THERMODYNAMICS OF AQUEOUS ELECTROLYTES AND HYDROGEN-BONDED NON-ELECTROLYTES OVER A WIDE RANGE OF TEMPERATURE AND PRESSURE

CENTRE FOR NEWFOUNDLAND STUDIES

TOTAL OF 10 PAGES ONLY
MAY BE XEROXED

(Without Author's Permission)

CAIBIN XIAO

001311


CENTRE FOR NFLD. STUDIES
MEMORIAL UNIVERSITY
OF NEWFOUNDLAND

THERMODYNAMICS OF AQUEOUS ELECTROLYTES AND HYDROGEN-BONDED NON-ELECTROLYTES OVER A WIDE RANGE OF TEMPERATURE AND PRESSURE

THE AQUEOUS TRIVALENT LANTHANIDE CATIONS AND THE METHANOL-WATER SYSTEM

by
Caibin Xiao

A thesis submitted to the
School of Graduate Studies
in partial fulfilment of the
requirements for the degree of
Doctor of Philosophy©

Department of Chemistry
Memorial University of Newfoundland

February, 1997

St. John's Newfoundland

National Library of Canada
Acquisitions and Bibliographic Services
395 Wellington Street
Ottawa ON K1A 0N4
Canada

Bibliothèque nationale du Canada
Acquisitions et services bibliographiques
395, rue Wellington
Ottawa ON K1A 0N4
Canada

Your file Votre référence

Our file Notre référence

The author has granted a non-exclusive licence allowing the National Library of Canada to reproduce, loan, distribute or sell copies of this thesis in microform, paper or electronic formats.

L'auteur a accordé une licence non exclusive permettant à la Bibliothèque nationale du Canada de reproduire, prêter, distribuer ou vendre des copies de cette thèse sous la forme de microfiche/film, de reproduction sur papier ou sur format électronique.

The author retains ownership of the copyright in this thesis. Neither the thesis nor substantial extracts from it may be printed or otherwise reproduced without the author's permission.

L'auteur conserve la propriété du droit d'auteur qui protège cette thèse. Ni la thèse ni des extraits substantiels de celle-ci ne doivent être imprimés ou autrement reproduits sans son autorisation.

0-612-36216-7

Canada

Abstract

Partial molar heat capacities and volumes of aqueous solutions are required to calculate the temperature- and pressure-dependence of chemical equilibrium constants over the wide range of conditions encountered in industrial and geochemical processes. Values for the standard partial molar heat capacities $C^{\circ}_{p,2}$ and volumes V°_{2} of aqueous electrolytes also provide much information about the nature of the ionic solvation because both functions are sensitive to the hydrated structure of ions in solution. This research addresses two major topics. The objective of the first part of the program is to explore the solvation of $M^{3+}(aq)$ ions by determining the apparent molar volumes and heat capacities of several trivalent lanthanide ions over a wide range of temperature and pressure, and interpreting the results by semi-empirical hydration models. The second objective is to examine the behaviour of partial molar volumes in the methanol-water system, as an example of a hydrogen bonded non-electrolyte, over a range of temperature and pressure that approaches the critical locus of the mixture.

Apparent molar heat capacities $C_{p,\phi}$ and volumes V_{ϕ} were derived from specific heat capacities and densities measured in a Sodev Picker flow microcalorimeter and vibrating-tube densimeter at pressure 0.1 MPa. For high-temperature volumetric measurements, a stainless-steel cell vibrating tube densimeter and a platinum cell vibrating-tube densimeter were constructed in the course of this research. These densimeters allowed measurement of the densities of solutions relative to the reference

fluid, water, at temperatures up to 600 K and pressures up to 30.0 MPa with an overall uncertainty less than 0.2 $kg \cdot m^3$.

Data for $C_{p,\phi}$ and V_ϕ for $LaCl_3(aq)$, $La(ClO_4)_3(aq)$, and $Gd(ClO_4)_3(aq)$ from 283.2 K to 338.2 K; $Nd(ClO_4)_3(aq)$, $Eu(ClO_4)_3(aq)$, $Er(ClO_4)_3(aq)$, and $Yb(ClO_4)_3(aq)$ from 283.2 K to 328.2 K; and $HCF_3SO_3(aq)$ and $NaCF_3SO_3(aq)$ from 283.2 K to 328.2 K, were analysed by means of the Pitzer equations to derive $C^o_{p,2}$, V^o_2, and expressions for the excess properties. The revised Helgeson-Kirkham-Flowers (HKF) model has been used to represent the temperature dependence of these standard partial molar properties within the experimental uncertainty. Plots of $C^o_{p,2}$ and V^o_2 at T = 298.15 K against the ionic radius of the six lanthanide cations clearly display the discontinuous behaviour known as the "gadolinium break". It was found that the ionic-radius dependence of V^o_2 is consistent with changes in the primary hydration number, while the effect of temperature on the behaviour of $C^o_{p,2}$ across the series suggests that secondary sphere hydration has a major effect on $C^o_{p,2}$.

Densities of $NaCF_3SO_3(aq)$ and $Gd(CF_3SO_3)_3(aq)$ were measured with the platinum-cell vibrating tube densimeter at temperatures from 323 K to 600 K and at pressures up to 20 MPa. Apparent molar volumes for $NaCF_3SO_3(aq)$ and $Gd(CF_3SO_3)_3(aq)$ calculated from the measured densities were represented by the Pitzer ion-interaction treatment. The temperature and pressure dependence of V^o_2 and the second virial coefficients in the Pitzer equation were expressed by empirical expressions in

which the compressibility of water was used as an independent variable. These treatments led to values of $V_2^o(NaCF_3SO_3, aq)$ from 283 K to 573 K and $V_2^o(Gd(CF_3SO_3)_3, aq)$ from 278 K to 473 K as functions of temperature and pressure, which are the first reported in the literature. The conventional values of $V_2^o(Gd^{3+}, aq)$ calculated from these data and $V_2^o(Na^+, aq)$ from the literature are in excellent agreement with extrapolations of low-temperature values of $V_2^o(Gd(ClO_4)_3, aq)$ based on the HKF approach. It was found that the effect of pressure on V_2^o for $Gd(CF_3SO_3)_3(aq)$ was more pronounced than that for common 1:1 and 2:1 aqueous electrolytes at temperatures near 298 K, and that this behaviour could be explained by the larger primary hydration shell for trivalent lanthanide cations.

Densities of $\{xCH_3OH + (1 - x)H_2O\}$ relative to water were measured in the vibrating tube densimeter at the temperatures T = (323, 373, 423, 473, 523, and 573 K) and at pressures of 7.0 MPa and 13.5 MPa. Excess molar volumes V_m^E for $\{xCH_3OH + (1 - x)H_2O\}$ were calculated from the experimental densities for the mixtures, using accurate equations of state for water and methanol. The data were treated with an extended corresponding-states model based on the properties of pure water. An empirical function was used to fit small differences between the compression factors of $\{xCH_3OH + (1 - x)H_2O\}$ and the compression factor of H_2O at the same reduced temperature and the same reduced pressure. The corresponding-states treatment reproduces the measured densities to within the experimental uncertainty of 0.0004 $g \cdot cm^{-3}$ at all of the temperatures and

pressures studied, except at T = 573 K and p = 13.5 MPa. The densities, excess molar volumes, partial molar volumes, isothermal compressions, and cubic expansion coefficients from the model are consistent with the limited literature data available. The behaviour of V_m^E at T = 573.6 K, and p = 13.7 MPa indicates either a very narrow region of (vapour + liquid) phase separation, or near-critical behaviour at x = 0.44 with the critical pressure $p_c \leq 13.5$ MPa.

Acknowledgements

I wish to express my appreciation and gratitude to my supervisor, Dr. Peter R. Tremaine for his guidance and inspiration throughout the course of this work.

I am grateful to Dr. J. M. Simonson of the Chemical and Analytical Division, Oak Ridge National laboratory for helpful collaborations and many useful discussions.

I am also grateful to Dr. H. Bianchi and Dr. R. J. Fernandez-Prini for providing the original densimeter design and components, and much help in the construction of the equipment. I would like to thank many other people who have assisted in various ways. First I thank Dr. Murray Brooker, Dr. Pujing Pan, and Dr. Dmitri Shvedov for helpful discussions. I also thank my colleagues in our lab: Mr. Zhongning Wang, Mr. Wei Xie, Ms. Jiangping Zhao, and Mr. Sean Quinlan for their help and encouragement. I am grateful to Miss Tram Pham for her assistance with experimental measurements for some results in Chapter III. Many thanks are due to Mr. Randy Thorne, Mr. Gerry Brown, and Mr. Lou Feltham for their excellent machining, electronic , and welding assistance.

I thank my wife Min Luo and my daughter Diandian for their support, understanding, and encouragement.

Financial support provided by the National Science and Engineering Research of Canada (NSERC), the International Association of Properties of Water and Steam (IAPWS), and Memorial University of Newfoundland are also gratefully acknowledged.

Contents

Page

Abstract II

Acknowledgement V

List of Tables XI

List of Abbreviations and Symbols XV

Part One. Introduction and Experimental Methods

I Introduction

I.1 Hydrothermal Solutions 5
I.2 Thermodynamics of Aqueous Solutions 6
I.2.1 Apparent Molar and Partial Molar Properties 6
I.2.2 Standard State and Excess Properties 9
I.2.3 Relationships 11
I.3 The Properties of Water 15
I.4 Solvation of Aqueous Electrolytes 19
I.4.1 Dielectric Saturation-Multi-Layer Model 21
I.4.2 Dielectric Saturation - Dielectric Constant as a Function of Radial Distance 23
I.4.3 Compressible-Continuum Model 26
I.4.4 Hydration Effects 29
I.4.5 The Helgeson Kirkham Flowers Model 36
I.5 Excess Properties 41
I.5.1 The Ornstein-Zernike Equation 41
I.5.2 Debye-Hückel Theory 43
I.5.3 Integral Equation Approaches 47
I.5.4 The Ion-Interaction Model 51
I.6 Near Critical Effects and Complications for Dilute Solutions 57
I.6.1 Dilute Near-Critical Solutions 58
I.6.2 Debye-Hückel Limiting Law near the Critical Point of the Solvent 61

II Experimental Methods

II.1 Picker Flow Calorimeter 66
II.1.1 The Principles of Operation 66
II.1.2 Absolute Calibration 73
II.2 Vibrating-Tube Densimeter 77
II.2.1 The Principle of the Vibrating Tube Densimeter 77
II.2.2 The Sodev Flow Densimeter 82
II.3 High-Temperature Densimeter 84
II.3.1 Construction and Operation of the High-Temperature Densimeters 84
II.3.2 Mechanical Characteristics of the Platinum Alloy Vibrating Tube densimeter 86
II.3.3 Bubble Point of Water at T = 574 K 87

Part Two. Partial Molar Heat Capacities and Volumes of Lanthanide $Ln^{3+}(aq)$ Ions

III Apparent Molar Volumes of Aqueous Sodium Trifluoromethanesulfonate and Aqueous Trifluoromethanesulfonic Acid at Temperatures from 283 to 600 K and Pressures up to 20 MPa.

III.1 Introduction 93
III.2 Experimental Section 94
III.3 Results 96
III.3.1 Low-Temperature Results 97
III.3.2 High-Temperature Results 103
III.4 Discussion 106
III.4.1 Experimental Uncertainties 106
III.4.2 The Concentration Dependence of $V_{\phi,2}$ and $C_{p,\phi,2}$ 115
III.4.3 Temperature Dependence of V_2^o, $\beta^{(o)V}$ and $\beta^{(1)V}$ 119
III.4.4 Standard Partial Molar Volumes for $CF_3SO_3^-(aq)$ 121

IV Apparent Molar Heat Capacities and Volumes of $LaCl_3(aq)$, $La(ClO_4)_3(aq)$,and $Gd(ClO_4)_3(aq)$ Between the Temperatures 283 K and 338 K.

IV.1 Introduction 125
IV.2 Experimental 125

IV.3 Results 128
IV.3.1 Apparent Molar Properties 128
IV.3.2 Hydrolysis of La^{3+}(aq) and Gd^{3+}(aq) 129
IV.3.3 Ion Interaction Model 134
IV.4 Discussion 146
IV.4.1 Literature Comparisons 146
IV.4.2 Extrapolation to Elevated Temperatures 151

V Apparent Molar Heat Capacities and Volumes of $Nd(ClO_4)_3$(aq), $Eu(ClO_4)_3$(aq), $Er(ClO_4)_3$(aq), and $Yb(ClO_4)_3$(aq) from the Temperatures 283 K to 328 K.

V.1 Introduction 160
V.2 Experimental 161
V.3 Results 162
V.4 Comparison with Literature Data 169
V.5 Standard Partial Molar Properties 179
V.6 Hydration Effects 185
V.7 Conclusions 192

VI Densities and Apparent Molar Volumes of $Gd(CF_3SO_3)_3$(aq) from the Temperatures 278 K to 472 K and Pressures up to 30 MPa.

VI.1 Introduction 194
VI.2 Experimental 195
VI.3 Results 196
V.3.1 Concentration Dependence of $V_{\phi,2}$ for $La(CF_3SO_3)_3$(aq) 197
V.3.2 Temperature- and Pressure-Dependence of $V_{\phi,2}$ for $Gd(CF_3SO_3)_3$(aq) 198
VI.4 Discussion 209
VI.4.1 The Pressure Effect 214
VI.4.2 Conventional Standard Partial Molar Volumes for Gd^{3+}(aq) 216
VI.5 Conclusion 219

Part Three. Thermodynamics of (Methanol + Water) at Elevated Temperature and Pressure.

VII Excess Molar Volumes and Densities of (Methanol + Water) at Temperatures Between 323 K and 573 K and Pressures of 0.1, 7.0 and 13.5 MPa.

VII.1 Introduction 221

VII.2 Experimental 222
VII.3 Results 223
VII.4 Corresponding-State Model 226
VII.5 Comparison with Literature Results 244
VII.6 Partial Molar Volumes, Isothermal Compressibility and Thermal Expansivity 245
VII.7 Near-Critical Behaviour at T = 573.6 K and p = 13.7 MPa 251

Part Four. Concluding Summary, References, and Appendices

VIII Concluding Summary 258

IX References 264

Appendix A: Tables of Experimental Results 282

Appendix B: Hydration Number of Aqueous Lanthanide Ions from Miyakawa *et al.*'s Model 337

List of Tables

Table III.1 Standard partial molar volumes V_2^o, virial coefficients $\beta^{(0)J}$ and $\beta^{(1)J}$ $\beta^{(0)V}$, $\beta^{(1)V}$, and C^J in equation (III.3.4) for $HCF_3SO_3(aq)$ at p = 0.10 MPa. 99

Table III.2 Standard partial molar heat capacities $C_{p,2}^o$, virial coefficients $\beta^{(0)J}$ and $\beta^{(1)J}$, and C^J in equation (III.3.5) for $HCF_3SO_3(aq)$ at p = 0.10 MPa. 99

Table III.3 Standard partial molar heat capacities $C_{p,2}^o$, virial coefficients $\beta^{(0)J}$ and $\beta^{(1)J}$, and C^J in equation (III.3.5) for $NaCF_3SO_3(aq)$ at p = 0.10 MPa. 107

Table III.4 Parameters for $NaCF_3SO_3(aq)$ in equations (III.3.7) - (III.3.9). 107

Table III.5 Calculated apparent molar volumes $V_{\phi,2}$ for $NaCF_3SO_3(aq)$. 108

Table III.6 The statistical uncertainties of densities $\delta\rho$ and the statistical errors in the apparent molar volumes $\delta V_{\phi,2}$ of 0.1 and 1.0 mol·kg^{-1} solutions as estimated from equation (III.4.1). 114

Table III.7 Comparing the relative densities of NaCl(aq) solutions and D_2O observed in this work with those calculated from the equations of state for NaCl(aq) and D_2O. . . 116

Table III.8 The conventional standard partial molar volumes V_2^o for $CF_3SO_3^-(aq)$ at 0.1 MPa for T < 373.15 K and at saturation pressures for T≥ 373.15 K. 122

Table IV.1 Values of parameters from the Pitzer ion-interaction model for $Gd(ClO_4)_3(aq)$, $La(ClO_4)_3(aq)$, and $LaCl_3(aq)$. 137

Table IV.2 The fitting parameters for equations (IV.3.3), (IV.3.6), (IV.3.8) and (IV.4.5) for the apparent molar heat capacities. 138

Table IV.3 The fitting parameters for equations (IV.3.4), (IV.3.7), and (IV.3.9) for the apparent molar volumes. 139

Table IV.4 Standard state properties of aquo-ions from 283.2 K to 338.2 K. 148

Table V.1 Values of parameters from the Pitzer ion-interaction model for aqueous $Nd(ClO_4)_3$, $Eu(ClO_4)_3$, $Er(ClO_4)_3$, $Yb(ClO_4)_3$ from the isothermal least square fits. . . . 166

Table V.2 The fitting parameters for equations (V.3.3), (V.3.7), (V.3.8), and (V.3.10) for the apparent molar volumes. 167

Table V.3 The fitting parameters for equations (V.3.2), (V.3.5), (V.3.6), and (V.3.9) for the apparent molar heat capacities. 168

Table V.4 Standard partial molar properties of aquo-ions from T = 283.2 K to 328.2 K from the parameters listed in tables V.2 and V.3. 180

Table VI.1 Standard partial molar volumes V_2^o of $La(CF_3SO_3)_3(aq)$ from equation (VI.3.2) 199

Table VI.2 Parameters for the standard partial molar volumes and excess properties $\beta^{(1)V}$ in equations (VI.3.2), (VI.3.4), and (VI.3.5) for $La(CF_3SO_3)_3(aq)$ 199

Table VI.3 The values of A_v in equation (VI.3.2) and densities of $H_2O(l)$ and NaCl(aq) ($m = 5.6940\ mol \cdot kg^{-1}$) used in this work. 200

Table VI.4 Coefficients for equations (VI.3.2) and (VI.3.6) to (VI.3.8) describing the temperature and pressure dependence of the parameters V_2^o, $\beta^{(o)V}$, and $\beta^{(1)V}$ for $Gd(CF_3SO_3)_3(aq)$ 205

Table VI.5 $V_{\phi,2}$ for $Gd(CF_3SO_3)_3(aq)$ at $p = p_{sat}$ and p= 25.0 MPa. 210

Table VI.6 The conventional standard partial molar volumes V_2^o for $Gd^{3+}(aq)$ at $p = p_{sat}$. 217

Table VII.1 Parameters in equations (VII.4.7) to (VII.4.10). 237

Table VII.2 Densities ρ, excess molar volumes V_m^E, partial molar volumes V_a and V_w, isothermal compressibilities κ_m and cubic expansion coefficients α_m of $\{xCH_3OH+(1-x)H_2O\}$. 238

Table A.II.1 The results from the flow-mimicking calibrations at T = 283.2, 288.2 and 298.2 K. 283

Table A.III.1 The experimental values of $\{(c_p\rho/c_{p,1}^*\rho_1^*) - 1\}$ and apparent molar heat capacities $C_{p,\phi,2}(HCF_3SO_3, aq)$. 285

Table A.III.2 The experimental values of $\{(c_p\rho/c^*_{p,1}\rho^*_1) - 1\}$ and apparent molar heat capacities $C_{p,\phi,2}(NaCF_3SO_3, aq)$. 289

Table A.III.3 Relative densities $\{\rho - \rho^*_1\}$ and apparent molar volumes $V_{\phi,2}$ of $HCF_3SO_3(aq)$ at p = 0.10 MPa. 292

Table A.III.4 Relative densities $\{\rho - \rho^*_1\}$ and apparent molar volumes $V_{\phi,2}$ of $NaCF_3SO_3(aq)$. 294

Table A.IV.1 The experimental values of $\{(c_p\rho/c^*_{p,1}\rho^*_1) - 1\}$ and apparent molar heat capacities $C_{p,\phi,2}(LaCl_3, aq)$. 298

Table A.IV.2 The experimental values of $\{(c_p\rho/c^*_{p,1}\rho^*_1) - 1\}$ and apparent molar heat capacities $C_{p,\phi,2}(La(ClO_4)_3, aq)$. 300

Table A.IV.3 The experimental values of $\{(c_p\rho/c^*_{p,1}\rho^*_1) - 1\}$ and apparent molar heat capacities $C_{p,\phi}$ for $\{La(ClO_4)_3 + HClO_4\}(aq)$ mixtures. 302

Table A.IV.4 Relative densities $\{\rho - \rho^*_1\}$ and apparent molar volumes V_ϕ for $\{La(ClO_4)_3 + HClO_4\}(aq)$ mixtures. 303

Table A.IV.5 The experimental apparent molar volumes $V_{\phi,2}$ and heat capacities $C_{p,\phi,2}$ for $Gd(ClO_4)_3(aq)$. 304

Table A.IV.6 The experimental values of $\{(c_p\rho/c^*_{p,1}\rho^*_1) - 1\}$ and apparent molar heat capacities $C_{p,\phi}$ for $\{Gd(ClO_4)_3 + HClO_4\}(aq)$ mixtures. 307

Table A.IV.7 Relative densities $\{\rho - \rho^*_1\}$ and apparent molar volumes V_ϕ for $\{Gd(ClO_4)_3 + HClO_4\}(aq)$ mixtures. 308

Table A.V.1 The experimental values of $\{(c_p\rho/c^*_{p,1}\rho^*_1) - 1\}$ and apparent molar heat capacities $C_{p,\phi}$ for $\{Ln(ClO_4)_3 + HClO_4\}(aq)$ mixtures. 309

Table A.V.2 Relative densities $\{\rho - \rho^*_1\}$ and apparent molar volumes V_ϕ for $\{Ln(ClO_4)_3 + HClO_4\}(aq)$. 316

Table A.V.3 The experimental apparent molar volumes $V_{\phi,2}$ and apparent molar heat capacities $C_{p,\phi}$ for $Eu(ClO_4)_3(aq)$ at T = 298.2 K. 323

Table A.VI.1 Densities ρ and apparent molar volumes $V_{\phi,2}$ of $La(CF_3SO_3)_3(aq)$ and $Gd(CF_3SO_3)_3(aq)$. 324

Table A.VI.2 Densities ρ and apparent molar volumes $V_{\phi,2}$ of $Gd(CF_3SO_3)_3(aq)$. 328

Table A.VII.1 Densities ρ and excess molar volumes V_m^E of $\{xCH_3OH + (1-x)H_2O\}$. 330

Table A.VII.2 Densities ρ(expt.) of methanol measured in this work and those ρ(calc.) from the equation of state (Goodwin, 1987). 335

List of Figures

Figure II.1 A schematic diagram of the Picker flow calorimeter 68

Figure II.2 Heat leak correction factor at T = 283.2 K. 76

Figure II.3 Schematic diagram of the vibrating-tube densimeter. 78

Figure II.4 Vibrating-tube densimeter and sample injection system. 88

Figure II.5 Electric circuit for measuring the resonance frequency of the vibrating tube densimeter 89

Figure II.6 Frequency response curve. 90

Figure II.7 Phase angle against frequency ratio. 90

Figure III.1 $V_{\phi,2}(HCF_3SO_3, aq)$ plotted as a function of the square root of molality. . . 100

Figure III.2 $V_{\phi,2}(NaCF_3SO_3, aq)$ plotted as a function of the square root of molality. . 101

Figure III.3 $C_{p,\phi,2}(HCF_3SO_3, aq)$ plotted as a function of the square root of molality. . 102

Figure III.4 $V_2^o(NaCF_3SO_3, aq)$ at temperatures between 283.15 K and 373.15 K plotted as a function of 1000/(T - 228). 104

Figure III.5 $V(NaCF_3SO_3, aq)$ at temperatures between 423.65 K and 600.48 K plotted as a function of $T\beta_1^*$. 105

Figure III.6 $V_{\phi,2}(NaCF_3SO_3, aq)$ at 0.1 MPa minus the Debye-Hückel limiting slope term according to equation (III.3.4) plotted as a function of molality. 109

Figure III.7 $V_{\phi,2}(NaCF_3SO_3, aq)$ minus the Debye-Hückel limiting slope term according to equation (III.3.4) plotted as a function of molality. 110

Figure III.8 $V_{\phi,2}(NaCF_3SO_3, aq)$ minus the Debye-Hückel limiting slope term according to equation (III.3.4) plotted as a function of molality. 111

Figure III.9 $V_{\phi,2}$ (observed) minus $V_{\phi,2}$ (calculated) from equations. (III.3.7) to (9) plotted as a function of temperature and molality. 112

Figure III.10 V_2^o(calculated) from equation (III.3.10) and from the isotherm-isobar least squares fittings plotted as a function of temperature. 120

Figure III.11 $\beta^{(0)V}$ and $\beta^{(1)V}$ for $NaCF_3SO_3$(aq) plotted as a function of temperature. . . 123

Figure IV.1 The apparent molar heat capacities of $La(ClO_4)_3$ (aq), plotted as a function of ionic strength after subtracting the Debye-Hückel limiting law (DHLL) term according to equation (IV.3.3). 130

Figure IV.2 The apparent molar heat capacities of $Gd(ClO_4)_3$ (aq), plotted as a function of ionic strength after subtracting the Debye-Hückel limiting law (DHLL) term according to equation (IV.3.3). 131

Figure IV.3 The apparent molar heat capacities of $LaCl_3$ (aq), plotted as a function of ionic strength after subtracting the Debye-Hückel limiting law (DHLL) term according to equation (IV.3.3). 132

Figure IV.4 The apparent molar volumes of $LaCl_3$ (aq), plotted as a function of ionic strength after subtracting the Debye-Hückel limiting law (DHLL) term according to equation (IV.3.3). 133

Figure IV.5 The apparent molar heat capacities of $La(ClO_4)_3$ (aq), plotted as a function of ionic strength after subtracting the Debye-Hückel limiting law (DHLL) term according to equation (IV.3.3). 140

Figure IV.6 The apparent molar heat capacities of $Gd(ClO_4)_3$ (aq), plotted as a function of ionic strength after subtracting the Debye-Hückel limiting law (DHLL) term according to equation (IV.3.3). 141

Figure IV.7 The apparent molar volumes of $La(ClO_4)_3$ (aq), plotted as a function of ionic strength after subtracting the Debye-Hückel limiting law (DHLL) term according to equation (IV.3.4). 142

Figure IV.8 The apparent molar volumes of $Gd(ClO_4)_3$ (aq), plotted as a function of ionic strength after subtracting the Debye-Hückel limiting law (DHLL) term according to equation (IV.3.4). 143

Figure IV.9 The standard partial molar heat capacities of $La(ClO_4)_3(aq)$ obtained from fitting equation (IV.3.3) to the experimental data at each temperature, and the extrapolation to elevated temperatures by fitting the entire matrix of data to equation (IV.4.5). 144

Figure IV.10 The standard partial molar volumes of $La(ClO_4)_3(aq)$ and $Gd(CLO_4)_3(aq)$ obtained from fitting equation (IV.3.4) to the experimental data at each temperature, and the extrapolation to elevated temperatures by fitting the entire matrix of data to equation (IV.3.9). 145

Figure IV.11 Comparison the standard partial molar heat capacities of $GdCl_3(aq)$ calculated from the standard partial molar heat capacities of $Gd(ClO_4)_3(aq)$ which are predicted by both equation (IV.3.8) and equation (IV.4.5) with the experiment data. . 150

Figure IV.12 Comparison the differences in V_2^o for $Cl^-(aq)$ and $ClO_4^-(aq)$ from different sources. 152

Figure IV.13 Comparison the differences in $C_{p,2}^o$ for $Cl^-(aq)$ and $ClO_4^-(aq)$ from different sources. 155

Figure IV.14 The temperature dependence of Pitzer's parameters $\beta^{(1)J}$ and $\beta^{(0)J}$ in equation (IV.3.3). 158

Figure IV.15 The temperature dependence of Pitzer's parameter $\beta^{(1)v}$ and $\beta^{(0)v}$ in equation (IV.3.4). 159

Figure V.1 Apparent molar volumes $V_{\phi,2}$ and apparent molar heat capacities $C_{p,\phi,2}$ of $Nd(ClO_4)_3(aq)$ plotted as a function of the square root of ionic strength $I^{1/2}$. 170

Figure V.2 Apparent molar volumes $V_{\phi,2}$ and apparent molar heat capacities $C_{p,\phi,2}$ of $Eu(ClO_4)_3(aq)$ plotted as a function of the square root of ionic strength $I^{1/2}$. 171

Figure V.3 Apparent molar volumes $V_{\phi,2}$ and apparent molar heat capacities $C_{p,\phi,2}$ of $Er(ClO_4)_3(aq)$ plotted as a function of the square root of ionic strength $I^{1/2}$ 172

Figure V.4 Apparent molar volumes $V_{\phi,2}$ and apparent molar heat capacities $C_{p,\phi,2}$ of $Yb(ClO_4)_3(aq)$ plotted as a function of the square root of ionic strength $I^{1/2}$ 173

Figure V.5 Apparent molar volumes $V_{\phi,2}$ and apparent molar heat capacities $C_{p,\phi,2}$ of $Eu(ClO_4)_3(aq)$ plotted as a function of square root ionic strength $I^{1/2}$ at T = 298.2 K. . . 174

Figure V.6 Standard partial molar volumes of $Nd(ClO_4)_3(aq)$ and $La(ClO_4)_3(aq)$ plotted as a function of temperature. 175

Figure V.7 Standard partial molar heat capacities $C^{\circ}_{p,2}$ of $Yb(ClO_4)_3(aq)$ obtained from fitting equation (V.3.2) to the experimental results at each temperature, and the extrapolation to elevated temperatures by fitting the entire matrix of results to equation (V.3.9a). 176

Figure V.8 The temperature dependence of the non-Born terms for aqueous trivalent cations. 177

Figure V.9 The standard partial molar volumes V°_2 of aqueous lanthanide perchlorates. 182

Figure V.10 The standard partial molar heat capacities $C^{\circ}_{p,2}$ of aqueous lanthanide perchlorates, $Al(ClO_4)_3(aq)$, and $Fe(ClO_4)_3(aq)$ plotted against ionic radius. 184

Figure V.11 The geometries of 8- and 9- coordinated $Ln^{3+}(aq)$ cations, and 6-coordinated metal cations as presented by Miyahawa *et al.*(1988). 188

Figure V.12 Plot of the hydration number of the lanthanides. 189

Figure VI.1 Apparent molar volumes of $La(CF_3SO_3)_3(aq)$ at 278 K and at 0.1 MPa, 7.0 MPa and 30.0 MPa 201

Figure VI.2 Apparent molar volumes of $La(CF_3SO_3)_3(aq)$ at 298 K and at 0.1 MPa, 7.0 MPa and 30.0 MPa 202

Figure VI.3 Apparent molar volumes of $La(CF_3SO_3)_3(aq)$ at 318 K and at 0.1 MPa, 7.0 MPa and 30.0 MPa 203

Figure VI.4 $V_{\phi,2}$ (observed) minus $V_{\phi,2}$ (calculated) from equations (VI.3.2), and (VI.3.6) to (VI.3.8) plotted as a function of temperature and molality. 206

Figure VI.5 $V_{\phi,2}\{Gd(CF_3SO_3)_3, aq\}$ minus the Debye-Hückel limiting slope term according to equation (VI.3.2) plotted as a function of molality. 207

Figure VI.6 $V_{\phi,2}\{Gd(CF_3SO_3)_3, aq\}$ minus the Debye-Hückel limiting slope term according to equation (VI.3.2) plotted as a function of molality. 208

Figure VI.7 $V_2^o\{Gd(CF_3SO_3)_3, aq\}$ calculated from equation (VI.3.8) plotted as a function of temperature. 211

Figure VI.8 $\beta^{(0)V}$ (upper) and $\beta^{(1)V}$ (lower) plotted as a function of temperature. 212

Figure VI.9 $V_{\phi,2}$ plotted as a function of the sqaure root molality m at T = 423 K. . . . 215

Figure VI.10 $V^o(Gd^{3+}, aq)$ as a function of temperature. 218

Figure VII.1 Deviations of the experimental densities of pure methanol ρ(expt) from those of Goodwin's equation of state ρ(calc). 225

Figure VII.2 Comparison of excess molar volume V_m^E at T = 323 K and p = 0.1 MPa. 227

Figure VII.3 Comparison of V_m^E in this work with V_m^E reported by Simonson *et al.* (1987) at p = 7.0 MPa. 228

Figure VII.4 Excess molar volumes V_m^E of $\{xCH_3OH + (1 - x)H_2O\}$ at T = 573.6 K and p = 13.7 MPa. 229

Figure VII.5 A schematic diagram of the dependence of V_m on x at p = 13.5 MPa. . . 230

Figure VII.6 The relative differences between the reduced compression factors of $\{xCH_3OH + (1- x)H_2O\}$ and H_2O, $\{Z_w(T_r, p_r) - Z_m(T_r, p_r, x)\}/Z_w(T_r, p_r)$, at the different temperatures and pressures. 234

Figure VII.7 Deviations of experimental excess molar volumes V_m^E(expt) from those V_m^E(calc) calculated from the model and deviations of the experimental densities ρ(expt) from those ρ(calc) calculated from the model. 243

Figure VII.8 Comparison of V_m^E predicted by the model with V_m^E estimated. 246

Figure VII.9 Comparison of partial molar volumes V_s and V_w calculated from the corresponding-states model with those from Easteal and Woolf (1985a) at T = 323 K and p = 0.1 MPa. 249

Figure VII.10 Comparison of (a) isothermal compression κ_m and (b) cubic expansion coefficient α_m with those from Easteal and Woolf (1985b). 250

Figure VII.11 Critical temperatures T_c of $\{xCH_3OH + (1 - x)H_2O\}$. 252

Figure VII.12 Molar volumes V_m of $\{xCH_3OH + (1 - x)H_2O\}$ at T = 573.6 K and p = 13.7 MPa. 254

Figure VII.13 Values for $(\partial V_m/\partial x)_{p,T}$ at T = 573.6 K and p = 13.7 MPa corresponding to the cubic spline function in figure VII.12. 255

Figure B.1 The gadolinium break estimated from equation (B.5) 340

Figure B.2 The heat capacity contributions of the ν_1 bands for the $Ln(H_2O)^{3+}$ 342

Abbreviations and Symbols

Abbreviations

aq	aqueous
CC	compressible-continuum (model)
cr	crystal state
DH	Debye-Hückel
DHLL	Debye-Hückel limiting law
EOS	equation of state
HKF	Helgeson-Kirkham-Flower (equation)
HNC	hypernetted chain (approximation)
ITS-68	International Temperature Scale-1968
ITS-90	International Temperature Scale-1990
MPB	modified Poisson-Boltzmann (equation)
MSA	mean spherical approximation
OZ	Ornstein-Zernike (equation)
PLL	phase-locked-loop
PM	primitive model
PY	Percus-Yevik (approximation)
RTD	platinum resistance device (thermometer)

Symbols[a]

α	activity; cubic expansion coefficient
β	equal to 1/(kT) or isothermal compressibility
$\beta^{(o)V}$, $\beta^{(1)V}$	adjustable parameters in the Pitzer equation for apparent molar volumes
$\beta^{(o)J}$, $\beta^{(1)J}$	adjustable parameters in the Pitzer equation for apparent molar heat capacities
$\gamma_{\pm}$	average activity coefficient
δY	statistical uncertainty associated with quantity Y
ΔY	finite increase in quantity Y
$\Delta_s Y$	Solvation (hydration) property Y
ϵ	static dielectric constant
ϵ_o	vacuum permittivity, 8.85419×10^{-12} $J^{-1}\cdot C^2\cdot m^{-1}$
ϵ_∞	high-frequency permittivity
η	a constant defined in Born equations
θ	solvent temperature parameter, equal to 228 K in HKF equations
κ	isothermal compressibility

μ	dipole moment of a molecule
μ_i	chemical potential of the component I
ν	$\nu = \nu 1 + \nu 2$, where $\nu 1$ and $\nu 2$ are numbers of cations, anions produced by dissociation of one molecule of electrolyte
ρ	density
ρ_i	number density of species i
ρ_l^*	density of water
τ	resonance period
ϕ	practical osmotic coefficient
ψ	equal to 260 MPa in HKF equations; phase angle
ω	vibrational frequency
ω_o	natural frequency
ω_i	Born coefficient for the ion i, defined by equation (I.4.36)
A	Helmholtz free energy
A_J	DHLL slope for apparent molar heat capacity
A_v	DHLL slope for apparent molar volume
A_ϕ	DHLL slope for activity coefficient and osmotic coefficient
c	speed of light, 2.99792458×10^{8} m·s^{-1}
c_p	massic heat capacity
C^V, C^J	ternary interaction parameters in Pitzer equations
C_p^o	standard partial molar heat capacity
$C_{p,\phi}$	apparent molar heat capacity
e	elementary charge, 1.602177×10^{-19} C
E	electric field strength
f	heat-leak correction factor
F_m	massic flow rate
F_v	volumetric flow rate
G	Gibbs free energy
H	enthalpy
I	ionic strength
I_a, I_b, I_c	moment of inertia
k	Boltzmann constant, 1.38066×10^{-23} J·K^{-1}
K	force constant; densimeter constant; equilibrium constant
L_ϕ	apparent molar enthalpy
Ln^{3+}	trivalent lanthanide cations
m	molality
n	hydration number
n_i	number of moles of species i
N_A	Avogadro constant
p	pressure

r_i	radius of ion i
$r_{cr,i}$	crystallographic radius of ion i
r_p	Pauling radius
R	gas constant, 8.314 $J \cdot K^{-1} \cdot mol^{-1}$
p_c	critical pressure
t	time
T	temperature
T_c	critical temperature
T_{cm}	critical temperature for a mixture
T_D	delay line temperature
V	volume
V_c	molar volume at the critical point
V_m	molar volume of a mixture
V^o	standard partial molar volume
$\bar{V}_i$	partial molar volume of component i
V_ϕ	apparent molar volume
x	mole fraction
Z_i	charge of ion i

---

[a] Symbols used in this thesis follow the convention used in the Journal of Chemical Thermodynamics. Symbols with subscript 1 refer to the properties for solvent water while symbols with subscript 2 and 3 refer to the properties for the major and the second major solutes, respectively, in solutions. The symbol with superscript * stands for the property of the pure single-phase substance while that with superscript o stands for the property of the hypothetical 1 molal ideal solution. Symbols for the units of quantities follow the definitions of the System International (SI). The absolute temperature scale used in this work is based on the ITS-68.

Part One. Introduction and Experimental Methods

Chapter I. Introduction

A knowledge of the equilibrium properties of aqueous systems is crucial for understanding many natural and industrial processes. The study of aqueous chemistry not only has great practical significance but also provides answers to fundamental questions about the nature of ionic solvation, ion-ion interactions, and hydrogen-bonding (Conway, 1981). Theoretical insights into the "structural" properties of aqueous solutions have been advanced by the development of statistical mechanics, quantum chemistry, and spectroscopy (Dogonadze *et al.*, 1986). Much of our knowledge about the behaviour of aqueous solutions, however, continues to be determined from painstaking direct experimental measurements of thermodynamic properties.

While a large amount of reliable experimental data for most classes of aqueous systems is available at T = 298.15 K and p = 0.1 MPa, many important applications require data for the thermodynamic properties of aqueous solutions under conditions of high temperature and high pressure; for example, in the modelling of geochemical processes and power plant chemistry. Unfortunately, only a few aqueous electrolytes and non-electrolytes have received the intense study required to provide a complete thermodynamic description over the full temperature and pressure range from the freezing point to the critical point of water (T = 273.15 K to 674 K, p = 0.1 to 22.2 MPa). The thermodynamic properties of solutes at extreme conditions are mainly estimated from

measurements at ambient conditions by a variety of empirical and semi-empirical methods. The investigation of model systems at both ambient and high temperature conditions is extremely important. Measurements on model systems provide reliable data for exploring the nature of aqueous solvation and, thus, for developing improved theoretical and empirical models.

A fundamental question in the study of aqueous electrolyte solutions is how the thermodynamic properties are determined by the charge, the ionic radius, and the structure of the hydrated ions. In the last two decades, reliable experimental data at elevated temperatures have been available for most common singly-charged and doubly-charged aquo-ions. It has been found that the behaviour of standard partial molar properties is dominated by configurational hydration effects at temperatures near 298.15 K, and by solvent polarization at high temperature (Cobble and Murray, 1981). In contrast to the M^{-}(aq) and M^{2-}(aq) ions, which have been well studied, the temperature- and pressure-dependent thermodynamic properties of the trivalent cations have not been examined. There are only a few M^{3-}(aq) cations whose partial molar heat capacities and volumes have been measured at temperatures beyond 298.15 K. The trivalent lanthanide cations are extremely interesting because the radii steadily decease across the series due to the lanthanide contraction effect, and their hydration numbers undergo an abrupt change in the middle of the series. Because their interactions with water are primarily electrostatic, the aqueous trivalent lanthanide cations serve as an ideal model system for

evaluating the effects of long-range polarization and short-range configurational hydration on thermodynamic properties.

In addition to electrostatic interactions between charged ions, hydrogen-bond formation and hydrophobic interactions are also important in determining thermodynamic properties of aqueous polyatomic ions, specially under sub-ambient conditions and at elevated temperature and pressure. It has been found that, at the critical point of water, the apparent molar properties of electrolyte solutions approach negative infinity, while the apparent molar properties of non-electrolyte solutions approach positive infinity (Wood *et al.*, 1991; Biggerstaff and Wood, 1985). This research measures the volumetric properties of the methanol-water system over a temperature and pressure range which covers the critical locus of the mixture to study the effect of near-critical conditions on the partial molar properties of a "typical" hydrogen-bonded non-electrolyte.

This thesis consists of four parts. In the first part, the theoretical background of aqueous chemistry relevant to this study is introduced. Then a description is given for the the theory and design of a new high-temperature vibrating tube densimeter constructed for this project. The principles and operation of the Picker flow microcalorimeter are also presented here. In the second part, the experimental results for the apparent molar heat capacities and apparent molar volumes of aqueous trifluoromethanesulfonic ("triflic") acid, sodium triflate, lanthanide perchlorates, and the lanthanide triflates are presented. Data treatments for excess properties by Pitzer's ion-ion interaction model and for the

standard partial molar properties by the HKF equations or empirical equations based on solvent density functions are discussed. The third part of this thesis presents results from volumetric studies of (methanol + water) over a wide range of p, T, x, and a modified corresponding-states model treatment for the pVT data of this system. A summary, references, and tables for experimental data are included in the last part of this thesis.

I.1 Hydrothermal Solutions

A hydrothermal solution is a hot aqueous solution. The thermodynamics of hydrothermal solutions are studied by geochemists in order to develop thermodynamic models for many geochemical processes. These include the formation of hydrothermal mineral deposits (Pirajno, 1992), water-rock interactions in enhanced oil recovery, and the possible origin of life from marine hydrothermal systems (Holm, 1992). The aqueous phase concerned in these geochemical systems typically contains species such as Na^+, K^+, Ca^{2+}, Mg^{2+}, Cl^-, SO_4^{2-}, CO_3^{2-}, Fe^{2+}, $Al(OH)_4^-$, and $AgCl_2^-$, at concentrations from a few ppm to near-saturation concentrations. The temperature of the aqueous phase ranges from ambient to 350 °C for the deep ocean hydrothermal vents and geothermal springs, and up to 1000 °C for magmatic fluids. Thermodynamic calculations play an essential role in determining fluid-mineral equilibra since direct experimental investigations of multi-phase equilibrium processes at very high temperatures and pressures are extremely difficult. The great difficulty involved in the equilibrium modelling of geochemical

systems is to collect thermodynamic data for the multi-component aqueous phase. Partial molar heat capacities and volumes must be known as a function of temperature and pressure to calculate the thermodynamic properties of aqueous electrolytes at high temperatures and pressures from the large experimental data base that exists for ambient conditions.

The aqueous phases in electrical power plants are less complicated than those in geochemical systems. However, very accurate thermodynamic data and theoretical models are required to calculate potential-pH diagrams, corrosion product solubilities, and the distribution of power cycle additives and contaminants between water and steam. These are used to provide a theoretical basis for on-line monitoring and chemistry control of the plant cycle water, to solve field problems, and to establish operational guidelines (Dooley and Bursik, 1995; Lindsay, 1989; Cobble and Lin, 1989).

Thermodynamic data for aqueous solutions at high temperature and pressure are also required in many other industrial and scientific areas. These include hydrometallurgy (Burkin, 1966), the hydrothermal synthesis of advanced materials (Lobachev, 1973), and the hydrothermal oxidation of toxic waste (Antal, 1995).

I.2 Thermodynamics of Aqueous Solutions

I.2.1 Apparent Molar and Partial Molar Properties

For simplicity, discussion is limited to binary systems, that is (water + single

solute). Symbols with subscript 1 refer to the properties for the solvent water and symbols with subscript 2 refer to the properties for solutes.

In studies of solution chemistry, the extensive properties of a solution are discussed in terms of the properties of the individual components. The latter are generally partial molar properties and apparent molar properties:

$$Y = n_1\bar{Y}_1 + n_2\bar{Y}_2 = n_2 Y_{\phi,2} + n_1 Y_1^* , \qquad \text{(I.2.1)}$$

where n_i and Y_i are the number of moles and the partial molar property, respectively, for component i; $Y_{\phi,2}$ is the apparent molar property and Y_1^* stands for the property of the pure solvent.

The partial molar properties are defined as:

$$\bar{Y}_i = (\partial Y/\partial n_i)_{T,p,n_{j\neq i}} . \qquad \text{(I.2.2)}$$

For example, the partial molar Gibbs energy is the chemical potential μ:

$$\mu_i = (\partial G/\partial n_i)_{T,p,n_{j\neq i}} . \qquad \text{(I.2.3)}$$

For non-electrolyte solutions, the composition variable is usually the mole fraction x of component 2, thus,

$$\bar{Y}_1 = Y - x(\partial Y/\partial x)_{pT}, \tag{I.3.4}$$

$$\bar{Y}_2 = Y - (1 - x)(\partial Y/\partial x)_{pT}. \tag{I.3.5}$$

For electrolyte solutions, the molality is used as the composition variable. Thus the partial molar properties are given by

$$\bar{Y}_1 = \{1 - m(\partial Y/\partial m)_{T,p}\}(M_1/1000), \tag{I.2.6}$$

$$\bar{Y}_2 = (\partial Y/\partial m)_{T,p}. \tag{I.2.7}$$

Apparent molar properties are defined by equations of the type,

$$Y_{\phi,2} = (Y - 1000\, Y_1^*/M_1)/m. \tag{I.2.8}$$

They are calculated from the quantities directly measured. For example, the apparent molar volume $V_{\phi,2}$ and $C_{p,\phi,2}$ are given by

$$V_{\phi,2} = \frac{1000(\rho_1^* - \rho)}{m\rho_1^*\rho} + \frac{M_2}{\rho}, \tag{I.2.9}$$

$$C_{p,\phi,2} = \frac{c_p(1 + mM_2) - c_{p,1}^*}{m}, \qquad \text{(I.3.10)}$$

where M_2 is the molar mass of the solute, ρ_1^* and $c_{p,1}^*$ are the density and the specific heat capacity of pure water, respectively; ρ and c_p are the density and the specific heat capacity of the solution, respectively. The apparent molar enthalpy $L_{\phi,2}$ can be obtained from measurements of the heat of solution or the heat of dilution:

$$L_{\phi,2} = \Delta\bar{H}_s - \Delta\bar{H}_s^o, \qquad \text{(I.2.11)}$$

$$L_{\phi,2}(m_2) - L_{\phi,2}(m_1) = \Delta\bar{H}_D(m_2 - m_1), \qquad \text{(I.2.12)}$$

where ΔH_s is the heat of solution and ΔH_s^o represents the heat of solution at infinite dilution; $\Delta H_D(m_2 - m_1)$ is the heat of dilution from molality m_2 to m_1.

I.2.2. Standard States and Excess Properties

Traditionally, standard states are used to describe the departure of the thermodynamic properties of a real solution from those of an ideal solution. For a solvent at temperature T and pressure p, the standard state is the pure phase of the solvent at T and p with an activity equal to unity. The chemical potential of the solvent μ_1 is given by

the expression:

$$\mu_1(T,p) = \mu_1^*(T,p) + RT \ln a_1(T,p) , \qquad \text{(I.2.13)}$$

where μ_1^* is the chemical potential of the pure solvent at T and p, and a_1 is the activity of the solvent. For a solute $M_{\nu_1}X_{\nu_2}$, the standard state is the hypothetical ideal solution at a standard molality $m^\circ = 1.0$ mol·kg^{-1}. The chemical potential is given by

$$\mu_2(T,p) = \mu_2^\circ(T,p) + \nu RT \ln a_2(T,p) , \qquad \text{(I.2.14)}$$

where μ_2° is the chemical potential for the hypothetical 1.0 mol·kg^{-1} ideal solution at T and p, a_2 is the activity of the solute, and $\nu = \nu_1 + \nu_2$.

The osmotic coefficient ϕ and average activity coefficient $\gamma_\pm$ are introduced to express the deviations of a real solution from the ideal behaviour of the standard states. They are defined as

$$\phi = -\frac{1000}{\nu m M_1} \ln a_1 , \qquad \text{(I.2.15)}$$

$$\gamma_\pm = a_2/m . \qquad \text{(I.2.16)}$$

Molar excess properties, Y^E, are defined by the general equation,

$$Y^E = Y(actual) - Y(ideal) . \qquad \text{(I.2.17)}$$

By the definition, the volume of mixing for an ideal solution is equal to zero at constant temperature and pressure, while the Gibbs free energy of mixing is given by

$$\Delta G_{mix} = RT\sum x_i \ln x_i . \qquad \text{(I.2.18)}$$

If we consider an electrolyte solution containing 1 kg of solvent (n_1 = 55.51 mole of solvent) and m moles of solute, the excess Gibbs free energy and the excess volume of the solution per mole of electrolyte are given by

$$\bar{G}^{E} = (\frac{n_1}{m}\mu_1 + \mu_2) - (\frac{n_1}{m}\mu_1^{*} + \mu_2^{o}) - RT(\frac{n_1}{m}\ln\frac{n_1}{n_1 + m} + \ln\frac{n_2}{n_1 + m}) , \qquad \text{(I.2.19)}$$

$$\bar{V}^{E} = (\frac{n_1}{m}\bar{V}_1 + \bar{V}_2) - (\frac{n_1}{m}V_1^{*} + V_2^{o}) , \qquad \text{(I.2.20)}$$

where V_1 and V_2 are the partial molal volumes of the solvent and the solute, respectively, $V_2^{o} = \lim_{m \to 0} V_{\phi,2}$ is the standard partial molar volume for the hypothetical 1 mol·kg^{-1} ideal solution, and V_1^{*} is the mole volume of the solvent.

I.2.3. Relationships

Combining equations (I.2.19), (I.2.13), and (I.2.14) yields the molar excess Gibbs free energy:

$$\bar{G}^{E} = \nu RT(\ln\gamma_{\pm} - \phi + \frac{n_1 + \nu m}{\nu m}\ln\frac{n_1 + \nu m}{n_1}) . \qquad (I.2.21)$$

For very dilute solutions,

$$\bar{G}^{E} = \nu RT(\ln\gamma_{\pm} + 1 - \phi) . \qquad (I.2.22)$$

According to the Gibbs-Duhem equation, only one of the two chemical potentials for a binary system is independent. Thus, the osmotic coefficient is related to the average activity coefficient in the expression:

$$\phi = 1 + 1/m \int m\, d\ln\gamma_{\pm} . \qquad (I.2.23)$$

For a binary solution in a single phase region, only three state variables are independent and, therefore, any three state variables may be used to define the complete thermodynamic state. All other thermodynamic properties can be derived from a thermodynamic potential which is a function of the three independent variables, generally G(T, p, x) or A(T, V, x). For example, the excess molar Gibbs free energy can be used as a thermodynamic potential to derive other excess or apparent molar properties.

$$L_{\phi} = -T^2[\partial(G_m^{E}/T)/\partial T]_{p,m} , \qquad (I.3.24)$$

$$C_{p,\phi,2} = C_{p,2}^{o} + (\partial L_{\phi} / \partial T)_{p,m}, \tag{I.3.25}$$

$$V_{\phi,2} = V_{2}^{o} + (\partial G_{m}^{E} / \partial p)_{T,m}, \tag{I.3.26}$$

where G_m^E is the excess molar Gibbs free energy and L_ϕ is the apparent relative molar enthalpy (Pitzer 1991).

From the equations above, two important thermodynamic identities are derived:

$$(\partial C_{p,\phi,2} / \partial p)_{T,m} = -T(\partial^2 V_{\phi,2} / \partial T^2)_{p,m}, \tag{I.3.27}$$

$$(\partial L_{\phi} / \partial p)_{T,m} = V_{\phi,2} - T(\partial V_{\phi,2} / \partial T)_{p,m}. \tag{I.3.28}$$

The significance of equations (I.3.27) and (I.3.28) is that they relate the volumetric measurements to the thermal measurements. The mutual agreement between values determined from measurements of $V_{\phi,2}$ and $C_{p,\phi,2}$ or $V_{\phi,2}$ and L_ϕ upon using these equations can be used to confirm that both sets of data are reliable. On the other hand, the estimation of $C_{p,\phi,2}$ and L_ϕ from $V_{\phi,2}$ may not be satisfactory because high quality data are needed to accurately calculate the pressure derivatives.

One of the basic applications of thermodynamics to hydrothermal systems is to obtain the Gibbs free energy change ($\Delta_r G°$) for a chemical or a phase equilibrium over a wider range of temperature and pressure. $\Delta_r G°$ and other thermodynamic data are available for many processes at T =298.15 K. Except for a few systems for which $\Delta_r G°$ or equilibrium constants can be measured directly by experimental methods, values for $\Delta_r G°$ at elevated temperatures are estimated through the following formula:

$$\Delta_r G°(T,p) = \Delta_r G°(298\,K, 0.1\,MPa) - \Delta_r S°(298\,K, 0.1\,MPa) + \int_{298}^{T} \Delta_r C_p^{\circ} dT - T\int_{298}^{T} \frac{\Delta_r C_p^{\circ}}{T} dT + \int_{0.1}^{p} \Delta_r V° dp \,, \qquad \text{(I.2.29)}$$

in which $\Delta_r C_p^{\circ}$, $\Delta_r V°$ and $\Delta_r S°$ are the standard heat capacity, volume and entropy of reaction, respectively. Generally, they are complex functions of temperature, pressure and composition.

Great effort has been made to develop global equations which can represent experimental data for all the partial molar properties, with the capability to predict thermodynamic properties over a wide range of temperature, pressure, and composition. For a few pure substances, very accurate equations of state (EOS) now are available. For binary aqueous solutions, the development of accurate EOS treatments is still in its infant stage. One of the best examples is the EOS for NaCl(aq) reported by Archer (1992). This EOS covers the temperature range from 250 K to 600 K, and pressures up to 100 MPa. In recent years, researchers at Oak Ridge National Laboratory have reported

unified EOSs for HCl(aq) and $CaCl_2$(aq) (Simonson *et al.*, 1990; Holmes *et al.*, 1987, 1994). These incorporate data from thermal, volumetric, and isopiestic measurements.

I.3 The Properties of Water

Because of its importance to industry and science, many precise experimental measurements for the thermal and volumetric properties of pure water have been made at temperatures ranging from the triple point to 1000 K and pressures up to 100 MPa, including the near-critical region. For example, extensive and accurate pVT measurements were made by Kell, Mclaurin and Whalley in Canada (Kell and Whalley, 1975; Kell *et al.*, 1978, 1989). Sixty years of international cooperation has resulted in unified equations of state for ordinary and the heavy water suitable for the accurate and speedy calculation of steam and liquid property values (Levelt Sengers, 1995; Kestin and Sengers, 1986; Haar *et al.*, 1984, Saul and Wagner, 1989). In the studies of aqueous chemistry, water is usually used as a reference fluid for density and heat capacity measurements. Moreover, as shown in the previous section, very accurate values for the properties of pure water are needed to obtain high quality data for the apparent or excess molar properties of aqueous solutions. The error associated with the density of water must be less than 0.00005 $g \cdot cm^{-3}$ in order to calculate V_m^E or $V_{\phi,2}$ for dilute aqueous solutions at all conditions of temperature and pressure. The heat capacity must be known to $\pm$ 0.0001 $J \cdot K^{-1} \cdot g^{-1}$ for accurate calculations of C_p^E and $C_{p,\phi,2}$.

The history of international collaboration in the development of formulations for the thermodynamic properties of light and heavy water has been described by Levelt Sengers (1995). To review the history and theory behind these most sophisticated EOS treatments is certainly beyond the scope of this section. However, it is worthwhile to describe the structure and main features of the EOS developed by Hill (1990), which is used at every stage of measurement presented in this thesis, and in the interpretation of experimental results.

The objective of developing any unified fundamental equation for the thermodynamic properties of water is to construct a Helmholtz function whose derivatives can represent all valid experimental data within the experimental uncertainties, including the near-critical-point region. The unified Helmholtz function (ψ/RT) suggested by Hill is

$$\bar{\Psi}(\bar{\rho},\bar{T}) \equiv \psi/RT = \bar{\Psi}_f + F(\bar{\Psi}_a - \bar{\Psi}_f)\,, \qquad \text{(I.3.1)}$$

in which $\bar{\Psi}_f = \bar{\Psi}_f(\bar{\rho},\bar{T})$ is the non-singular part of the dimensionless Helmholtz function, called the "far-field" function, and $\bar{\Psi}_a = \bar{\Psi}(\bar{\rho},\bar{T})$ is the singular part of the dimensionless Helmholtz function, the "revised-extended scaling equation" of Levelt Sengers, Kamagar-Parsi, Balfour and Sengers (Levelt Sengers *et al.*, 1983). In equation (I.3.1), $F(\bar{\rho},\bar{T})$ is a function of "distance" from the critical point, which acts as a "switching function". The value of $F(\bar{\rho},\bar{T})$ is unity at the critical point, where all its derivatives are zero, and zero

everywhere outside the critical region.

The function $\bar{\Psi}_n$ used by Hill is exactly equivalent to the $\bar{P}$ function given by Levelt Sengers *et al.* (1983). The $\bar{P}$ function consists of one part, P_{reg}, and another part, ΔP, that contains the critical anomalies. ΔP was constructed in such a way that its derivatives with respect to the independent variables (chemical potential and temperature) have power law behaviour near the critical point, and that the critical exponents of these properties satisfy the scaling laws. Following the theory of critical universality, Levelt Sengers *et al.* (1983) used the values of the critical exponents obtained theoretically from the three-dimension Ising model.

The far-field equation is in the form

$$\bar{\Psi}_f = \ln\bar{\rho} + \bar{\Psi}_o + \bar{\Psi}_1(\bar{\rho},\bar{T}) \ , \qquad \text{(I.3.2)}$$

where the first two terms pertain to the ideal gas, and $\bar{\Psi}_1(\bar{\rho},\bar{T})$ is a complicated function with 64 adjustable parameters which were obtained by fitting the unified equation (I.3.1) to a large number of experimental data.

Hill's EOS reproduces all the experimental data for density, speed of sound, specific heat, throttling coefficients, and virial coefficients within the experimental uncertainty. For example, the densities obtained from Hill's EOS are within 20 to 30 parts per million of the values measured by Kell and Whalley from T = 273.15 K to 573.15 K at pressures up to 100 MPa.

Since Hill's EOS fully incorporates the revised-extended scaling equation of Levelt Senger, Kamagar-Parsi, Balfour and Sengers, the EOS is capable of providing a highly accurate representation of all the thermodynamic data in the near-critical region.

Pruss and Wagner (1995) reported a new EOS for water as a candidate for the new scientific formulation of IAPWS at the 12th IAPWS conference. The new EOS was based on the new international temperature scale ITS-90 and updated experimental data. This EOS contains 54 parameters in the non-singular residual part of the Helmholtz function (versus 64 parameters used in this part of Hill's EOS). Pruss and Wagner introduced a two-parameter non-analytical term to account for the critical anomalies in the second derivatives of the Helmholtz function. This non-analytic function is expressed in terms of the reduced variables $\tau = T_c/T$ and $\delta = \rho/\rho_c$ so that no switching function was needed. Pruss and Wagner's EOS reproduces the selected experimental data to within the experimental uncertainty, even including data in the metastable supercooled region. Both Hill's formulation and Pruss and Wagner's formulation have very similar accuracy over the range of interest. Hill's EOS is, however, compatible with the dielectric constant data for water compiled by Archer and Wang (1990). We have used Hill's EOS to calculate densities, specific heat capacities, and other thermodynamic properties for water in this research.

The EOS for D_2O has been formulated by Hill *et al.* (1982). This EOS represents pVT data, specific heat capacities, and speed of sound for whole range of liquid and

vapour states from the triple point up to 873 K and 100 MPa to within the experimental uncertainties, except at conditions very close to the critical point. For example, the estimated uncertainty associated with densities of the saturated liquid at 573 K is about 0.1 $kg \cdot m^{-3}$.

I.4 Solvation of Aqueous Electrolytes

The theory of ionic solvation began with the Born model (Born, 1920). The physical picture of the model is very simple. In the Born model, ions are viewed as rigid conducting spheres of radius r_i, bearing a charge $Z_i e$, where e is the electronic charge, and the solvent is taken to be a structureless dielectric continuum. The Gibbs free energy resulting from the transfer of ions from vacuum into the solvent is given by

$$\Delta_t G^\circ = \sum \frac{-\eta Z_i^2}{r_i}\left(1 - \frac{1}{\epsilon}\right), \qquad \text{(I.4.1)}$$

$$\eta = e^2 N_A/(8\pi\epsilon_o), \qquad \text{(I.4.2)}$$

where N_A is Avogadro's constant, ϵ_o is the permittivity of a vacuum, and ϵ is the static dielectric constant of the solvent (water).

From equation (I.4.1), other thermodynamic properties for the solvation process

can be derived:

$$\Delta_s S^\circ = -(\partial \Delta_s G^\circ / \partial T)_p = \sum \frac{\eta Z_i^2}{r_i} (\frac{\partial \ln \epsilon}{\partial T})_p , \qquad \text{(I.4.3)}$$

$$\Delta_s V^\circ = (\partial \Delta_s G^\circ / \partial p)_T = \sum \frac{\eta Z_i^2}{r_i} (\frac{\partial \ln \epsilon}{\partial p})_T , \qquad \text{(I.4.4)}$$

$$\Delta_s C_p^\circ = T(\partial \Delta_s S^\circ / \partial T)_p = \sum \frac{\eta Z_i^2 T}{r_i} [(\frac{\partial^2 \ln \epsilon}{\partial T^2})_p - (\frac{\partial \ln \epsilon}{\partial T})_p^2] . \qquad \text{(I.4.5)}$$

In making numerical calculations based on equations above, the radius of the solvated ion is needed. Traditionally, the radii obtained from X-ray measurements on ionic crystals, i.e. the crystallographic radii, are used in the Born model. The calculated values for $\Delta_s G^\circ$ and $\Delta_s H^\circ$ from equations (I.4.1) to (I.4.4) for the alkali metal cations and halide anions are numerically too high, in some cases they are nearly 50% higher than the experimental values (Bockris and Reddy, 1970). However, calculated values are of the same order of magnitude as the experimental results. This supports the premise that ion-solvent interactions arise largely from coulombic forces.

Many modifications have been made to improve the Born model by using a so-called "effective radius" and/or by introducing an "effective" dielectric constant in the

region near the ion. For example, it was found that, by adding 8.5 nm to the radii of the positive ions and 1.0 nm to those of the negative ions, one can remove the discrepancy between the calculated and observed values (Bockris and Reddy, 1970). Because of dielectric saturation caused by the high electric field of the ions, it is expected that the dielectric constant in the vicinity of ions is much lower than that in bulk water. The physical effect of using a smaller value for the effective dielectric constant is the same as using a larger value for the effective radius. Both reduce the overestimation of the ion-solvent interaction in the Born model. The approach using an effective dielectric constant may be carried out in a more physically rigorous way.

I.4.1 Dielectric Saturation: Multi-Layer Model

Beveridge and Schnuelle (1975) had used the reaction field technique to determine the electrostatic energy of a charge in a dielectric medium which is partitioned into concentric shells characterized by different dielectric constants. The charged ion polarizes the surrounding molecules, and the polarized solvent molecules create a reaction field (depolarization field). The free energy can be calculated from the interaction of the charge with the reaction field. They obtained a general equation for the Gibbs free energy of a n-layer model. For the one-layer model,

$$\Delta_t G^\circ = \sum \eta Z_i^2 [(\frac{1}{\epsilon_1} - 1)(\frac{1}{r_i} - \frac{1}{r_{i,1}}) + (\frac{1}{\epsilon r_{i,1}} - \frac{1}{r_i})] , \qquad (I.4.6)$$

and for the two-layer model,

$$\Delta_s G^\circ = \sum \eta Z_i^2 [(\frac{1}{\epsilon_{i,2}} - 1)(\frac{1}{r_{i,1}} - \frac{1}{r_{i,2}}) + (\frac{1}{\epsilon_{i,1}} - 1)(\frac{1}{r_i} - \frac{1}{r_{i,1}}) + \frac{1}{\epsilon r_{i,2}} - \frac{1}{r_i}] , \qquad \text{(I.4.7)}$$

where $r_{i,1}$ is equal to r_i plus the thickness of the first layer, and $r_{i,2}$ is equal to $r_{i,1}$ plus the thickness of the second layer; $\epsilon_{i,1}$ and $\epsilon_{i,2}$ are the dielectric constants of the solvent in the first and the second layers, respectively.

Abraham and Marcus (Abraham *et al.*, 1983; Abraham and Marcus, 1986) used the one-layer model to calculate the electrostatic contribution to the thermodynamic properties for the ion-solvation process. In their approach, r_i is taken as the crystallographic ionic radius; ϵ_1 is $1.05n_D^2$ (where n_D is the solvent refractive index); and $\partial\epsilon_1/\partial T$ is -1.60×10^{-3} K^{-1}. The reason for assigning the value $1.05n_D^2$ to ϵ_1 is that the water molecules in the first layer have no freedom of thermal motion under the strong electric field of ions and no orientational polarization contribution to the dielectric constant.

The thickness of the first layer was either taken to be the value of the solvent radius (28 nm) or calculated from the experimental value for $\Delta_s G^\circ$ at T = 298.15 K.

Abraham and Marcus (1986) assumed that the standard thermodynamic functions were composed of a neutral part and an electrostatic part:

$$\Delta_s Q^\circ = \Delta Q_E^\circ + \Delta Q_N^\circ , \qquad \text{(I.4.8)}$$

where ΔQ_E° and ΔQ_N° denote the electrostatic and nonelectrostatic contributions. Values of ΔQ_N° are estimated from the corresponding solvation parameters of non-polar gaseous solution with the following equation

$$\Delta Q_N^\circ = a + b r . \qquad \text{(I.4.9)}$$

The parameters a and b are obtained by fitting equation above to the experimental data for noble gases.

The values of $\Delta_s G^\circ$ for a few $M^+(aq)$ calculated from Abraham and Marcus's model are much closer to the observed values than those obtained with the original Born equation at temperatures from 283 K to 573 K. At temperatures higher than 423 K, the calculated and observed $\Delta_s S^\circ$ values are in fair agreement. Like the Born model, Abraham and Marcus's approach fails to give even a qualitative representation for $\Delta_s C_p^\circ$ in the temperature range $283\ K \le T \le 573\ K$. Because little was known about the thickness and dielectric constant of the first layer, or their variation with temperature, these parameters in Abraham and Marcus's model were selected arbitrarily.

I.4.2 Dielectric Saturation: Dielectric Constant as a Function of Radial Distance

If the dielectric constant is a function of the electric field, and thus a function of the distance r measured from the center of the ion, the electrostatic contribution to the hydration energy is given by

$$\Delta_s G^\circ = -\eta Z_i^2 \{ \frac{1}{r_c} - \int_{r_c}^{\infty} [\epsilon(r) r^2]^{-1} dr \} , \qquad \text{(I.4.10)}$$

where r_c is the ionic radius and η is defined by equation (I.4.2).

Different approaches use different functions for $\epsilon(r)$. Dandurand and Schott (1992) used a empirical function of the type

$$\epsilon(r) = \epsilon_B \exp(-K_n / r^n) \qquad n = 0, 1, 2, ... \qquad \text{(I.4.11)}$$

which is not explicitly dependent on the electric field. In equation (I.4.11), ϵ_B is the dielectric constant of bulk water, $K_n = (\ln \epsilon_B)/r_c^n$.

Bacher and Porter (1986) used a function $\epsilon(r)$ derived from Debye's classical theory for static permittivity,

$$\epsilon(r) = 1 + \frac{\epsilon_\infty - 1}{\epsilon_\infty + 2}(\epsilon + 2) + \frac{4\pi\epsilon\mu r^2}{Zev}[-\frac{1}{y} + \coth(y)] , \qquad \text{(I.4.12)}$$

with the abbreviation $y = (\epsilon + 2)Ze\mu/(3kTr^2\epsilon)$. In equation (I.4.12), v is the volume of a water molecule, μ is the dipole moment of the water molecule, and ϵ_∞ is the high-frequency permittivity, which was taken to be the square of the refractive index.

Bucher and Porter found that $\Delta_s G^\circ$ was sensitive to r_c, the lower limit of integration. They chose r_c to be the Pauling radius r_P plus an empirical correction term δr,

which was taken to be $\delta r = 17$ nm for univalent ions and 35 nm for divalent ions. The average deviation between the calculated $\Delta_s G°$ and the experimental Gibbs free energy of hydration was 29 kJ·mol^{-1} for univalent ions and and 110 kJ·mol^{-1} for divalent ions.

Bontha and Pintauro (1992) used Booth's equation for $\epsilon(r)$,

$$\epsilon(r) = n^2 + \frac{3(\epsilon_B - n^2)}{\zeta E}[\coth(\zeta E) - \frac{1}{\zeta E}] , \qquad \text{(I.4.13)}$$

where $\zeta = 5\mu(n^2 + 2)/(2kT)$. The constants in equation (I.4.13) n, μ, and k are the optical refractive index, the dipole moment of a solvent molecule, and the Boltzmann constant, respectively. E(r) is the scalar electric field strength which satisfies the Poisson equation,

$$\nabla\cdot[\epsilon(r)\cdot E(r)] = 0 . \qquad \text{(I.4.14)}$$

In a polar medium, the macroscopic field is given by the expression

$$E(r) = \frac{1}{\epsilon(r)}\frac{Ze}{r^2} . \qquad \text{(I.4.15)}$$

After simultaneously solving equations (I.4.14) and (I.4.15), both ϵ(r) and E(r) are obtained as functions of radial coordinates r.

Bontha and Pintauro have shown that the effect of dielectric saturation is significant, and that, while Abraham and Marcus' model gave the approximate magnitude

of the dielectric saturation for univalent ions, it underestimated the values for divalent ions. On calculating the value for $\Delta_s G^\circ$, Bontha and Pintauro included the energy needed to form a cavity and to modify the solvent. This term was estimated according to the methods used by Abraham and Lizzi (1978). If the Goldschmidt ionic radius was used in the model, the calculated $\Delta_s G^\circ$ agreed very well with the experimental values at T = 298.15 K.

I.4.3 Compressible-Continuum Models

The strong electric field of an ion effects not only the orientational polarization of water molecules around the ion, but also the number density of water molecules in the region near the ion (Frank, 1955; Wood *et al.*, 1981, 1994; Quint and Wood, 1985). Thus the electric field strength E itself is a function of the dielectric constant $\epsilon\{(\rho_N(r),r\}$, where $\rho_N(r)$ is the number density of water. Wood and Quint have shown that E, ϵ and ρ_N satisfy the following equations:

$$E^2 = \int_{\rho_{N,\infty}}^{\rho_N} 2/\{\epsilon_o \rho_N^2 \kappa_T (\frac{\partial \epsilon}{\partial \rho_N})_{E,T}\} d\rho_N \ , \qquad \text{(I.4.16)}$$

and

$$E = Ze/(4\pi\epsilon_o \epsilon r^2) \ , \qquad \text{(I.4.17)}$$

and

$$\epsilon = n_D^2 + \alpha_B \pi \rho_N (n^2+2)\mu L\{\beta\mu(n^2+2)E/kT\}/4\pi\epsilon_o E\,, \qquad \text{(I.4.18)}$$

where κ_T is the isothermal compressibility near the ion; n_D is the optical refractive index of the solvent; α is the molecular polarizability; μ is the dipole moment of a water molecule; and $L\{y\} = [\coth\{y\} - 1/y]$ is the langevin function. In equation (I.4.17), α_B = 0.884, and β was adjusted at each temperature so that the equation gives the exact value for the dielectric constant of bulk water at E = 0.

Because ρ_N is a function of E, κ_T must be a function of E, ρ_N, and T,

$$\kappa_T = \kappa_T^o / \{1 - (\epsilon_o/2)\rho_N \kappa_T^o \int_0^{E^2} (\partial^2\epsilon/\partial\rho_N^2)_{E,T} dE^2\}\,, \qquad \text{(I.4.19)}$$

where κ_T^o is the compressibility at E = 0 and the integration is performed at constant ρ_N and T.

Values for $(\partial\epsilon/\partial\rho_N)_{E,T}$ and $(\partial^2\epsilon/\partial\rho_N^2)_{E,T}$ were obtained through tedious differentiation of equation (I.4.18). After solving equations (I.4.16-I.4.19) numerically, E can be obtained as a function of the radial coordinate r. Then the free energy for ionic hydration is calculated as

$$\Delta_t G^o = -\int_{q=0}^{Ze}\int_{r=\infty}^{r_c} E dq dr\,. \qquad \text{(I.4.20)}$$

Other thermodynamic properties such as $\Delta_s V^\circ$, $\Delta_s C_p^\circ$ were obtained by the appropriate numerical differentiation of equation (I.4.20).

Wood *et al.* (1994) have compared the pair-correlation function $\rho(r)/\rho^*$ of NaCl(aq) from the compressible-continuum (CC) model with that from a Monto-Carlo simulation at the supercritical temperature of water, T = 723.15 K, and a low steam density, $\rho = 0.01$ g·cm^{-3}. They also compared the apparent molar heat capacity and apparent molar volumes of NaCl(aq) calculated from CC model and the Born model with those observed experimentally at temperatures from T = 640 K to 680 K and at pressure p = 28 MPa (Majer *et al.*, 1991). Although the CC model gave a more reasonable description of the structure of hydrated ion than the simple Born model, the latter gave surprisedly good predictions for both the apparent molar heat capacities and apparent molar volumes at those conditions. This simulation by Wood *et al.* (1994) demonstrated the complexity of the solvation process at high temperature, and showed that the compression of the solvent caused by the extremely high electric field of the ion and high compressibility of the solvent needs to be considered. They suggested that the success of the simple Born model was due to the fortuitous cancelation of many important effects under high temperature conditions.

All the models discussed above improved the Born model by considering the dielectric constant of the solvent in the vicinity of the ion to be a function of the distance measured from the center of the ion. However, these models all ignored the structure of

water close to the hydrated ions.

I.4.4 Hydration Effects

An ion exists in aqueous solution in the hydrated form. The structure of hydrated ions has been investigated by means of X-ray and neutron diffraction, spectroscopy, and computer simulation (Ohtaki and Radnai, 1993). A few models have attempted to define a hydration number and to consider the effect of structure and hydration number.

In order to calculate the entropies and enthalpies of hydration, the partition function of the hydrated ions is needed. Although some of the vibrational and rotational frequencies for the internal motions in the primary solvation spheres of hydrated ions have been obtained by means of Raman and IR spectra, the entire vibrational and rotational modes can be only estimated with a electrostatic model or a quantum chemistry approach.

Eley and Evens (1938) made the first calculation of this kind for ions, based on an electrostatic model. Later, several electrostatic models were reported in which the short-range interactions between the solvent molecule and the ion and between the solvent molecules in the hydration sphere were considered (Muirhead-Gould and Laidler, 1966; Goldman and Bates, 1972; Tremaine and Goldman, 1978; Marcus, 1986; Tanger and Pitzer, 1989). Among them, it is worth mentioning Goldman and Bates' model, which has been used to calculate the Gibbs free energy of aqueous ions at high temperature by

Tremaine and Goldman (1978).

The Gibbs free energy for the hydration process in Goldman and Bates' model consists of three terms:

$$\Delta_z G^\circ = \Delta G^\circ_{Born} + \Delta E + RT(\partial \ln Q / \partial T)_p , \qquad \text{(I.4.21)}$$

where ΔE is the electrostatic energy of the short-range interaction, and ΔG°_{Born} is the Born term which arises from the long-range interactions between the hydrated ion and the solvent. The last term in equation (I.4.21) is due to the rotational and vibrational freedom of the hydrated ion.

ΔE represents the change in zero-point energy of the following process:

$$nH_2O(g) + \text{ion } r_c(g) \rightarrow (\text{ion } r_c \cdot nH_2O)(g).$$

The quantity ΔE was taken to consist of a sum of potential energies:

$$E = E_{i-d} + E_{i-id} + E_l + E_{la} + E_{rep} + \frac{1}{2} hc \sum \omega_i . \qquad \text{(I.4.22)}$$

In the equation above, the last term corrects the change in the zero-point vibrational energy of the hydration process in the gaseous phase. E_{i-d} represents the energy of interaction of the charge on the central ion with the permanent, off-center dipoles of the n water molecules in the first hydration shell; E_{i-id} is the energy of interaction of the charge on the central ion with the n dipoles induced by this charge; E_l is the dispersion interaction energy of the central ion with the surrounding primary water molecules; E_{la} is

the energy of the interaction between the primary water molecules around the central ion. E_{rep} is the repulsion term, which has the form:

$$E_{rep} = B/r^{12} . \qquad \text{(I.4.23)}$$

The value of the repulsion constant B was determined by solving the equation,

$$(\partial E/\partial r)_{r=r_c+r_w} = 0 , \qquad \text{(I.4.24)}$$

where r_c is the ionic radius and r_w = 12.6 nm represents the dimension of a water molecule.

The quantity Q was taken as a product of translational, rotational and vibrational partition functions, and hence,

$$(\partial lnQ/\partial T)_p = (\partial lnQ_{trans}/\partial T)_p + (\partial Q_{rot}/\partial T)_p + (\partial lnQ_{vib}/\partial T)_p . \qquad \text{(I.4.25)}$$

Goldman and Bates showed that the terms $(\partial \ln Q_{trans}/\partial T)_p$ and $(\partial \ln Q_{rot}/\partial T)_p$ take the simple forms, -5n/(2T) and (3 - 2n)/(2T), respectively, where n is the hydration number.

There are (5n - 3) vibrational modes arising from the motions of the bound water molecules with respect to the central ion. Goldman and Bates assumed that two of these modes can be attributed to oscillations of the bound water molecules about their smallest and largest principle axes of inertia. The frequencies of these models were estimated as

$$\omega_a^o = \frac{1}{2\pi c}\left(\frac{D_\pm}{I_a}\right)^{1/2}, \qquad \text{(I.4.26)}$$

$$\omega_c^o = \frac{1}{2\pi c}\left(\frac{D_\pm}{I_c}\right)^{1/2}, \qquad \text{(I.4.26)}$$

where I_a and I_c are the principal moments of inertia of the gaseous hydrate about its smallest and largest principal axes, respectively, and c is the speed of light. $D_\pm$ in equations (I.4.25) and (I.4.26) is the potential energy of a bound water molecule, given by

$$D_\pm = \frac{|Z|e\mu}{(r\pm s)^2}\sum_{l=0}^{\infty}\left(\frac{a}{r\pm s}\right)^{2l} - \frac{\delta_2\mu^2}{(r\pm s)^3}, \qquad \text{(I.4.27)}$$

where δ_2 is a numerical constant whose value is dependent on n, s is the distance between the center of the dipole and the oxygen atom, μ is the dipole moment of the water molecule, and a is the length of the dipole.

The remaining (5n - 5) fundamental vibrational frequencies in the gaseous hydrated ion were estimated by assuming that each of those frequencies is the same as the frequency of the fundamental breathing model (Goldman and Bates, 1972). These were calculated from the equations,

$$\omega_f^o = \frac{1}{2\pi c}\left(\frac{K^*}{R}\right)^{1/2}, \qquad \text{(I.4.28)}$$

and

$$R = M_{H_2O} M_{ion} / (M_{H_2O} + M_{ion}) \,. \tag{I.4.29}$$

The force constant in equation (I.4.28) was determined from

$$K = \frac{1}{n} \left(\frac{\partial^2 E}{\partial r^2} \right) \tag{I.4.30}$$

Finally,

$$\left(\frac{\partial \ln Q_{vib}}{\partial T} \right) = \frac{1}{T} \left[\frac{(5n-5) X_f e^{-X_f}}{1 - e^{-X_f}} + \frac{X_a e^{-X_a}}{1 - e^{-X_a}} + \frac{X_c e^{-X_c}}{1 - e^{-X_c}} \right] , \tag{I.4.31}$$

where $X_j = (hc\omega_j^o)/kT$.

The Born term was evaluated through

$$\Delta G^o_{Born} = \frac{N_A (Ze)^2}{2} \left(\frac{1}{r_c} - \frac{1}{r_g} \right) + \frac{N_A (Ze)^2}{2 r_c} \left(\frac{1}{\epsilon} - 1 \right) , \tag{I.4.32}$$

in which the first term arises from the difference between the radius of the gaseous ion and the aqueous ion. Here, r_c is the effective radius of the hydrated ion which was taken to be the radius of a uniform sphere, equal in volume to the volume of the hydrated ion,

$$r_e / nm = [r_c^3 + n(12.6)^3]^{1/3} \,. \tag{I.4.33}$$

The calculated Gibbs free energies, enthalpies and entropies are in excellent agreement with experimental values for 5 univalent cations, 4 univalent anions, 4 divalent cations, and 3 trivalent cations at T = 298 K.

Goldman and Bates' model is much more complicated than many other treatments that are based on Born model. For example, the enthalpy calculation in Goldman and Bates' approach consists of more than ten terms. The major factors contributing to the success of the model may be the following: First, the dipole of the water molecules was considered to be off-centred to allow for the possibility that positive and negative ions of the same size and charge are unequally hydrated. Second, the ion-solvent interaction energies were explicitly dependent on the structure and the hydration number of the hydrated ion. Goldman and Bates demonstrated that the energies of the short-range interactions between the ion and the surrounding water molecules were of the same order of magnitude as the long-range interaction described by Born model. Therefore, for physical realistic models of ionic hydration, the first hydration shell must be appropriately modelled. Third, although the term $RT^2(\partial \ln Q/\partial T)_p$ was not significant for $\Delta_r H°$, it is the major contribution to entropy. Finally, as required for any physically realistic model, some basic physical properties of the ion such as mass, polarizability and ionization potential of the ion must be considered.

Tremaine and Goldman (1978) extended this approach to calculate the Gibbs free energy function, $(\bar{G}_T^\circ - \bar{G}_{298}^\circ)$, for 14 group 1A, 2A, 3A and 3B cations and trivalent

lanthanides and actinide, from T = 323 K to 623 K. The calculation employs a temperature-independent primary hydration number as the only adjustable parameter. Above 423 K, the standard state partial molar Gibbs free energies predicted by the model reproduce the available experimental data much more accurately than those obtained by assuming that the heat capacities at T = 298 K are invariant with temperature.

Modified Born models have been used successfully to predict the Gibbs free energies and entropies of ionic hydration processes at T = 298 K. Some models predict reasonable values for the temperature dependencies of $\Delta_s S°$ and $\Delta_s G°$. Unfortunately, none of the models discussed above are adequate for calculating $\Delta_s C_p°$ and $\Delta_s V°$, even for a qualitative representation of the temperature dependence of $C_p°$ in the low temperature region. For many aqueous electrolytes, $C_p°$ first increases dramatically with temperature, reaching a maximum between 323 K to 358 K, and then declines dramatically as the temperature increases further. The Born model predicts that $(\partial C_p°/\partial T)_p$ is always negative and fails to describe the sharp increase of $C_p°$ at low temperature (Wei and Blum, 1995). In Goldman and Bates' model, the contribution to $C_p°$ by the internal modes of motion in the gaseous hydrated ion can be estimated from the partition function (equation I.4.25). The increase in $C_p°$(NaCl, aq) from T = 273 K to 333 K due to these internal modes is only 40 $J \cdot K^{-1} \cdot mol^{-1}$. This is much less than the experimental value of 150 $J \cdot K^{-1} \cdot mol^{-1}$. Certainly, structural effects beyond the first hydration shell have great influence on the temperature dependence of $C_p°$. This is not surprising if we note that the huge difference

between ice and liquid water at the same temperature cannot be explained by the change in the vibrational contribution(Eisengerg and Kauzmann, 1969). The remarkable change in heat capacity is undoubtedly associated with the distortion, and perhaps the breaking, of hydrogen bonds. It is not realistic to model $C^{\circ}_{p,s}$ for aqueous electrolytes without a knowledge of the subtle structure of the solvent beyond the first hydration shell.

I.4.5 The Helgeson Kirkham Flowers Model

Helgeson and Kirkham (1976) and Helgeson, Kirkham and Flowers (1981) appreciated that the large negative values of the partial molar heat capacities and volumes of aqueous electrolytes at high temperature could be described by the Born model. They assumed that the standard partial molar properties consist of two contributions: an electrostatic term, derived from the Born equation, and a nonelectrostatic term. The nonelectrostatic terms were empirically selected to be asymptotic functions of temperature which dominate at low temperature and approach constant values at high temperature. This consideration is consistent with the assumption that the high temperature behaviour of aqueous electrolytes is dominated by long-range electrostatic interactions (Cobble *et al.*, 1981).

In the Helgeson-Kirkham-Flower ("HKF") model, the standard partial molar volume was given by

$$V_j^o = a_{1,j} + a_{2,j}p + \frac{a_{3,j} + a_{4,j}pT}{T - \theta_j} - \omega_j Q \ , \qquad \text{(I.4.34)}$$

where p and T refer to the pressure in bars and the temperature in K, and a_{ij} corresponds to adjustable parameters characteristic of the jth species. These are independent of temperature and pressure. They are determined by fitting the equation to experimental data or by empirical correlations. The terms Q and ω in equation are derived from Born equation and given by

$$Q = \frac{1}{\epsilon}(\partial \ln \epsilon / \partial p)_T \ , \qquad \text{(I.4.35)}$$

$$\omega_j = \eta Z_j^2 / r_{e,j} \ , \qquad \text{(I.4.36)}$$

where Z_j is the charge of the jth ion and $\eta = 6.9466 \times 10^6$ nm·J·mol^{-1}, defined by equation (I.4.2). An effective radius r_e was used in the Born equation rather than crystallographic radii. By regression analysis of the experimental data available at that time, Helgeson and Kirkham (1976) found that the effective radii r_e for anions could be taken to be equivalent to their crystallographic radii. The effective radii of cations could be related to their crystallographic counterparts r_c by

$$r_{e,j} = r_{c,j} + 0.94 Z_j \ . \qquad \text{(I.4.37)}$$

The isobaric temperature dependence of the standard partial molar heat capacity was represented by

$$C^{\circ}_{p_r,j} = c_{1,j} + \frac{c_{2,j}T}{T-\theta_j} + \omega_j T X_{pT} \,, \tag{I.4.38}$$

where p_r stands for a reference pressure, $c_{1,j}$ and $c_{2,j}$ designate pressure/temperature-independent coefficients, and

$$X_{p_r,T} = \frac{1}{\epsilon(p_r,T)}\left[\left(\frac{\partial^2 \ln \epsilon(p_r,T)}{\partial T^2}\right)_{p_r} - \left(\frac{\partial \epsilon(p_r,T)}{\partial T}\right)^2_{p_r}\right] . \tag{I.4.39}$$

Use of equation (I.4.38) and the thermodynamic identity given by equation (I.2.27) leads to the following general equation for C°_{pj} as a function of temperature and pressure,

$$C^{\circ}_{pj} = c_{1,j} + \frac{c_{2,j}T}{T-\theta_j} - \frac{\theta_j T[2a_{2,j}(p-p_r) + a_{4,j}(p^2-p_r^2)]}{(T-\theta_j)^2} + \omega_j T X_{pT} \,. \tag{I.4.40}$$

The HKF equations have been revised recently to be consistent with new experimental results for C°_{pj} and V°_j at extremes of temperature (Tanger and Helgeson, 1988; Shock and Helgeson, 1988). The effective radius of the ion in the revised HKF equations is a function of temperature and pressure,

$$r_{e,j} = r_{c,j} + |Z_j|[k_j + g(T,p)] \ , \qquad \text{(I.4.41)}$$

where $r_{c,j}$ is the crystallographic radius of the ion, k_j is zero for the anion and 9.4 nm for cation. The term g(T,p) in equation (I.4.41) is a function of temperature and pressure related to the properties of the solvent. The differences between equations (I.4.37) and (I.4.41) are only important at temperatures above 473 K and pressures above 200 MPa.

The nonelectrostatic terms for standard partial molar volumes and standard partial molar heat capacities in the revised HKF model are

$$V^{\circ}_{j,n} = a_{1,j} + \frac{a_{2,j}}{\Phi + p} + \frac{1}{T - \Theta}\left(a_{3,j}T + \frac{a_{4,j}}{\Phi + p}\right) \ , \qquad \text{(I.4.42)}$$

$$C^{\circ}_{p,j,n} = c_{1,j} + \frac{c_{2,j}}{(T-\Theta)^2} - \frac{2T}{(T-\Theta)^3}(a_{3,j})(p - p^{\circ}) + a_{4,j}\ln\frac{\Phi + p}{\Phi + p^{\circ}} \ , \qquad \text{(I.4.43)}$$

where Θ = 228 K and Φ = 260 MPa, p° = 0.1 MPa is the reference pressure. The parameters $a_{i,j}$ and $c_{i,j}$ are characteristic parameters for electrolytes, independent of temperature and pressure.

Helgeson and co-workers have intensively analyzed the experimental data for a wide class of electrolytes using HKF approach. Parameters in the HKF equations have now been tabulated for many electrolytes (Tanger and Helgeson, 1988; Shock and

Helgeson, 1988). A computer code for calculating the standard state thermodynamic properties of aqueous electrolytes over a temperature range of 273 to 1000 K and pressures up to 500 MPa according to the HKF model is now available (Johnson *et al.*, 1992). The HKF approach has been widely used in the modelling of geochemical systems and in some industrial applications.

For many aqueous systems, the thermodynamic properties of the solute are only known at T = 298.15 K. For such species, the coefficients in the HKF equations have been estimated through empirical correlations (Shock and Helgeson, 1988). The validity of the HKF model for some of these systems is questionable. Some of its limitations are discussed in the later chapters. For most aqueous electrolyte systems, the properties at high temperature calculated by HKF model are extrapolations based on temperature-dependent data at low temperatures. The extrapolation of $C^{\circ}_{p,2}$ from low temperature to high temperature can be quite successful. For example, Hovey and Tremaine (1986) reported $C^{\circ}_{p,2}(AlCl_3, aq)$ over range 283 K ≤ T ≤ 328 K. The values of $C^{\circ}_{p,2}(AlCl_3, aq)$ at T = 373 K and T = 423 K obtained by extrapolating the experimental data using HKF model were -504.9 $J \cdot K^{-1} \cdot mol^{-1}$ and -739.7 $J \cdot K^{-1} \cdot mol^{-1}$, respectively. Later, Conti *et al.* (1992) reported the experimental values $C^{\circ}_{p,2}(AlCl_3, aq)$ = -490 $J \cdot K^{-1} \cdot mol^{-1}$ and -720 $J \cdot K^{-1} \cdot mol^{-1}$, at T = 373 K and 423 K, respectively. The agreement is within the combined experimental uncertainty.

I.5 Excess Properties

As discussed in Section I.2, apparent molar properties may be expressed in terms of ideal properties and excess properties,

$$Y_{\phi,2} = Y_2^{\circ}(T,p) + Y^{EX}(T,p,m) \; . \tag{I.5.1}$$

In equation (I.5.1), Y_2° is the standard partial molar property, i.e., the property of the solute in the hypothetical 1 molal standard state, and it is only dependent on the nature of the ion-solvent interactions; Y^{EX} is the excess property which is determined by ion-ion interactions in solution. The previous section discussed the standard partial molar properties. This section briefly presents a few statistical mechanical approaches for treating the excess properties of electrolyte solutions in the primitive model.

I.5.1 The Ornstein-Zernike Equation

The Ornstein-Zernike (OZ) equation is an important relation in the statistical mechanics of dense fluids (Lee, 1988). It defines the direct correlation function $c_{ij}(r)$ in terms of the total correlation function $h_{ij}(r)$ through a convolution integral:

$$h_{ij}(r) = c_{ij}(r) + \sum_{k=1}^{s} \rho_k \int h_{ik}(r,r')c_{kj}(r,r')dr' \; , \tag{I.5.2}$$

where ρ_k is the number density of the kth species. Although the direct correlation

function does not have a simple physical meaning, it is always short-ranged and related to the compressibility derivatives $[\partial(\mu/kT)/\partial\rho]_T$ (Lee, 1988).

Various approximate integral equation approaches for treating dense fluids originate in solutions for the OZ equation based on approximate relations between $c_{ij}(r)$ and $h_{ij}(r)$. Normally, three approximations are employed to solve this equation:

(i) the hypernetted chain (HNC) approximation,

$$c_{ij}(r) = g_{ij}(r) - 1 - \ln g_{ij}(r) - \beta u_{ij}(r) \; ; \tag{I.5.3}$$

(ii) the Percus-Yevik (PY) approximation,

$$c_{ij}(r) = g_{ij}(r)\{1 - \exp[\beta u_{ij}(r)]\} \; ; \tag{I.5.4}$$

(iii) the mean spherical approximation (MSA),

$$c_{ij}(r) = -\beta u_{ij}(r) \; ; \; r \geq d_{ij} \; . \tag{I.5.5}$$

Here $\beta = 1/kT$; $g_{ij}(r)$ is the pair correlation function $g_{ij}(r) = h_{ij}(r) - 1$; and $d_{ij} = (d_i + d_j)/2$ where d_i and d_j are the hard spherical diameters of the ith and jth species. The function $u_{ij}(r) = Z_i Z_j e^2/(4\pi\epsilon\epsilon_o r)$ in equations (I.5.3) to (I.5.5) is the electrostatic potential between charged ions i and j.

In the mean spherical approximation, equation (I.5.5) reflects the asymptotic behaviour of the direct correlation function at infinite dilute ($r \to \infty$) at which only binary

interactions contribute to the excess properties of the solution. If a further approximation is made for the total correlation function,

$$h_{ij} = e^{-\beta u_{ij}} - 1 = -\frac{w_{ij}}{kT}, \qquad \text{(I.5.6)}$$

where w_{ij} is the potential of mean force. The traditional Debye-Hückel equation can be derived from the OZ equation.

I.5.2 Debye-Hückel Theory

The derivation of the Debye-Hückel (DH) theory can be found in any standard physical chemistry text, for example Atkins (1990). The two important results from DH theory are the DH limiting law and the Debye screened potential.

For the mean activity coefficients of a single electrolyte solution, the limiting law is

$$\ln\gamma_{\pm} = -|Z_+ Z_-| A_\phi I^{1/2}, \qquad \text{(I.5.7)}$$

where A_ϕ is the Debye-Hückel limiting law (DHLL) slope for activity coefficients and I is the ionic strength. Other excess properties of aqueous electrolyte solutions can be derived from the pressure or temperature derivatives of the DHLL expression for the mean activity coefficient. Essentially, all the excess properties approach zero at a rate

proportional to the square root of the ionic strength.

The difficulty applying the cluster expansion method to ionic systems is that the Mayer-f-integration diverges due to the long-range columbic potential $(Ze)/(4\pi\epsilon_o\epsilon r)$ (Ben-Naim, 1992). This difficulty does not exist in DH theory in which ions are screened by a cloud of the ions of the oppositive charge. The average electric potential experienced by a unit charge at distance r is due to interaction with the central ion i and its cosphere,

$$\psi_i(r) = \frac{Z_i e}{4\pi\epsilon_o\epsilon r} e^{-\kappa r}, \tag{I.5.8}$$

where κ is the inverse Debye length,

$$\kappa^2 = \frac{8\pi e^2}{\epsilon_o\epsilon kT} I. \tag{I.5.9}$$

The screened potential can be also derived from the OZ relation (Lee, 1988). With the approximations given by equations (I.5.5 and I.5.6) , the OZ equation becomes

$$-w_{ij}(r) = \frac{Z_i Z_j e^2}{4\pi\epsilon_o\epsilon r} + \sum_l \beta\rho_l \int dr' \frac{Z_i Z_j e^2}{4\pi\epsilon_o\epsilon r'} w_{lj}(r - r') . \tag{I.5.10}$$

Solving this integral equation, we have

$$w_{ij} = \frac{Z_i Z_j e^2}{4\pi\epsilon_o \epsilon r} e^{-\kappa r} . \qquad \text{(I.5.11)}$$

This result is the same as equation (I.5.8) because $w_{ij}(r) = Z_j e\psi_i(r)$.

It is well known that the Debye-Hückel theory gives correct limiting behaviour for electrolytes at infinite dilution, and that it is also useful at finite but very low concentrations. In practice, it is very difficult to obtain accurate experimental data for aqueous electrolyte solutions with molalities less than 0.1 mol·kg^{-1}. The Debye-Hückel limiting laws are crucially important for extracting standard partial molar properties by providing a means of extrapolating experimental data to infinite dilution. There are still gaps between the highest concentration at which the limiting laws are valid and the lowest concentrations which experimental methods can access. Many attempts have been made to extend the range of the validity of the DH theory. Improvements in the DH theory range from fully empirical to quite fundamental (Desnoyers and Jolicoeur, 1983).

In the original treatment of Debye and Hückel (1923), ions were viewed as point charges. If some distance σ for the closest approach of other ions to the central ion is assumed, the limiting law for the mean activity coefficient is given by

$$\ln\gamma_{\pm} = -\frac{A_{\phi}(Z_{+}Z_{-})I^{1/2}}{1 + \sigma B I^{1/2}} , \qquad \text{(I.6.12)}$$

where $B = 50.29/(\epsilon T)^{1/2}$. If a is assumed to be about 30 nm, $\sigma \cdot B \approx 1$ at T = 298.15 K, .

Thus,

$$\ln\gamma_{\pm} = -\frac{A_{\phi}(Z_{+}Z_{-})I^{1/2}}{1 + I^{1/2}} . \qquad \text{(I.5.13)}$$

This is the limiting term in Guggeheim's equation (Guggenheim and Turgeon, 1955). The excess apparent molar heat capacity and volume corresponding to equation (I.5.13) are (Hovey, 1988)

$$C_{p,\phi,2} - C_{p,2}^{o} = 1.5\frac{|Z_{+}Z_{-}|A_{J}}{I}[I - 2I^{1/2} + 2\ln(1 + I^{1/2})] + B_{J}I , \qquad \text{(I.5.14)}$$

and

$$V_{\phi,2} - V_{2}^{o} = 1.5\frac{|Z_{+}Z_{-}|A_{V}}{I}[I - 2I^{1/2} + 2\ln(1 + I^{1/2})] + B_{V}I , \qquad \text{(I.5.15)}$$

Equations (I.5.13 - I.5.15) extend the range of the validity of the DH theory. The difference between equation (I.5.13) and equation (I.5.7) may be significant at high temperature because the temperature derivatives of $\sigma \cdot BI^{1/2}$ become larger at T >> 298 K.

Another main source of inaccuracy in the DH treatment for extending the limiting law lies in the linearization of the Poisson-Boltzmann equation. Many nonlinear Poisson-

Boltzmann treatments have been reported, and the range of the usefulness of these models is somewhat larger than the DH theory (Desnoyers and Jolicoeur, 1983; Kjellander, 1995). As an example, Outhwaite *et al.* (1991, 1993) formulated a modified Poisson-Boltzmann (MPB) equation. It was found that both structural and thermodynamic properties from the MPB agree well with the results from Monte Carlo simulations for 1:1, 1:2, 3:1, and 2:2 electrolytes in the primitive model. The discrepancies for the pair correlation function only occur at high concentrations for ions with asymmetric valence or large variations in ion size.

I.5.3 Integral Equation Approaches

The most accurate integral equation has been found to be the hypernetted chain (HNC) equation (Desnoyers and Jolicoeur, 1983). However, the HNC equation can only be solved numerically. Although the mean spherical approximation (MSA) does not give accurate structural results, it has been solved analytically for both symmetric and asymmetric electrolytes (Blum, 1975) and it provides useful insights into the solvation of ions (Wei and Blum, 1995) and ion-ion interactions (Blum and Hoye, 1976). Moreover, studies have shown that MSA gives satisfactory predictions for the excess Gibbs free energy for the primitive model (PM). Now we briefly introduce the mean spherical approximation and its application to the aqueous electrolyte systems.

For charged hard spheres of unequal diameters, the pair potential is

$$u_{ij} = Z_i Z_j e^2/(4\pi\epsilon_o \epsilon r)\,, \quad r > d_{ij}\,;$$
$$u_{ij} = \infty\,, \qquad\qquad r < d_{ij}\,, \tag{I.5.16}$$

where $d_{ij} = (d_i + d_j)/2$.

The MSA assumptions are

$$c_{ij}(r) = -\frac{Z_i Z_j e^2}{4\pi\epsilon_o \epsilon k T r}\,, \quad r > d_{ij}\,. \tag{I.5.17}$$

$$g_{ij}(r) = 0\,, \quad r < d_{ij}\,; \tag{I.5.18}$$

Blum (1975) has solved the OZ equation with the above approximation for PM. As in the DH theory, a characteristic length, the shielding parameter Γ, appears in this theory,

$$2\Gamma = a\{\sum_{i=1}^{n} \rho_i [\frac{Z_i - (\pi/2\Delta) d_i^2 P_n}{1 + \Gamma d_i}]\}^{1/2}\,. \tag{I.5.19}$$

The symbols in equation (I.5.19) are defined as follows:

$$P_n = \frac{1}{\Omega} \sum \rho_k d_k z_k/(1 + \Gamma d_k)\,, \tag{I.5.20}$$

$$\Omega = 1 + \frac{\pi}{2\Delta}\sum \rho_k d_k^3/(1+\Gamma d_k)\,, \tag{I.5.21}$$

$$\xi_n = \sum \rho_k (d_k)^n\,,\ n = 0,1,2,3\,, \tag{I.5.22}$$

$$\Delta = 1 - \pi\xi_3/6\ ,\ \alpha^2 = 4\pi\beta e^2/(4\pi\epsilon\epsilon_o)\,. \tag{I.5.23}$$

The degree of equation (I.5.19) depends on the number of ions involved. The numerical solution can be obtained either from the Newton-Raphson formula or by a simple iteration of some estimated initial value of Γ.

A important feature of equation (I.5.19) is that as the size $d_i \to 0$, the term 2Γ approaches κ, the Debye inverse length.

The excess internal energy is given by

$$\Delta E = -\frac{e^2}{4\pi\epsilon_o\epsilon}\{\Gamma\sum_{i=1}^{n}\rho_i Z_i^2/(1+\Gamma d_i) + \frac{\pi}{2\Delta}\Omega P_n^2\}\,. \tag{I.5.24}$$

By using using the thermodynamic relation $[\partial(\beta\Delta A)/\partial\beta)_\rho = \Delta E]$, one obtains the excess free energy ΔA, which satisfies a simple formula,

$$\beta\Delta A = \beta\Delta E + \Gamma^3/(3\pi)\,. \tag{I.5.25}$$

The osmotic coefficient and the excess activity coefficient are given by

$$\phi - 1 = -\frac{\Gamma^3}{3\pi\xi_o} - \frac{\alpha^2}{8\xi_o}\left(\frac{P_n}{\Delta}\right)^2 , \tag{I.5.26}$$

$$\Delta \ln \gamma_{\pm} = \frac{1}{\xi_o}\left[\beta\Delta E - \frac{\alpha_o^2 P_n^2}{8\Delta_o^2}\right] , \tag{I.5.27}$$

which are very similar to the Debye-Hückel formulas (equation I.5.12). The inverse screening length κ is equal to 2Γ in the MSA.

This very simple theory gave surprisingly accurate osmotic coefficients for many monovalent salts in water at T = 298 K (Triolo *et al.*, 1978). It has been demonstrated that the MSA yields excellent representations for the osmotic coefficients and activity coefficients of a wide class of aqueous electrolyte over a large range of temperature at ionic strengths up to 6 mol·kg^{-1}, if only one adjustable parameter, the ionic diameter, is used as a function of density and temperature (Watanasiri *et al.*, 1982; Sun *et al.*, 1994). The activity coefficients and osmotic coefficients of mixtures can be calculated in a predictive manner from the adjustable parameters obtained from solutions of single electrolytes (Lee, 1988; Ball *et al.*, 1985).

I.5.4 The Ion Interaction Model

While the integral equation approaches succeed in describing the thermodynamic and structural properties of aqueous electrolyte solutions, the mathematical calculations for the osmotic coefficients and activity coefficients are cumbersome. The calculations for properties such as apparent molar heat capacity and volume are very much more tedious. During the last two decades, a compact and convenient model, the Pitzer ion-interaction model, has been widely used to interpolate experimental data and to model complex aqueous systems (Pitzer, 1973, 1991).

Pitzer (1973) expanded the excess Gibbs energy of the electrolyte solution in a virial series,

$$\frac{G^{EX}}{RT} = n_w f(I) + \frac{1}{n_w}\sum_{ij} \lambda_{ij}(I) n_i n_j + \frac{1}{n_w}\sum_{ijk} \mu_{ijk} n_i n_j n_k + \cdots , \qquad \text{(I.5.28)}$$

where n_w is the number of moles of solvent; n_i, n_j and n_k are the moles of solutes i, j and k; λ_{ij} and μ_{ijk} are virial coefficients related to binary and ternary ionic interactions; and f(I) is an electrostatic term that converges to the DH limiting law as $I \to 0$.

Comparing the equation above to the following Guggenheim equations (Guggenheim, 1955) for a single electrolyte MX,

$$\frac{G^{EX}}{n_w RT} = -\frac{4}{3} A_\phi I^{3/2} \tau(I^{1/2}) + 2\sum_M \sum_X \beta_{MX} m_M m_X , \qquad \text{(I.5.29)}$$

one observes that the second virial coefficient λ_{ij} in Pitzer equation is expressed as a function of the ionic strength, while β_{MX} in the Guggenheim equations is independent of

$$\tau(x) = (\frac{3}{x^2})[\ln(1+x) - x + (\frac{x^2}{2})] \ , \qquad \text{(I.5.30)}$$

$$\phi - 1 = -(\frac{A_\phi}{3} I^{1/2})\tau(I^{1/2}) + \beta_{MX} m \ , \qquad \text{(I.5.31)}$$

the ionic strength. Pitzer has shown that the ionic-strength dependence of β_{MX} is required to represent experimental osmotic coefficients at T = 298 K up to molalities of 2 mol·kg^{-1}. Furthermore, Pitzer (1973) has also shown that the dependence of the second virial coefficient on the ionic strength could be derived from the exponential DH theory.

The pair distribution function in the DH theory is given by

$$g_{ij}(r) = \exp(-Z_i e\psi_j / kT) \ , \ r > \sigma \ ;$$
$$g_{ij}(r) = 0 \ , \ r < \sigma \ , \qquad \text{(I.5.32)}$$

where $\sigma = d_{ij}$ which is the distance of closest approach between oppositely charged ions.

Pitzer used an expansion of equation (I.5.32) up to the third term:

$$g_{ij}(r) = 1 - \frac{Z_i e\psi_j}{kT} + \frac{1}{2}(\frac{Z_i e\psi_j}{kT})^2 \ . \qquad \text{(I.5.33)}$$

The first two terms on the right side correspond to the linerized DH approximation. The following expression for osmotic coefficient was obtained from equation (I.5.32) through standard statistical mechanical relationships.

$$\phi - 1 = -\frac{\kappa^3}{24\pi\rho(1+\kappa\sigma)} + c\left[\frac{2\pi\sigma^3}{3} + \left(\frac{1}{48\pi\rho}\right)\left(\frac{\kappa^4\sigma}{c^2(1+\kappa\sigma)^2}\right)\right], \qquad \text{(I.5.34)}$$

Here c is molarity, κ is the Debye inverse length, and ρ is the total number density of ions. This equation agrees with Monto Carlo results for concentrations up to I = 0.5 M, to within the computational uncertainty. This equation also fit the experimental data for HBr very well with σ used as an adjustable parameter. It can be seen from equation (I.5.34) that the second virial coefficient is a function of the composition or the ionic strength.

If $\lambda(I)$ is a function of I, the function for the osmotic coefficient corresponding to equation (I.5.28) is different from equation (I.5.31). The expressions for the activity coefficient and osmotic coefficient for a single electrolyte can be derived from the appropriate derivatives of G^{EX}(equation I.5.28),

$$\phi - 1 = |Z_M Z_X| f^{\phi} + m(2\nu_M\nu_X/\nu)B^{\phi}_{MX} + m^2[2(\nu_M\nu_X)^{1/2}/\nu]B^{\phi}_{MX}, \qquad \text{(I.5.35)}$$

and

$$\ln\gamma_{\pm} = |Z_M Z_X| f^{\gamma} + m(2\nu_M\nu_X/\nu)B^{\gamma}_{MX} + m^2[2(\nu_M\nu_X)^{1/2}/\nu]C^{\gamma}_{MX}, \qquad \text{(I.5.36)}$$

where $f^{\phi} = (df/dI - f/I)/2$ and $f^{\gamma} = (df/dI)/2$. The second virial coefficients B^{ϕ}_{MX} and B^{γ}_{MX} in equations are functions of I and $\lambda(I)$ (Pitzer, 1973).

The term f^{ϕ} in equation (I.5.35) has the same form as the first term in equation (I.5.34) derived from the Debye-Hückel radial distribution function, $-A_{\phi}[I^{1/2}/(1 + bI^{1/2})]$. A empirical function B^{ϕ} for the second virial coefficient was used by Pitzer (1973), rather than the one in equation (I.5.34), that is

$$B^{\phi} = \beta^{(0)} - \beta^{(1)}\exp(-\alpha I^{1/2}) \,. \qquad \text{(I.5.37)}$$

where $\beta^{(0)}$, $\beta^{(1)}$ and α are three adjustable parameters for each solute. Pitzer selected equation (I.5.37) for B^{ϕ} because of its simple form and useful limiting properties: (1) finite value at I = 0; (2) rapid change linear in $I^{1/2}$ at low ionic strength; and (3) smooth approach to a limiting value at high I.

Pitzer (1973) found that these equations could be fitted to the experimental osmotic coefficients for eight 1:1 salts and five 2:1 or 1:2 salts at ionic strengths up to 2 $mol \cdot kg^{-1}$ within the experimental uncertainties, with fixed values for a =2.0 $kg^{1/2} \cdot mol^{-1/2}$ and b = 1.2 $kg^{1/2} \cdot mol^{-1/2}$. Other thermodynamic properties can be derived from equation (I.5.41) since the coefficients in each expression are simply related to one another through standard thermodynamic relations. For example, the expressions for partial molar heat capacities and volumes are given by

$$C_{p,\phi,2} = C^{\circ}_{p,2} + \nu|Z_M Z_X|(A_J/2b)\ln(1 + bI^{1/2}) - 2\nu_M\nu_X RT^2[mB'_{MX} + m^2(\nu_M\nu_X)C'_{MX}], \quad \text{(I.5.38)}$$

where

$$A_J = (\partial A_L/\partial T)_p \; ; \; A_L = 4RT^2(\partial A_\phi/\partial T)_p \, . \tag{I.5.39}$$

$$B^J_{MX} = (\partial^2 B_{MX}/\partial T^2)_{pJ} + (2/T)(\partial B_{MX}/\partial T)_{pJ} \, , \tag{I.5.41}$$

and

$$V_{\phi,2} = V_2^\circ + |z_M z_X|(A_V/2b)\ln(1 + bI^{1/2}) + 2\nu_M \nu_X RT[mB^V_{MX} + m^2(\nu_M \nu_X)^{1/2} C^V_{MX}] \, , \tag{I.5.42}$$

$$C^J_{MX} = (\partial^2 C_{MX}/\partial T^2)_p + (2/T)(\partial C_{MX}/\partial T)_p \, , \tag{I.5.40}$$

where

$$A_V = 2A_\phi RT[3(\partial \ln \epsilon/\partial p)_T + (\partial \ln V_w/\partial p)_T] \, , \tag{I.5.43}$$

$$B^V_{MX} = (\partial \beta_{(o)}/\partial p)_T + (\partial \beta^{(1)}/\partial p)_T g(\alpha I^{1/2}) \, , \tag{I.5.44}$$

$$C^V_{MX} = (\partial C_{MX}/\partial p)_T = (\partial C^\phi_{MX}/\partial p)_T/2|z_M z_X|^{1/2} \, . \tag{I.5.45}$$

For a single electrolyte solution with molality less than 1 mol·kg^{-1}, the ternary

interaction parameters C^J and C^V are generally not needed.

The Debye-Hückel parameters A_ϕ, A_J and A_V are calculated from the pVT properties of water given by an EOS (Hill, 1991; Haar *et al.*, 1984) and an expression for the temperature and pressure dependence of the dielectric constant of water (See, for example, Bradley and Pitzer, 1979; Archer and Wang, 1990;, and Helgeson and Kirkham, 1974).

It is well known that there are sharp minima in the plots of $\ln\gamma_\pm$ and ϕ - 1 against molality. This behaviour is largely described by the composition-dependent second virial coefficients B^ϕ_{MX} and B^γ_{MX} in the Pitzer equations. Thus, to fit experimental data at very high concentrations, the Pitzer equations require fewer parameters than other similar approaches (Lietzke and Stoughton, 1962). The other remarkable feature about the Pitzer equation is that the parameters derived from single and binary electrolyte systems can be used with success to predict thermodynamic properties in systems containing many more ionic components.

Pitzer parameters, $\beta^{(0)}$,$\beta^{(1)}$ and C have been compiled for more than 200 single aqueous electrolytes at T = 298 K, and along with the temperature derivatives, $\beta^{(0)L}$, $\beta^{(1)L}$ and C^L for more than 100 electrolytes (Pitzer and Mayorga, 1974a, 1974b). The experimental activity coefficients and osmotic coefficients of these systems can be represented within experimental error for dilute solutions up to ionic strengths of about 6 mol·kg^{-1}. The Pitzer treatment has been used to successfully represent the

thermodynamic properties of systems such as NaCl(aq), KCl(aq), $MgCl_2$(aq), $CaCl_2$(aq), Na_2SO_4(aq), K_2SO_4(aq), $MgSO_4$(aq), HCl(aq) and NaOH(aq), over a wide range of concentration and temperatures (Pitzer, 1989, 1991, 1993; Rogers and Pitzer, 1991; Silvester and Pitzer, 1977). Mixing parameters for many common cation-cation pairs and anion-anion pairs at T = 298 K are also available (Pitzer, 1991; Pitzer and Kim, 1974). As a result, thermodynamic properties now can be expressed in a single unified equation over the whole range of concentration, that is, from infinite dilution to saturation.

I.6 Near Critical Effects and Complications for Dilute Solutions

Apparent molar properties are derived from experimental data for macroscopic properties, such as density and specific heat capacity. They can be divided into two parts: the property at the hypothetical ideal standard state, the so-called standard partial molar property, and a correction term arising from nonideal behaviour caused by solute-solute interactions, the so-called excess property. The theories of conventional solution chemistry are based on the premise that the properties of solutions can be predicted by adding a correction term to the properties of the ideal standard state. This has the advantage that the standard partial molar properties of an electrolyte solution, for example NaCl(aq), can be further divided into contributions from individual ions, Na^+(aq) and Cl^-(aq). Thus the standard partial molar properties of $NaClO_4$(aq) can be calculated through $Y°(NaClO_4, aq) = Y°(NaCl, aq) - Y°(HCl, aq) + Y°(HClO_4, aq)$. Although it is

more difficult to develop a similar additivity rule that applies to the excess properties, parameters in the Pitzer ion-ion interaction model evaluated from single electrolyte data may be used to predict parameters for electrolyte mixtures.

Unfortunately, this procedure cannot be applied to solutions at conditions close to the critical point of water because both the standard partial molar properties and Debye-Hückel limiting slope become divergent under near-critical conditions. It is troublesome to predict a finite value for the property of a solution by making a correction on an infinite value. In the following section, we shall briefly discuss how the standard partial molar properties diverge along different paths approaching the critical point of water.

I.6.1 Dilute Near-Critical Solutions

As demonstrated by Levelt Sengers (1991), the major features of standard partial molar properties near the critical point of water can be explained by the expansion of a classical Helmholtz free energy function.

In the van der Waals theory of critical phenomena for pure fluids, the second and the third derivatives of Helmholtz free energy with respect to volume vanish at the critical point. The basic assumption in the Taylor expansion of a classical Helmholtz free energy is that all the leading terms are nonzero except of $(\partial^2 A/\partial V^2)_{pT}$ and $(\partial^3 A/\partial V^3)_{pT}$. Now we use the partial molar volume as a example to show the divergence and the path-dependence of the divergence as $T \to T_c$ and $x \to 0$.

The partial molar volumes of the solvent $\bar{V}_2$ and the solute $\bar{V}_1$ are defined by

$$\bar{V}_1 = V - x(\partial V/\partial x)_{pT}, \tag{I.6.1}$$

$$\bar{V}_2 = V + (1 - x)(\partial V/\partial x)_{pT}, \tag{I.6.2}$$

where V is the molar volume of the solution, x is the mole fraction of the solute, and $(\partial V/\partial x)_{pT}$ is related to the derivatives of Helmholtz free energy by the following relationship (Levelt Sengers, 1991):

$$(\partial V/\partial x)_{pT} = -(\partial V/\partial p)_{Tx}\cdot(\partial p/\partial x)_{VT} = A_{Vx}/A_{VV}. \tag{I.6.3}$$

In the equation above, A_{Vx} represents $(\partial^2 A/\partial V\partial x)_{pT}$ and A_{VV} represents $(\partial^2 A/\partial V^2)_{pT}$. This notation for the derivatives of A will be used in the following discussion.

Expanding A_{Vx} and A_{VV} at the critical point of the solvent, we have,

$$\left(\frac{\partial V}{\partial x}\right)_{pT} = \frac{-A^c_{Vx}}{A^c_{VVx}x + A^c_{VVT}(\delta T) + A^c_{VVVV}(\delta V)^2/2 + \cdots}, \tag{I.6.4}$$

where the subscript c indicates that the quantities are evaluated at T_c and p_c of the solvent.

On the critical line, $\delta T = 0$ and $(\delta V)^2$ is of higher order than x. It follows from equation (I.6.4) that, for small x,

$$(\partial V/\partial x)_{pT} = -(RT_c/A^c_{Vx})\cdot x^{-1} . \qquad (I.6.5)$$

Thus, $\bar{V}_2$ diverges as x^{-1}, while $\bar{V}_1$ approaches to the value of $V_c + RT_c/A^c_{Vx}$, which is finite but not equal to the critical volume of the solvent.

Along the coexistence curve at $T = T_c$,

$$(\partial V/\partial x)_{pT} = -\{A^c_{Vx}/[A^c_{VVx} + 3(A^c_{Vx})^2/RT_c]\}\cdot x^{-1} . \qquad (I.6.6)$$

So that $\bar{V}_2$ diverges as x^{-1} and $\bar{V}_1$ approaches to the limiting value of

$$\bar{V}_1(x=0) = V_c - A^c_{Vx}/[A^c_{VVx} + 3(A^c_{Vx})^2/RT_c] . \qquad (I.6.7)$$

Again, $\bar{V}_1$ does not equal V_c at the limit of $x = 0$.

Along the critical isotherm-isobar,

$$(\partial V/\partial x)_{pT} = -sign(A^c_{Vx})|2A^c_{Vx}/9A^c_{VVVV}|^{1/3}\cdot x^{-2/3} . \qquad (I.6.8)$$

So that $\bar{V}_2$ diverges as $x^{-2/3}$ and $\bar{V}_1$ is finite, given by

$$\bar{V}_1 = V_c + (-sign A^c_{Vx})|2A^c_{Vx}/9A^c_{VVVV}|^{1/3}\cdot x^{1/3} . \qquad (I.6.9)$$

Thus $\bar{V}_1$ nonlinearily approaches V_c on the critical isotherm-isobar.

The path dependence of $\bar{V}_1$ and $\bar{V}_2$ was first observed by Krichevskii and Makarevich for $\{SF_6 + CO_2\}$ (cited by Rozen, 1976). On moving along the critical curve

toward the critical the point of SF_6, the limiting value of the partial molar volume of SF_6 at $x(CO_2) \to 0$ does not coincide with that of the pure solvent (198 $cm^3 \cdot mol^{-1}$), but actually becomes negative (-230 $cm^3 \cdot mol^{-1}$). On moving to the critical point of SF_6 along the critical isotherm isobar, $\bar{V}_1$ approaches -40 $cm^3 \cdot mol^{-1}$.

I.7.2 The Debye-Hückel Limiting Law Near the Critical Point of the Solvent

Applying the Debye-Hückel limiting law at the critical point of the pure solvent leads to unphysical results (Levelt Sengers *et al.*, 1986). For example, the apparent molar volume diverges not only at the solvent critical point, but also at molality $m > 0$ because the Debye-Hückle limiting slope is

$$A_V = 2A_\phi RT[3(\partial \ln \epsilon / \partial p)_T + (\partial \ln V_w / \partial p)_T] , \qquad \text{(I.6.10)}$$

in which the last term is the isothermal compressibility.

This problem can be avoided by considering A_ϕ is a function of V and T, instead of p and T. At finite molality, we have

$$V_\phi - V^\circ = (\frac{\partial \ln \gamma_\pm}{\partial p})_{Tm} = -3m^{1/2}(\frac{\partial A_\phi}{\partial V})_T(\frac{\partial V}{\partial p})_{Tm} . \qquad \text{(I.6.11)}$$

The factor $(\partial A_\phi / \partial V)_T$ is finite and the last factor $(\partial V / \partial p)_{Tm}$, which is proportional to the compressibility of the solution, diverges only at $m = 0$ and the critical point of the

solvent.

From equation (I.6.11), one can see that the DH effect becomes of secondary importance when the critical point of the solvent is approached, the dominant term along the critical isotherm-isobar being proportional to $(\partial V/\partial p)_{Tm}$ which diverges as $x^{-2/3}$ in the classical theory.

Why do these effect happen? We have a dilemma: infinite dilution and criticality. The criticality of a mixture, $(\partial x/\partial G)_{pT}$, diverges at the critical line but vanishes in the infinite-dilution limit. We cannot transfer the criticality of a mixture to the criticality of the pure solvent by taking the solution towards infinite dilution (Chang *et al.*, 1984). The properties of a dilute solution near the critical point of the solvent are not a perturbation of the state of the pure solvent at the same condition. Thus, many traditional concepts of solution physical chemistry become useless near the critical point of the solvent.

At the critical point of the solvent, the properties of dilute solutions are finite but the standard partial molar properties and partial molar properties may diverge. In order to avoid this mathematical difficulty, one may model the total properties of a dilute solution directly. The Gibbs free energy G(T, p, x), uses T and p as independent variables. It is not an appropriate thermodynamic potential for an equation of state because some of the second derivatives diverge strongly at the critical point of the pure solvent. The appropriate function for this range is the Helmholtz energy with the independent variables T, ρ, and x (Levelt Sengers, 1991; Levelt Sengers *et al.*, 1986). The advantage in using

the Helmholtz energy as the thermodynamic potential is that the second derivatives remain finite (or diverge weakly in the nonclassical description), but the detailed behaviour of the derivatives of A(V, ρ, x) with respect to composition variable as x → 0 or x → 1 is not well known. On the other hand, a binary solution with mole fraction not close to 0 or 1 can be described by G(T, p, x) since the thermodynamic behaviour in this range is essentially the same as the one described by A(T, V) for a pure substance according to Griffith and Wheeler's theory (Griffith and Wheeler, 1970). The nonclassical behaviour can be incorporated into the model based on G(T, p, x).

An equation of state for aqueous NaCl solution formulated on the thermodynamic potential A(T, V, x) was reported by Pitzer and Tanger (Pitzer, 1989). The basic assumption was that the pressure of aqueous NaCl solution could be expressed in the series:

$$p = p(H_2O, T, \rho') + y\{b_{10} + b_{11}(\rho' - 1) + \cdots\} + y^2\{b_{20} + \cdots\} , \qquad \text{(I.6.12)}$$

where ρ' is the reduced density $\{\rho(H_2O)/\rho_c(H_2O)\}$ of water, and y is the mole ratio $n(NaCl)/n(H_2O)$. The Helmholtz energy was obtained by integration with respect to pressure and the addition of the pressure-independent terms: one for ideal mixing and another proportional to the NaCl content. Other thermodynamic properties were obtained by appropriate derivatives of the Helmholtz energy. For example,

$$C_{p,m}(H_2O) = C_{V,m}(H_2O,T,\rho') + yV_c(T/\rho')\{(\rho^2 b_{10}/\rho' T^2) + y(d^2 b_{20}/dT^2) - (\rho' \ln\rho' + 1)(d^2 b_{11}/dT^2)\} + yc(NaCl,T) . \quad \text{(I.6.13)}$$

All the parameters in equations (I.6.12 and 13) depend only on temperature and are analytic functions of temperature. The model reproduces the coexistence curve of NaCl(aq) very well. The apparent molar heat capacities calculated from equation (I.6.13) agree remarkably with the measurements of White *et al.* (1988) along a near-critical path (32.1 MPA) from 600 to 700 K, with all of the features in this range.

Since all the parameters and their derivatives with respect to T are analytic at any reduced density ρ' and temperature T, the critical behaviour of NaCl(aq) is the same as that of pure water at the same temperature and reduced density. No special features for mixtures, or ionic systems have been incorporated into the model.

In summary, the divergences in the apparent molar and partial molar properties of aqueous solutions near the critical point of water are caused by using an inappropriate reference state and selecting inappropriate thermodynamic potentials with T, p as independent variables. The behaviour of dilute solutions near the critical point of water does not add a new feature to the critical phenomena of fluids. The critical phenomena of dilute solutions ought to be understood in terms of concept of universality, within the theoretical framework of Griffith and Wheeler for multi-component systems.

It is worth mentioning that Pitzer (1990) and Levelt Sengers and Given (1993)

have indicated that ionic fluids might have classical critical exponents rather than nonclassical critical exponents due to the nature of the long-range columbic force. The theoretical and experimental investigations on this subject are continuing as an area of active reaearch (Narayanan and Pitzer, 1994, 1995).

Chapter II. Experimental Methods

Apparent molar heat capacities and volumes of aqueous electrolytes are calculated from relative specific heat capacities and densities, which are usually measured with Picker-type flow calorimeters and vibrating-tube densitometers. They can also be obtained from the temperature and pressure dependence of apparent molar enthalpies, activity coefficients, and equilibrium constants through temperature and pressure derivatives. Experimental methods developed during the last two decades to measure these properties have been reviewed in detail by Marsh and O'Hare (1994) and others (Picker *et al*, 1971; Oscarson *et al*, 1988). In this chapter, we discuss the Picker flow microcalorimeter and the vibrating-tube densimeter constructed and used in this work.

II. 1 Picker Flow Microcalorimeter

II.1.1 The Principles of Operation

Since the Picker flow microcalorimeter was first invented (Picker *et al.*, 1971), it has been widely used to determine the heat capacities and heats of mixing of aqueous electrolytes and non-electrolytes near T = 298.15K. It was adapted by Wood's group at the University of Delaware for use under high temperature and pressure conditions (Smith-Magowan and Wood, 1981; White and Wood, 1982). The construction and principles of operation have been described by Picker *et al.* (1971), Desnoyers *et*

al.(1976), Smith-Magowan and Wood (1981), and White and Wood (1982). In this section, we briefly discuss the operating principles, then the setup of the Picker flow microcalorimeter in our laboratory, and finally the calibration procedures.

The design of the Picker microcalorimeter is shown schematically in figure II.1.1. It consists of two symmetrical cells (sample cell and reference cell) that are made of a 1.1 mm o.d. platinum tube to which are connected heaters (Zener diodes) in the up-stream area of each tube and two sensitive temperature sensors in the down-stream area. Assuming there are no heat losses, the heat capacity flux ($\rho F_m c_p$) times the temperature increase (ΔT) is equal to the power input to the cell (W), where ρ is the density of the fluid, F_m is its mass flow rate, and c_p is the specific heat capacity of the fluid. The specific heat capacity in each cell is given by $c_p = W \rho F_m/\Delta T$. Identical temperature increases in both cells can be achieved by changing the ratio of the power delivered to the heaters. Thus, the specific heat capacity $c_{p,1}$ of the fluid in the reference cell is related to $c_{p,2}$ of the fluid in the sample cell through the expression:

$$c_{p,1}/c_{p,2} = W_1 F_{m1} \rho_1/(W_2 F_{m2} \rho_2) , \qquad \text{(II.1.1)}$$

where the subscripts 1 and 2 refer to the sample fluid and the reference fluid, respectively. The two cells are connected in series by a delay line, in which the volumetric flow rates F_{v1} and F_{v2} at the interface between the sample fluid and the reference are assumed to be equal. The mass flow rate F_{m1} of the sample fluid is related to the mass flow rate F_{m2} of

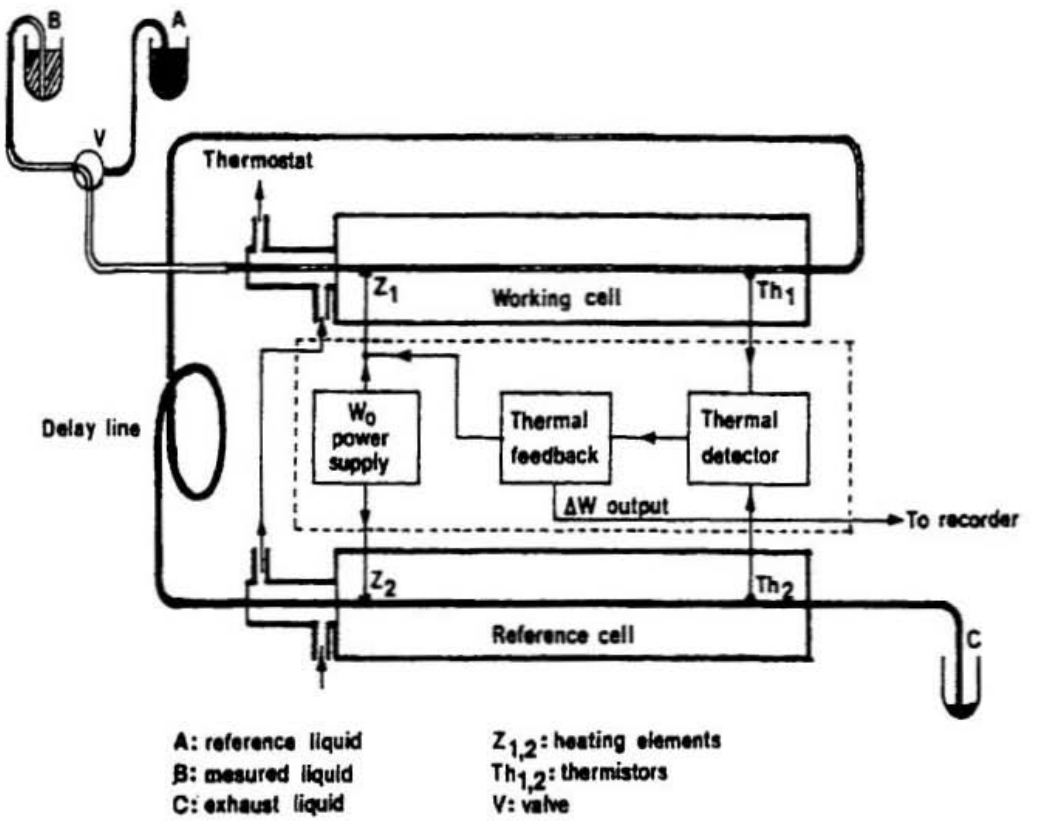


Figure II.1 A schematic diagram of the Picker flow calorimeter

the reference fluid through the expression:

$$F_{m1}/\rho_{1,T_D} = F_{v1} = F_{v2} = F_{m2}/\rho_{2,T_D} , \qquad \text{(II.1.2)}$$

where T_D indicates the temperature of the fluids in the delay line. Combining equations (II.1.1) and (II.1.2), we have

$$c_{p,1}/c_{p,2} = W_1\rho_{2,T_D}/\{W_2\rho_{1,T_D}\} . \qquad \text{(II.1.3)}$$

The electronic circuit was designed in such a way that a constant power (W_o) was supplied equally to both cells and a bias DC voltage, negative or positive, was applied to the heater on sample cell to maintain the temperature of this cell equal to the temperature of the reference cell. If the temperature of the fluids in the delay line is maintained at a value equal to the mean temperature of the fluids in the calorimeter cells. Then,

$$c_{p,2} = \left(\frac{W_o + \Delta W}{W_o}\right)\frac{c_{p,1}\rho_1}{\rho_2} , \qquad \text{(II.1.4)}$$

where ΔW is the extra power delivered to the heater on the sample cell.

The output from the feedback circuit is a DC voltage V that is proportional to the bias power ΔW supplied to the sample cell. The proportionality constant r is determined in the electronic calibration as:

$$r = I_c V_2/V , \qquad \text{(II.1.5)}$$

where I_c is the calibration current and V_2 is the voltage drop across the heater on the sample cell. If the voltage V_1 across the heater on the reference cell, V_2, and the total heating current I_o are measured, W_o is given by

$$W_o = I_o(V_1 + V_2)/4 \,. \qquad \text{(II.1.6)}$$

In practice, the current I_o in equation (II.1.4) and I_c in equation (II.1.3) were determined by measuring the voltages across standard resistors that were connected in series with the heating circuits.

During the measurements, the reference fluid water usually flows through the system from a large reservoir under the influence of gravity, and the solution under investigation introduced into the calorimeter by use of a six-port rotary valve or some other means. Because of the presence of the delay line between the two cells, there is a time interval when the solution is in the sample cell and water is in the reference cell, while the thermal detector unit gives a steady output voltage V. The specific heat capacity of the solution is calculated as

$$c_{p,2} = (1 + \Delta W/W_o)c_{p,1}\,\rho_1/\rho_2 \,. \qquad \text{(II.1.7)}$$

where $\Delta W = rV$.

All of the heat capacity measurements in this work were performed with a Picker flow microcalorimeter (Sodev model CP-C) specially fitted with platinum cells for the

study of severely corrosive solutions. The calorimeter was connected to a Sodev thermal detection unit (model DT-C) that was used for tuning and calibrating the calorimeter and for detecting the output of the differential calorimetric signal. The temperature of the calorimeter was controlled to ± 0.01 K by a Sodev high flow, high stability circulating fluid pump (Model PC-B) and a temperature control unit (Model CT-L). The thermistor (Omega, 44107) used to measure the temperature of the calorimeter was calibrated with a Hewlett-Packard 2804A quartz-crystal thermometer traceable to NBS standards. The differential output V, voltages across the two heaters V_1 and V_2, the heating current I_o, and the resistance of the thermistor were measured by a Hewlett-Packard (HP 3457A) multichannel digital multimeter and were recorded by a computer through a Hewlett-Packard interface card with an HPIB-BASIC program written by the author. It usually took twenty minutes to collect 180 data points for the differential output of the calorimeter and the vibrational period of the densitometer (discussed in the next section) during a single injection of solution. After the signal was recorded, the average values of the parameters in equations (II.1.6) and (II.1.7), as well as temperatures of the calorimeter and the densimeter, were printed out in a table format.

The advantage of the Picker calorimeter over a batch calorimeter is its ability to measure the *relative* specific heat capacity instead of the absolute heat capacity. In measurements with batch calorimeters, the specific heat capacity of the fluid is determined by measuring the temperature change corresponding to a given energy. In

order to obtain the absolute specific heat capacity with the uncertainty less than 0.1 per cent, the temperature measurements in the batch calorimeter need to be accurate to ±0.1 mK, which is very difficult in practice. Problems associated with solvent volatility restrict the use of batch calorimeters for solutions at elevated temperatures.

The detection limit of the relative specific heat capacity ($c_{p,2} - c_{p,1}$) is about 7×10^{-5} $J\cdot K^{-1}\cdot g^{-1}$ if ΔT is set to be 1.6 K. The statistical uncertainty of the relative specific heat capacity was estimated to be 0.5 per cent (Picker *et al.*, 1971, Desnoyers *et al.*, 1976). The major systematic error arises from heat losses (Desnoyers *et al.*, 1976). Equation (II.1.7) is correct if all the applied power serves to increase the temperature of the fluids in the flow cells. In practice, there is a loss of heating power between the heating element and the calorimeter jacket through convection, radiation, and conduction through the leads and the cell walls. Desnoyers *et al.* (1976) recommended that a calibration based on the known specific heat capacity of NaCl(aq) could be used to eliminate the systematic error due to such heat losses. After introducing a heat-loss correction factor f (White *et al.*, 1982), equation II.1.5 is modified to be

$$c_{p,2} = (1 + \Delta W f / W_o) c_{p,1} \rho_1 / \rho_2 \ . \qquad \text{(II.1.8)}$$

The heat-loss correction factor may be determined by a calibration based on the specific heat capacities and densities of NaCl(aq) solutions as in the expression:

$$f = \frac{(c_p \rho)_{std} - c_{p,w} \rho_w}{(c_p \rho)_{expt} - c_{p,w} \rho_w} , \qquad \text{(II.1.9)}$$

where $(c_p\rho)_{expt}$ and $(c_p\rho)_{std}$ are the product of the specific heat capacity and density for the standard NaCl(aq) solution measured in the calibration experiments and that calculated from the literature data (Archer, 1991), respectively. In this work, carefully prepared NaCl(aq) standard solutions with m = 1.0 mol·kg^{-1} were used and the heat-loss correction factors were found to be 1.005 ± 0.005. In other words, the specific heat capacity and the apparent molar heat capacity for a 1 mol·kg^{-1} NaCl(aq) solution determined with the Picker calorimeter used in this work without any correction agree with the specific heat capacity and the apparent molar heat capacity calculated from the equation of state by Archer with a systematic bias of 0.00025 ± 0.00025 J·K^{-1}·g^{-1} and 0.25 ± 0.25 J·K^{-1}·mol^{-1}, respectively.

II.1.2 Absolute Calibration

In order to establish the calibration procedure for the Picker calorimeter in our laboratory, a method for the absolute calibration of flow calorimeters (White and Wood, 1982) was also used to determine the heat-loss correction factor. In this experiment, one high-precision syringe pump was used to supply a constant flow of water (1.2 cm^3·min^{-1}) through the reference cell, delay line, and sample cell. A second high-precision syringe

pump was used to give an extra flow through the reference cell to mimic a difference in the heat capacity of the fluids. Applying equations (II.1.1) and (II.1.8) and noting that the densities and the heat capacities of the fluids in both cells are identical, we have the following expression for the heat-loss correction factor:

$$f = F_b W_o/(F_a \Delta W) \qquad \text{(II.1.8)}$$

where F_a is the mass flow rate from the main pump and F_b is the mass flow rate of the incremental flow that mimics the change in the heat capacity in the sample cell. The results are presented in table A.II.1. The heat-loss correction factors at T = 283.15 K are shown in figure II.2.

As shown in figure II.1.2, the heat-loss correction factor is not dependent on ΔW, because ΔW is usually less than 10 per cent of the main heater power W_o. The average of the heat-loss correction factors obtained in 18 measurements at T = 283.15 K is 1.0030 with standard deviation 0.0028. During the same period of time, chemical calibrations using 0.98858 mol·kg^{-1} NaCl(aq) solution and values of density and specific heat capacity of NaCl(aq) calculated from the equation of state for NaCl(aq) by Archer (1992) were performed. Although the heat-loss correction factor from this chemical calibration (1.0125 ± 0.0042) was larger than that obtained from the absolute calibration, the agreement between them was within the combined error. To check this, we calculated apparent molar heat capacity for 0.99889 molal NaCl(aq) using the heat-loss correction

factor 1.003 obtained from the absolute calibration. The average value 65.42 ± 0.56 $J \cdot K^{-1} \cdot mol^{-1}$ agreed with that calculated from the EOS of Archer (66.77 $J \cdot K^{-1} \cdot mol^{-1}$) within the uncertainty of ± 2 $J \cdot K^{-1} \cdot mol^{-1}$ associated with EOS in this molality range. The average value of the heat-loss correction factors was 1.0060 ± 0.0041 and 1.0026 ± 0.0048 at T = 288.15 K and T = 298.15 K, respectively. These agreed well with the average values 1.0068 ± 0.0088 and 1.0026 ± 0.0064 obtained from the chemical calibrations at T = 288.15 and T = 298.15 K, respectively. In optimizing the parameters in the equation of state for NaCl(aq), Archer used the heat capacity data for NaCl(aq) solutions at temperatures between 278.15 K and 358.15 K measured by batch calorimeters (Tanner and Lamb, 1978). Our results appeared to support the results for NaCl(aq) at T = 298.15 K that Archer (1992) had selected. We notice that the apparent molar heat capacities for NaCl(aq) solution with m = 1 $mol \cdot kg^{-1}$ obtained by Perron *et al.* with earlier models of the Picker calorimeter are systematically higher than those from Archer's equation of state by about 2 $J \cdot K^{-1} \cdot mol^{-1}$ at T = 298.15 K and about 4 $J \cdot K^{-1} \cdot mol^{-1}$ at T = 308.15 K (Archer, 1992).

As a brief conclusion, the heat-loss correction factors obtained from the flow-mimicking calibration agreed with those from the chemical calibration using NaCl(aq) and the values of density and specific heat capacity calculated from EOS of Archer (1992). The chemical calibration can be used routinely to remove the small systematic error caused by the heat power loss in this instrument.

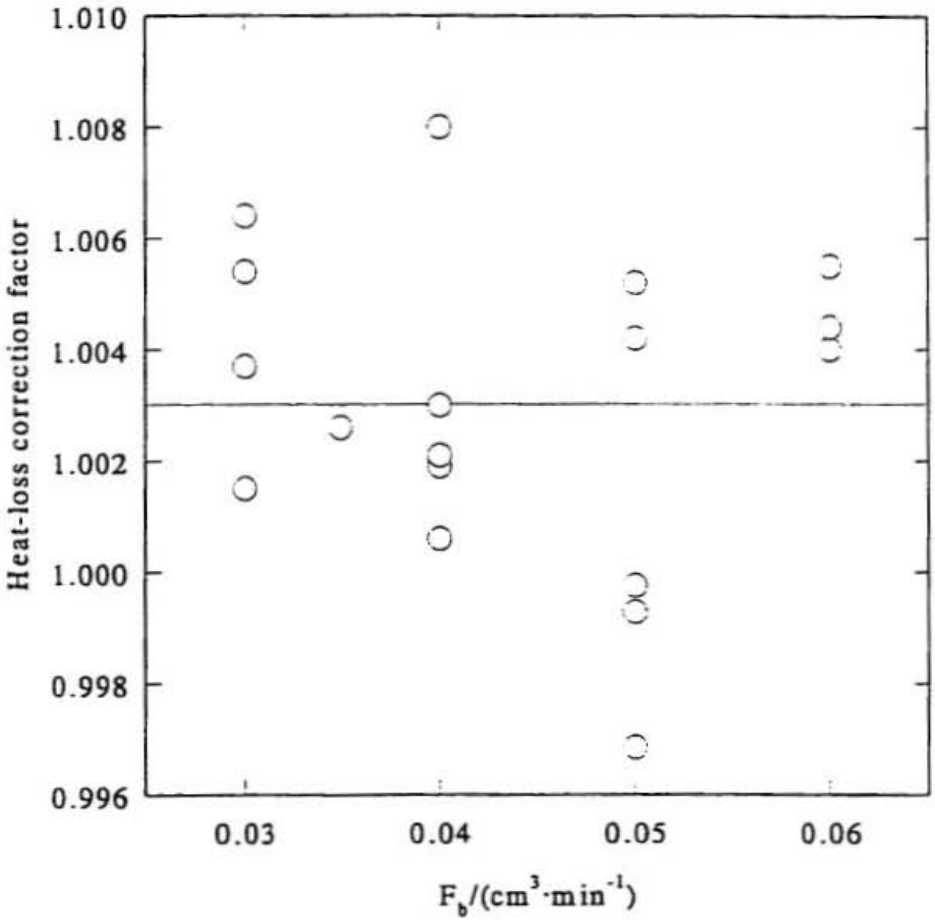


Figure II.2 Heat leak correction factor at T = 283.2 K

II.2 Vibrating Tube Densimeter

Kratky *et al.* (1969) first demonstrated that very precise fluid densities could be obtained by measuring the natural vibrational frequency of tubes containing the fluid under investigation. Picker *et al.* (1974) reported a compact vibrating tube densimeter which operated under flow conditions and allowed fast density measurements with ppm precision. Since then, the two commercial vibrating tube densimeters manufactured by Sodev Inc. and Anton Paar Instruments Ltd. have been widely used in the investigation of the volumetric properties of fluids. The operational temperature of these commercial densimeters is generally less than 423 K. A high-temperature version of the vibrating tube densimeter was constructed by Wood and coworkers (Albert and Wood, 1984, Wood *et al*, 1989, Majer, 1991). Several other high-temperature densimeters have been constructed using variations of the Wood and Paar designs as reported by Corti *et al.* (1990), Simonson *et al.* (1992), and by Xiao *et al.* (1997). In this section, the principle of the vibrating tube densimeter is first discussed and then the Sodev densimeter used in this work for low-temperature measurements is described. The high-temperature densimeters constructed in this project will be presented in the Section II.2.2.

II.2.1 The Principle of the Vibrating Tube Densimeter

The principle of the vibrating tube densimeter was briefly discussed by Albert and

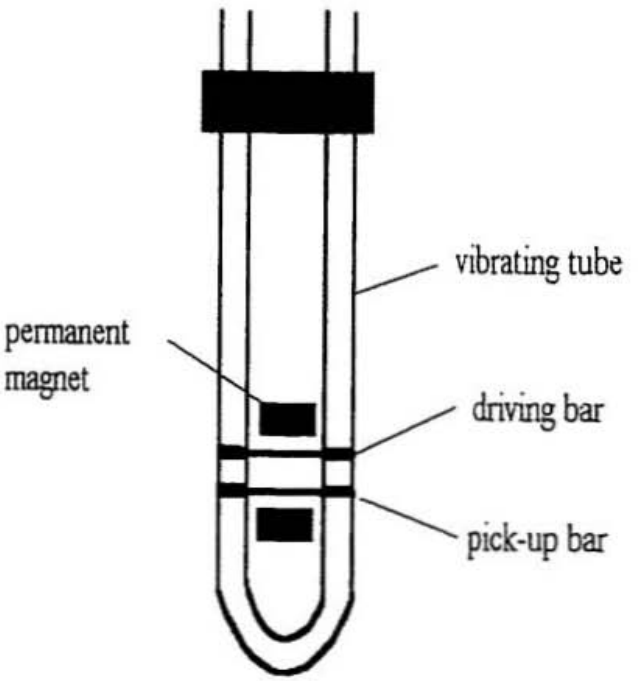


Figure II.3 Schematic diagram of the vibrating tube densimeter

Wood (1984). The essential features of the instrument are shown in figure II.3. The fluid under investigation is placed inside the vibrating tube. The tube is driven to vibrate by the force generated by the interaction between the permanent magnetic field and an alternating current through the metal bar labelled as "driving bar". The other metal bar labelled as "pick-up" serves to sense the vibration. When the tube is set in motion from the static equilibrium position by an initial displacement, and if the elastic force is proportional to the displacement x with a stiffness coefficient k and the vibration is not damped, the differential equation of motion that governs the free vibration of this system is given by

$$m(d^2x/dt^2) + kx = 0 \ , \qquad \text{(II.2.1)}$$

or

$$d^2x/dt^2 + \omega^2 x = 0 \ , \qquad \text{(II.2.2)}$$

where m is the mass of the tube and $\omega = (k/m)^{1/2}$ is the natural frequency of vibration.

For a real system, damping must be considered. If the damping force is proportional to the velocity dx/dt with a positive proportionality coefficient c, the equation of motion is given by

$$m(d^2x/dt^2) + c(dx/dt) + kx = 0 \ , \qquad \text{(II.2.3)}$$

or

$$d^2x/dt^2 + 2\xi\omega(dx/dt) + \omega^2 x = 0 \ , \qquad \text{(II.2.4)}$$

where ξ is equal to $c/(2m\omega)$ and is called the "damping factor" (Shabana, 1992).

The natural frequency $\omega = (k/m)^{1/2}$ is the only quantity needed for calculating the density of the fluid in the tube regardless of whether the vibration is damped or undamped. The density of the fluid inside the tube ρ is related to ω as in following expression

$$\rho = (k/\omega^2 - m)/V_t \ , \qquad \text{(II.2.5)}$$

where V_t is the volume of the vibrating tube. If the natural frequency ω_o for a reference fluid is measured, the relative density $\rho - \rho_o$ is given by

$$\rho - \rho_o = K(1/\omega^2 - 1/\omega_o^2) \ , \qquad \text{(II.2.6)}$$

where ρ_o is the density of the reference fluid. The characteristic constant $K = k/V_t$ can be determined in a calibration run with two fluids of known-density.

We now discuss the forced vibration of the damped system. If a current $i_{drv} = i_o\sin(\omega_f t)$ is supplied to the driving bar, the tube will be driven to vibrate by a periodic force $F(t) = F_o\sin(\omega_f t)$. The differential equation of motion is then given by

$$d^2x/dt^2 + 2\xi\omega(dx/dt) + \omega^2 x = F(t) \ . \qquad \text{(II.2.7)}$$

Solving equation (II.2.7) yields

$$x = x_o \beta Sin(\omega_f t - \psi) , \qquad \text{(II.2.8)}$$

where $x_o = F_o/k$. The magnification factor β and the phase angle ψ are given by

$$\beta = 1/\sqrt{(1 - r^2)^2 + (2r\xi)^2} , \qquad \text{(II.2.9)}$$

and

$$\psi = \tan^{-1}\left(\frac{2r\xi}{1 - r^2}\right) , \qquad \text{(II.2.10)}$$

in which $r = \omega_f/\omega$ is the frequency ratio.

It is clear from equation (II.2.10) that the phase angle must equal $\pi/2$ and does not depend on the damping factor or other characteristic constants of the tube at the resonance condition ($r = 1$). Thus, if the driving force F(t) is exactly $\pi/2$ out of phase with the displacement at certain frequency ω_f, this frequency must equal the natural frequency ω. The resonance condition does *not* correspond to the maximum of the magnification factor β which occurs at $r = (1 - 2\xi^2)^{1/2}$.

As the tube vibrates in the permanent magnetic field, the current i_{ind} induced in the pickup bar is proportional to the velocity of the vibrating tube:

$$i_{ind} \propto dx/dt \propto \cos(\omega_f t - \psi) .$$

At resonance, $i_{ind} \propto \sin(\omega_o t)$ or $\sin(\omega_o t + \pi)$, depending on the polarity of the magnet. This is the basic relationship which governs the design of electronic circuit for the measurement of the natural frequency of the vibrating tube densimeter.

Since at resonance i_{ind} has the same frequency and the same phase angle as i_{drv}, the simplest design of the electronic circuit is to use the amplified pickup signal to drive the tube. At this condition, the natural frequency of the tube is equal to both the frequency of the sinusoid i_{drv} and sinusoid i_{ind} which can be measured with a frequency meter. This design is subject to electronic noise. An improved electronic circuit based on a phase-lock-loop has been reported by Wood *et al.* (1989). It allows reliable density measurements at larger noise levels, which are usually caused by the large heating current of the high-temperature furnace.

II.2.2 The Sodev Flow Densimeter

The prototype of the commercial Sodev densimeter was described by Picker *et al.* (1974). The mechanism to drive the vibrating tube and to sense the vibration is different from the one sketched in figure II.2.1. The mechanical and electronic principles are the same as those discussed in the previous section. The reproducibility of densities measured in the densimeter was estimated to be about 2×10^{-6} g·cm^{-3} if calibrations were performed daily (Picker *et al.*, 1974).

All density measurements in this work at p = 0.1 MPa were performed with a

Picker-type flow densimeter (Sodev model 03-D) connected to a high speed, high stability circulating pump and a temperature control unit (Sodev models PC-B and CT-L). Temperature was monitored by a thermistor placed in the circulating fluid lines. This thermistor was calibrated by the same procedure as that for the calorimeter. Thermistor resistances were measured with a Hewlett-Packard multichannel multimeter (HP 3457A). Time periods were recorded by a Hewlett-Packard universal counter (HP 5328A) with an integration time of 30 seconds. The universal counter was interfaced to a computer through a Hewlett-Packard HP-IB interface. Normally 160 of these 30 second average time periods were collected by the computer for each experimental run. These recorded time periods were averaged over intervals corresponding to the baseline and peak by the computer to give the values for $\tau = 1/\omega$ and $\tau_o = 1/\omega_o$ required in equation (II.2.6). These are printed out in a data table along with the calorimeter results.

The calibration constant K in equation (II.2.6) was determined daily with a standard NaCl(aq) solution (m = 1.0 mol·kg^{-1}). The reference values of the densities for water and the NaCl(aq) solution were calculated from the equation of state of water reported by Hill (1992) and the equation of state of NaCl(aq) reported by Archer (1992). The reproducibility of the calibration constants at four days interval was about ±0.04%.

II.3 High-Temperature Densimeter

II.3.1 Construction and Operation of the High-Temperature Densimeters

A vibrating-tube densimeter was constructed according to the design of Albert and Wood (1984), as modified by Corti and Fernandez-Prini (1990). The densimeter and the flow system for injecting fluids are shown schematically in figure II.4. Briefly, the U-shaped vibrating tube was made from a 304 stainless steel tube or (90% platinum + 10% iridium) alloy tube (2 mm diameter, 0.2 mm wall thickness), silver soldered into two holes set in a cylindrical brass block (5.5 cm in diameter and 20 cm in length), in which a slot (10 cm long, 3 cm wide and 2.75 cm deep) had been machined. Two inconel rods (0.3 mm diameter), mounted on the tube with ceramic adhesive, rested between the poles of a permanent magnet fixed to the brass block, as shown in figure II.4. These were connected to a feedback amplifier via fine silver wires which are attached and insulated by ceramic adhesive where they passed through the block. One of the rods carried the electrical current which drove the vibration of the tube. The other carried the induced current which was measured to sense the frequency of vibration.

The densimeter unit was placed inside a much larger, heavily insulated cylindrical brass block (20 cm outside diameter, 5.5 inner diameter and 30 cm in length) which served as an oven. Heat was provided by two strands of insulated (nickel + chromium) heating wire wound around the brass cylinder in a symmetrical counter-current configuration to minimize electromagnetic inductance. The temperature of the

oven was controlled by an Omega CN2012 temperature controller, and measured by a 100 Ω Platinum RTD located near the outer circumference of the block. The RTD was calibrated to an estimated accuracy of ±0.05 K by measuring the freezing points of tin and lead (supplied by NIST as standard reference materials). The temperature of the densimeter itself was measured by another 100 Ω platinum RTD located as shown in figure II.4. The large thermal mass and well-insulated shell of the brass oven provided stable temperature control. The temperature fluctuation measured by the 100 Ω platinum RTD in the densimeter was less than 0.02 K at T = 573 K.

Immediately before the entrance to the oven, the inlet and outlet ends of the densimeter U-tube passed through a small brass block which served as a preheater. The temperature of the preheater was controlled independently to 0.2 K by an Omega nozzle heater (HBA-103027) and Omega CN76000 PID temperature controller.

The sample injection system consisted of a Constammetric II high pressure liquid chromatographic (h.p.l.c.) pump (LDC/Milton Roy) equipped with a six port h.p.l.c. rotary valve and a 15 cm^3 sample injection loop, heat exchanger and preheater. Fluids were injected into the densimeter cell at a constant mass flow rate which corresponds to a volumetric flow rate from the pump of about 0.032 $cm^3 \cdot s^{-1}$ at T = 298 K. The pressure of the flow system was maintained by a nitrogen cylinder and a back-pressure regulator (Tescom model 26-1700). The system pressure was measured by an Omega PX951 pressure transducer traceable to NIST standards and an Omega DP41-E process

indicator. The RTDs were monitored with a Hewlett Packard 34401A digital voltmeter.

The electronic circuit design originated from the phase-locked loop (PLL) described by Wood *et al.* (1989) It is sketched in figure II.5. Frequencies were measured with a Hewlett Packard 5316 A counter.

II.3.2 The Mechanical Characteristics of the Platinum Alloy Vibrating Tube

The mechanical characteristics of the vibrating tube must be understood to test and fine-tune each vibrating tube densimeter. Because the (90% platinum + 10% iridium) alloy tube is softer than the 304 stainless steel-tube, its damping factor is bigger. To measure the damping factor, the amplitude of the pick-up (point "T.P" in figure II.5) was measured at different frequencies for both the stainless-steel tube densimeter and the platinum-alloy tube densimeter at T = 298.15 K. The frequency response curve for the platinum-alloy tube densimeter is shown in figure II.6. The damping factor for the platinum-alloy tube densimeter was determined to be $\xi = 0.0055$ by means of the bandwidth method (Shabana, 1992) from the frequency response curve figure II.6, while a similar frequency response curve yielded $\xi = 0.001$ for the stainless steel-tube densimeter.

The phase angle ψ behaviour from equation (II.2.10) is shown in figure II.7. Clearly, the phase angle curve near resonance for the stainless-steel tube densimeter is much steeper than that for the platinum alloy-tube densimeter. Thus, in order to

accurately determine the resonance frequency for the platinum alloy-tube densimeter, special care was needed in the tuning of the phase-lock-loop to ensure the phase angle between the pick-up signal and driving signal was exactly π.

II.3.3 The Bubble Point of Water at T = 574 K

The period and the amplitude of the vibrating tube are so sensitive that the vibrating tube densimeter can be used to determine the bubble point of the fluid inside (Crovetto and Wood, 1991). Since the saturation pressure and temperature of water is known very precisely, the bubble point can be used to check the accuracy of the temperature and pressure measurements in the working instrument.

The bubble point of water at T = 574 K was measured with the stainless-steel tube densimeter. In this measurement, the flow rate of water was maintained at 0.2 $cm^3 \cdot min^{-1}$ and the pressure of the system was gradually reduced from a value slightly higher than the saturation pressure of water. The temperature and the pressure of the densimeter and the densities calculated from the vibrational period are presented in figure II.8. Clearly, a significant density drop occurred at p = 8.68 MPa and a recorded temperature of 573.83 K. Considering the uncertainties in the pressure and temperature measurements, the bubble point pressure and temperature were estimated to be 8.68 ±0.01 MPa and 573.83 ± 0.05 K, respectively. The saturation temperature at p = 8.68 ±0.01 MPa calculated from the equation of state of Hill (1990) is 573.94 ± 0.11 K. These values agree with the

measured bubble point temperature and pressure within the estimated experimental uncertainties. Additionally, the steam densities obtained in this experiment agreed with the densities calculated from the EOS of Hill (1990) to within the experimental uncertainty of $\pm 0.2\ kg \cdot m^{-3}$.

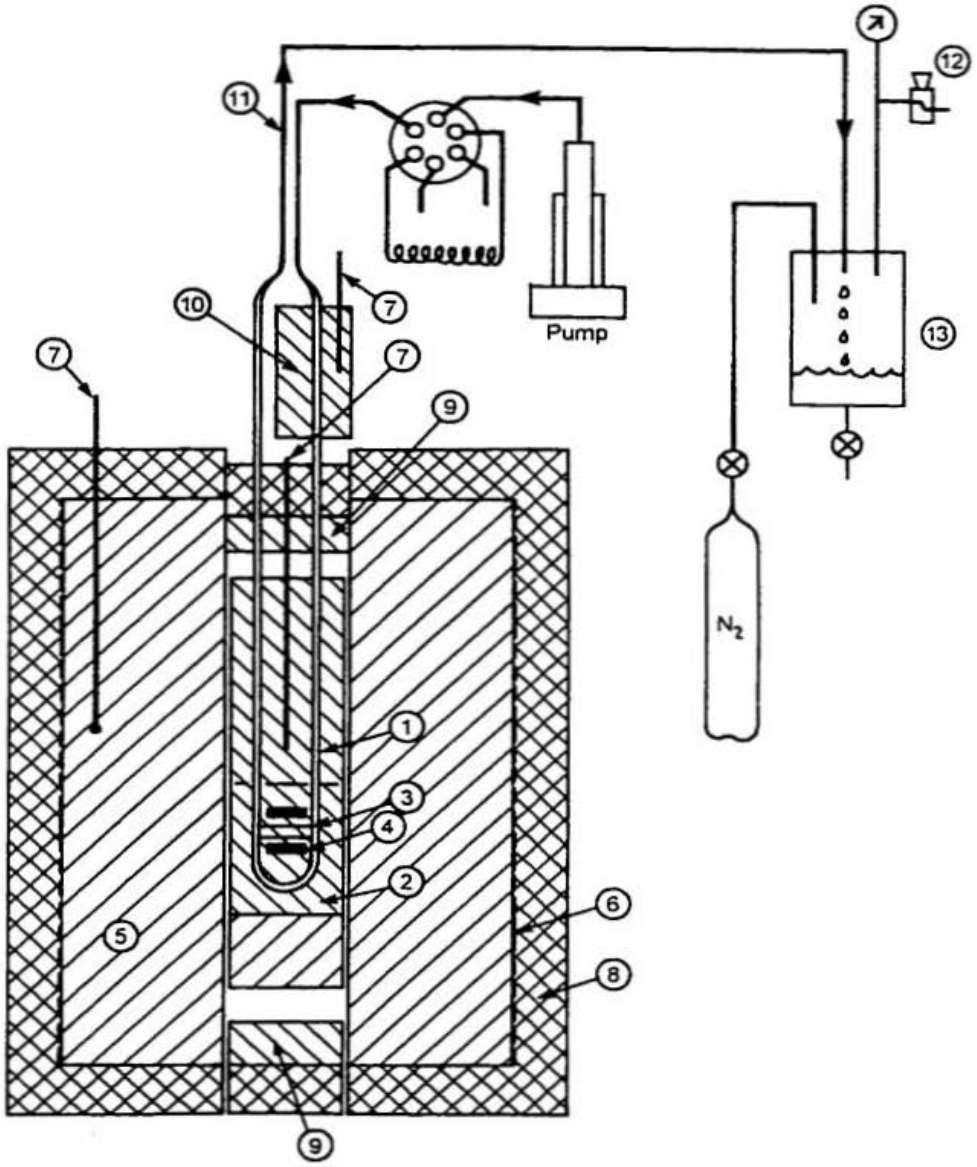


Figure II.4 Vibrating tube densimeter and sample injection system. 1, U-shaped vibrating tube; 2, densimeter cell body; 3, Inconel rods for sensing and driver current; 4, permanent magnet; 5, brass oven; 6, insulated wire; 7, RTD; 8, thermal insulator; 9, brass heat shield; 10, brass pre-heater; 11, heat exchanger; 12, back-pressure regulator; 13, receiver vessel.

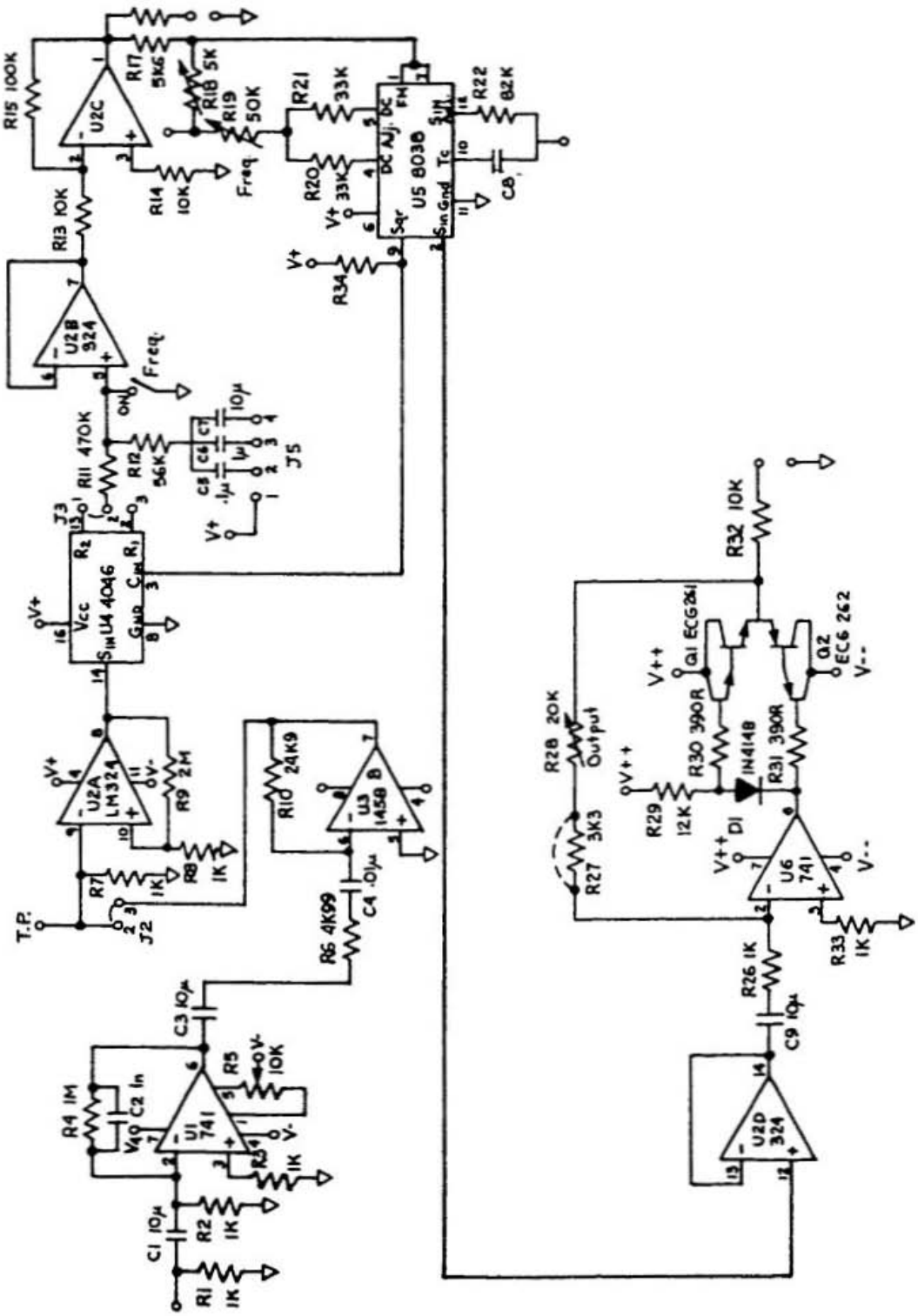


Figure II.5. Electric circuit for measuring the resonance frequency of the vibrating-tube

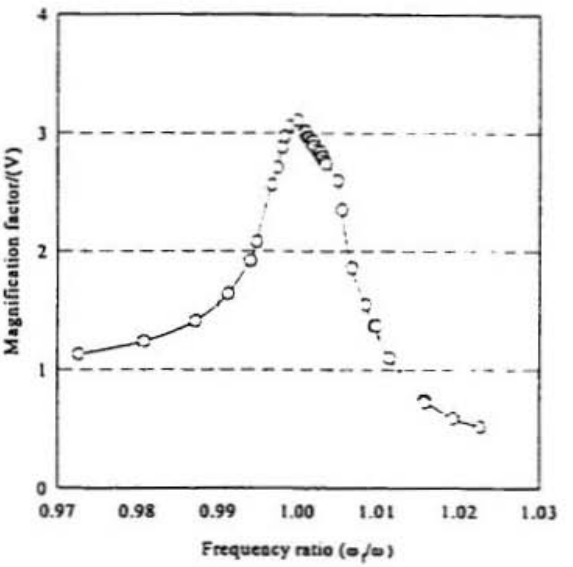


Figure II.6 Frequency response curve

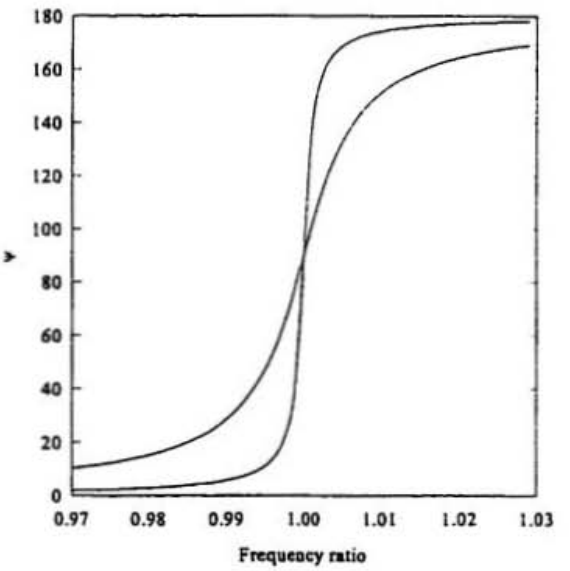


Figure II.7 Phase angle against frequency ratio

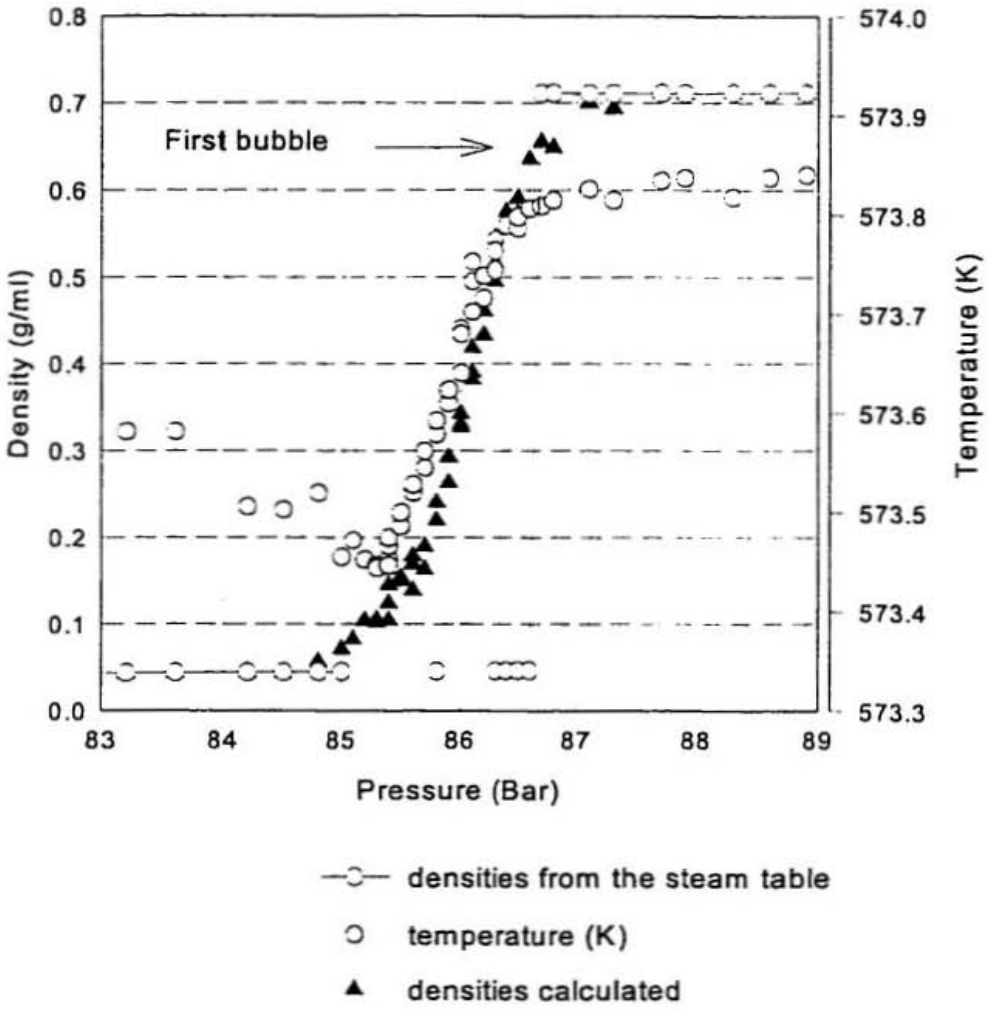


Figure II.8 Bubble point of water at T = 474 K

Part Two. Thermodynamics of Aqueous Trivalent Lanthanide Cations

Chapter III. Apparent Molar Volumes and Heat Capacities of Aqueous Sodium Trifluoromethanesulfonate and Aqueous Trifluoromethanesulfonic Acid at Temperatures from 283 K to 600 K and Pressures up to 20 MPa.

III.1 Introduction

Trifluoromethanesulfonic acid HCF_3SO_3(aq) is one of the strongest monobasic acids known (Lawrance, 1986). Its conjugate base $CF_3SO_3^-$(aq) is similar to the perchlorate anion in that it is considered to be a very poor ligand for most metal cations. Trifluoromethanesulfonate ("triflate") salts have extremely high thermal stability and are resistant to both reductive and oxidative cleavage (Leonard and Swaddle, 1975). They have been used as an alternative to perchlorates for hydrothermal experiments requiring noncomplexing and non-oxidizing anions. For example, Palmer and Drummond (1988) used sodium triflate as an inert supporting electrolyte in thermodynamic studies of hydrolysis and metal complexation at high temperatures. Except for the electrical conductances for $NaCF_3SO_3$(aq) (Ho and Palmer, 1995) and the apparent molar volumes for $Gd(CF_3SO_3)_3$(aq) and $La(CF_3SO_3)_3$(aq) (Xiao *et al.*, 1996), no other thermodynamic properties for triflates have been reported. In order to interpret our experimental results for lanthanide triflates, values for thermodynamic properties of the triflate anion are needed. In this chapter, we report apparent molar volumes for $NaCF_3SO_3$(aq) from 283 K to 600 K and pressures up to 20 MPa, and apparent molar volumes for HCF_3SO_3(aq) at

0.1 MPa and at temperatures between 283 K and 328 K.

III.2 Experimental Section

The stock solution of trifluoromethanesulfonic (triflic) acid was prepared from trifluoromethanesulfonic acid (Alfa, 99 per cent). The concentration of the stock solution was determined by titration against tri(hydroxymethyl)aminomethane (TRIS) using methyl red as indicator. Solid sodium triflate was obtained by neutralizing triflic acid (Alfa, 99 per cent) with NaOH solution (40 per cent). The salt was recrystallized twice from water, digested for one week, then filtered, and dried at 120 °C to constant weight. The stock solution of sodium triflate was prepared from the purified salt. More dilute solutions were prepared by diluting the stock solution with water by mass.

Ultrapure NaCl(cr) (Alfa, 99.99 per cent) that had been dried at 200 °C for 20 hours was used to prepare the sodium chloride solutions needed for the calibration of the densimeter. D_2O was supplied and analysed by Atomic Energy of Canada Ltd. (mass fraction 0.9952 of D_2O, mass fraction 0.0048 of H_2O).

The relative specific heat capacities and the relative densities of $NaCF_3SO_3(aq)$ and $HCF_3SO_3(aq)$ at 0.1 MPa were measured in the Sodev CP-C flow microcalorimeter and the Sodev 03D vibrating flow densimeter equipped with platinum cells. The temperature of the calorimeter and the densimeter were controlled to ±0.01 K by a Sodev CT-L circulating bath. The thermistors (Omega, 44107) used to measure the temperature

of the calorimeter and the densimeter were calibrated with a Hewlett-Packard 2804A quartz-crystal thermometer traceable to NIST standards. Pure water and a standard solution of NaCl(aq) (2.1536 mol·kg^{-1}) were used to calibrate the densimeter and to determine the heat-loss correction factor for the calorimeter.

Densities of $NaCF_3SO_3$(aq) at pressures other than 0.1 MPa were measured in the high-temperature platinum vibrating tube densimeter in which the U-shaped vibrating tube (2 mm diameter, 0.2 mm wall thickness) was made from a (90% platinum +10% iridium) alloy. The structure of the densimeter system is the same as described in chapter II, except for the differences described below. The sample injection system consisted of a Constammetric II high pressure liquid chromatographic (HPLC) pump (LDC/Milton Roy) equipped with a two-position six-port valve and a 15 cm^3 sample injection loop which was made from 3.2 mm o.d. PEEK tubing (Upchurch Scientific). The sample in the loop was loaded by a filling syringe and pre-pressurized to the system pressure by a second HPLC pump before being pushed into the densimeter. Water delivered by the HPLC pump at flow rate of 0.016 cm^3·s^{-1}could be directed through the six-port valve into the densimeter to act as a reference fluid, or it could be directed into the sample loop to force the sample into the densimeter. The 100 Ω platinum RTD that was used to measure the temperature of the densimeter was calibrated to an estimated accuracy of ±0.02 K by measuring the ice point of water and the freezing points of tin and lead (supplied by NIST as standard reference materials). An NaCl(aq) solution with m = 2.1536 mol·kg^{-1} was

used to calibrate the densimeter at all conditions except for T = 600.45 K and T = 374.77 K, at which a more concentrated NaCl(aq) solution (m = 4.3477 mol·kg^{-1}) was used.

III.3 Results

The density of fluids in the vibrating tube densimeter was determined from the expression

$$\rho = \rho_i^* + K(\tau - \tau_w) , \qquad \text{(III.3.1)}$$

where ρ and ρ_i^* are the densities of the fluid and the reference fluid (water), respectively; τ and τ_w are the resonance periods for the fluid and water, respectively; and K is a characteristic constant determined by calibration with the reference fluids water and NaCl(aq) solution (equation II.2.6). The densities of water were obtained from the equation of state reported by Hill (1990) while the densities of the standard NaCl(aq) solutions were obtained from the equation of state reported by Archer (1992).

Apparent molar volumes $V_{\phi,2}$ and apparent molar heat capacities $C_{p,\phi,2}$ were calculated from densities and specific heat capacities according to the usual definitions

$$V_{\phi,2} = 1000(\rho_i^* - \rho)/(m\rho\rho_i^*) + M/\rho , \qquad \text{(III.3.2)}$$

$$C_{p,\phi,2} = c_p M + (c_p - c_{p,1}^*)/m \ , \qquad \text{(III.3.3)}$$

where m is the molality, M is molar mass (150.0795 g·mol^{-1} for HCF_3SO_3, and 172.0602 g·mol^{-1} for $NaCF_3SO_3$), and c_p and $c_{p,1}^*$ are the specific heat capacities of solution and water, respectively. The experimentally determined relative densities (ρ - ρ_1^*) and apparent molar volumes are listed in Table A.III.1 for HCF_3SO_3(aq) and Table A.III.2 for $NaCF_3SO_3$(aq). The experimental values of $\{(c_p \cdot \rho / c_{p,1}^* \cdot \rho_1^*) - 1\}$ and apparent molar heat capacities are presented in Table A.III.3 for HCF_3SO_3(aq) and Table A.III.4 for $NaCF_3SO_3$(aq).

III.3.1 Low-Temperature Results

The Pitzer ion-interaction equation (Pitzer, 1991) for a 1-1 electrolyte was used to represent the concentration dependence of $V_{\phi,2}$ and $C_{p,\phi,2}$:

$$V_{\phi,2} = V_2^o + 2A_v \ln(1 + b\sqrt{I})/b + 2RTm[\beta^{(o)V} + 2\beta^{(1)V} f(I)] + C^V m^2 \ , \qquad \text{(III.3.4)}$$

$$C_{p,\phi,2} = C_{p,2}^o + 2A_J \ln(1 + b\sqrt{I})/b - 2RT^2 m[\beta^{(o)J} + 2\beta^{(1)J} f(I)] + C^J m^2 \ , \qquad \text{(III.3.5)}$$

where V_2^o and $C_{p,2}^o$ are the standard partial molar volume and the standard partial molar heat capacity, respectively; A_v and A_j are the Debye-Hückel limiting slopes evaluated using the dielectric constant of water compiled by Archer and Wang (1990) and the equation of state of water by Hill (1990); and b = 1.2 $kg^{1/2}$·$mol^{-1/2}$. In equations (III.3.4) and (III.3.5), T is the temperature, R = 8.314 J·K^{-1}·mol^{-1}; $\beta^{(o)V}$, $\beta^{(1)V}$, $\beta^{(o)J}$,and $\beta^{(1)J}$ are fitting parameters, and the function f(I) is given by

$$f(I) = \{1 - (1 + \alpha\sqrt{I})\exp(-\alpha\sqrt{I})\}/(\alpha^2 I)\,, \qquad \text{(III.3.6)}$$

where α = 2.0 $kg^{1/2}$·$mol^{-1/2}$ and I is the ionic strength. The ternary interaction parameters C^V and C^J in equations (III.3.4) and (III.3.5) are needed only for HCF_3SO_3(aq) solutions at the molalities up to 8.1 mol·kg^{-1}.

Equation (III.3.4) was fitted to the apparent molar volumes of HCF_3SO_3(aq) at each temperature by the method of least squares. The resulting values of V_2^o, $\beta^{(o)V}$ and $\beta^{(1)V}$ are presented in Table III.1. The calculated values for $V_{\phi,2}$ after subtracting the Debye-Hückel limiting law (DHLL) term are shown in figure III.1. Equation (III.3.5) was fitted to the apparent molar heat capacities of HCF_3SO_3(aq) and those of $NaCF_3SO_3$(aq) at each experimental temperature. Weights proportional to the solution molality were used in the least squares fitting for $NaCF_3SO_3$(aq). The results from these fittings are presented in Tables III.2 and III.3, and illustrated in figures III.2 and III.3.

Table III.1. Standard partial molar volumes V_2°; virial coefficients $\beta^{(0)V}$, $\beta^{(1)V}$, and C^V in equation (III.3.4) for HCF_3SO_3(aq) at p = 0.10 MPa.

T/K	V_2°	$10^4 \cdot \beta^{(0)V}$	$10^4 \cdot \beta^{(1)V}$	C^V
	$cm^3 \cdot mol^{-1}$	$kg \cdot mol^{-1} \cdot MPa^{-1}$	$kg \cdot mol^{-1} \cdot MPa^{-1}$	$kg^2 \cdot cm^3 \cdot mol^{-3}$
283.2	73.92	-1.570	2.647	0.06055
298.2	75.83	-1.256	0.4032	0.04664
313.2	77.24	-0.9612	-0.4706	
328.2	78.11	-1.876	5.458	0.07074

Table III.2. Standard partial molar heat capacities $C_{p,2}^\circ$; virial coefficients $\beta^{(0)J}$, $\beta^{(1)J}$, and C^J in equation (III.3.5) for HCF_3SO_3(aq) at p = 0.10 MPa.

T/K	$C_{p,2}^\circ$	$10^5 \cdot \beta^{(0)J}$	$10^5 \cdot \beta^{(1)J}$	C^J
	$J \cdot K^{-1} \cdot mol^{-1}$	$kg \cdot mol^{-1} \cdot K^{-2}$	$kg \cdot mol^{-1} \cdot K^{-2}$	$J \cdot kg \cdot K^{-1} \cdot mol^{-3}$
283.2	133.7	1.124	-4.098	0.8202
298.2	159.0	1.232	-1.799	0.9725
313.2	166.3	0.7996	-0.2536	
328.2	162.8	1.127	-1.800	1.093

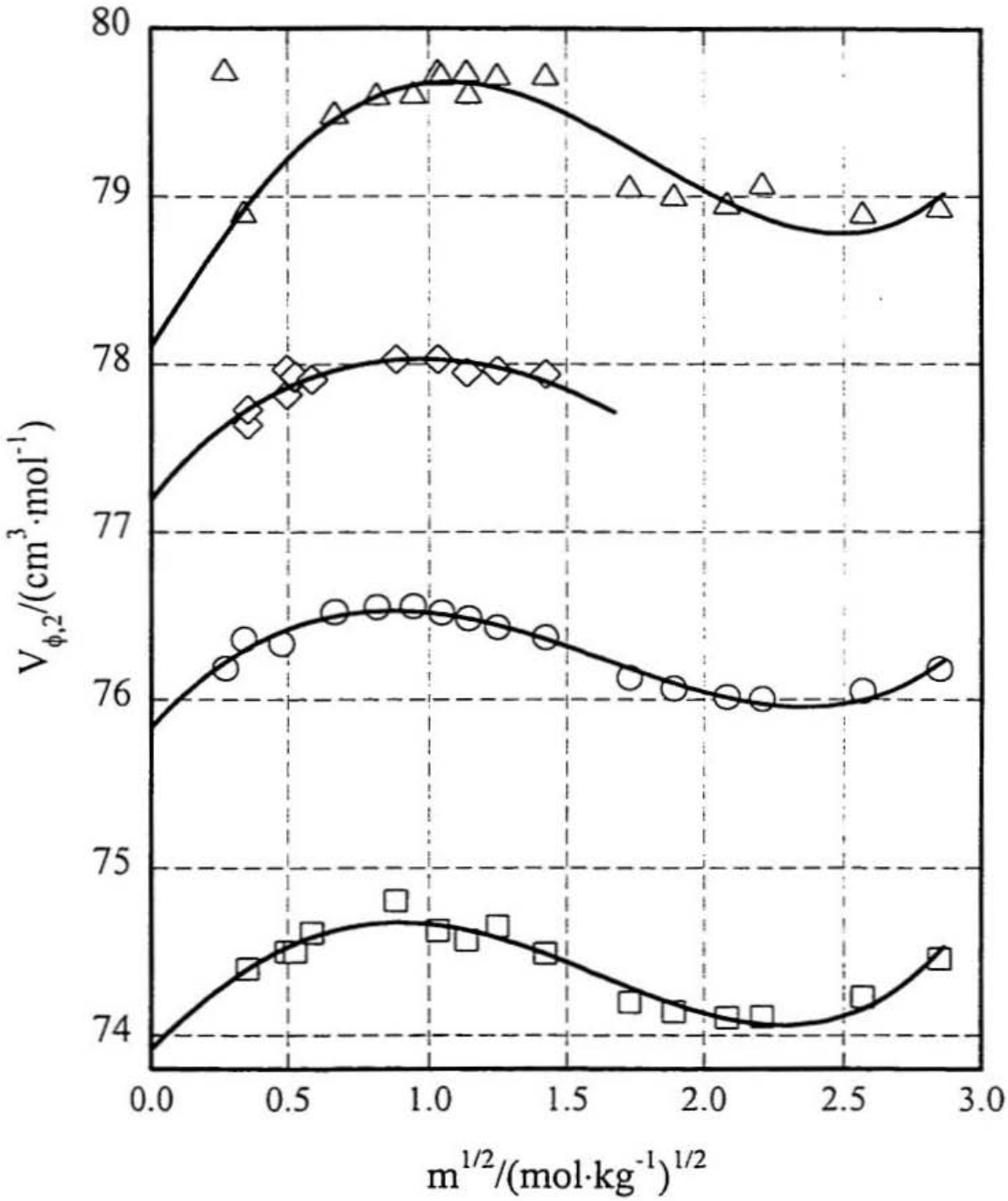


Figure III.1 Plots of $V_{\phi,2}(HCF_3SO_3, aq)$ against the square root of molality: □, T = 283.2 K; ○, T = 298.2 K; ◇, T = 313.2 K; Δ, T = 328.2 K; Lines, the least square fits to equation (III.3.4)

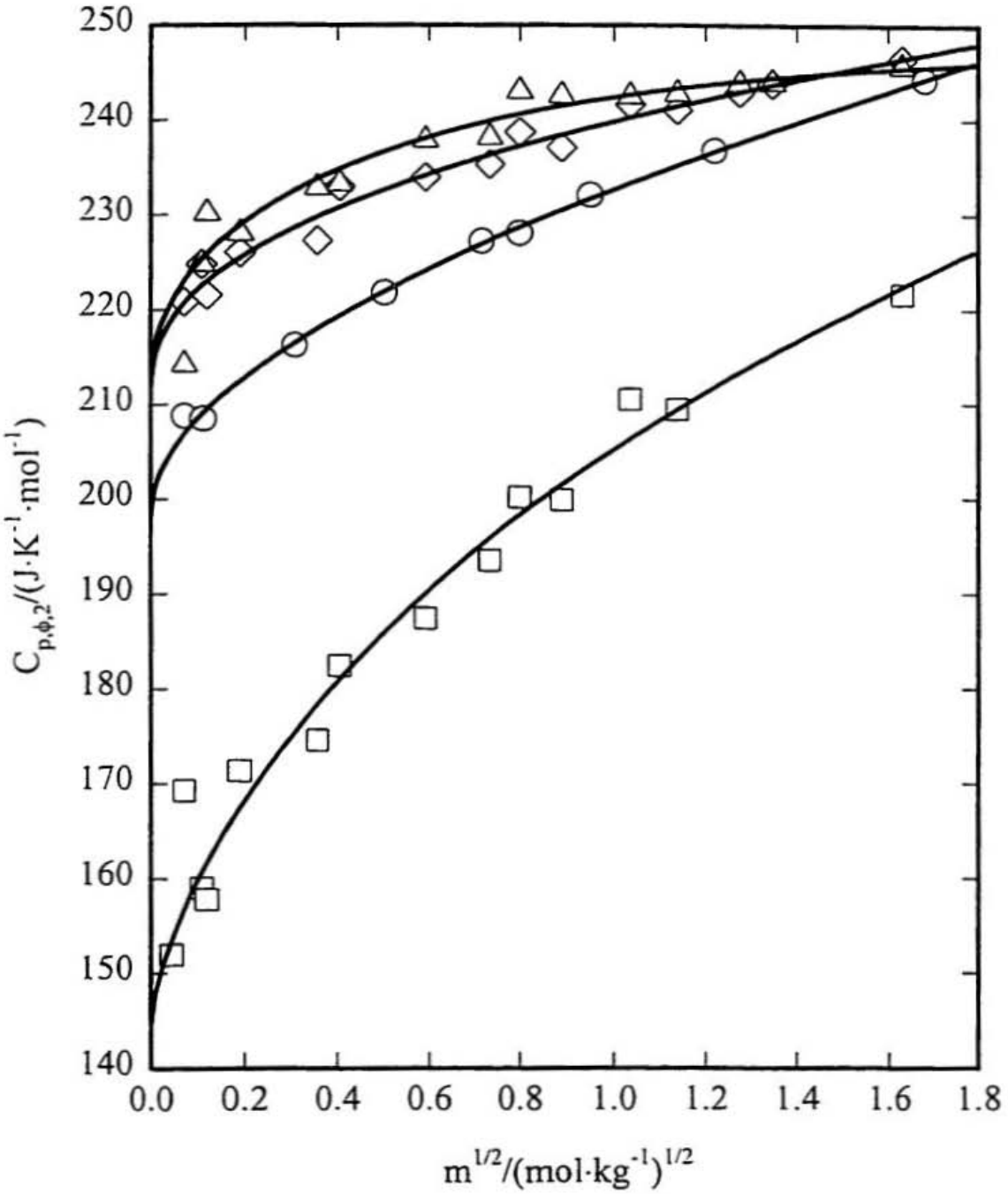


Figure III.2 Plots of $C_{p,\phi,2}(NaCF_3SO_3, aq)$ against the square root of molality: ○, T = 283.2 K; □, T = 298.2 K; Δ, T = 313.2 K; ◇, T = 328.2 K; Lines, the least square fits to equation (III.3.5)

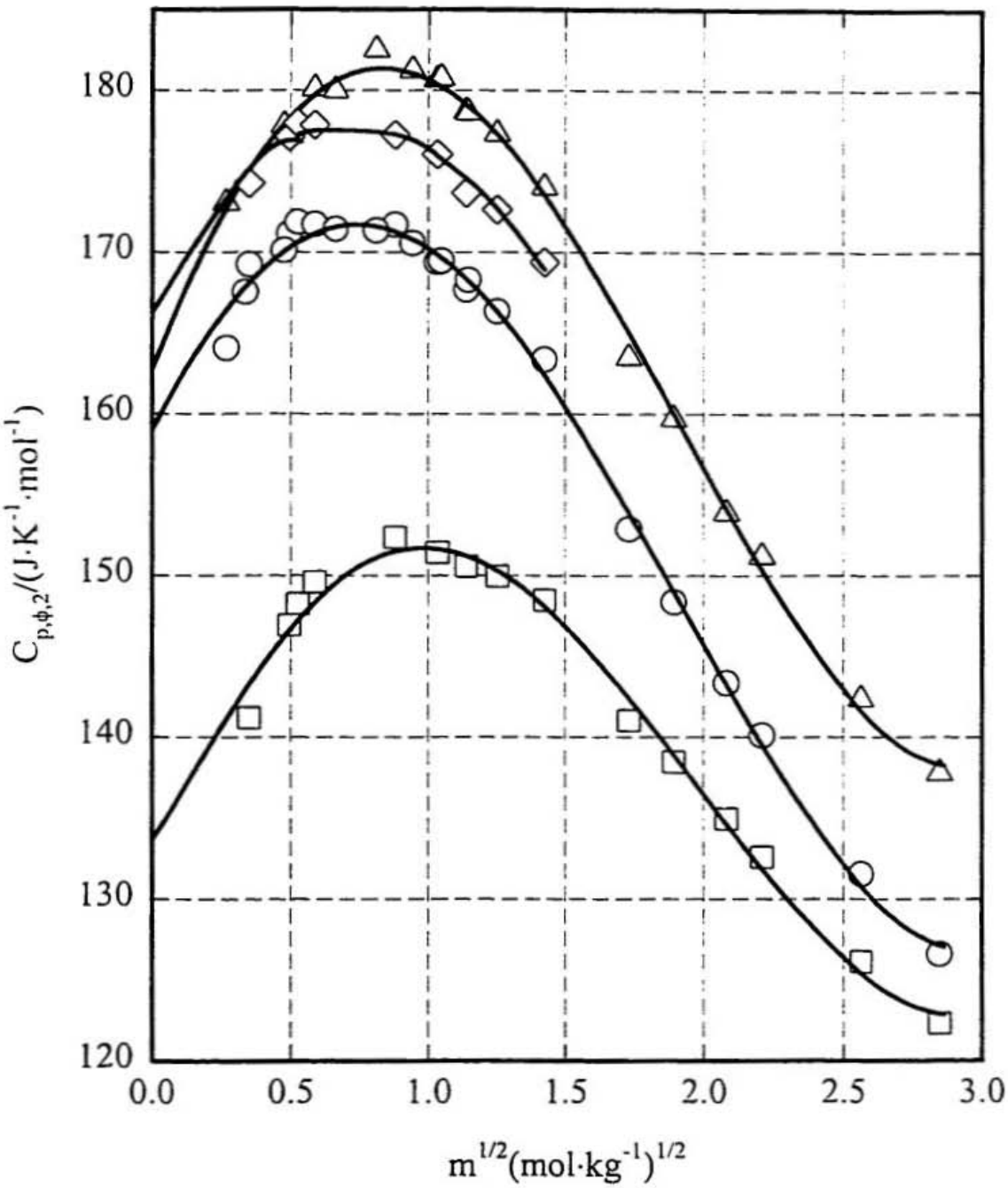


Figure III.3 Plots of $C_{p,\phi,2}(HCF_3SO_3, aq)$ against the square root of molality: ○, T = 283.2 K; □, T = 298.2 K; ◇, T = 313.2 K; Δ, T = 328.2 K; Lines, the least square fits to equation (III.3.5)

III.3.2 High-Temperature Results

The Pitzer theory does not consider the temperature dependence of V_2^o, $\beta^{(o)V}$ and $\beta^{(1)V}$. For many electrolytes, the steep increase in V_2^o as the temperature increases from 273 K to about 373 K can be described by a function of the form $\{a_1 + a_2/(T - 228)\}$ with two adjustable parameters a_1 and a_2 (Helgeson and Kirkham, 1976). It has been demonstrated by Anderson *et al.* (1991), Simonson et al. (1994), and Tremaine *et al.* (1996) that the compressibility coefficient of the solvent water $\beta_1^* = -(1/V)(\partial V/\partial p)_T$ is a good independent variable to formulate simple empirical equations to represent the behaviour of V_2^o with at elevated temperatures.

The values for $V_2^o(NaCF_3SO_3, aq)$ at temperatures between 283 K and 373 K, obtained by fitting equation (III.3.3) to the isothermal-isobaric data, are shown in figure III.4 as a function of 1/(T - 228). Clearly, a two-parameter term $\{a_1 + a_2/(T - 228)\}$ can be used to represent V_2^o well within the experimental uncertainty. In the high temperature region (T > 475 K), the data for V_2^o at different pressures follow a nearly linear dependence on $T \cdot \beta_1^*$, as shown in figure III.5. It was also found that $\beta^{(o)V}$ and $\beta^{(1)V}$ display behaviour similar to V_2^o at high temperature. As a result, the following empirical expressions were used to represent the temperature and pressure dependencies of V_2^o, $\beta^{(o)V}$ and $\beta^{(1)V}$:

$$\beta^{(o)V} = a_1 + a_2\beta_1^* + a_3 T\beta_1^*, \qquad \text{(III.3.7)}$$

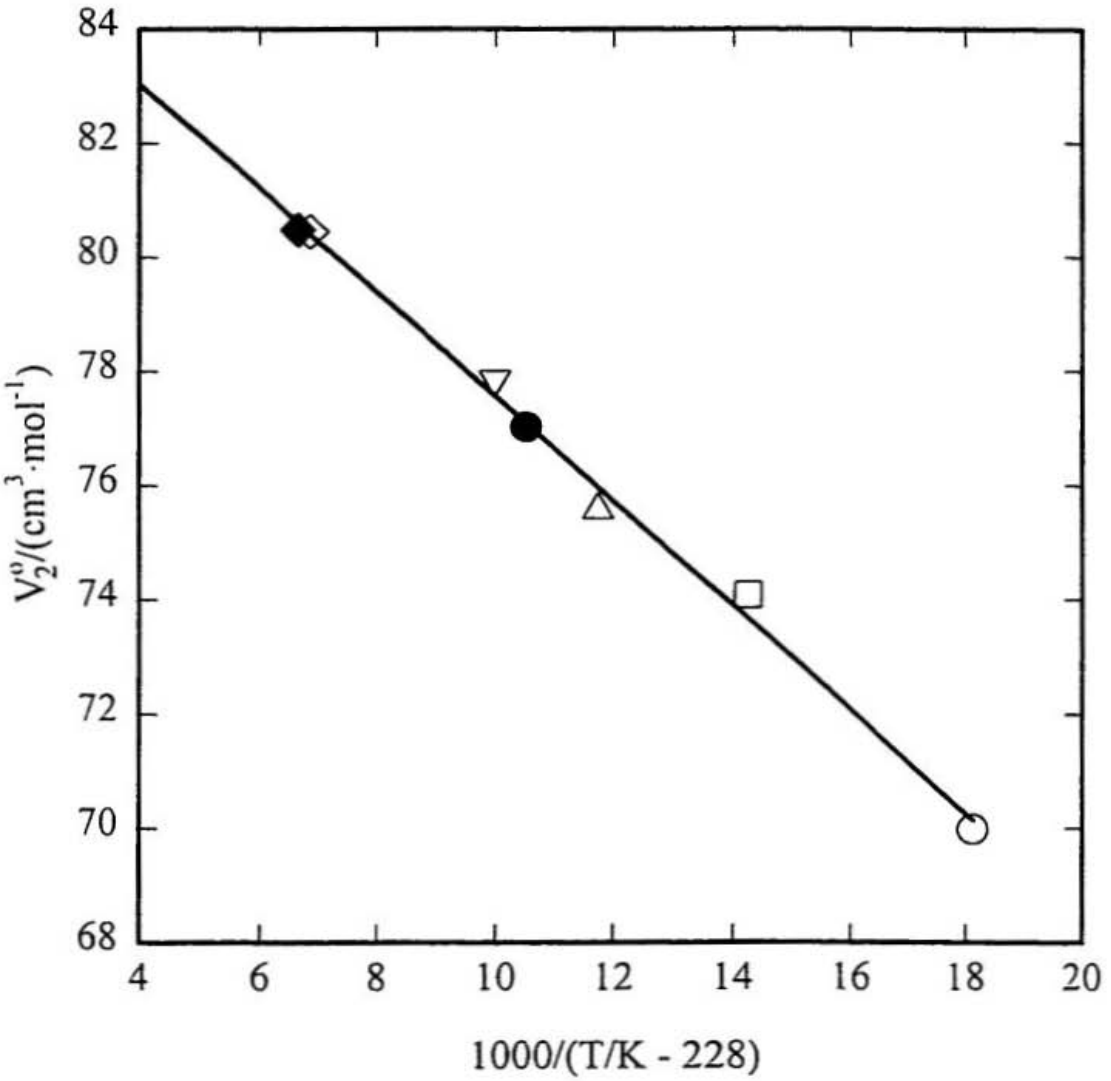


Figure III.4 $V_2^{\circ}(NaCF_3SO_3, aq)$ at temperatures between 283.15 K and 373.15 K plotted against 1000/(T - 228): ○, 283.15 K, 0.1 MPa; □, 298.15, 0.1 MPa; Δ, 313.15 K, 0.1 MPa; ●, 323.05 K, 10.60 MPa; ▽, 328.15 K, 0.1 MPa; ◇, 373.12 K, 0.50 MPa; ◆, 374.77 K, 10.01 MPa.

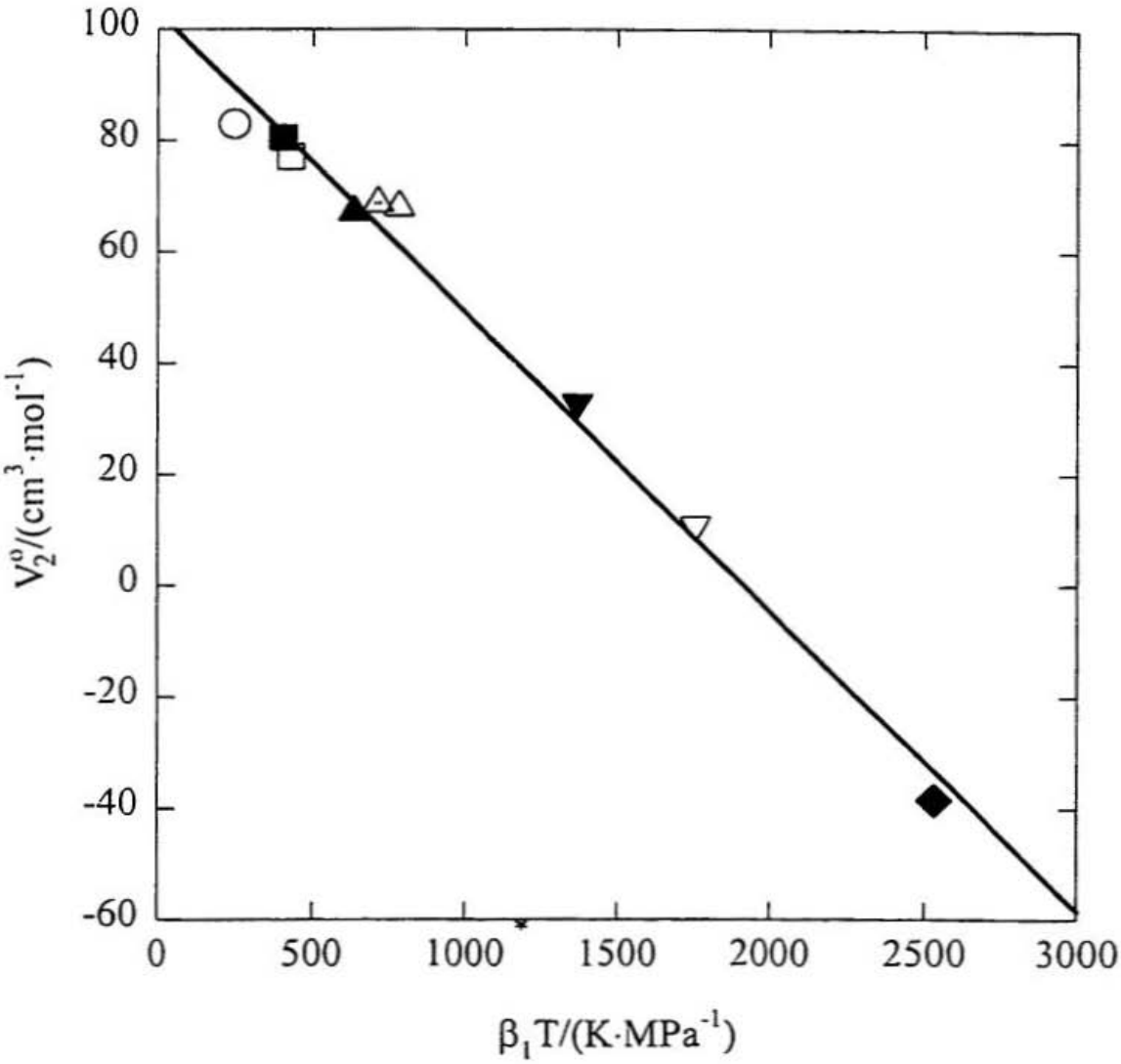


Figure III.5 $V_2^o(NaCF_3SO_3, aq)$ at temperatures between 423.65 K and 600.48 K plotted against $T\beta_1^*$: ○, 422.65 K, 10.20 MPa; ■, 475.93 K, 10.18 MPa; □, 476.05 K, 2.13 MPa; ▲, 523.57 K, 20.40 MPa; Δ, 523.55 K, 10.15 MPa; Δ, 524.85 K, 4.56 MPa; ▽, 573.39 K, 10.13 MPa; ▼, 573.32 K, 19.87 MPa; ◆, 600.48, 20.2 MPa.

$$\beta^{(1)V} = a_4 + a_5/T + a_6 T + a_7 \beta_1^* + a_8 T^2 \beta_1^* , \qquad \text{(III.3.8)}$$

$$V_2^o = a_9 + a_{10}/(T - 228) + a_{11} T + a_{12} \beta_1^* + a_{13} T \beta_1^* . \qquad \text{(III.3.9)}$$

Equations (III.3.7 to III.3.9) were fitted to the experimental data at all temperatures, pressures and molalities by the method of least squares with weights proportional to the solution molality, except for data at T = 600.48 K for which a weighting factor 0.2·m was assigned. The fitted parameters a_i to a_{13} in equations (III.3.7 to III.3.9) are listed in table III.4. Plots of the fitted results for ($V_{\phi,2}$ - DHLL) against molality are compared with the experimental data in figures III.6 to III.8. The values for V_2^o at saturation pressure p = p_{sat}, and p = 20.0 MPa are listed in Table III.5 at rounded temperatures and molalities . The deviations between the calculated and the observed values of $V_{\phi,2}$ are shown in figure III.9.

III.4 Discussion

III.4.1 Experimental Uncertainties

The errors associated with density measurements in a vibrating-tube densimeter have been discussed by Majer *et al.* (1991), Corti *et al.* (1990) and Oakes *et al.* (1995).

Table III.3. Standard partial molar heat capacities $C^{\circ}_{p,2}$; virial coefficients $\beta^{(0)J}$ and $\beta^{(1)J}$ in equation (III.3.5) for $NaCF_3SO_3(aq)$.

T/K	$C^{\circ}_{p,2}$	$10^6 \cdot \beta^{(0)J}$	$10^6 \cdot \beta^{(1)J}$
	$J \cdot K^{-1} \cdot mol^{-1}$	$kg \cdot mol^{-1} \cdot K^{-2}$	$kg \cdot mol^{-1} \cdot K^{-2}$
283.2	144.5	-8.363	-84.99
298.2	198.1	-6.836	-7.950
313.2	211.9	-2.256	-0.1500
328.2	210.2	4.245	-23.60

Table III.4. Parameters for $NaCF_3SO_3(aq)$ in equations (III.3.7) - (III.3.9).

Parameter	For $\beta^{(0)V}$	Parameter	For $\beta^{(1)V}$	Parameter	For V°
a_1	-1.11410×10^{-3}	a_4	-2.12439×10^{-2}	a_9	48.6573
a_2	5.06841	a_5	5.08354	a_{10}	-1.21195
a_3	-8.41287×10^{-3}	a_6	4.09029×10^{-5}	a_{11}	7.77104×10^{-2}
		a_7	-21.4177	a_{12}	1.13856×10^{5}
		a_8	4.80441×10^{-5}	a_{13}	-2.41696×10^{2}

Table III.5. Calculated apparent molar volumes $V_{\phi,2}$ ($cm^3 \cdot mol^{-1}$) for $NaCF_3SO_3(aq)$.

	m/(mol·kg^{-1})							
T/K	0.0	0.10	0.25	0.50	0.75	1.00	1.30	1.60
				$p = p_{sat}$ [a]				
283.15	70.40	70.88	71.16	71.52	71.82	72.11	72.43	72.74
298.15	73.46	74.05	74.39	74.76	75.02	75.24	75.46	75.65
323.15	76.83	77.59	77.98	78.35	78.56	78.11	78.82	78.88
373.15	80.91	82.08	82.61	83.04	83.25	83.35	83.38	83.35
423.15	82.51	84.47	85.28	85.95	86.30	86.50	86.62	86.65
473.15	80.04	83.67	85.07	86.26	86.97	87.45	87.86	88.15
523.15	66.79	74.68	77.52	79.95	81.49	82.63	83.72	84.61
573.15	10.79	34.80	43.22	50.41	54.97	58.41	61.72	64.46
598.15	-89.39	-34.31	-14.49	2.52				
				P = 20.0 MPa				
473.15	80.12	83.60	85.16	86.51	87.26	87.71	88.02	88.16
523.15	69.99	76.97	79.87	82.41	83.92	84.94	85.77	86.33
573.15	31.27	49.34	56.39	62.49	66.22	68.84	71.14	72.85
598.15	-30.94	5.66	19.72	31.86				

[a] Saturation pressure for $T \geq 373.15$ K and 0.10 MPa for $T < 373.15$ K.

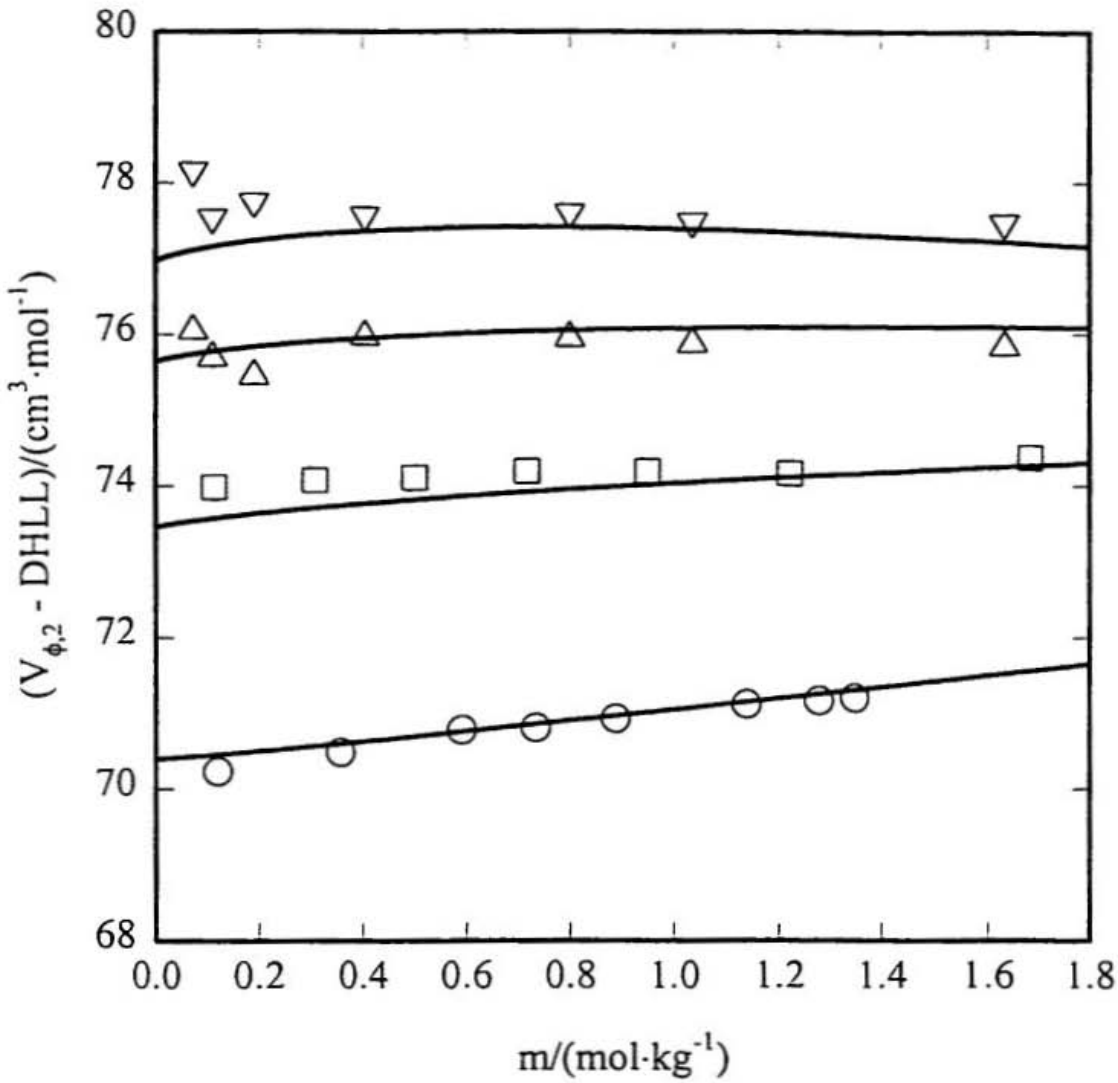


Figure III.6 $V_{\phi,2}(NaCF_3SO_3, aq)$ at 0.1 MPa minus the Debye-Hückel limiting slope term according to equation (III..3.4) plotted against molality: ○, 283.15 K; □, 298.15; Δ, 313.15 K; ▽, 328.15 K.

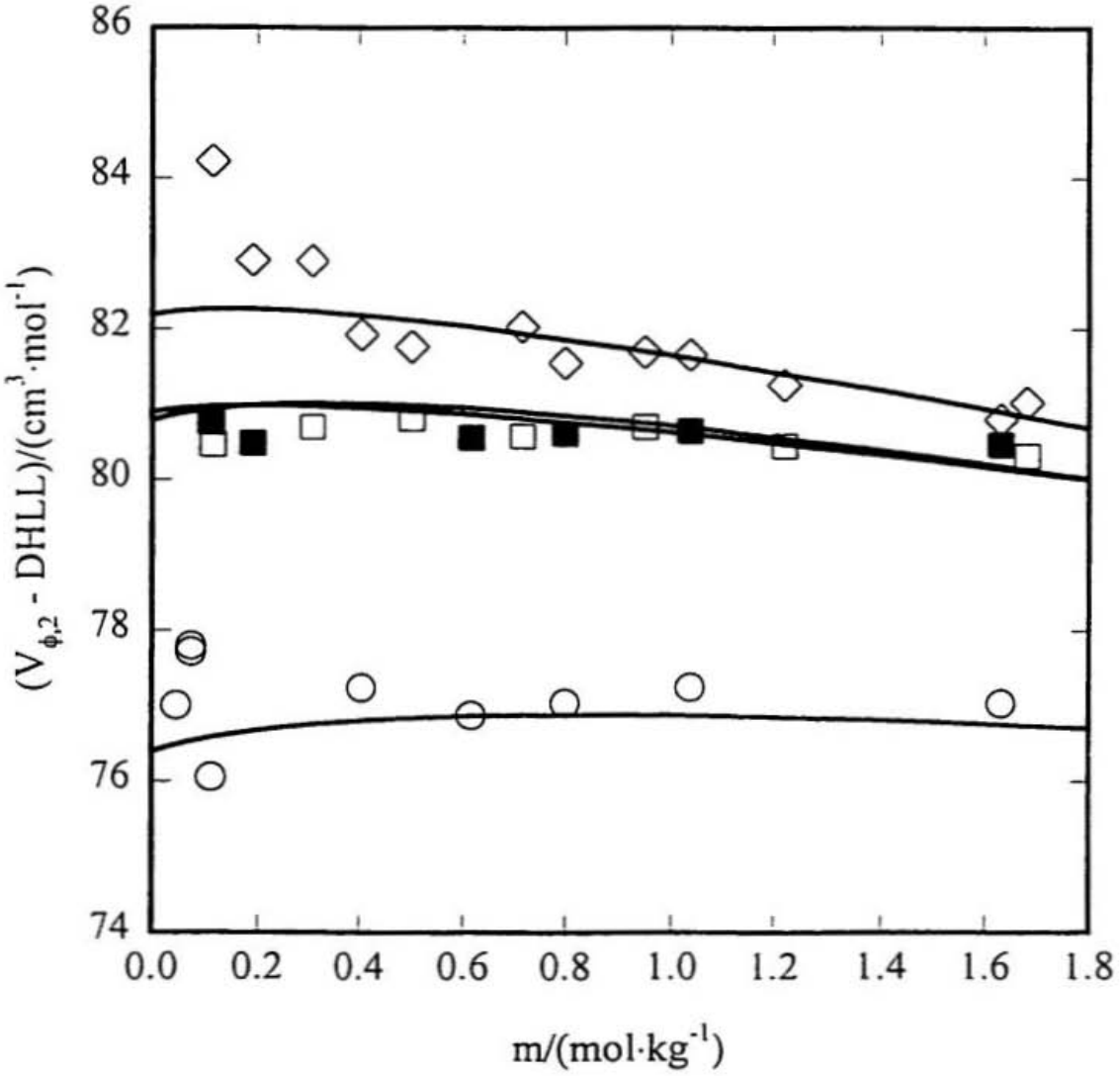


Figure III.7 $V_{\phi,2}(NaCF_3SO_3, aq)$ minus the Debye-Hückel limiting slope term according to equation (III.3.4) plotted against molality: ○, 323.05 K, 10.60 MPa; □, 373.12, 0.50 MPa; ■, 374.77 K, 10.01 MPa; ◇, 422.65 K, 10.20 MPa.

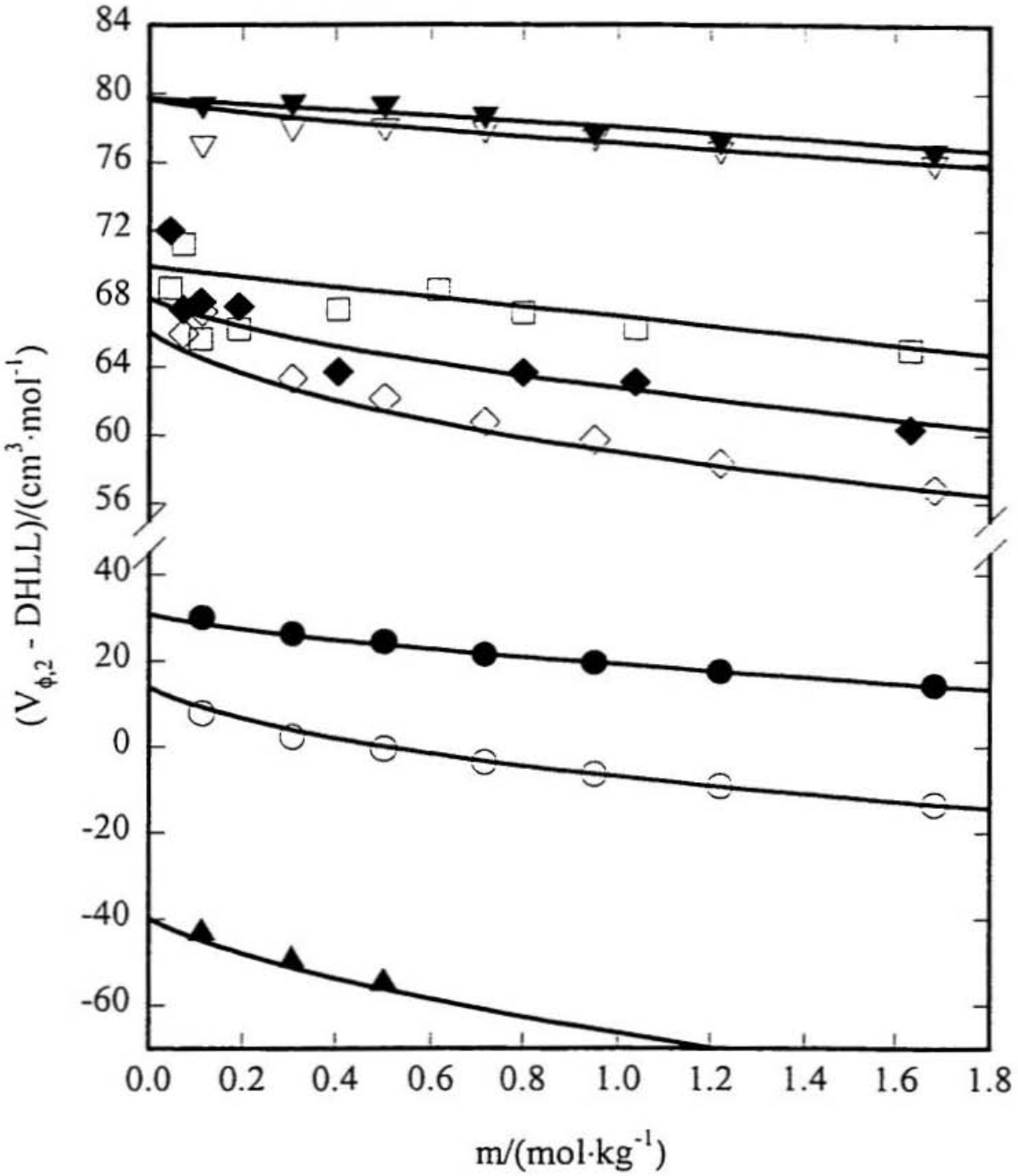


Figure III.8 $V_{\phi,2}(NaCF_3SO_3, aq)$ minus the Debye-Hückel limiting slope term according to equation (III.3.4) plotted against molality: ▲, 600.48 K, 20.20 MPa; ○, 573.39 K, 10.13 MPa; ●, 573.32 K, 19.87 MPa; ◇, 524.85 K, 4.56 MPa; ◆, 523.55 K, 10.15 MPa; □, 523.57 K, 20.40 MPa; ▽, 476.05 K, 2.13MPa; ▼, 475.93 K, 10.18 MPa.

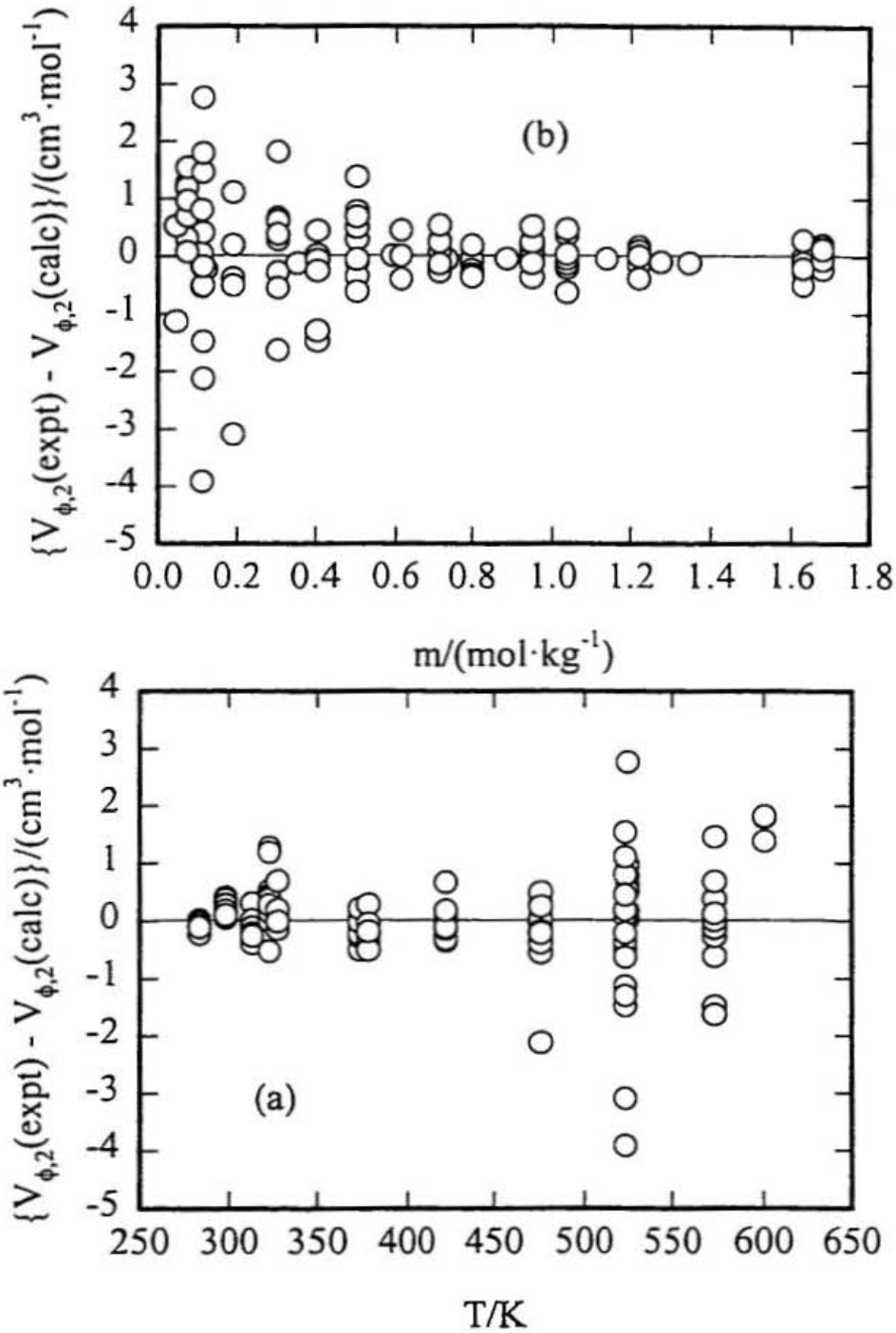


Figure III.9 $V_{\phi,2}$ (observed) minus $V_{\phi,2}$ (calculated) from equations. (III.3.7) - (III.3.9) plotted aganist temperature and molality: a, temperature; b, molality.

These may be divided into two sources: statistical uncertainty and systematic error. The statistical uncertainty is contributed from the random errors associated with the calibration constant, the periods measured for water and the solution under investigation, and the fluctuations of temperature and pressure. It may be estimated through the expression

$$\delta\rho = \{(\rho - \rho_1^*)^2(\delta K/K)^2 + 8[K\tau(\delta\tau)]^2 + [\beta_w^* \rho_1^*(\delta p)]^2 + [\alpha_1^* \rho_1^*(\delta T)]^2\}^{1/2}, \qquad \text{(III.4.1)}$$

where $\delta\rho$ is the statistical uncertainty of density. Here, δK, and $\delta\tau$ denote the standard deviations of calibration constant, and vibrational periods, respectively; α_1^* is the thermal expansion coefficient of water. The terms in equation (III.4.1) are not totally independent. For instance, the statistical error in the vibrational period arises from electronic noise and also from the temperature and pressure fluctuations. For this reason, δT and δp in equation (III.4.1) were taken to represent only the differences in temperature and pressure between the measurement on water and the measurement on the solution. For all measurements in this work, $\delta T < 0.02$ K, $\delta p < 0.01$ MPa, and $\delta K = 0.002$K. The standard deviation $\delta\tau$ varied at different conditions and was calculated by averaging about 20 values. The statistical uncertainties of densities $\delta\rho$, estimated from equation (III.4.1) for all measurements on the platinum-tube, are listed in table III.6. The error associated with $V_{\phi,2}$ as calculated from $\delta\rho$ are also presented in table III.6.

Table III.6. The statistical uncertainties of densities $\delta\rho$ and the statistical errors of apparent molar volumes $\delta V_{\phi,2}$ of 0.1 and 1.0 molal solutions as estimated from equation (III.4.1).

T/K	p/MPa	$\delta\rho$/(kg·m^{-3})		$\delta V_{\phi,2}$/(cm^3·mol^{-1})	
		m = 0.1	m = 1.0	m = 0.1	m = 1.0
323.05	10.60	0.17	0.24	1.70	0.24
373.15	0.50	0.02	0.18	0.21	0.18
374.77	10.01	0.17	0.28	1.70	0.24
422.65	10.20	0.08	0.18	0.93	0.20
476.05	2.13	0.03	0.16	0.40	0.20
475.93	10.18	0.10	0.20	1.35	0.25
524.85	0.46	0.04	0.16	0.64	0.22
523.55	10.15	0.09	0.18	1.40	0.25
523.57	20.40	0.10	0.18	1.56	0.25
573.39	10.13	0.05	0.12	0.95	0.22
573.32	19.87	0.05	0.12	0.93	0.25
600.48	20.20	0.12		2.4	

The systematic error results mainly from the uncertainties in the calibration constant K and the non-linearity of the densimeter. The accuracy of K depends on accuracy of the densities of the two reference fluids. Non-linearity of the densimeter occurs if the vibrating-tube does not vibrate harmonically or if it is not at its resonance frequency. In table III.7, the relative densities of several NaCl(aq) solutions and D_2O measured in this work are compared with those from the literature (Archer, 1992; Hill *et al.*, 1982). Except in two cases in which $\delta\rho \geq 0.40$ kg·m^{-3}, $\delta\rho$ are generally not larger than the statistical errors estimated with equation (III.4.1) and listed in Table III.6. This suggests that systematic errors may not be a major problem in this work. The deviation between the calculated and experimental values for $V_{\phi,2}$ are shown in figure III.9. Except for three measurements at T = 523.6 K, the deviations are consistent with the statistical uncertainties estimated from equation (III.4.1).

III.4.2 The Concentration Dependence of $V_{\phi,2}$ and $C_{p,\phi,2}$

The values of $V_{\phi,2}(HCF_3SO_3, aq)$ and the values of $C_{p,\phi,2}(HCF_3SO_3, aq)$ are plotted against the square root of the molality in figures III.1 and III.3. The values of $V_{\phi,2}$ and $C_{p,\phi,2}$ at T = 298.2 K first increase with $m^{1/2}$ in accordance with the Debye-Hückel limiting law, then reach a maximum at m = 1.0 mol·kg^{-1}, and then decrease as the molality increases further. In the plot of $V_{\phi,2}$ against $m^{1/2}$, there is a minimum at m = 5.1 mol ·kg^{-1}. The maximum in the curve of $C_{p,\phi,2}$ shifts to low molality as temperature is

Table III.7. Comparison of the relative densities of NaCl(aq) solutions and D_2O measured in this work with those calculated from equations of state for NaCl(aq)[19] and D_2O.[20]

m/(mol·kg^{-1})	$(\rho - \rho_i^*)$/(kg·m^{-3}) (obs.)	$(\rho - \rho_i^*)$/(kg·m^{-3}) (literature[d])	$\delta\rho$/(kg·m^{-3})	T/K	p/MPa
1.2167[a]	45.52	45.46	-0.06	373.18	0.50
2.3287[a]	83.34	83.44	0.10	373.15	0.50
2.1536[a]	77.92	77.66	-0.26	373.19	0.83
2.3287[a]	133.88	134.28	0.40	573.34	10.14
0.11513[b]	4.29	4.52	0.23	374.75	9.99
0.48795[b]	18.90	18.70	-0.20	374.68	10.02
0.98795[b]	43.59	43.63	0.04	475.94	2.15
0.98795[b]	42.74	42.96	0.21	475.81	10.22
2.1536[b]	77.02	77.25	0.23	374.74	10.00
D_2O[b][c]	105.06	104.91	-0.15	374.75	10.06
D_2O[b][c]	100.19	100.48	0.28	422.59	10.13
D_2O[b][c]	101.14	101.08	-0.06	422.75	19.63
D_2O[b][c]	92.18	92.64	0.46	475.90	2.15

[a] Calibration constant K determined from the standard NaCl(aq) solution with m = 4.3477 mol·kg^{-1}.

[b] Calibration constant K determined from the standard NaCl(aq) solution with m = 2.1536 mol·kg^{-1}.

[c] Data for mass fraction 0.9952 D_2O and 0.0048 H_2O, corrected to 1.000 D_2O.

[d] Hill (1990); Archer (1992); Hill *et al.* (1982).

raised to T = 328.2 K, while the maximum in the curve for $V_{\phi,2}$ is not sensitive to the temperature change. This unusual molality dependence of $V_{\phi,2}$ and $C_{p,\phi,2}$ has not been observed for other aqueous solutions of strong acids, such as HCl(aq), $HClO_4$(aq), and H_2SO_4(aq), or for aqueous solutions of simple electrolytes, such as NaCl(aq), KCl(aq), and $CaCl_2$(aq). However, similar maxima in the molality dependence of $V_{\phi,2}$ and $C_{p,\phi,2}$ and minima in $V_{\phi,2}$ at higher molalities have been observed for aqueous electrolytes such as tetraakylammonium salts (Franks and Smith, 1967; Wen and Satio, 1964; Leduc and Desnoyers, 1973), aqueous weak electrolytes such as the piperidine (Kiyohara *et al.*, 1975), and aqueous nonelectrolytes such as t-BuOH (Avedikian *et al.*, 1975).

The common feature of those solutes are that they have a hydrophobic group and a polar group that can form hydrogen-bonds with water. The abnormal molality dependence of $V_{\phi,2}$ and $C_{p,\phi,2}$ has been attributed to the effect of "hydrophobic structure making" (Avedikian *et al*, 1975) and to the formation of clathrate-like structures for the tetraalkylammonium salts (Wen and Satio, 1964).

Infrared absorption spectra of aqueous triflic acid indicated that addition products of the type $(CF_3SO_3H)_n \cdot H_3O^+$ may exist in the concentrated solutions (Balicheva *et al.*, 1973). Several solid triflic acid hydrates $H_{2n+1}O_n^+CF_3SO_3^-$ have been identified in the phase diagram of $(CF_3SO_3H + H_2O)$ (Delaplan *et al.*, 1975a). The melting points of these hydrates varied from T = - 61 °C for n = 5 to T = 34.5 °C for n = 1. The crystal structures of these hydrates have been reported by Delaplan *et al.* (1975a and 1975b) for

n = ½ and 2 and by Lundgren (1978a and 1978b) for n = 4 and 5. The structures of these solid hydrates generally consist of an infinite series of layers that are composed of discrete $H_{2n+1}O_n^+$ and $CF_3SO_3^-$ ions linked together by hydrogen bonds. For the higher hydrates (n = 4 and 5), there is a hydrogen-bond connection between the different layers and $CF_3SO_3^-$ ions are interspersed in the cavities formed between these layers. Two of the sulphonate oxygen atoms are hydrogen-bonded to water molecules to form a three-dimensional network of hydrogen bonds. For the lower hydrates (n = 2 and ½), there is no hydrogen-bond connection between the different layers and the hydrogen-bonded layers are separated by normal van der Waals distances between the $-CF_3$ groups of different layers.

Although the structure of solutions in the molality range of $0 < m < 8.1$ mol·kg^{-1} at temperatures between 283 K and 328 K may not be the same as any structures of the solid hydrates, it is commonly believed that the structures of hydrates persist to a certain degree in solutions. The values of $V_{\phi,2}$ first increase with the increase of molality in accordance with the Debye-Hückel limiting law. Upon further addition of acid to the solution, we speculate that $CF_3SO_3^-$ resides in voids between the hydrogen-bonded cluster of $H_{2n+1}O_n^+$ and the oxygens on the sulphonate group enhance the three-dimensional hydrogen-bonding network. This will cause $V_{\phi,2}$ to decrease. $V_{\phi,2}$ continues to decrease with further increases in concentration until the solution reaches a stage at which $CF_3SO_3^-$ begins to weaken the hydrogen bonding between the layers. This

corresponds to the stoichiometry of the solid hydrates with n = 2 and ½. From this stage on, the value of $V_{\phi,2}(CF_3SO_3H, aq)$ will increase with increasing of molality.

The behaviour of $C_{p,\phi,2}$ is more difficult to account for. The maxima in the $C_{p,\phi,2}$ curves in the low concentration region of figure III.3 do correspond to the maxima in the plots of $V_{\phi,2}$ against $m^{1/2}$ in figure III.1,. The structure-making effect of $CF_3SO_3^-$ ion discussed above may also account for the abnormal concentration dependence of $C_{p,\phi,2}$.

III.4.3 Temperature Dependence of V_2^o and $\beta^{(o)V}$

The values of V_2^o obtained by fitting equation (III.3.4), and equations (III.3.6) to (III.3.9) to the entire matrix of data are shown in figure III.10. The individual points are the values of V_2^o obtained by fitting equation (III.3. 3) to isobaric data at each temperature. The differences lie within the combined error of the fits. The pressure dependence of V_2^o was not significant over the range $p_{sat} \leq p \leq 10$ MPa and $T < 423$ K, and so no extra pressure dependence parameters were included for the low temperature region in equations (III.3.7) to (III.3.9). Since only two sets of $V_{\phi,2}$ at $p > 0.1$ MPa and $T < 373$ K were used in optimizing the parameters in equations (III.3.7) to (III.3.9), equation (III.3.7) may not be entirely accurate in representing the pressure dependence of V_2^o in this temperature region. It is of interest to note that the maximum in the curve of V_2^o against temperature in figure III.10 appears at about 423 K. This is much higher than the values obtained for the maxima of ordinary 1-1 and 2-1 aqueous electrolytes such as NaCl(aq)

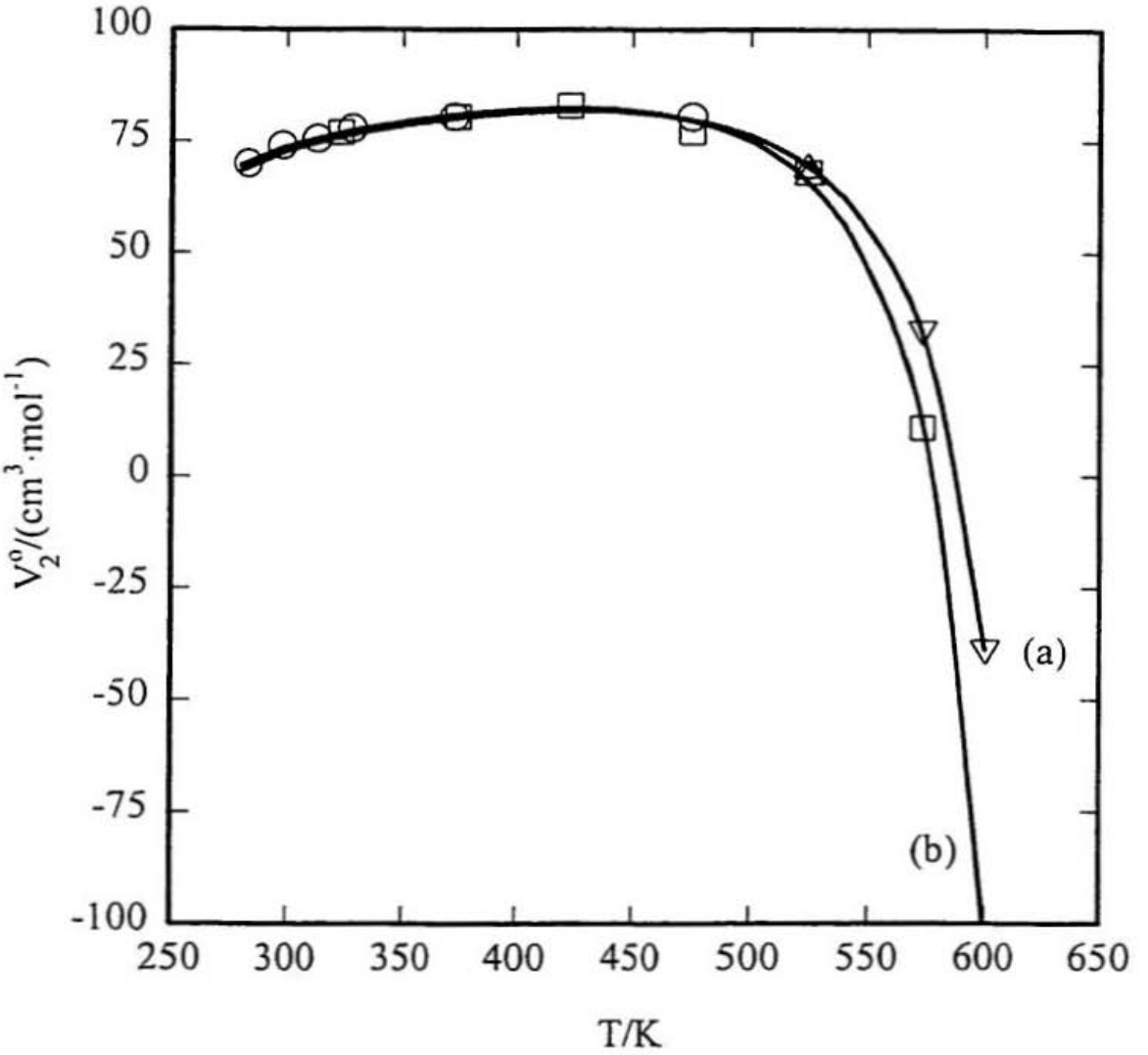


Figure III.10 V_2^o ($NaCF_3SO_3$, aq) calculated from equation (III.3.10) and from the isotherm-isobar least squares fits plotted against temperature: Symbols, from isothermal fittings; lines from equation (III.3.1); ○, p = 0.10 MPa; □, p = 10 MPa; ▽, p = 20 MPa; Δ, $p = p_{sat}$; line (a), p = 20 MPa; line (b), $p = p_{sat}$.

(Simonson *et al.*, 1994) and $CaCl_2$(aq) (Oakes *et al.*, 1995), which occur near T = 323 K. It has been shown in many studies that V_2^o of aqueous electrolytes at $p = p_{sat}$ first increases to a maximum, then decreases toward negative infinity as the temperature is increased toward the critical point of water (Helgeson and Kirkham, 1976). This behaviour reflects the increasing importance of long-range solvent polarization by the charge on ions, and is described quite well by the Born model. The electrostatic effect of $CF_3SO_3^-$(aq) is expected to be less pronounced than that of Cl^-(aq) because the $CF_3SO_3^-$(aq) anion has a larger radius so that the maximum in V_2^o is shifted to a higher temperature.

The second viral coefficients $\beta^{(o)V}$ and $\beta^{(1)V}$ are shown in figure III.11 as functions of temperature at $p = p_{sat}$ and p = 20.0 MPa. The temperature dependence of $\beta^{(o)V}$ is similar to those for NaCl(aq) (Simonson *et al*, 1994), $CaCl_2$(aq) (Oakes *et al*, 1995), and $MgCl_2$(aq) (Phutela *et al*, 1987), although quite different fitting expressions for $\beta^{(o)V}$ were used in their treatments.

III.4.4 Standard Partial Molar Volumes for $CF_3SO_3^-$(aq)

The conventional standard partial molar volumes {$V°(H^+, aq) \equiv 0$} for $CF_3SO_3^-$(aq) can be calculated from values of V_2^o for $NaCF_3SO_3$(aq) and those for Na^+(aq) which are taken from the compilation by Tanger and Helgeson (1988) as cited by Shock and Helgeson (1988). These are listed in Table III.8. The values for $V°(Na^+, aq)$ were derived by fitting the revised Helgeson-Kirkham-Flowers equation (Helgeson, Kirkham

Table III.8. The conventional standard partial molar volumes V_2^o for $CF_3SO_3^-$(aq) at 0.1 MPa for T < 373.15 K and at $p = p_{sat}$ for T≥ 373.15 K.

T/K	$V^o(CF_3SO_3^-, aq)$ / $cm^3 \cdot mol^{-1}$	T/K	$V^o(CF_3SO_3^-, aq)$ / $cm^3 \cdot mol^{-1}$
283.15	72.70(73.95)[a]	373.15	80.51
298.15	74.66(75.86)	423.15	82.61
313.15	76.15(77.24)	473.15	81.74
328.15	77.47(78.30)	523.15	72.39
343.15	78.57	573.15	26.09

[a] The numbers in parenthesis are the values for $V_2^o(HCF_3SO_3, aq)$

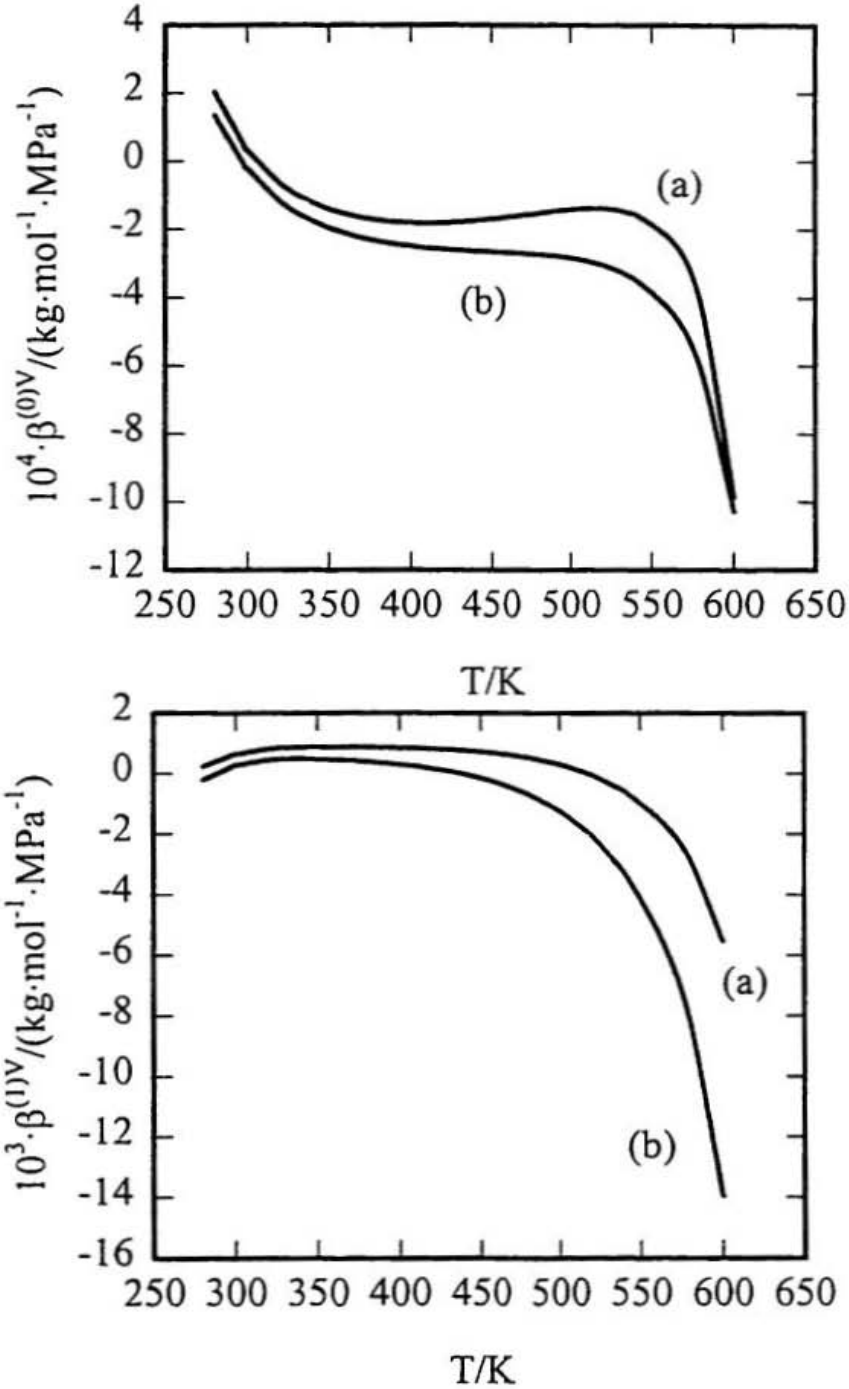


Figure III.11 $\beta^{(0)V}$ and $\beta^{(1)V}$ for $NaCF_3SO_3(aq)$ plotted against temperature: (a), p = 20.0 MPa; (b), $p = p_{sat}$.

and Flowers, 1981) to V°(HCl, aq) obtained by Ellis and McFadden (1972) at temperatures 298 ≤ T ≤ 473 K and data for V°(NaCl, aq) by Grant-Taylor (1981), L'vov *et al.*(1981) and Gates (1985) at temperatures up to 575 K. The agreement with experiment is ~ ± 2 $cm^3 \cdot mol^{-1}$. The values of $V_2^o(CF_3SO_3^-, aq)$ calculated from $NaCF_3SO_3(aq)$ at T = (283.15, 298.15, 313.15, and 328.15) K are systematically higher than the corresponding values of $V_2^o(HCF_3SO_3, aq)$ by about 1 $cm^3 \cdot mol^{-1}$. The conventional standard partial molar heat capacities for $C_{p,\phi}(CF_3SO_3^-, aq)$ calculated from $NaCF_3SO_3$ are also systematically higher than those from HCF_3SO_3. The reason for the discrepancy is unknown.

The triflate anion is larger in size than those for other simple anions and oxy-anions (r = 32.8 nm, as estimated from the volume of liquid anhydrous triflic acid) and, as expected, the value $V_2^o(CF_3SO_3^-, aq)$ = 74.66 $cm^3 \cdot mol^{-1}$ at 298.15 K is higher than {$V_2^o(Cl^-$, aq) = 28.88 $cm^3 \cdot mol^{-1}$, $V_2^o(ClO_4^-, aq)$ = 44.1 $cm^3 \cdot mol^{-1}$, and $V_2^o(SO_4^{2-}, aq)$ = 19.5 $cm^3 \cdot mol^{-1}$} (Marcus, 1993; Helgeson *et al.*, 1981). The triflate anion has the second largest V_2^o among 43 common monovalent anions in the compilation of Marcus (1993). The large effective radius is an attractive property in studies aimed at characterizing thermodynamics of cation hydration since its contribution to solvent polarization through the Born equation is smaller than that of other non-complexing anions.

Chapter IV. Apparent Molar Heat Capacities and Apparent Molar Volumes of $LaCl_3(aq)$, $La(ClO_4)_3(aq)$ and $Gd(ClO_4)_3(aq)$ at Temperatures from 283 to 338K

IV.1 Introduction

Values for $C^o_{p,2}$ and V^o_2 of aqueous $LaCl_3(aq)$, $La(ClO_4)_3(aq)$, and $Gd(ClO_4)_3(aq)$ at 298 K have been reported by Spedding *et al.* (1966b, 1966d, 1975a, 1975b, 1975c) and Spitzer *et al.*(1979). In addition, $C^o_{p,2}$ of gadolinium chloride was determined by Jekel *et al.* (1964) from 273.15 to 373.15 K using the integral heat of solution method. Densities of $LaCl_3(aq)$ from 288 to 328 K were measured by Isono (1984). To our knowledge, no other temperature-dependent values of $C^o_{p,2}$ and V^o_2 have been reported for the trivalent rare-earth elements.

The complexation of $La^{3+}(aq)$ with $NO_3^-(aq)$ and $Cl^-(aq)$ has been studied by several spectroscopic methods (Chen and Detellier, 1992; Silber *et al.*, 1990; Breen and Horrocks, 1983). The lanthanide cation, however, forms only a very weak complex with $ClO_4^-(aq)$ (Chen and Detellier, 1992). To minimize complexation, we used the lanthanum perchlorate and gadolinium perchlorate salts for our measurements to determine $C^o_{p,2}$ and V^o_2 of the simple cations.

IV.2 Experimental

Lanthanum perchlorate and gadolinium perchlorate were prepared from their

oxides by the procedure reported by Spedding *et al.* (1966d). Approximately 50 g of the oxide was added slowly to a slightly less-than-equivalent amount of 1.7 mol·dm^{-3} $HClO_4$(aq) with stirring. The mixture was heated at T = 353 K for several hours to yield a clear solution with only a little oxide power remaining. This solution was titrated with perchloric acid to pH 2. A sharp titration curve was observed with an equivalent point at pH = 3. After the solution was heated for several minutes, the pH changed to 4 or greater. The solution was again adjusted to pH 2 and heated for several hours to dissolve the remaining solid or colloidal oxide further. This process was carried out several times until the pH did not change from the equivalence value of pH 3-3.5. The final solution was filtered through a fine sintered glass filter. The pH of the filtrate was about 3.3.

Two kinds of stock solutions of perchlorate were used for our measurements. The first were solutions prepared directly from the procedure above with pH = 3.3. The second were solutions with pH = 1, prepared by adding a mass of 40 g of 0.5 mol·dm^{-3} $HClO_4$(aq) to 350 g of the first stock solution. More dilute solutions were prepared by diluting each stock solution with water by mass.

Lanthanum chloride solution was prepared by dissolving the anhydrous salt in water. A milky mixture resulted with pH = 7. Hydrochloric acid (1 mol·dm^{-3}) was added to the mixture to adjust the pH to 2, and the mixture was then heated for several hours. When the pH exceeded 4, HCl(aq) was added to adjust the pH to 2 and the mixture was heated again. This process was repeated until a clear solution with a constant pH = 2 was

obtained. The stock solution was obtained by filtering the solution through a fine sintered glass filter. More dilute solutions were prepared by diluting the stock solution with water by mass.

The concentrations of $HClO_4$(aq) and HCl(aq) were determined by titration with tris(hydroxymethyl)aminomethane (TRIS) using methyl red as indictor. The concentrations of La^{3+}(aq) and Gd^{3+}(aq) were determined by titration with ethylene diamine tetra acetic acid (EDTA) using xylenol orange as indictor and hexamethylenetetramine to buffer the solution at pH ≈ 6.0. Lanthanum chloride was also standardized by determining chloride concentration by the usual silver chloride gravimetric procedure. The results agreed with those obtained by titration to within 0.1 per cent.

Nanopure water (resistivity >17 MΩ·cm) was used to prepare all solutions. The $HClO_4$(aq) and HCl(aq) were obtained by dilution of 15 mol·kg^{-1} HCl(aq) and 23 mol·kg^{-1} $HClO_4$(aq), both Fisher A.C.S. certified reagent grade. Lanthanum oxide (mass fraction: 0.999), gadolinium oxide (mass fraction: 0.999) and TRIS (mass fraction: 99.9) were purchased from Aldrich. Reagent grade anhydrous lanthanum chloride and utrapure sodium chloride were purchased from Alfa.

The experimental procedures are the same as described in Chapters II and III. A standard NaCl(aq) solution with m = 0.9958 mol·kg^{-1} and pure water were used to calibrate the densimeter and to determine the heat-loss correction factor.

IV.3 Results

IV.3.1 Apparent Molar Properties

The experimentally determined relative densities ($\rho - \rho_1^*$) and heat capacity ratios [$c_p\rho/(c_{p,1}^* \rho_1^*) - 1$] at each of the experimental temperatures are listed in tables A.IV.1 to A.IV.7. Tables A.IV.1 to A.IV.7 also give the experimental apparent molar volumes V_ϕ and heat capacities $C_{p,\phi}$ which were calculated from these data using densities and specific heat capacities of pure water taken from Hill (1992). By definition

$$Y_\phi^{expt} = \{Y(solution) - 55.509 Y_1^*\}/(m_2 + m_3) \qquad (IV.3.1)$$

where Y_1^* is the molar heat capacity or volume of pure $H_2O(l)$, and m_2 and m_3 are the molality of the salt and perchloric acid, respectively. The effect of the small amount of excess acid was subtracted by means of the procedure used by Hovey and Tremaine (1986). Briefly, the contribution of each solute can be described by Young's rule (Young and Smith, 1954; Reilly and Wood, 1969):

$$Y_\phi^{expt} = \frac{m_2}{m_2 + m_3} Y_{\phi,2} + \frac{m_3}{m_2 + m_3} Y_{\phi,3} + \delta \,. \qquad (IV.3.2)$$

Here, $Y_{\phi,2}$ and $Y_{\phi,3}$ are the values for the hypothetical solution of the pure components with speciation and ionic strength identical to the mixture; δ is an excess mixing term, which usually may be ignored in calculating the properties of the major components where there is a common anion. Both V_ϕ and $C_{p,\phi}$ of $HClO_4(aq)$ from T = 283 to T = 338

K were calculated as functions of ionic strength and temperature by applying the equations reported by Hovey *et al.* (1988). The resulting values of $C_{p,\phi,2}$ and $V_{\phi,2}$ for $LaCl_3(aq)$, $La(ClO_4)_3(aq)$ and $Gd(ClO_4)_3(aq)$ from equation (IV.3.2) are tabulated in the tables A.IV.1 to A.IV.7, and plotted in figures IV.1 to IV. 4.

IV.3.2 Hydrolysis of $La^{3+}(aq)$ and $Gd^{3+}(aq)$

The hydrolysis of trivalent lanthanides has been critically reviewed by Baes and Mesmer (1976). Aqueous Gd^{3+} and La^{3+} do not undergo appreciable hydrolysis in solutions with pH < 6 at m < 1.0 mol·kg^{-1}. In addition, no inner-sphere complexes have been detected by UV-visible (Silber *et al.*, 1990) or luminescence spectroscopy (Breen and Horrocks, 1983). A ^{139}La NMR study (Chen and Detellier, 1992), however, has shown that $La^{3+}(aq)$ forms a weak complex with $ClO_4^-(aq)$ with a formation constant of K = 0.03. To confirm the magnitude of the effects of hydrolysis and complexation on the experimental values of $C_{p,\phi}$ and V_ϕ, two sets of $La(ClO_4)_3(aq)$ and $Gd(ClO_4)_3(aq)$ solutions were studied at T = 298.2 K and T = 313.2 K. One set of measurements used solutions with the mole ratio $n(La^{3+})/n(ClO_4^-) = 0.33$ or $n(Gd^{3+})/n(ClO_4^-) = 0.33$, whose pH lay in the range 3.3 to 5.3. The other set of measurements used solutions containing excess $HClO_4(aq)$ sufficient to maintain pH = 2. The apparent molar properties for the salts, as determined from the two sets of results, are listed in tables A.IV.3, A.IV.4, A.IV.6 and A.IV.7 and illustrated in figures IV.3 and IV.4. The largest differences in

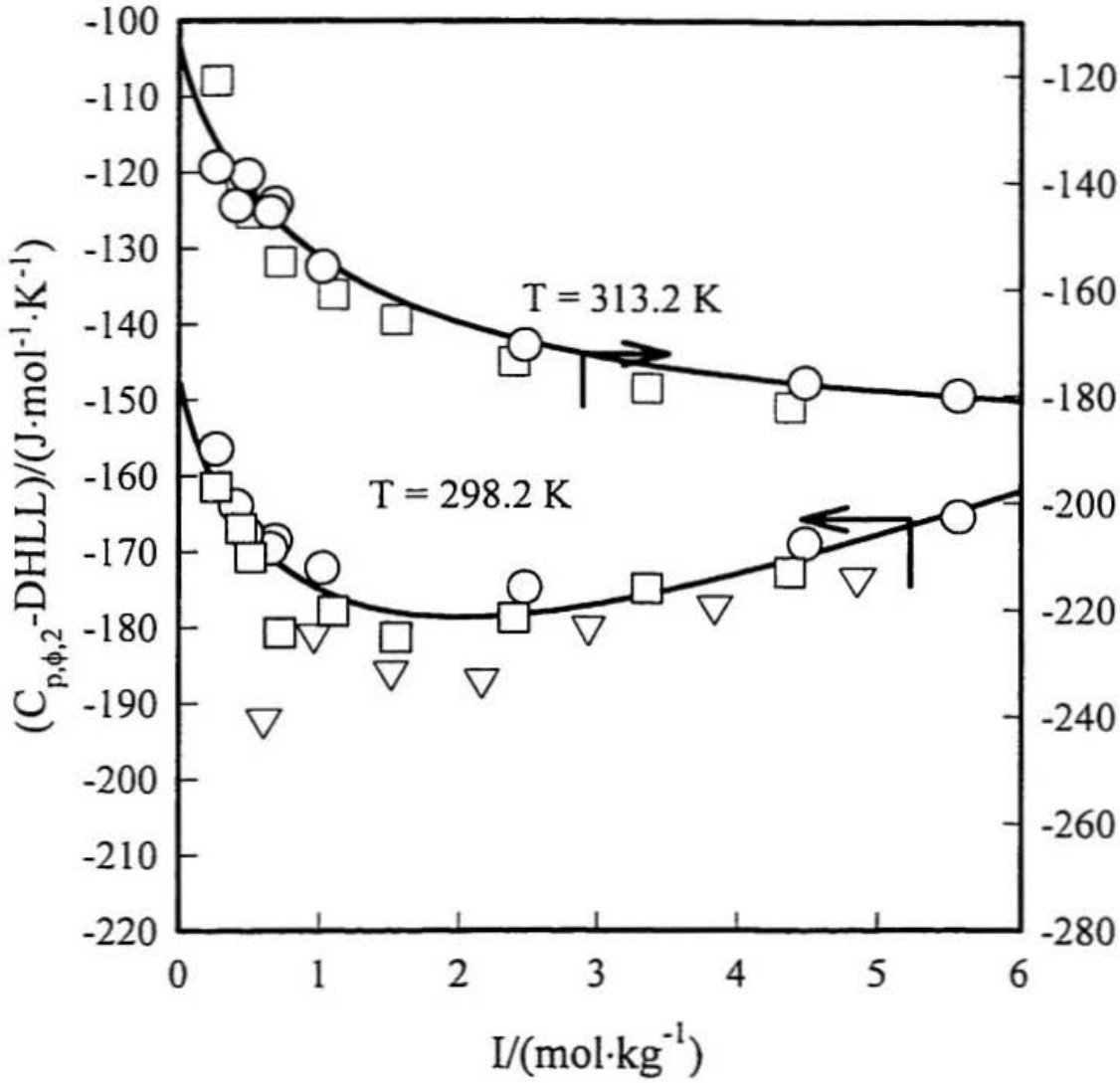


Figure IV.1. The apparent molar heat capacities of $La(ClO_4)_3(aq)$, plotted as a function of ionic strength after subtracting the Debye-Hückel limiting law (DHLL) term according to equation (IV.3.3). The least square fits to equation (IV.3.3) are shown as solid curves. □, solutions with pH=2.4; ○, solutions with pH=3-5; ▽, Spedding *et al.* (1975c).

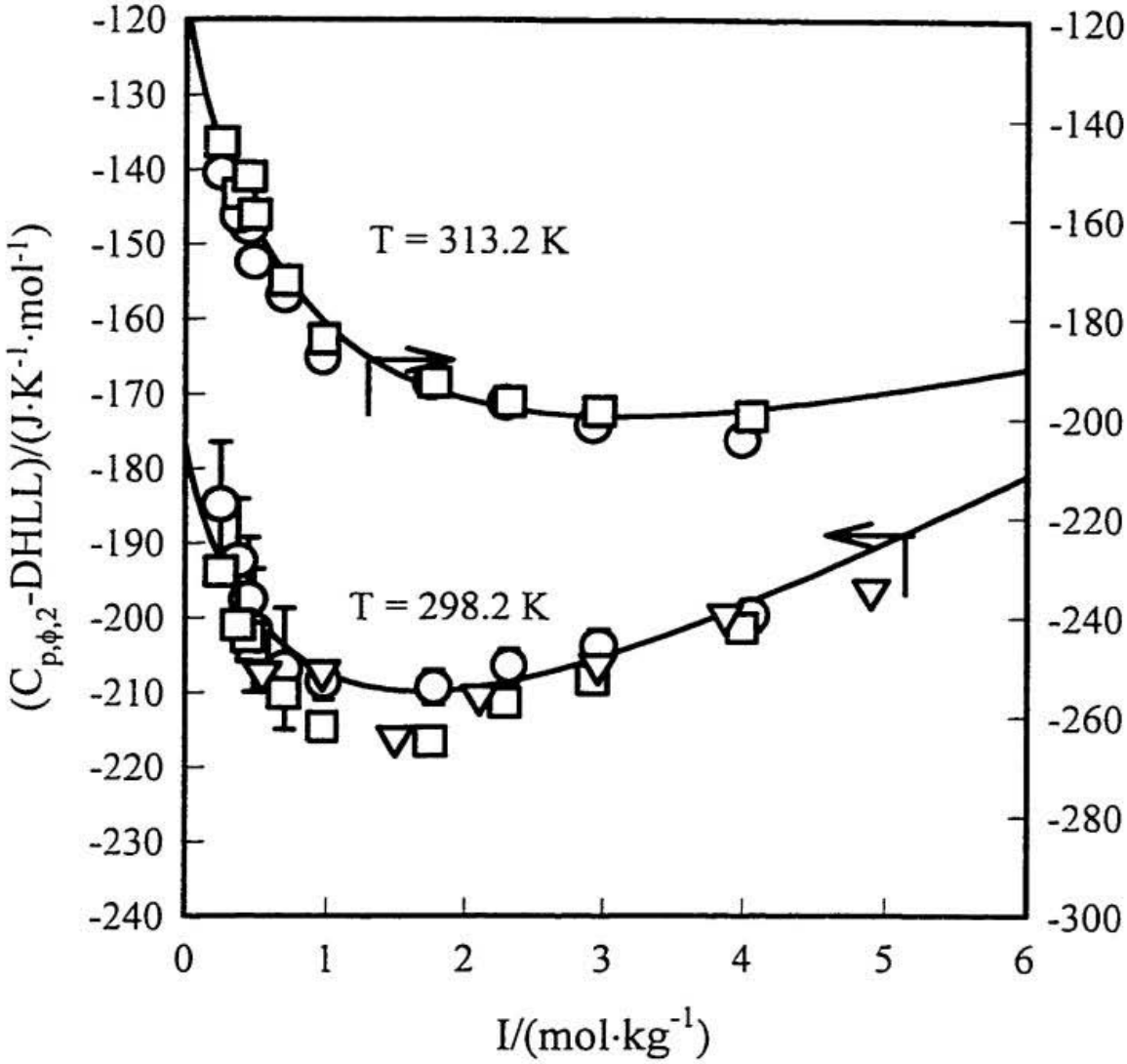


Figure IV.2. The apparent molar heat capacities of $Gd(ClO_4)_3(aq)$, plotted as a function of ionic strength after subtracting the Debye-Hückel limiting law (DHLL) term according to equation (IV.3.3). The least square fits to equation (IV.3.3) are shown as solid curves. □, solutions with pH=2.4; ○, solutions with pH=3-5; ▽, Spedding *et al.* (1975c).

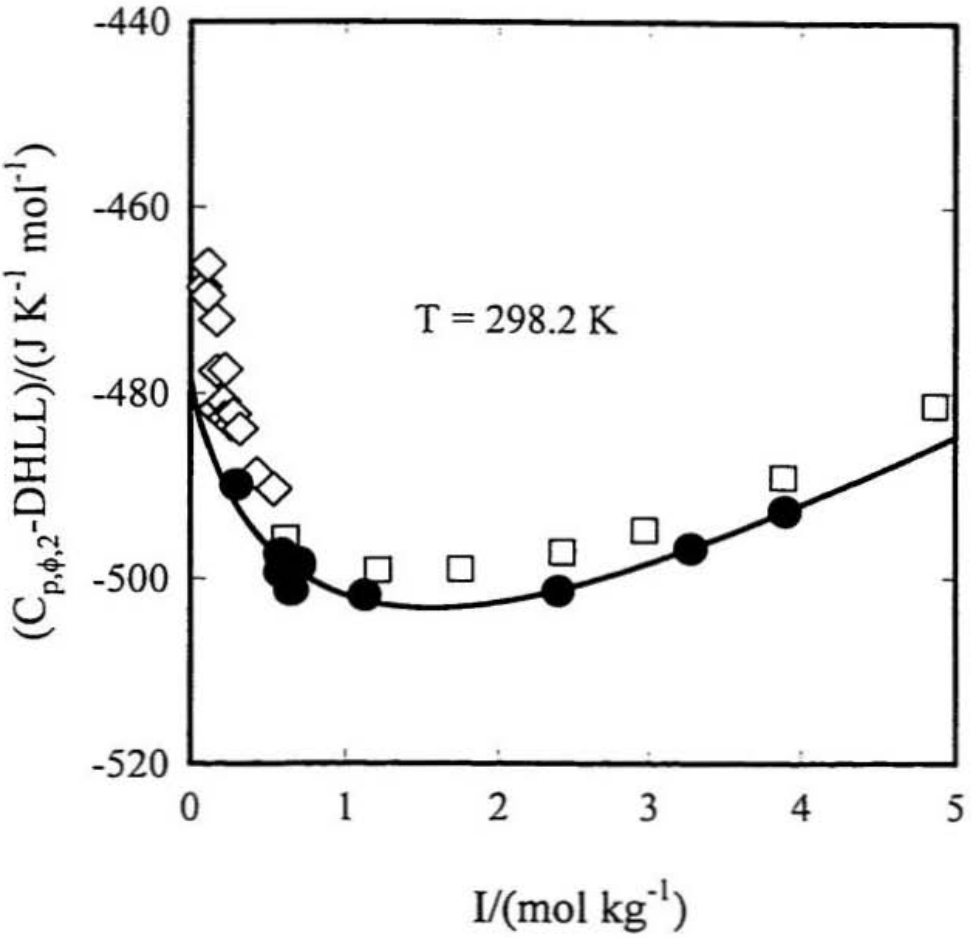


Figure IV.3. The apparent molar heat capacities of $LaCl_3(aq)$, plotted as a function of ionic strength after subtracting the Debye-Hückel limiting law (DHLL) term according to equation (IV.3.3). The least square fits to equation (IV.3.3) are shown as solid curves. ●, this work; □, Spedding *et al.* (1966d); ◇, Spitzer *et al.* (1979).

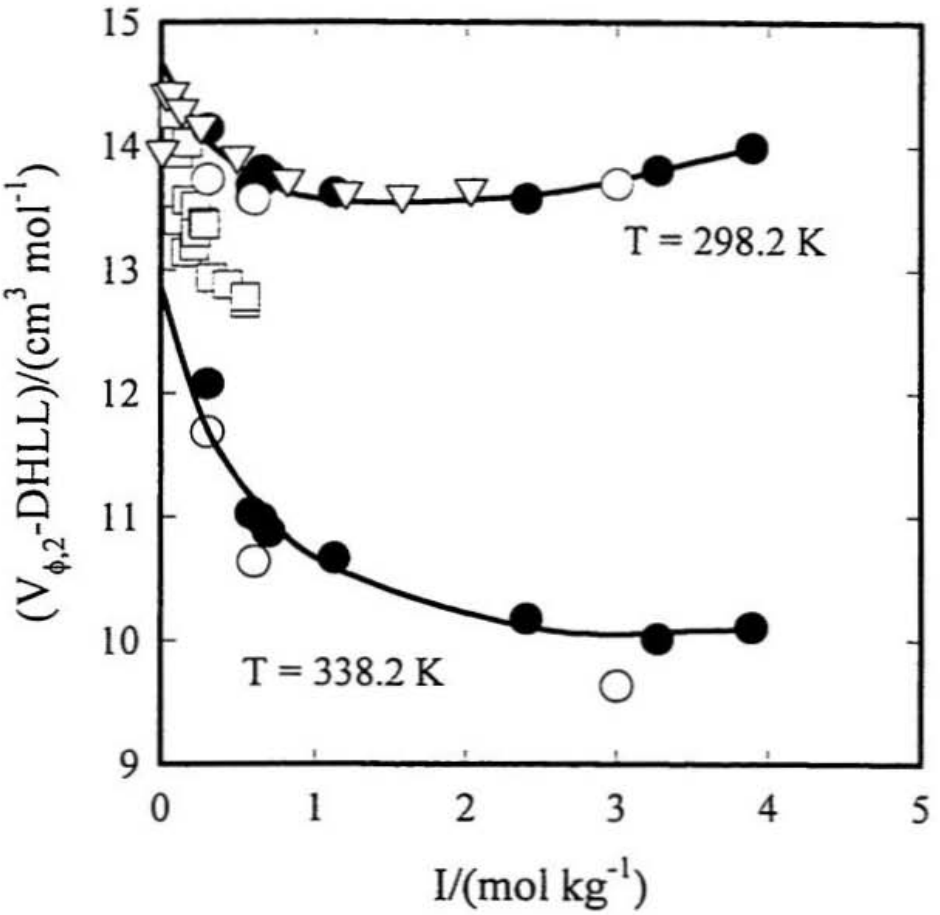


Figure IV.4. The apparent molar volumes of $LaCl_3$(aq), plotted as a function of ionic strength after subtracting the Debye-Hückel limiting law (DHLL) term according to equation (IV.3.3). The least square fits to equation (IV.3.4) are shown as solid curves. ●, this work; □, Spedding *et al.* (1975a); ◇, Spitzer *et al.* (1979); ○, Isona (1984).

$C_{p,\phi,2}$ and $V_{\phi,2}$, observed at low concentrations of $La(ClO_4)_3$, are less than 10 $J \cdot K^{-1} \cdot mol^{-1}$ and 1 $cm^3 \cdot mol^{-1}$, respectively, which is within the experimental uncertainty in this concentration range. The good agreement within those two sets of data shows that there is no apparent effect of hydrolysis in aqueous solutions with pH < 5.3.

IV.3.3 Ion Interaction Model

The Pitzer ion interaction model has been successfully used to treat the heat capacities of many aqueous electrolyte systems (Pitzer, 1991), for example HCl (Tremaine *et al.*,1986), $AlCl_3$ (Conti *et al.*, 1992), $MgCl_2$, $CaCl_2$ and $SrCl_2$ (Phutela *et al.*, 1987). At solution concentrations below 1 $mol \cdot kg^{-1}$, the ternary interaction parameters C^J and C^V are not needed. Thus, the equations for fitting experimental heat capacities and volumes are the following:

$$C_{p,\phi,2} = C^0_{p,2} + (6A_J/b)\ln(1+bI^{1/2}) - 6RT^2 m\beta^{(0)V} - 12RT^2 m\beta^{(1)V} f(I), \qquad (IV.3.3)$$

$$V_{\phi,2} = V^0_2 + 6A_V \ln(1+bI^{1/2})/b + 6RTm\beta^{(0)V} + 12RTm\beta^{(1)V} f(I), \qquad (IV.3.4)$$

where b=1.2 $kg^{1/2} \cdot mol^{-1/2}$. A_J in equation (IV.3.3) and A_V in equation (IV.3.4) are the Debye-Hückel limiting slopes for the heat capacity and for the volume, respectively, whose values were taken from the compilation by Pitzer (1991). Here, m is molality of the solute, I is the ionic strength, and f(I) is given by equation (III.3.6).

The Pitzer theory does not consider the temperature dependence of the β parameters. We adopted the equations used by Phutela and Pitzer (1987) for some 1:2 electrolytes, and express $\beta^{(i)\gamma}$ as:

$$\beta^{(0)J} = c_3/T + c_4 + c_5 T , \qquad \text{(IV.3.6a)}$$

$$\beta^{(1)J} = c_6/T + c_7 + c_8 T , \qquad \text{(IV.3.6b)}$$

$$\beta^{(0)V} = v_3 + v_4 T , \qquad \text{(IV.7a)}$$

$$\beta^{(1)V} = v_5/T + v_6 + v_7 T . \qquad \text{(IV.7b)}$$

By definition, $C^{\circ}_{p,2}$ and V°_2 are the standard partial molar heat capacity and standard partial molar volume, respectively. The temperature dependence was modelled by the revised HKF equations proposed by Tanger and Helgeson (1988):

$$C^{\circ}_{p,2} = c_1 + \frac{c_2}{(T-\Theta)^2} + \omega T X , \qquad \text{(IV.3.8)}$$

$$V^{\circ}_2 = v_1 + \frac{v_2}{T-\Theta} - \omega Q . \qquad \text{(IV.3.9)}$$

Here c_1, c_2, v_1 and v_2 are species-dependent fitting parameters, and Θ = 228 K is a solvent-dependent parameter. The term ωTX and ωQ are the electrostatic contributions to the standard heat capacity and standard volume according to the Born equation, in which X, Q and ω are given by

$$Q = \frac{1}{\varepsilon}\left(\frac{\partial \ln \varepsilon}{\partial P}\right)_T, \qquad \text{(IV.3.10)}$$

$$X = \frac{1}{\varepsilon}\left[\left(\frac{\partial^2 \ln \varepsilon}{\partial T^2}\right)_P - \left(\frac{\partial \ln \varepsilon}{\partial T}\right)_P^2\right], \qquad \text{(IV.3.11)}$$

$$\omega = \frac{Z^2 \eta}{r_e}, \qquad \text{(IV.3.12)}$$

where ϵ is the static dielectric constant of water, η=6.9466×10^{-5} J·m^{-1}·mol^{-1}, Z is ionic charge, and r_e is an effective electrostatic radius of the ion: r_e=r_{cryst}+0.94·Z for cations; r_e=r_{cryst} for anions (Shock and Helgeson, 1988). Data for the X and Q were taken from Helgeson and Kirkham (1976).

Equations (IV.3.3) and (IV.3.4) were fitted to the experimental data at each temperature by the Marquardt-Levenberg non-linear square algorithm within the commercial software SigmaPlot©. The fitted values for the βs and standard partial properties are listed in the table IV.1. The entire array of data at all temperatures and all concentrations was then used to optimize the parameters in equations.(IV.3.3) to (IV.3.9) by the SigmaPlot curve fitting program. The results are listed in tables IV.2 and IV.3, and also illustrated in figures IV.5 to IV.8. The extrapolated high temperature behaviour of $C^{\circ}_{p,2}$ and V°_2 is illustrated by figures IV.9 and IV.10.

Table IV.1. Values of parameters from the Pitzer ion-interaction model for $Gd(ClO_4)_3$(aq), $La(ClO_4)_3$(aq) and $LaCl_3$(aq)[a]

T/K	V_2^o [b]	$RT\beta^{(0)V}$ [c]	$RT\beta^{(1)V}$ [d]	$C_{p,2}^o$ [e]	$RT^2\beta^{(0)J}$ [f]	$RT^2\beta^{(1)J}$ [g]
			$La(ClO_4)_3$			
283.2	84.68(0.45)	1.400	-9.551	-315.7(4.8)	-22.19	12.93
298.2	94.12(0.59)	0.8277	-14.70	-176.7(5.6)	-10.29	138.4
313.2	99.36(0.70)	0.4171	-17.52	-115.7(5.2)	-7.066	244.2
328.2	101.1(0.58)	-0.0495	-14.38	-108.9(7.3)	-6.587	288.8
338.5	103.2(0.60)	-0.0822	-18.23	-111.6(8.3)	-0.4549	284.8
			$LaCl_3$			
283.2	13.18(0.52)	0.7897	-6.256	-549.9(3.6)	-16.70	78.6
298.2	14.71(0.17)	0.3980	-5.038	-478.6(2.0)	-8.94	108.3
313.2	13.98(0.31)	0.3128	-5.000	-420.0(1.7)	-10.13	214.0
328.2	13.39(0.39)	0.4755	-10.93	410.2(2.4)	-4.269	190.6
338.2	10.50(0.30)	0.0025	-6.15	-411.6(3.1)	-4.269	210.8
			$Gd(ClO_4)_3$			
283.2	84.15(0.46)	0.7942	-6.25	-271.3(4.8)	-15.40	21.68
298.2	90.91(0.60)	0.1141	-5.954	-148.6(2.5)	-5.320	96.84
313.2	96.34(0.25)	-0.1315	-10.27	-114.5(4.9)	0.6727	130.6
328.2	99.80(0.35)	-0.2440	-15.44	-93.87(4.7)	1.754	226.3
338.2	101.16(0.4)	-0.5293	-15.43	-103.3(3.21)	2.832	252.2

[a] The figures in parentheses are the standard deviations of each of the parameters;
[b] $cm^3 \cdot mol^{-1}$; [c] $kg \cdot mol^{-1} \cdot bar^{-1}$; [d] $kg \cdot mol^{-1} \cdot bar^{-1}$; [e] $J \cdot K^{-1} \cdot mol^{-1}$; [f] $J \cdot K^{-1} \cdot mol^{-1}$; [g] $J \cdot K^{-1} \cdot mol^{-1}$

Table IV.2. The fitting parameters for equations (IV.3.3), (IV.3.6), (IV.3.8), and (IV.4.5) for the apparent molar heat capacities.

parameter	$La(ClO_4)_3(aq)$	$LaCl_3(aq)$	$Gd(ClO_4)_3(aq)$
	Equation (IV.4.5)		
$c_1/(J\cdot K^{-1}\cdot mol^{-1})$	$1.713\times10^{2}(6.7)$	$-1.038\times10^{2}(8.94)$	$1.835\times10^{2}(5.3)$
$c_2/(J\cdot K\cdot mol^{-1})$	-1.672×10^{5}	-1.015×10^{5}	-1.475×10^{5}
$c_3/(J\cdot K^{2}\cdot kg^{-1})$	-5.898×10^{-1}	-0.2367×10^{-1}	-4.729×10^{-1}
$c_4/(J\cdot K^{1}\cdot kg^{-1})$	3.595×10^{-3}	1.2405×10^{-3}	2.886×10^{-3}
$c_5/(J\cdot kg^{-1})$	-5.484×10^{-6}	-1.580×10^{-6}	-4.391×10^{-6}
$c_6/(J\cdot K^{2}\cdot kg^{-1})$	-8.162×10^{-1}	-5.975×10^{-1}	-3.558×10^{-1}
$c_7/(J\cdot K^{1}\cdot kg^{-1})$	4.756×10^{-3}	5.996×10^{-3}	1.497×10^{-3}
$c_8/(J\cdot kg^{-1})$	-6.001×10^{-6}	-1.234×10^{-5}	-6.101×10^{-7}
	Equation (IV.3.8)		
$c_1/(J\cdot K^{-1}\cdot mol^{-1})$	$2.328\times10^{2}(7.2)$	$-5.598\times10^{1}(8.7)$	$3.75\times10^{2}(5.3)$
$c_2/(J\cdot K\cdot mol^{-1})$	-1.068×10^{6}	-7.235×10^{5}	-9.484×10^{5}
$c_3/(J\cdot K^{2}\cdot kg^{-1})$	-6.928×10^{-1}	-2.077×10^{-1}	-5.240×10^{-1}
$c_4/(J\cdot K^{1}\cdot kg^{-1})$	4.321×10^{-3}	1.283×10^{-3}	3.255×10^{-3}
$c_5/(J\cdot kg^{-1})$	-6.749×10^{-6}	-1.514×10^{-6}	-5.045×10^{-6}
$c_6/(J\cdot K^{2}\cdot kg^{-1})$	6.393×10^{-1}	-1.148×10^{0}	-6.691×10^{-1}
$c_7/(J\cdot K^{1}\cdot kg^{-1})$	-5.553×10^{-3}	8.406×10^{-3}	-5.918×10^{-3}
$c_8/(J\cdot kg^{-1})$	1.197×10^{-5}	-1.445×10^{-5}	1.257×10^{-5}

Table IV.3. The fitting parameters for equations (IV.3.4), (IV.3.7) and (IV.3.9) for the apparent molar volumes.

parameters	$La(ClO_4)_3$(aq)	$LaCl_3$(aq)	$Gd(ClO_4)_3$(aq)
$v_1/(cm^3 \cdot mol^{-1})$	143.6	38.72(0.86)	140.2(0.93)
$v_2/(cm^3 \cdot K \cdot mol^{-1})$	-2592	-5812(67.3)	-2440(72.3)
$v_3/(kg \cdot mol^{-1} \cdot MPa^{-1})$	3.300×10^{-1}	7.350×10^{-4}	3.047×10^{-3}
$v_4/(kg \cdot mol^{-1} \cdot K^{-1} \cdot MPa^{-1})$	-9.851×10^{-6}	-1.877×10^{-6}	-9.674×10^{-6}
$v_5/(kg \cdot mol^{-1} \cdot K \cdot MPa^{-1})$	7.362×10^{1}	-2.902×10^{1}	9.855×10^{1}
$v_6/(kg \cdot mol^{-1} \cdot MPa^{-1})$	-4.679×10^{-1}	1.992×10^{-1}	-6.301×10^{-1}
$v_7/(kg \cdot mol^{-1} \cdot K^{-1} \cdot MPa^{-1})$	7.213×10^{-4}	-3.469×10^{-4}	9.892×10^{-4}

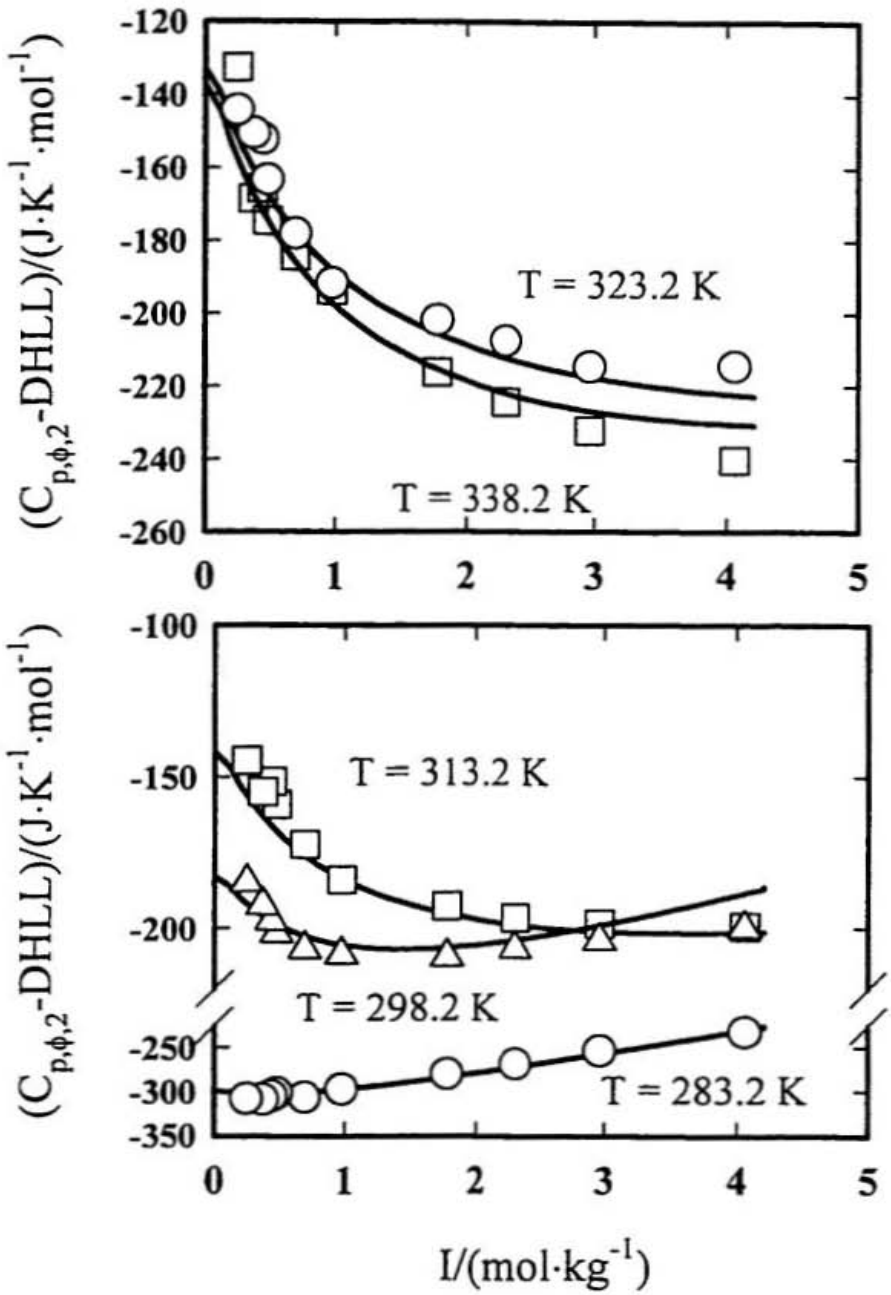


Figure IV.5. The apparent molar heat capacities of $La(ClO_4)_3(aq)$, plotted as a function of ionic strength after subtracting the Debye-Hückel limiting law (DHLL) term according to equation (IV.3.3). The least square fits to equations (IV.3.3), (IV.3.6), and (IV.4.5) are shown as solid curves.

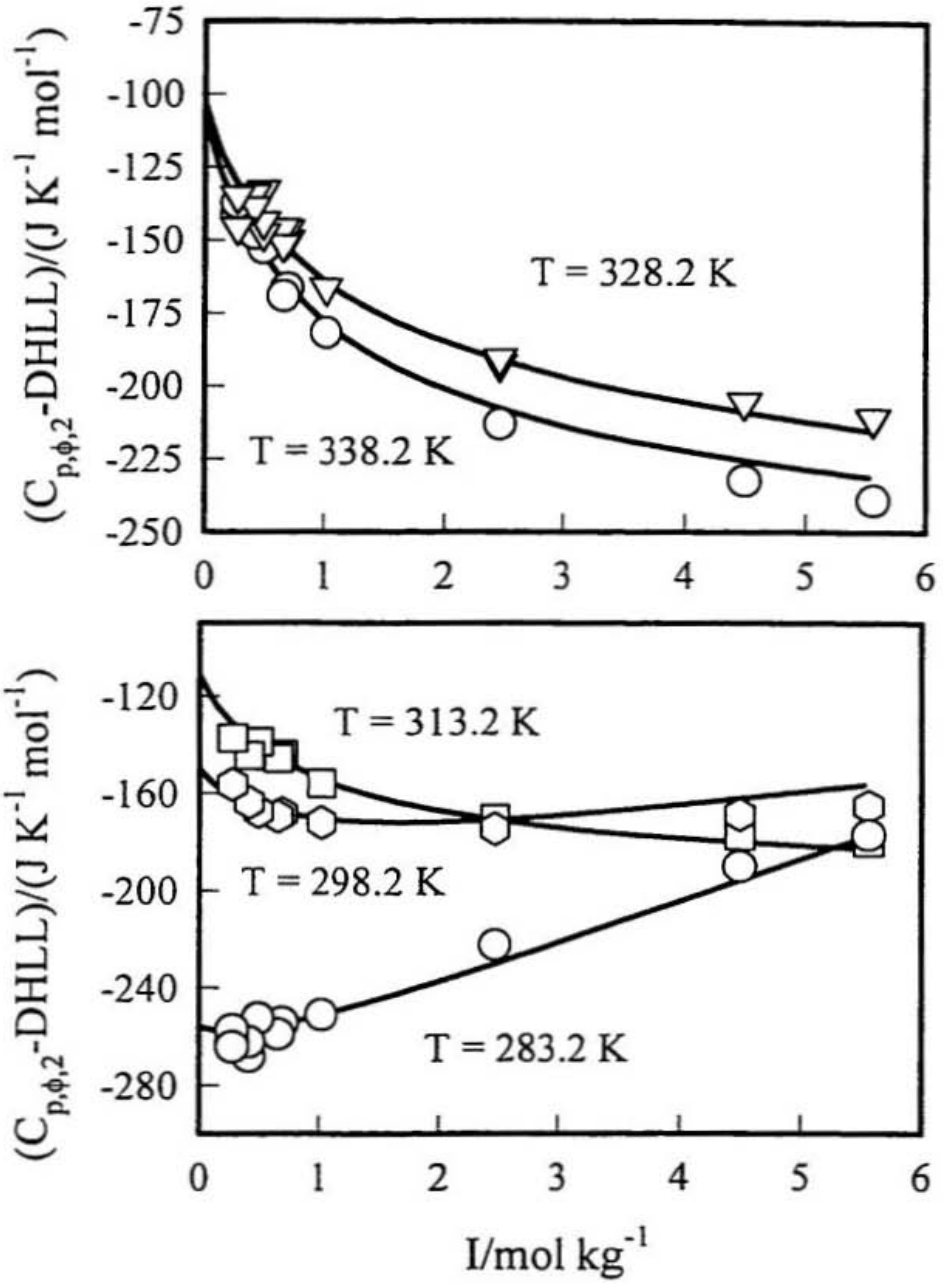


Figure IV.6. The apparent molar heat capacities of $Gd(ClO_4)_3(aq)$, plotted as a function of ionic strength after subtracting the Debye-Hückel limiting law (DHLL) term according to equation (IV.3.3). The least square fits to equations (IV.3.3), (IV.3.6), and (IV.4.5) are shown as solid curves.

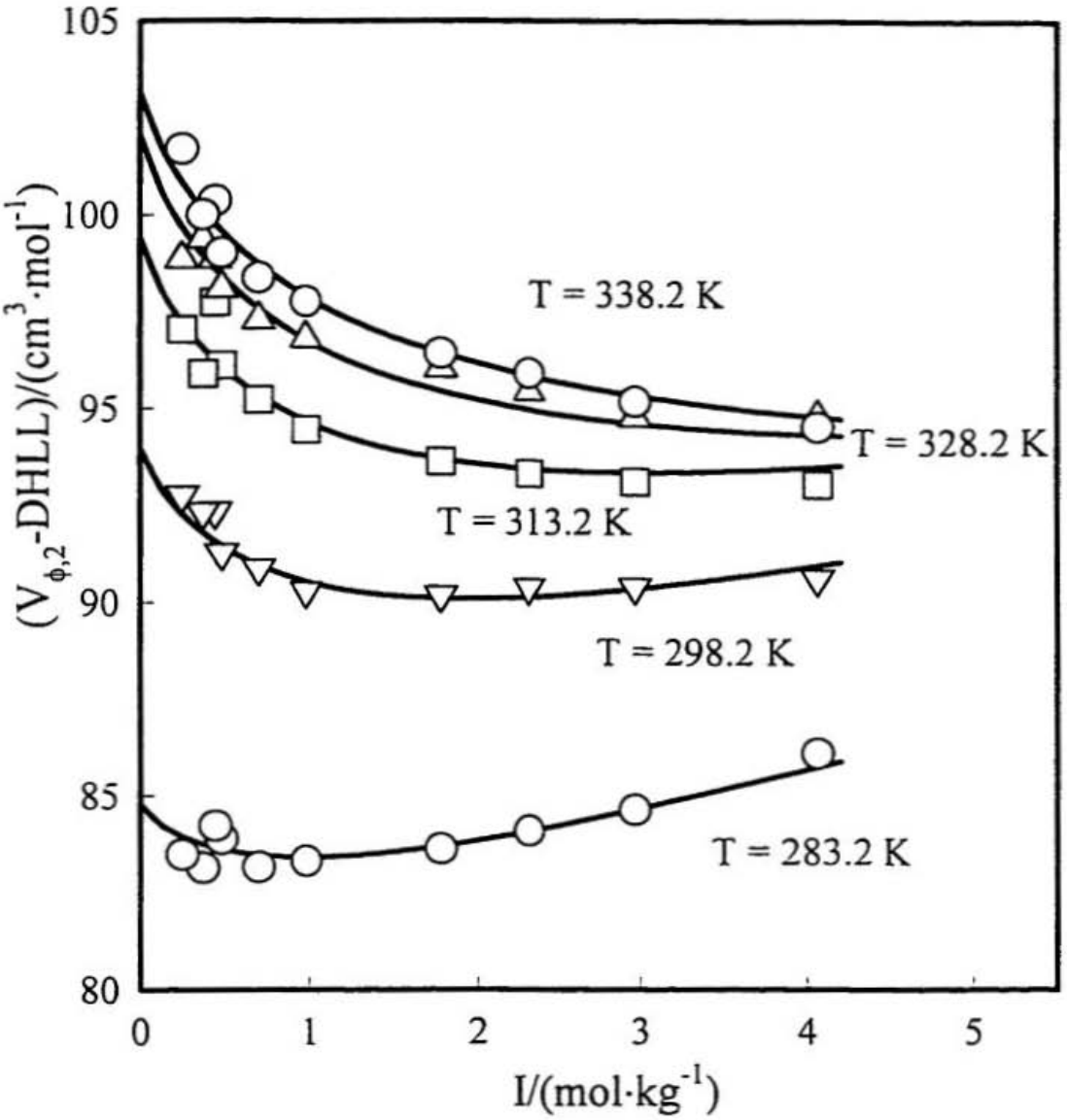


Figure IV.7. The apparent molar volumes of $La(ClO_4)_3(aq)$, plotted as a function of ionic strength after subtracting the Debye-Hückel limiting law (DHLL) term according to equation (IV.3.4). The least square fits to equations (IV.3.4), (IV.3.7), and (IV.3.9) are shown as solid curves.

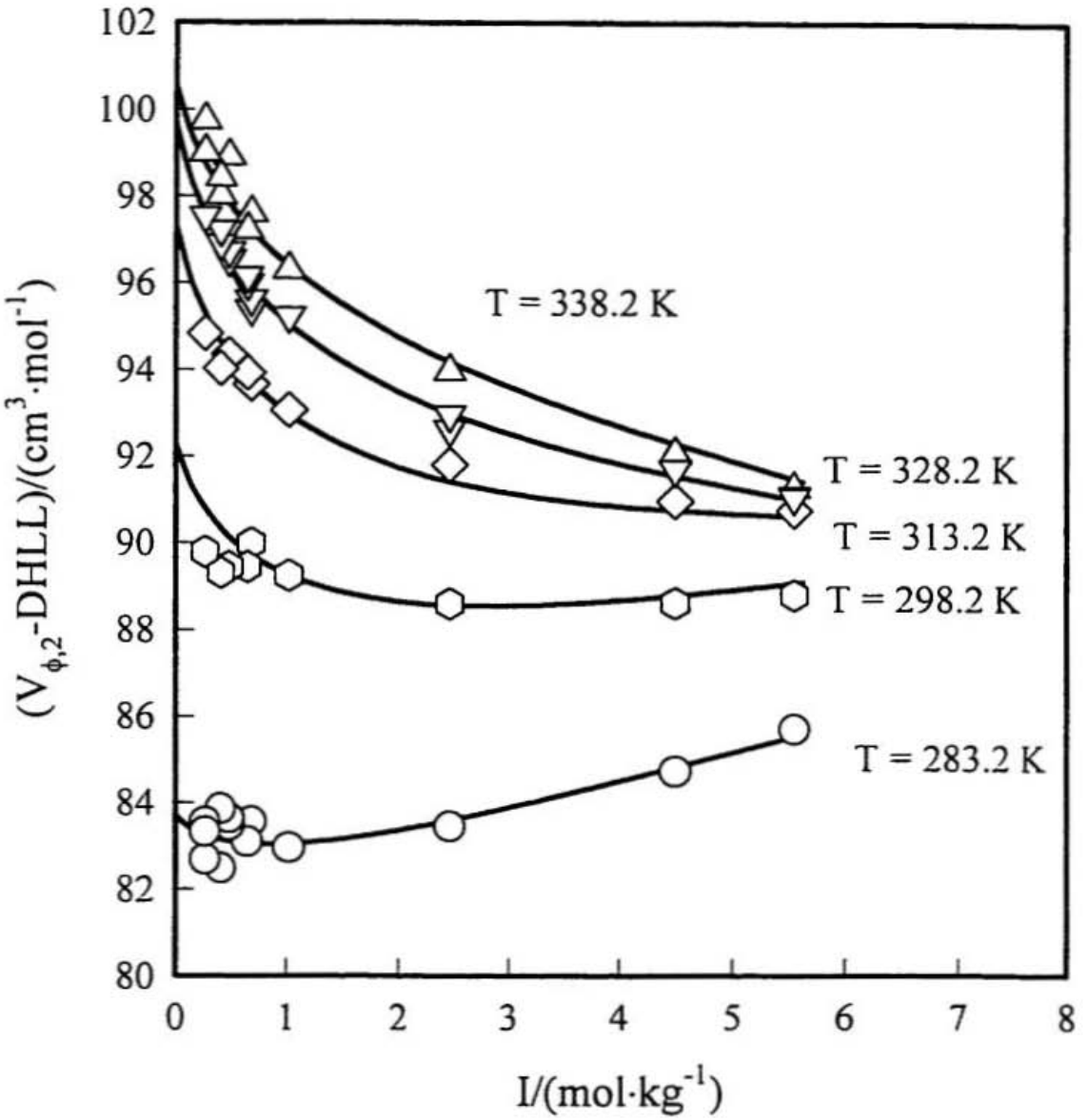


Figure IV.8. The apparent molar volumes of $Gd(ClO_4)_3(aq)$, plotted as a function of ionic strength after subtracting the Debye-Hückel limiting law (DHLL) term according to equation (IV.3.4). The least square fits to equations (IV.3.4), (IV.3.7), and (IV.3.9) are shown as solid curves.

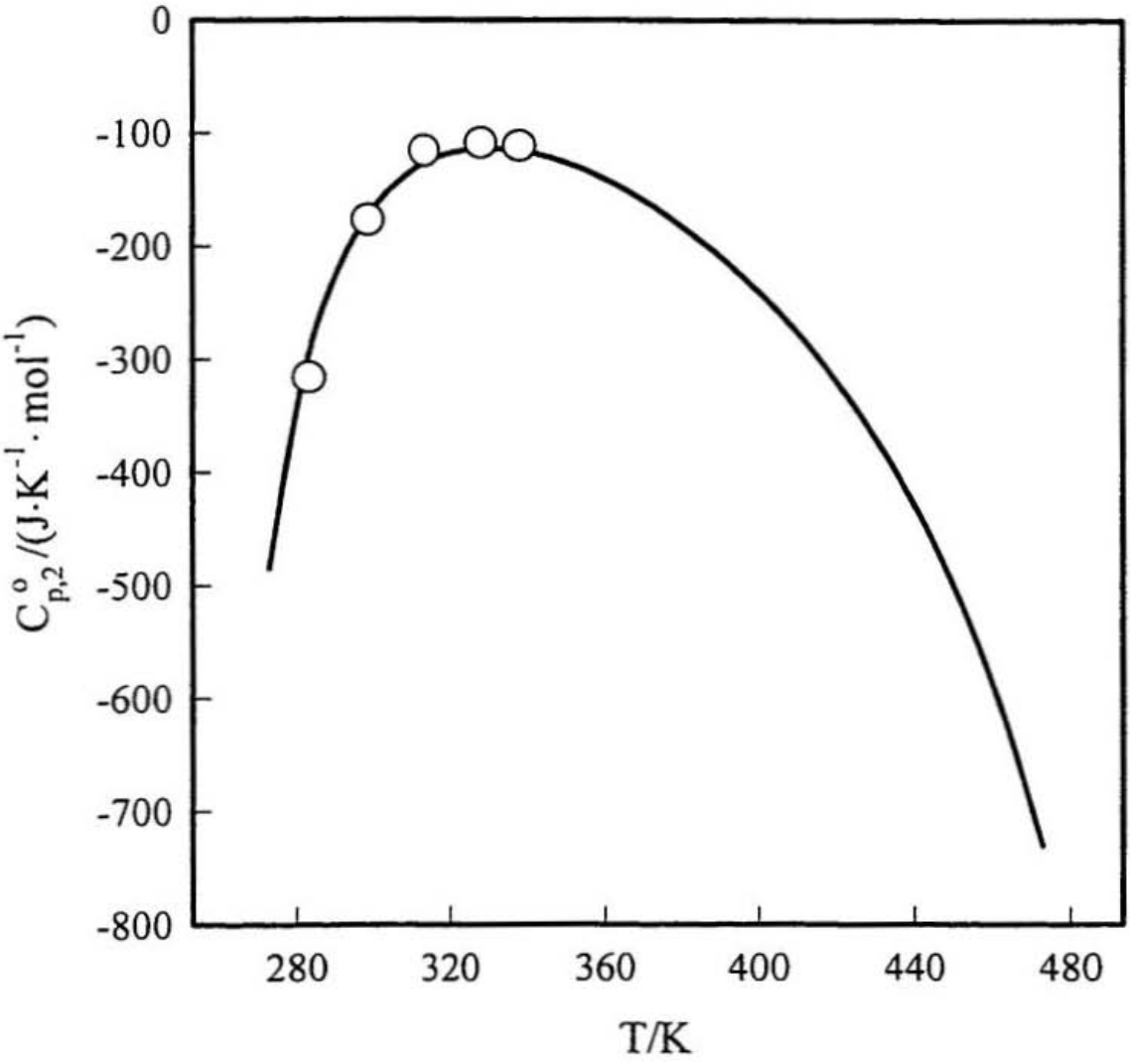


Figure IV.9. The standard partial molar heat capacities of $La(ClO_4)_3(aq)$ obtained from fitting equation (IV.3.3) to the experimental data at each temperature (shown as circles), and the extrapolation to elevated temperatures by fitting the entire matrix of data to equation (IV.4.5) (shown as a solid curve).

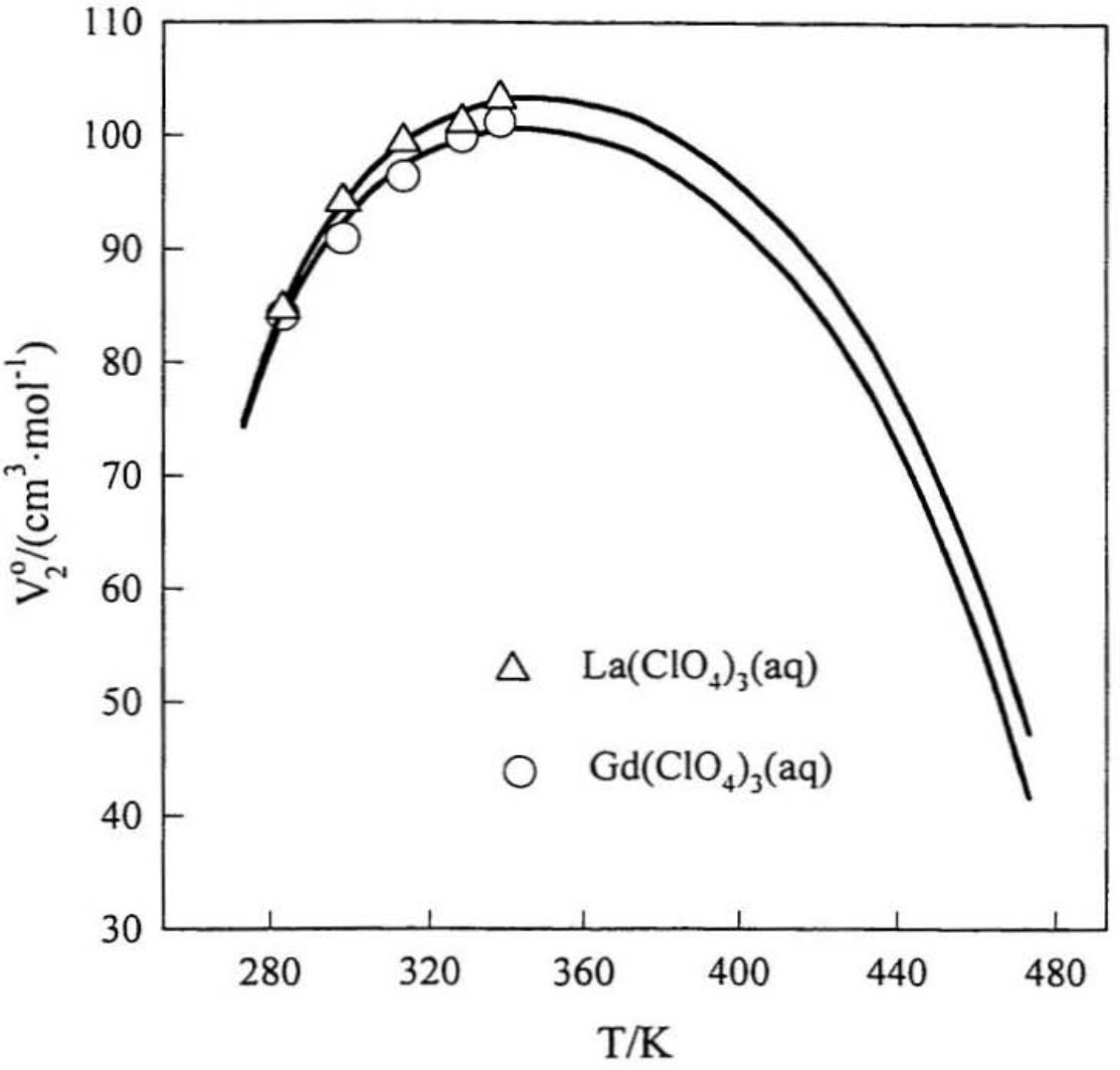


Figure IV.10. The standard partial molar volumes of $La(ClO_4)_3(aq)$ (shown as Δ) and $Gd(ClO_4)_3(aq)$ (shown as ○) obtained from fitting equation (IV.3.4) to the experimental data at each temperature, and the extrapolation to elevated temperatures by fitting the entire matrix of data to equation (IV.3.9) (shown as solid curves).

IV.4 DISCUSSION

IV.4.1 Literature Comparisons

The apparent molar heat capacities of aqueous $La(ClO_4)_3$ and $Gd(ClO_4)_3$ at T = 298.15 K from Spedding *et al.* (1975a) are compared with our results in figures IV.3 and IV.4. At m > 0.4 $mol \cdot kg^{-1}$, values for $C_{p,\phi,2}$ of both $Gd(ClO_4)_3(aq)$ and $La(ClO_4)_3(aq)$ agree with Spedding's results to within 5 $J \cdot K^{-1} \cdot mol^{-1}$. At lower molalities, these results deviate from our values by 5 to 10 $J \cdot K^{-1} \cdot mol^{-1}$. Consequently, values of $C^{\circ}_{p,2}$ calculated by extrapolating Spedding's data to infinite dilution are more negative than our results by about 25 $J \cdot K^{-1} \cdot mol^{-1}$ and 43 $J \cdot K^{-1} \cdot mol^{-1}$ for $La(ClO_4)_3$ and $Gd(ClO_4)_3$, respectively. The values of $C_{p,\phi,2}(LaCl_3, aq)$ are compared with Spedding's data in the figure IV.3. Our values for $C_{p,\phi,2}$ ($LaCl_3$,aq) agree to within 1 $J \cdot K^{-1} \cdot mol^{-1}$ with the values reported by Spedding *et al.* (1975b). Both sets appear to be more negative than those of Spitzer *et al.* (1979), which are at lower concentrations, by about 5 $J \cdot K^{-1} \cdot mol^{-1}$. The value $C^{\circ}_{p,2}(LaCl_3$, aq) = -478.6 $J \cdot K^{-1} \cdot mol^{-1}$ obtained by extrapolating our data to m = 0 by the Pitzer equation (IV.3.3) differs from the value of -465 $J \cdot K^{-1} \cdot mol^{-1}$ reported by Spitzer *et al.*(1979). The values of $V_{\phi,2}$ of both $La(ClO_4)_3(aq)$ and $Gd(ClO_4)_3(aq)$ agree with Spedding's results (Spedding *et al.*, 1975c) at T = 298.15 K to within about 1.5 $cm^3 \cdot mol^{-1}$ over the molality range of our experiments. Our results for $V_{\phi,2}$ of $LaCl_3(aq)$ at T = 298.2 K and T = 328.2 K are plotted in figure IV.4. These agree with Spedding *et al.* (1966d) and Isona (1984) within 0.2 $cm^3 \cdot mol^{-1}$. Our measurements yield $V^{\circ}_2(LaCl_3$, aq) = 14.71 $cm^3 \cdot mol^{-1}$ which is

quite good agreement with the value 14.6 $cm^3 \cdot mol^{-1}$ reported by Spitzer *et al.* (1979).

The sharp curvature in the Debye-Hückel corrected plots at low concentrations (figures IV.1-8) was found in both the Pitzer treatment reported here, and in an analysis with the Guggeheim equations for $AlCl_3$(aq) (Hovey and Tremaine, 1986). This behaviour may arise from the neglect of higher order terms in the limiting law, which are important for asymmetrical electrolytes (Cassel and Wood, 1974; Friedman and Krishnan, 1974). Pitzer (1991) treats this problem through higher order ion-interaction parameters. The approach works well for activity coefficients (Roy *et al.*, 1983), but may be less valid for enthalpy, heat capacity and volume. Equations (IV.3.3) to (IV.3.8) are successful in representing the concentration-dependence of our data to within the experimental uncertainty, and the extrapolated values at infinite dilution, $C^{\circ}_{p,2}$ and V°_2 are consistent with those of other workors.

The standard partial molar properties of La^{3+}(aq) and Gd^{3+}(aq) can be calculated from the results in table IV.1 on the basis of the usual convention ($C^{\circ}_{p,2}(H^+) \equiv 0$, $V^{\circ}_2(H^+) \equiv 0$) and these are listed in table IV.4. Taking V°_2 of Cl^-(aq) at temperatures 298.15 K, 313.15 K and 323.15 K from the fitting equation reported by Pogue and Atkinson (1988), and that of ClO_4^-(aq) from Hovey *et al.* (1988), the V°_2 of $La(ClO_4)_3$ and $LaCl_3$ yield two sets of values for $V^{\circ}_2(La^{3+}, aq)$. The agreement is within 1 $cm^3 \cdot mol^{-1}$ at these three temperatures. To check the self-consistency between $V^{\circ}_2(LaCl_3, aq)$ and

Table IV.4. Standard state properties of aquo-ions from 283.2 K to 338.2 K.

	V°_{2}/(cm^3·mol^{-1})				
T/K	Cl^-(aq)[a]	ClO_4^-(aq)[b]	La^{3+}(aq)[c]	La^{3+}(aq)[d]	Gd^{3+}(aq)[d]
283.2	--	41.63	--	-40.21	-40.74
298.2	17.80	44.04	-38.69	-38.00	-41.21
313.2	17.97	46.24	-39.93	-39.36	-42.38
328.2	17.74	47.31	-39.83	-40.83	-42.13
338.2	--	47.95	--	-40.66	-42.69
	$C^{\circ}_{p,2}$/(J·K^{-1}·mol^{-1})				
T/K	Cl^-(aq)[a]	ClO_4^-(aq)[b]	La^{3+}(aq)[c]	La^{3+}(aq)[d]	Gd^{3+}(aq)[d]
283.2	-149.47	-62.30	-101.5	-128.8	-87.0
298.2	-126.23	-24.68	-99.9	-102.8	-73.6
313.2	-114.76	-10.22	-75.7	-85.0	-87.5
328.2	-110.17	-4.58	-79.7	-95.2	-87.7
338.2	-109.53	-3.40	-83.0	-101.4	-93.1

[a] Hovey *et al.* (1988); [b] Tremaine *et al.* (1986); [c] calculated from measurements on $LaCl_3$(aq); [d] calculated from measurements on $La(ClO_4)_3$(aq) or $Gd(ClO_4)_3$(aq).

$V^{\circ}_{2}(La(ClO_4)_3, aq)$, we plot the values of $\{V^{\circ}_{2}(Cl^-, aq) - V^{\circ}_{2}(ClO_4^-, aq)\}$ from different sources in figure IV.11. The values of $\{V^{\circ}_{2}(Cl^-, aq) - V^{\circ}_{2}(ClO_4^-, aq)\}$ calculated from our results for aqueous $LaCl_3$ and $La(ClO_4)_3$ agree well with those calculated for the results for HCl(aq) and $HClO_4$(aq) reported by Pogue and Atkinson (1988) and Herrington *et al.* (1985).

Temperature-dependent values for $C^{\circ}_{p,2}(Cl^-, aq)$ and $C^{\circ}_{p,2}(ClO_4^-, aq)$ have been reported from Tremaine's laboratory (Hovey *et al.*, 1988; Tremaine *et al.*, 1986) and by Pogue and Aktinson (1988). There are significant differences between these two sets. These differences are magnified when used to calculate $C^{\circ}_{p,2}(M^{3+}, aq)$ from values for the 3:1 electrolytes. The values for $C^{\circ}_{p,2}(M^{3+})$ in table IV.3 are based on $C^{\circ}_{p,2}(Cl^-, aq)$ from Tremaine *et al.* (1986) and $C^{\circ}_{p,2}(ClO_4^-, aq)$ from Hovey *et al.* (1988). The resulting value for $C^{\circ}_{p,2}(La^{3+}, aq)$ at T = 298.15 K from $La(ClO_4)_3$(aq) is in reasonable agreement with that from $LaCl_3$(aq), but the values from both salts differ by up to 28 $J \cdot K^{-1} \cdot mol^{-1}$ at other temperatures. The probable sources of the discrepancy are complexation between La^{3+}(aq) and Cl^-(aq) and the accumulation of the uncertainties associated with the values $C^{\circ}_{p,2}$ for $LaCl_3$(aq), $La(ClO_4)_3$(aq), HCl(aq) and $HClO_4$(aq). The heat capacities reported by Pogue and Atkinson (1988) give a much larger disagreement. While the values in table IV.3 lie within the combined experimental uncertainty, more accurate values for $C^{\circ}_{p,2}(Cl^-, aq)$ and $C^{\circ}_{p,2}(ClO_4^-, aq)$ are needed at temperatures other than 298.15 K. Values of $\{C^{\circ}_{p,2}(Cl^-, aq) - C^{\circ}_{p,2}(ClO_4^-, aq)\}$ from our laboratory (Hovey *et al.*, 1988), Pogue and

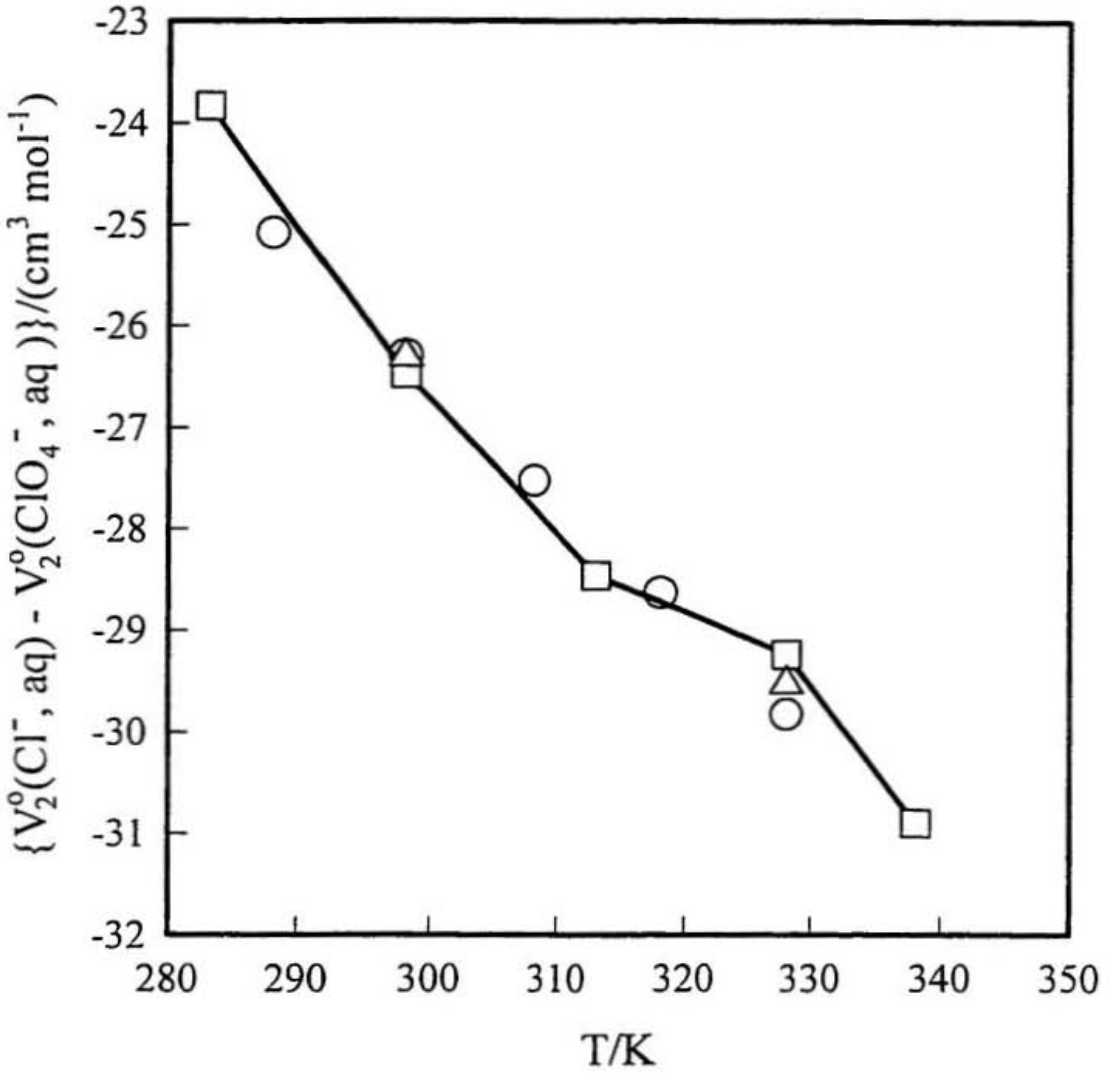


Figure IV.11. Comparison of the differences in V_2° for $Cl^-(aq)$ and $ClO_4^-(aq)$ from different sources. ○, calculated from $V_2^\circ(HCl, aq)$ (Pogue *et al.*, 1988) and $V_2^\circ(HClO_4, aq)$ (Pogue *et al.*, 1988); Δ, calculated from $V_2^\circ(HCl, aq)$ (Pogue *et al.*, 1988) and $V_2^\circ(HClO_4, aq)$ (Herrington *et al.*, 1985); □, calculated from $V_2^\circ(LaCl_3, aq)$ and $V_2^\circ(La(ClO_4)_3, aq)$, this work.

Atkinson (1988), and Mastroianni and Criss (1972) are plotted in figures IV.12. While all four sets agree with each other at T = 298.15 K, the disagreement at other temperatures is significant. Values calculated from $C^{\circ}_{p,2}$(NaCl, aq) (Archer, 1992) and $C^{\circ}_{p,2}$($NaClO_4$, aq) (Mastroianni and Criss, 1972) support our results at the lowest and highest temperatures studied, but new experimental measurements are clearly needed. The major uncertainties appear to lie with results for the perchlorates.

IV.4.2 Extrapolation to Elevated Temperatures

In recent years, the geochemical community has made much use of the semi-empirical extended Born model for ionic hydration proposed by Helgeson, Kirkham and Flowers (Helgeson and Kirkham, 1976; Helgeson, Kirkham, and Flower, 1981; Tanger and Helgeson, 1988; Shock and Helgeson, 1988). In the revised "HKF" model (Tanger and Helgeson, 1988), V°_2 of an aqueous electrolyte is expressed as

$$V_2^{\circ} = a_1 + a_2/(\psi + p) + \{a_3 + a_4/(\psi + p)\}/(T - \Theta) - \omega Q \,, \qquad \text{(IV.4.1)}$$

where Ψ=260 MPa and a_1, a_2, a_3 and a_4 are characteristic parameters for electrolytes, independent of temperature and pressure. This equation has been somewhat successful in reproducing the temperature and pressure dependence of experimental results. The following thermodynamic identity,

$$(\partial C^{\circ}_{p,2}/\partial p)_T = -T(\partial^2 V_2^{\circ}/\partial T^2)_p \,, \qquad \text{(IV.4.2)}$$

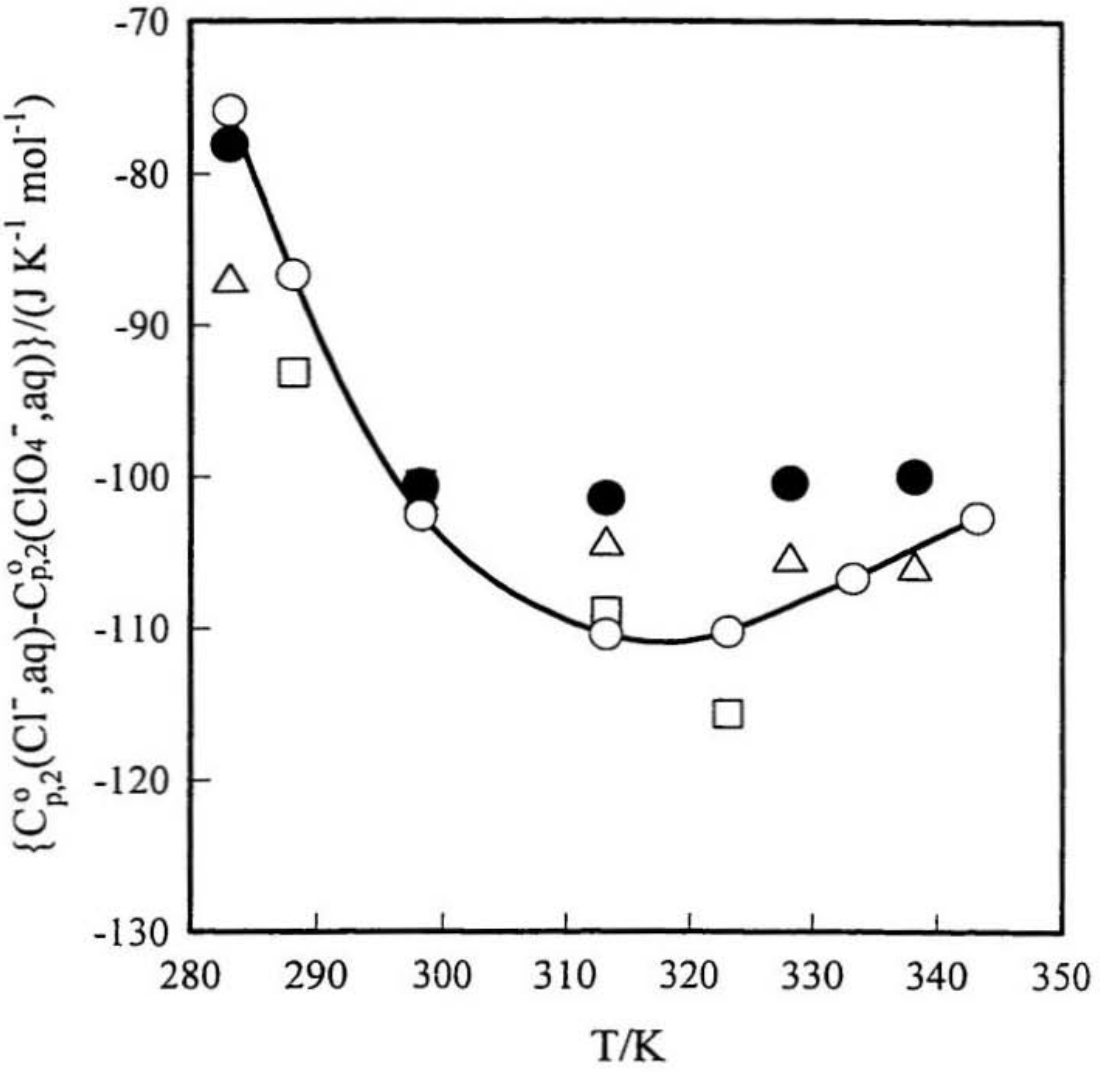


Figure 12. Comparison of the differences in $C^{\circ}_{p,2}$ for $Cl^-(aq)$ and $ClO_4^-(aq)$ from different sources. ●, calculated of $C^{\circ}_{p,2}(LaCl_3, aq)$ and $C^{\circ}_{p,2}(La(ClO_4)_4, aq)$, this work; ○ and —, calculated from $C^{\circ}_{p,2}(NaCl, aq)$ (Archer, 1992) and $C^{\circ}_{p,2}(NaClO_4, aq)$ (Mastroianni *et al.*, 1972); Δ, calculated from $C^{\circ}_{p,2}(HClO_4, aq)$ (Hovey *et al.*, 1988) and $C^{\circ}_{p,2}(HCl, aq)$ (Tremaine *et al.*, 1988); □, calculated from $C^{\circ}_{p,2}(HClO_4, aq)$ (Pogue *et al.*, 1988) and $C^{\circ}_{p,2}(HCl, aq)$ (Pogue *et al.*, 1988).

yields an expression for the temperature dependence of the standard partial heat capacity from the equation (IV.4.1),

$$C_{p,2}^{\circ}(T,p) = C_{p,2}^{\circ}(T,p_r) - [a_3(p-p_r) + a_4 \ln\{(\Psi+p)/(\Psi+p_r)\}]T/(T-\Theta)^3 + \omega TX + c(T), \quad \text{(IV.4.3)}$$

where p_r is the reference pressure, usually 100 kPa. The integration constant c(T) was empirically selected by Helgeson and his coworkers to be $c/(T-\Theta)^2$, in which c is independent of temperature and pressure, to give the isobaric expression for $C_{p,2}^{\circ}$ listed here as equation (IV.3.8). A simpler form of equation (IV.4.3) arises if we consider an integration constant of the form:

$$c(T) = -c'T/(T-\Theta)^3, \quad \text{(IV.4.4)}$$

so that isobaric expression for $C_{p,2}^{\circ}$ is given by

$$C_{p,2}^{\circ} = c_1 + c_2 T/(T-\Theta)^3 + \omega TX. \quad \text{(IV.4.5)}$$

The fitting parameters for equation (IV.3.8), as well as equation (IV.4.5), are listed in table IV.2. For both $Gd(ClO_4)_3$(aq) and $La(ClO_4)_3$(aq), equation (IV.4.5) gives better fit to the experimental values for $C_{p,2}^{\circ}$ than equation (IV.3.8). The standard deviations are 8.0 $J \cdot K^{-1} \cdot mol^{-1}$and 10.4 $J \cdot K^{-1} \cdot mol^{-1}$ for $Gd(ClO_4)_3$ and $La(ClO_4)_3$, respectively, when equation (IV.3.8) is used, and 3.2 $J \cdot K^{-1} \cdot mol^{-1}$ and 5.6 $J \cdot K^{-1} \cdot mol^{-1}$ for

$Gd(ClO_4)_3$ and $La(ClO_4)_3$, respectively, when equation (IV.4.5) is used.

Aqueous $GdCl_3$ and $AlCl_3$ are the only trivalent salts whose standard partial heat capacities have been reported at temperatures above 338 K (Jekel *et al.*, 1964; Conti *et al.*, 1992). In order to test the validity of the extrapolation model, values in table IV.3 were used to calculate the $C^{\circ}_{p,2}$ parameters for $GdCl_3$(aq) according to equations (IV.3.8) and (IV.4.5). The extrapolated values for $C^{\circ}_{p,2}$ are compared in figure IV.13 with those reported by Jekel *et al.* (1964). The largest difference between $C^{\circ}_{p,2}(GdCl_3, aq)$ from equation (IV.4.5) and the experimental values in the temperature range of 283 to 373 K is 25 $J \cdot K^{-1} \cdot mol^{-1}$. The agreement is well within the combined experimental uncertainties.

The high temperature behaviour of the $C^{\circ}_{p,2}$ function is dominated by the Born term and thus is heavily dependant on formula used for the effective radius. For these salts, the simple rule to obtain the effective radius for trivalent cations suggested by Helgeson *et al.* (1976, 1981) appears to adequate. Hovey and Tremaine (1988) also used the Helgeson effective radius and the HKF model to extrapolate the low temperature $C^{\circ}_{p,2}$ function of Al^{3+}(aq) to elevated temperatures. Conti *et al.* (1992) recently measured $C^{\circ}_{p,2}$ of $AlCl_3$(aq) at T = (323 K, 373 K and 423 K). Their results led to values of $C^{\circ}_{p,2}$ at these temperatures which agree closely with the extrapolated results (Conti *et al.*, 1992; Tremaine and Xiao, 1996).

A detailed evaluation of limitations in the Born equation has been reported by Wood *et al.* (1994). Although the success of the model is fortuitous, the classical Born

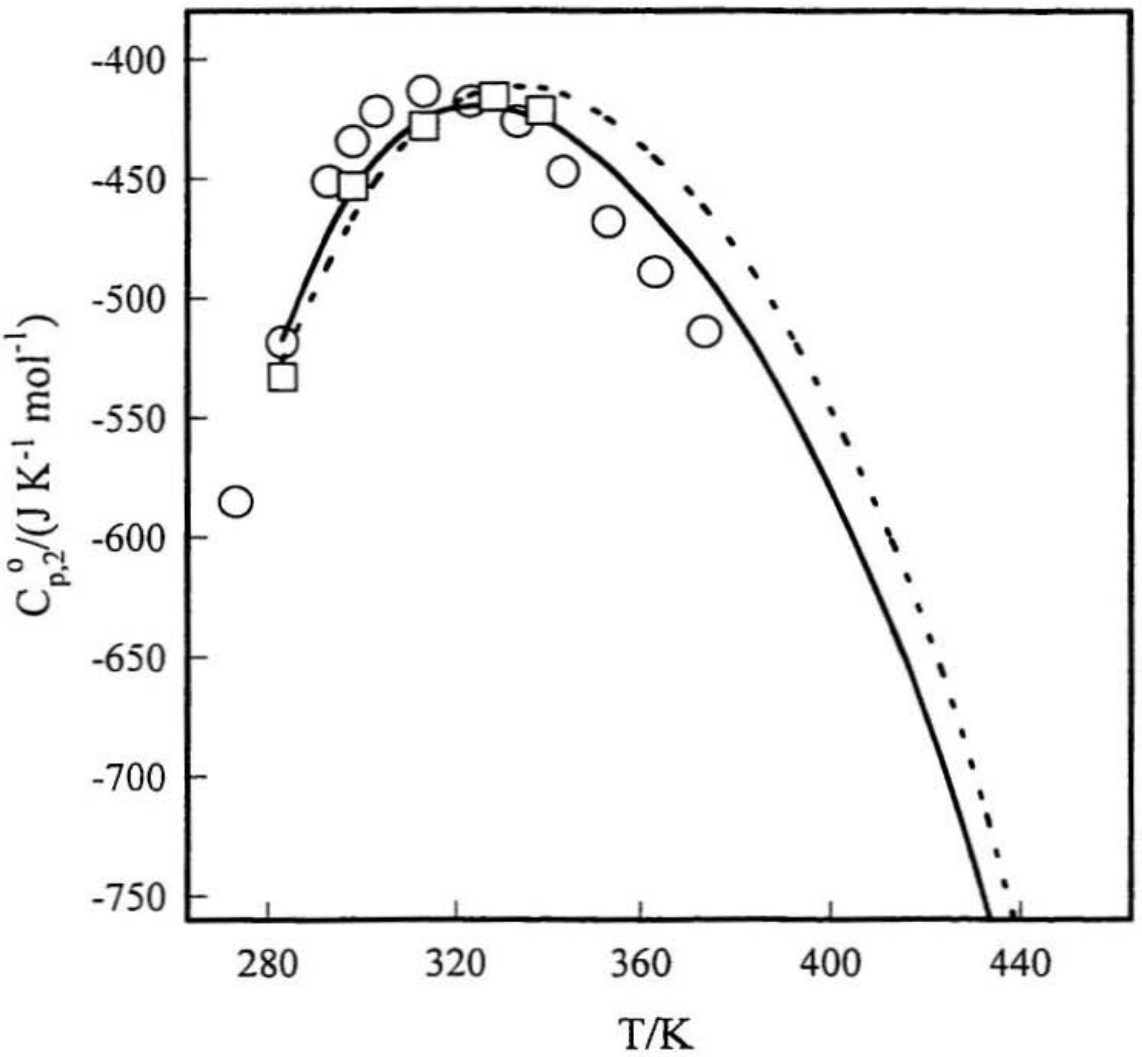


Figure IV.13. Comparison of the standard partial molar heat capacities of $GdCl_3(aq)$ calculated from the standard partial molar heat capacities of $Gd(ClO_4)_3(aq)$ which are predicted by both equation (IV.3.8) and equation (IV.3.9) with the experiment data. Dash line, equation (IV.3.8); solid line equation (IV.4.5); ○, Jekel *et al.* (1964); □, this work.

equation yields radial distribution functions beyond the primary coordination sphere that are approximately consistent with those from molecular dynamics simulations up to about T = 573 K. The results presented here suggest that equations (IV.3.8) and (IV.4.5) are useful pragmatic tools for predicting temperature-dependent heat capacity functions for M^{3+}(aq) ions over an extended range of temperature.

The steep curvature in $C^{\circ}_{p,2}$ and V°_{2} at T < 298.15 K is attributed to hydrogen-bonding effects, represented by the empirical "non-Born" terms in equation (IV.3.8) and (IV.4.5). The temperature-dependence of $C^{\circ}_{p,2}$ for $La(ClO_4)_3$(aq) and $Gd(ClO_4)_3$(aq) T < 298 K is less pronounced than that observed for $FeCl_3$(aq) (Hovey, 1988) and $AlCl_3$(aq) (Hovey *et al.*, 1986). Neutron and X-ray scattering studies (Ohtaki and Radnai, 1993) revealed significant differences between the La^{3+}(aq) and Gd^{3+}(aq) ions with hydration numbers of 9 and 8, respectively, and those of Al^{3+}(aq) and Fe^{3+}(aq), which have a well-defined hydration number of 6. More discussion about the hydration effects on $C^{\circ}_{p,2}$ will be given in the next chapter.

The form of equations (IV.3.6) and (IV.3.7) for the temperature dependence of the ß parameters is purely empirical and, thus, temperature-dependent Pitzer parameters from the global fitting procedure may have limited validity beyond the experimental temperature range of 283 to 338 K. In figures IV.14 and IV.15, the values of $ß^{(i)J}$ and $ß^{(i)v}$ are compared with the functions fitted to equations (IV.3.6) and (IV.3.7) with the global fitting parameters. Clearly, experimental measurements extending to temperatures well

above 338 K are needed to unambiguously determine the temperature-dependence of the β parameters in this model.

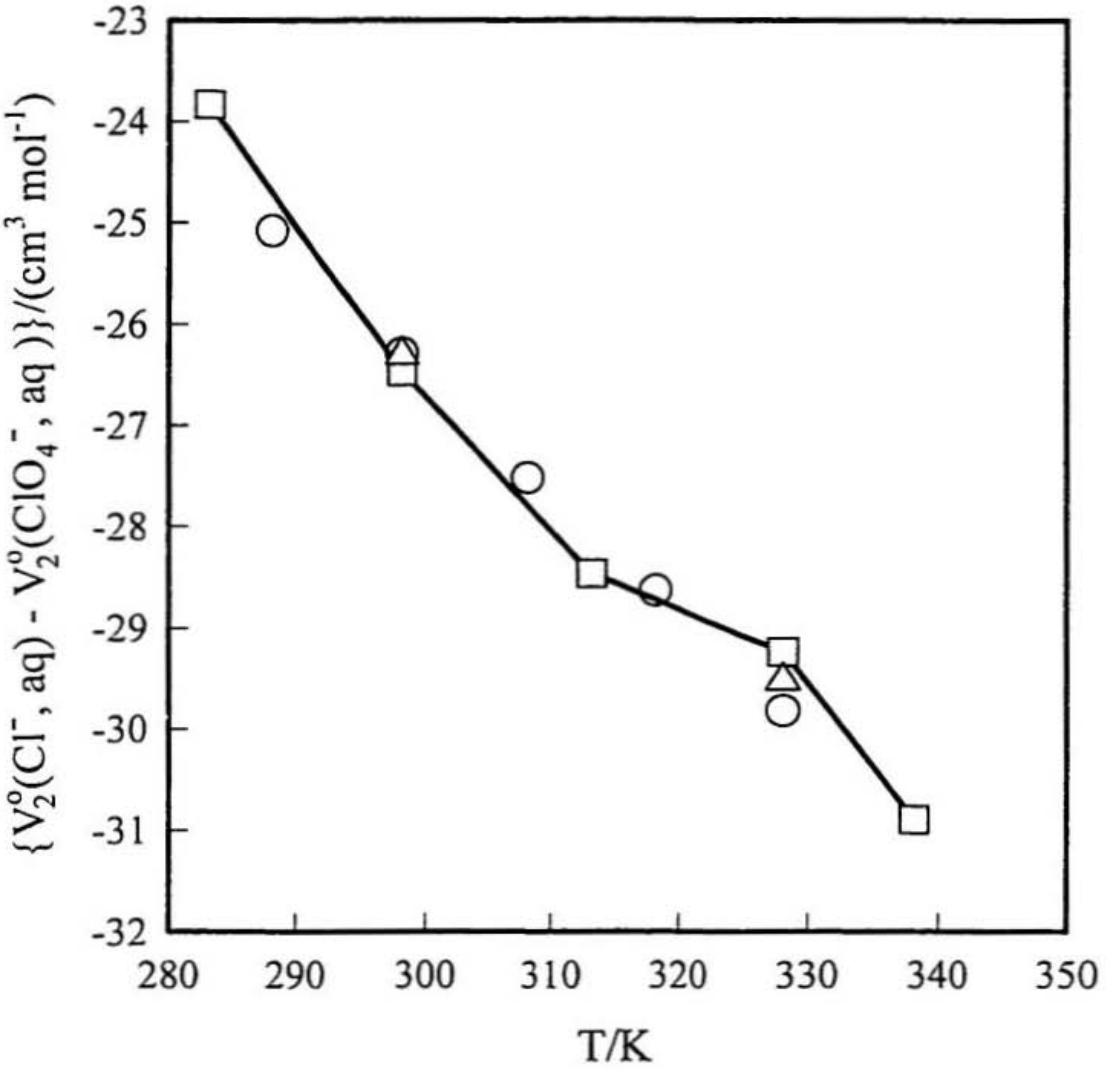


Figure V.14. The temperature dependence of Pitzer's parameters $\beta^{(1)J}$ and $\beta^{(0)J}$ in quation (IV.3.3). The circles are the results obtained by fitting equation (IV.3.3) to experimental data at each temperature. The solid line shows the results from fitting equations (IV.3.3), (IV.3.6), and (IV.4.5) to the entire matrix of experimental data from 283.2 K to 338.2 K.

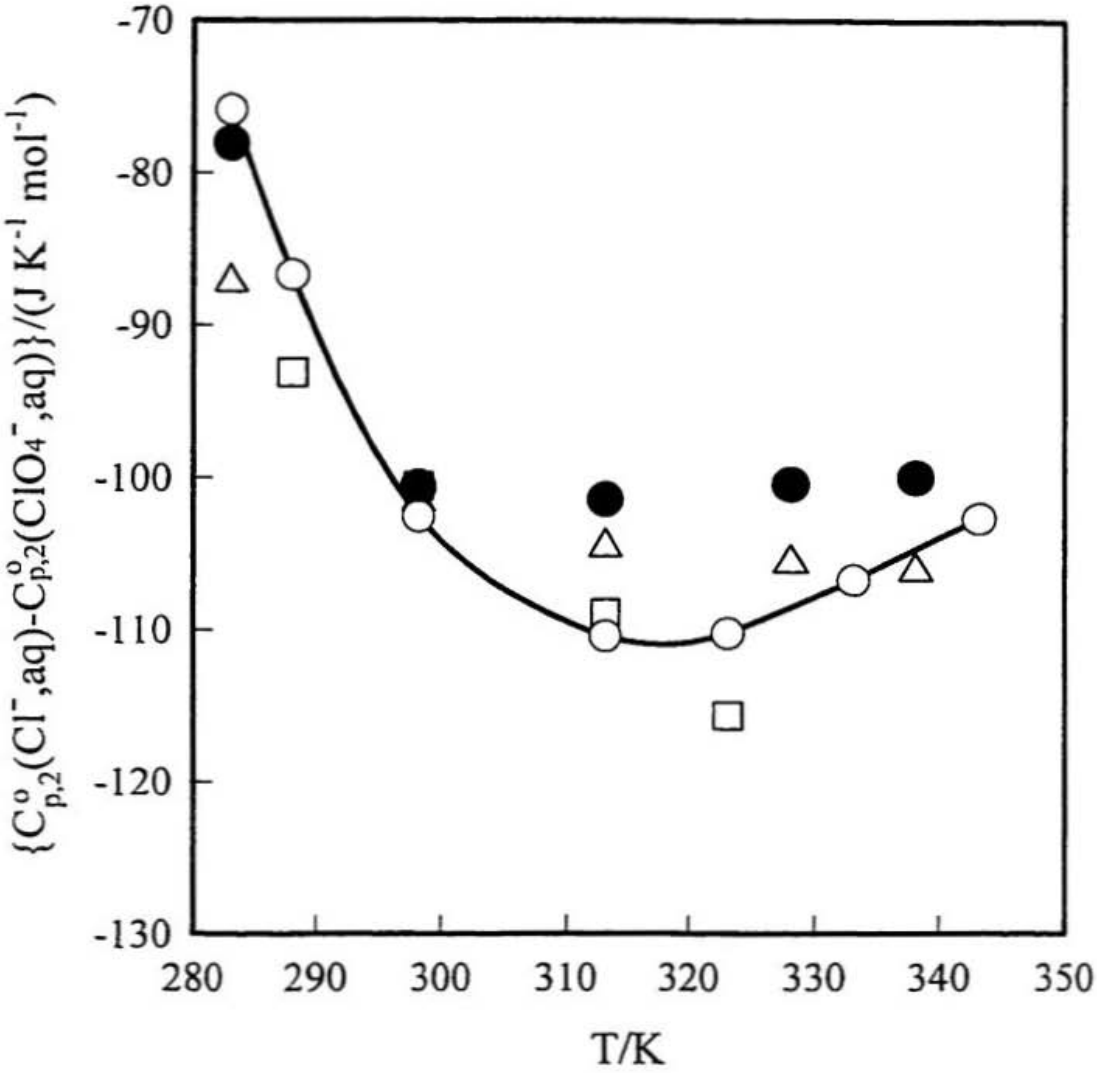


Figure V.15. The temperature dependence of Pitzer's parameters $\beta^{(1)v}$ and $\beta^{(0)v}$ in equation (IV.3.4). The circles are the results obtained by fitting equation (IV.3.4) to experimental data at each temperature. The solid line shows the results from fitting equations (IV.3.4), (IV.3.7), and (IV.3.9) to the entire matrix of experimental data from 283.2 K to 338.2 K.

Chapter V. Apparent Molar Heat Capacities and Volumes of $Nd(ClO_4)_3(aq)$, $Eu(ClO_4)_3(aq)$, $Er(ClO_4)_3(aq)$ and $Yb(ClO_4)_3(aq)$ from the Temperatures 283 K to 328 K

V.1 Introduction

In the previous chapter, apparent molar heat capacities $C_{p,\phi,2}$ and apparent molar volumes $V_{\phi,2}$ were reported for $LaCl_3(aq)$, $La(ClO_4)_3(aq)$, and $Gd(ClO_4)_3(aq)$ at temperatures in the range 283 K ≤ T ≤ 338 K. In this chapter, we report values of $C_{p,\phi,2}$ and $V_{\phi,2}$ for four other lanthanide perchlorates, $Nd(ClO_4)_3(aq)$, $Eu(ClO_4)_3(aq)$, $Er(ClO_4)_3(aq)$, and $Yb(ClO_4)_3(aq)$ at the temperatures T = (283.2, 298.2, 313.2 and 328.2 K).

Lanthanide perchlorates $Ln(ClO_4)_3(aq)$ serve as model systems, useful in understanding the thermodynamic properties of aqueous trivalent cations. The trivalent lanthanide cations from La^{3+} to Lu^{3+} are characterized by the progressive filling of the 4f orbital. The ionic radii decrease regularly across this series as the number of 4f electrons is increased, due to the lanthanide contraction effect. Although their chemical and physical properties are believed to be predominantly electrostatic in nature, and thus are determined by size differences, many structural and thermodynamic studies indicate that some properties of $Ln^{3+}(aq)$ do not vary smoothly along the series (Spedding *et al.*, 1966a, 1966b, 1966d, 1975a, 1975b; Rard and Spedding, 1985; Cossy and Merbach, 1988; Kanno and Hiraishi, 1980). This phenomenon has been interpreted as reflecting a

change in the number of water molecules in the primary coordination sphere of these ions, the so-called "gadolinium break" (Rard, 1985; Rizkalla and Choppin, 1991). Generally, it is believed that lanthanide cations from $La^{3+}(aq)$ to $Nd^{3+}(aq)$ have a hydration number of approximately nine while those from $Tb^{3+}(aq)$ to $Lu^{3+}(aq)$ have a hydration number of eight. Both $Eu^{3+}(aq)$ and $Gd^{3+}(aq)$ are thought to have an intermediate value, representing an equilibrium mixture of these two hydration numbers (Rizkalla and Choppin, 1991; Choppin, 1971; Ohtaki and Radnai, 1993).

The behaviour of the standard partial molar heat capacities $C^{\circ}_{p,2}$ and volumes V°_{2} is dominated by configurational hydration effects ("structural" effects) at temperatures near 298.15 K, and by long-range solvent polarization ("field") effects at high temperatures (Cobble and Murray, 1981). Thus, the values for $C^{\circ}_{p,2}$ and V°_{2} of aqueous ions at high temperatures are determined primarily by their size and charge (Corti, 1992; Wood *et al.*, 1994). Accurate measurements of $C_{p,\phi,2}$ and $V_{\phi,2}$ for the aqueous lanthanide perchlorates near ambient conditions are needed to further our understanding of the solvation of trivalent cations under conditions where configurational hydration effects are important.

V.2 Experimental

Standard solutions of $Nd(ClO_4)_3(aq)$, $Eu(ClO_4)_3(aq)$, $Er(ClO_4)_3(aq)$, and $Yb(ClO_4)_3(aq)$ were prepared from the oxides (Aldrich, mass fraction: 0.999) with a small excess of acid to prevent hydrolysis, by the same procedure described in our previous

chapter. The concentrations of the stock solutions were ~ 0.7 mol·kg^{-1} with a final pH = 3. Less concentrated solutions were prepared by diluting the stock solution with water and perchloric acid by mass. A second set of solutions of $Eu(ClO_4)_3(aq)$ was prepared by diluting the stock solution with water only. The pH of the second set varied from pH = 3 for the most concentrated solution, to pH = 5.3 for the most dilute solution. The concentrations of $HClO_4(aq)$ were determined by titration with tris(hydroxy methyl)aminomethane (TRIS) using methyl red as indicator. The concentrations of the lanthanide salts were determined by titration with ethylene diaminetetraacetic acid (EDTA) using xylenol orange as indicator and methenamine to buffer the solution. Other experimental procedures are identical to those described in our previous chapter.

V.3 Results

The experimentally determined relative densities ($\rho - \rho_1^*$) and massic heat capacity ratios $\{(c_p \cdot \rho / c_{p,1}^* \cdot \rho_1^*) - 1\}$ at each of the experimental temperatures are listed in tables A.V.1 to A.V.3. Tables A.V.1 and A.V.3 also give the experimental apparent molar volumes $V_{\phi,2}$ and apparent molar heat capacities $C_{p,\phi,2}$ which were calculated from these results using densities and specific heat capacities of pure water taken from Hill (1990). By definition,

$$Y_\phi = \{Y(sln) - 55.509 Y_1^*\}/(m_2 + m_3), \qquad \text{(V.3.1)}$$

where Y_1^* is the molar heat capacity or molar volume of pure $H_2O(l)$, and m_2 and m_3 are the molalities of the salt and perchloric acid, respectively. The effect of the small amount of excess acid was subtracted by the same procedure described in Chapter IV. The resulting values of $C_{p,\phi,2}$ and $V_{\phi,2}$ are also tabulated in tables A.V.1 to A.V.3.

The Pitzer ion interaction model (Pitzer, 1992) was used to treat the molality dependance of $C_{p,\phi,2}$ and $V_{\phi,2}$. At molalities below 1 mol·kg^{-1}, the ternary interaction parameters are not needed. Thus, the equations for representing the experimental apparent molar heat capacities and volumes were the following:

$$C_{p,\phi,2} = C_{p,2}^{o} + (6A_J/b)\ln(1 + bI^{1/2}) - 6RT^2 m\beta^{(o)J} - 12RT^2\beta^{(1)J}f(I), \qquad (V.3.2)$$

and

$$V_{\phi,2} = V_2^{o} + (6A_V/b)\ln(1 + bI^{1/2}) + 6RTm\beta^{(o)V} + 12RT\beta^{(1)V}f(I), \qquad (V.3.3)$$

where b = 1.2 kg$^{1/2}$·mol$^{-1/2}$. The terms A_J in equation (V.3.2) and A_V in equation (V.3.3) are the Debye-Hückel limiting slopes for the apparent molar heat capacity and the apparent molar volume, respectively, whose values were taken from the compilation by Pitzer (1992). Here, f(I) is given by

$$f(I) = \{1 - [(1 + aI^{1/2})\exp(-aI^{1/2})]\}/(a^2 I), \qquad (V.3.4)$$

where a = 2.0 kg$^{1/2}$·mol$^{-1/2}$. The expressions used to describe the temperature dependence

of the β parameters are the same as those in Chapter IV:

$$\beta^{(0)J} = (c_3/T) + c_4 + c_5 T, \qquad \text{(V.3.5)}$$

$$\beta^{(1)J} = (c_6/T) + c_7 + c_8 T, \qquad \text{(V.3.6)}$$

$$\beta^{(0)V} = v_3 + v_4 T, \qquad \text{(V.3.7)}$$

and

$$\beta^{(1)V} = (v_5/T) + v_6 + v_7 T. \qquad \text{(V.3.8)}$$

By definition, $C^{\circ}_{p,2}$ and V°_2 are the standard partial molar heat capacity and standard partial molar volume, respectively. The temperature dependence of $C^{\circ}_{p,2}$ and V°_2 was modelled by the Helgeson-Kirkham-Flowers ("HKF") equations, as revised by Tanger and Helgeson (1988). At constant pressure, these take the form:

$$C^{\circ}_{p,2} = c_1 + \{c_2/(T-\Theta)^2\} + \omega T X, \qquad \text{(V.3.9a)}$$

$$V^{0}_{2} = v_1 + \{v_2/(T-\Theta)\} - \omega Q. \qquad \text{(V.3.10)}$$

Here, c_1, c_2, v_1, and v_2 are species-dependent fitting parameters, and Θ = 228 K is a

solvent-dependent parameter associated with the anomolous behavior of supercooled water (1988). The terms ωTX and ωQ are the electrostatic contributions to the standard partial molar heat capacity and standard partial molar volume according to the Born equation, where X and Q are functions of the temperature and pressure derivatives of the static dielectric constant of water, and ω is a function of the ionic charge Z and an effective ionic radius r_e. The values for X and Q were taken from Helgeson and Kirkham (1976) and the values of ω for the lanthanide perchlorates were taken from Shock and Helgeson (1988).

An alternative non-Born term for the standard partial molar heat capacity was successfully used in our previous treatment of the temperature dependence of $C^{o}_{p,2}$. With this non-Born term, the expression for the standard partial molar heat capacity is written as:

$$C^{o}_{p,2} = c_1 + \{c_2 T/(T-\Theta)^3\} + \omega TX. \qquad \text{(V.3.9b)}$$

Equations (V.3.2) and (V.3.3) were fitted to the experimental results at each temperature by the Marquardt-Levenberg algorithm in the commercial software package SigmaPlot©. The fitted values for the βs and standard partial molar properties from the isothermal fits are listed in table V.1. The entire array of values at all temperatures and molalities was then used to optimize the parameters in equations (V.3.2) to (V.3.9). The fitted parameters are listed in tables V.2 and V.3, and the fitted expressions are plotted in

Table V.1. Values of parameters from the Pitzer ion-interaction model for aqueous $Nd(ClO_4)_3$, $Eu(ClO_4)_3$, $Er(ClO_4)_3$, $Yb(ClO_4)_3$ from the isothermal least square fits[a]

T/K	V_2^o [b]	$RT\beta^{(0)V}$ [c]	$RT\beta^{(1)V}$ [c]	$C^0_{p,2}$ [d]	$RT^2\beta^{(0)J}$ [e]	$RT^2\beta^{(1)J}$ [e]
			$Nd(ClO_4)_3$			
283.2	80.63(0.7)	1.459	-11.52	-317.0(8.0)	-21.07	-15.17
298.2	88.55(0.2)	0.4465	-8.553	-185.9(3.0)	-10.96	115.0
313.2	93.60(0.2)	0.02948	-9.975	-126.7(6.2)	-4.515	191.8
328.2	96.34(0.4)	-0.3965	-10.03	-124.80(2.2)	1.935	192.10
			$Eu(ClO_4)_3$			
283.2	82.95(0.8)	0.3141	-1.078	-277.9(3.1)	-16.29	-33.71
298.2	91.02(0.2)	0.2337	-9.307	-157.4(6.1)	-6.426	87.08
313.2	95.24(0.2)	-0.3285	-8.022	-97.60(3.5)	-3.929	211.5
328.2	97.97(0.2)	-0.6642	-9.083	-119.5(1.4)	2.853	155.9
			$Er(ClO_4)_3$			
283.2	77.63(0.6)	0.7226	1.092	-274.0(4.8)	-18.92	-35.81
298.2	89.51(0.2)	0.3647	-8.608	-142.3(2.6)	-5.333	70.81
313.2	94.43(0.2)	-0.0572	-9.852	-101.7(2.3)	-0.4457	134.9
328.2	97.61(0.9)	-0.4880	-11.47	-105.14(4.5)	4.807	146.53
			$Yb(ClO_4)_3$			
283.2	78.51(0.8)	0.9016	-3.076	-262.3(3.9)	-21.12	-8.415
298.2	87.88(0.1)	0.3344	-7.870	-137.9(2.8)	-7.634	91.99
313.2	93.08(0.3)	0.0082	-10.96	-94.11(2.1)	-2.779	173.9
328.2	96.04(0.3)	-0.2599	-13.73	-78.06(2.0)	0.9704	244.7

[a] the figures in parentheses are the standard deviations of the parameters.
[b] $cm^3 \cdot mol^{-1}$; [c] $cm^3 \cdot kg \cdot mol^{-2}$; [d] $J \cdot K^{-1} \cdot mol^{-1}$; [e] $J \cdot K^{-1} \cdot mol^{-2} \cdot kg$

Table V.2. The fitting parameters for equations (V.3.3), (V.3.7), (V.3.8) and (V.3.10) for the apparent molar volumes of aqueous $Nd(ClO_4)_3$, $Eu(ClO_4)_3$, $Er(ClO_4)_3$, and $Yb(ClO_4)_3$

Parameter	$Nd(ClO_4)_3$(aq)	$Eu(ClO_4)_3$(aq)	$Er(ClO_4)_3$(aq)	$Yb(ClO_4)_3$(aq)
v_1/($cm^3 \cdot mol^{-1}$)	1.394×10^{2}	1.357×10^{2}	1.450×10^{2}	1.393×10^{2}
v_2/($kg \cdot mol^{-1} \cdot K$)	-2.668×10^{4}	-2.212×10^{4}	-3.023×10^{4}	-2.672×10^{4}
v_3/($kg \cdot mol^{-1} \cdot MPa^{-1}$)	3.9318×10^{-3}	3.413×10^{-3}	2.657×10^{-3}	2.971×10^{-3}
v_4/($kg \cdot mol^{-1} \cdot K^{-1} \cdot MPa^{-1}$)	-1.248×10^{-5}	-1.126×10^{-5}	-8.463×10^{-6}	-9.379×10^{-6}
v_5/($kg \cdot mol^{-1} \cdot K \cdot MPa^{-1}$)	7.870×10^{1}	9.564×10^{1}	6.464×10^{1}	7.204×10^{1}
v_6/($kg \cdot mol^{-1} \cdot MPa^{-1}$)	-5.023×10^{-1}	-6.244×10^{-1}	-3.857×10^{-1}	-4.474×10^{-1}
v_7/($kg \cdot mol^{-1} \cdot K^{-1} \cdot MPa^{-1}$)	7.863×10^{-4}	1.007×10^{-3}	5.587×10^{-4}	6.790×10^{-4}

Table V.3. The fitting parameters for equations (V.3.2), (V.3.5), (V.3.6) and (V.3.9) for the apparent molar heat capacities of aqueous $Nd(ClO_4)_3$, $Eu(ClO_4)_3$, $Er(ClO_4)_3$, and $Yb(ClO_4)_3$

Parameters	$Nd(ClO_4)_3$(aq)	$Eu(ClO_4)_3$(aq)	$Er(ClO_4)_3$(aq)	$Yb(ClO_4)_3$(aq)
		Equation (V.3.9b)		
c_1/(J·K^{-1}·mol^{-1})	1.587×10^{2}	1.747×10^{2}	1.945×10^{2}	2.151×10^{2}
c_2/(J·K·mol^{-1})	-1.628×10^{5}	-1.414×10^{5}	-1.550×10^{5}	-1.645×10^{5}
c_3/(kg·mol^{-1}·K^{-1})	-5.029×10^{-1}	-1.053×10^{0}	-7.871×10^{-1}	-5.886×10^{-1}
c_4/(kg·mol^{-1}·K^{-2})	3.017×10^{-3}	6.664×10^{-3}	4.934×10^{-3}	3.632×10^{-3}
c_5/(kg·mol^{-1}·K^{-3})	-4.510×10^{-6}	-1.053×10^{-5}	-7.716×10^{-6}	-5.602×10^{-6}
c_6/(kg·mol^{-1}·K^{-1})	-2.170×10^{0}	2.211×10^{0}	7.071×10^{-1}	-2.327×10^{0}
c_7/(kg·mol^{-1}·K^{-2})	1.365×10^{-2}	-1.504×10^{-2}	-5.724×10^{-3}	1.384×10^{-2}
c_8/(kg·mol^{-1}·K^{-3})	-2.090×10^{-5}	2.600×10^{-5}	1.146×10^{-5}	-1.980×10^{-5}
		Equation (V.3.9a)[a]		
c_1/(J·K^{-1}·mol^{-1})	2.233×10^{2}	2.380×10^{2}	2.522×10^{2}	2.761×10^{2}
c_2/(J·K·mol^{-1})	-1.047×10^{6}	-9.427×10^{5}	-9.836×10^{5}	-1.039×10^{6}
c_3/(kg·mol^{-1}·K^{-1})	-6.948×10^{-1}	-1.031×10^{0}	-8.671×10^{-1}	-7.471×10^{-1}
c_4/(kg·mol^{-1}·K^{-2})	4.318×10^{-3}	6.589×10^{-3}	5.488×10^{-3}	4.710×10^{-3}
c_5/(kg·mol^{-1}·K^{-3})	-6.706×10^{-6}	-1.052×10^{-5}	-8.672×10^{-6}	-7.425×10^{-6}
c_6/(kg·mol^{-1}·K^{-1})	1.918×10^{-1}	2.773×10^{0}	2.533×10^{0}	1.686×10^{-1}
c_7/(kg·mol^{-1}·K^{-2})	-2.566×10^{-3}	-1.973×10^{-2}	-1.827×10^{-2}	-3.135×10^{-3}
c_8/(kg·mol^{-1}·K^{-3})	6.799×10^{-6}	3.530×10^{-5}	3.290×10^{-5}	8.936×10^{-6}

[a] Used in calculating $C^{o}_{p,2}$ (Ln^{3+}, aq) in Table V.4.

figures V.1 to V.5 for comparison with the experimental data.

The temperature dependence of $C^{\circ}_{p,2}$ and V°_{2} is illustrated in figures V.6 and V.7 with data for $C^{\circ}_{p,2}\{Yb(ClO_4)_3,aq\}$ and V°_{2} $\{Nd(ClO_4)_3,aq\}$ from table V.1. The behaviour at elevated temperatures is tightly constrained by the Born terms in equations (V.3.9) and (V.3.10), which contain no adjustable parameters. The non-Born term contributions to the HKF heat capacity model ($C^{\circ}_{p,2}$ - ωTX) are plotted in figure V.8.

V.4 Comparison with Literature Data

Experimental values of $C_{p,\phi,2}$ and $V_{\phi,2}$ for $Eu(ClO_4)_3(aq)$, with and without excess perchloric acid, are plotted against the square root of ionic strength in figure V.5. It can been seen that $C_{p,\phi,2}$ and $V_{\phi,2}$ of $\{Eu(ClO_4)_3 + HClO_4\}(aq)$ do not significantly differ from those of $Eu(ClO_4)_3(aq)$ alone. This result is consistent with those for $Gd(ClO_4)_3(aq)$ and $La(ClO_4)_3(aq)$ in Chapter VI. It suggests that there is no apparent effect of hydrolysis in aqueous solutions with pH < 5.3.

The apparent molar volumes and apparent molar heat capacities of $Nd(ClO_4)_3(aq)$, $Eu(ClO_4)_3(aq)$, $Er(ClO_4)_3(aq)$, and $Yb(ClO_4)_3(aq)$ at T = 298.15 K from Spedding *et al.* (1975a) are compared with our results in figures V.1 to V.5. The experimental values of $V_{\phi,2}$ in this work agree with Spedding's results at T = 298.15 K to within about 1 $cm^3 \cdot mol^{-1}$, over the molality range of our experiments. The extrapolated values of V°_{2} for $Nd(ClO_4)_3(aq)$, $Eu(ClO_4)_3(aq)$, $Er(ClO_4)_3(aq)$, and $Yb(ClO_4)_3(aq)$,

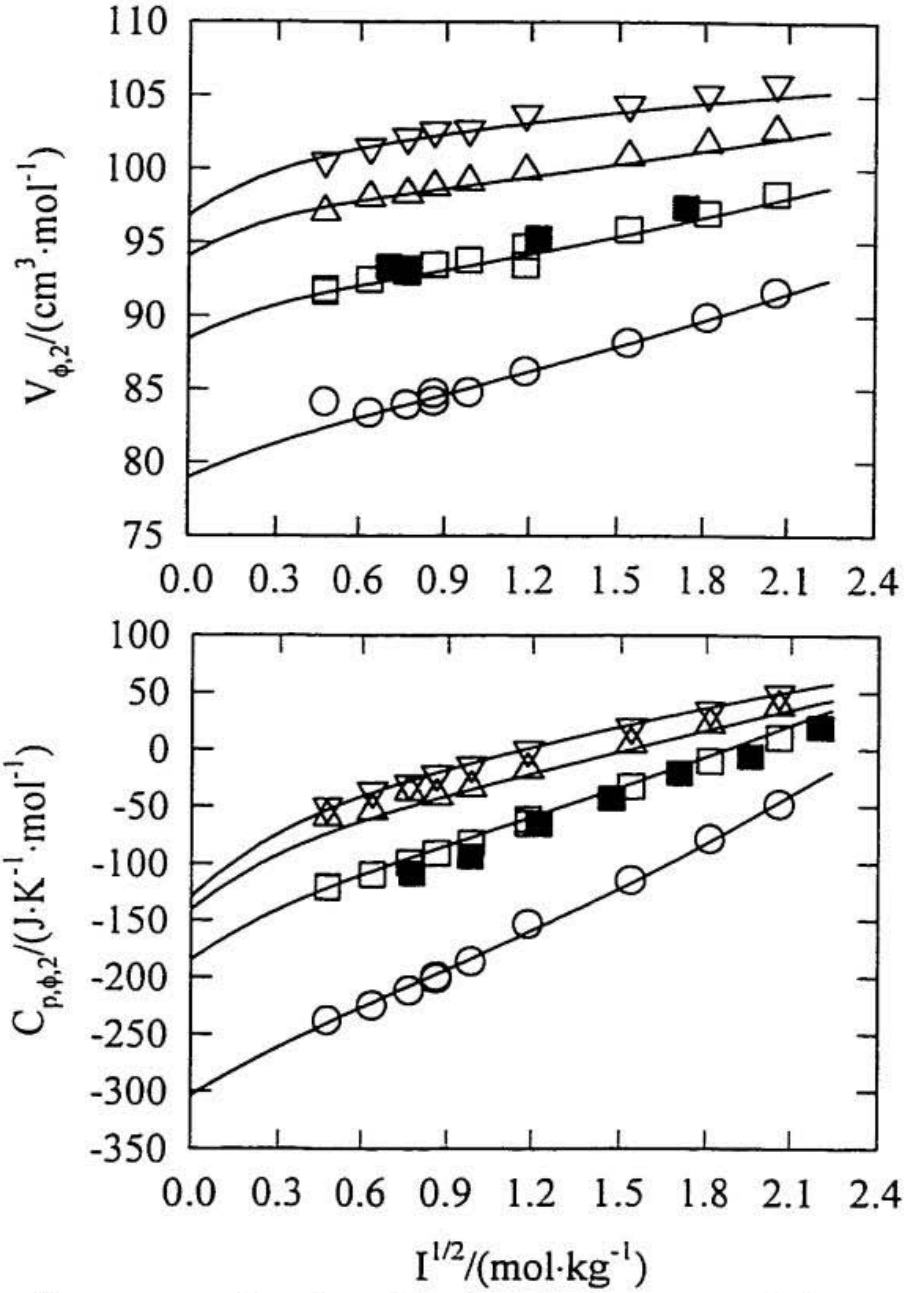


Figure V.1. The apparent molar volumes $V_{\phi,2}$ (upper) and apparent molar heat capacities $C_{p,\phi,2}$ (lower) of $Nd(ClO_4)_3(aq)$ plotted as a function of the square root of ionic strength, $I^{1/2}$: ○, T = 283.2 K; □, T = 298.15 K; ■, T = 298.15 K (Spedding *et al.*, 1975a, 1975c); Δ, T = 313.2 K; ∇, T = 328.2 K. The least-squares fits of equations (V.3.2) to (V.3.10) are shown as solid lines.

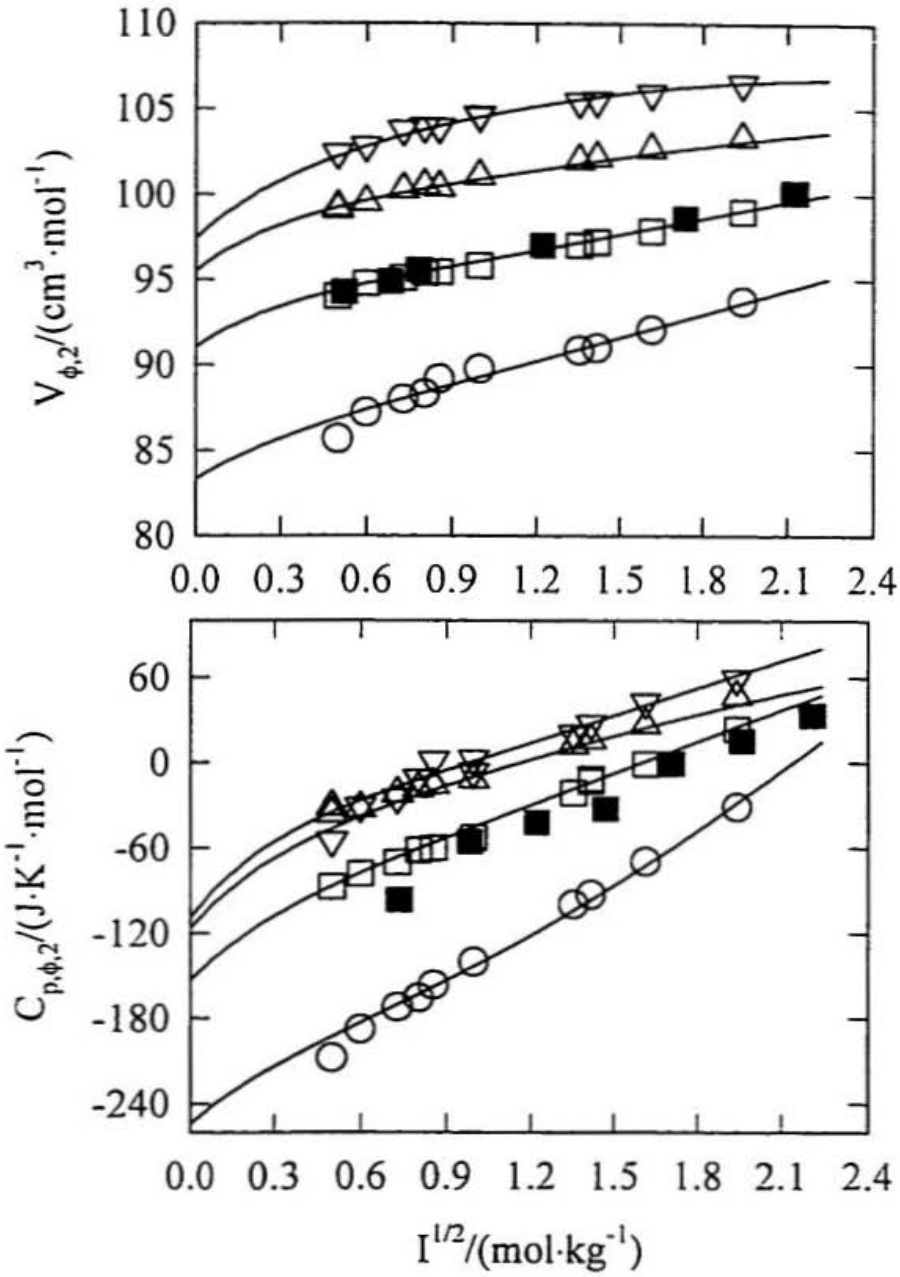


Figure V.2. The apparent molar volumes $V_{\phi,2}$ (upper) and apparent molar heat capacities $C_{p,\phi,2}$ (lower) of $Eu(ClO_4)_3(aq)$ plotted as a function of the square root of ionic strength, $I^{1/2}$: o, T = 283.2 K; □, T = 298.15 K; ■, T = 298.15 K (Spedding *et al.*, 1975a, 1975c); Δ, T = 313.2 K; ∇, T = 328.2 K. The least-squares fits of equations (V.3.2) to (V.3.10) are shown as solid lines.

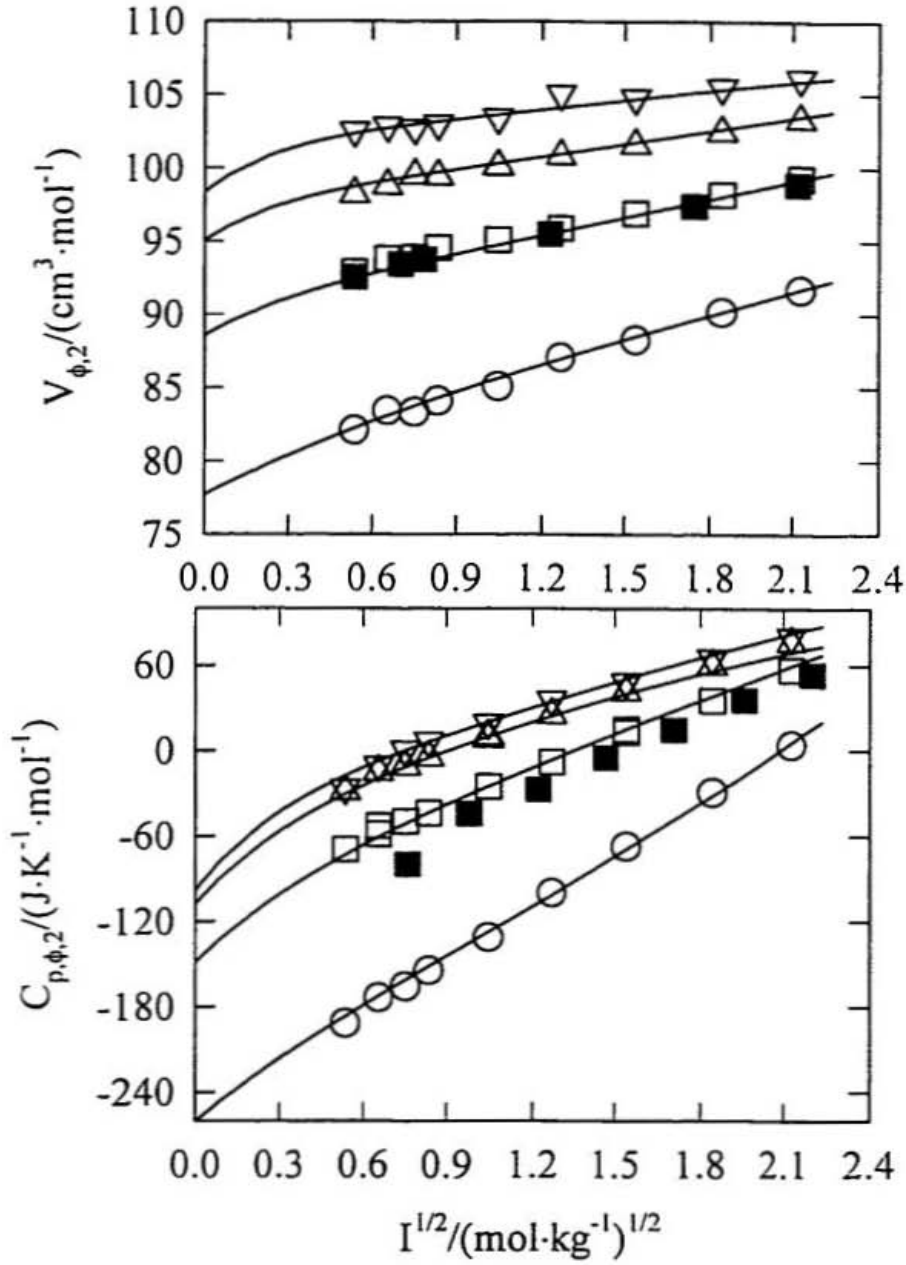


Figure V.3. The apparent molar volumes $V_{\phi,2}$ (upper) and apparent molar heat capacities $C_{p,\phi,2}$ (lower) of $Er(ClO_4)_3$(aq) plotted as a function of the square root of ionic strength, $I^{1/2}$: o, T = 283.2 K; □, T = 298.15 K; ■, T = 298.15 K (Spedding *et al.*, 1975a, 1975c); Δ, T = 313.2 K; ∇, T = 328.2 K. The least-squares fits of equations (V.3.2) to (V.3.10) are shown as solid lines.

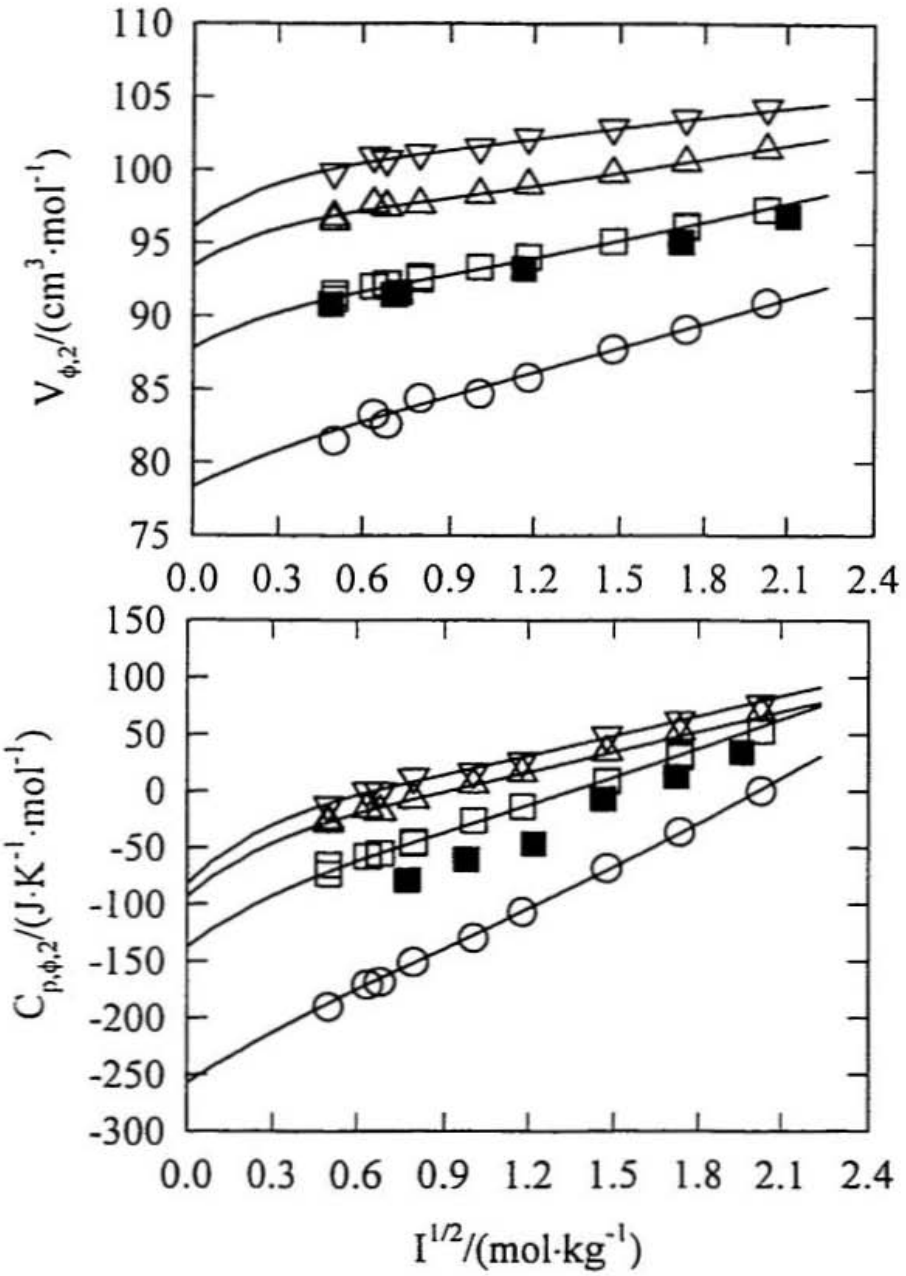


Figure V.4. The apparent molar volumes $V_{\phi,2}$ (upper) and apparent molar heat capacities $C_{p,\phi,2}$ (lower) of $Yb(ClO_4)_3(aq)$ plotted as a function of the square root of ionic strength, $I^{1/2}$: o, T = 283.2 K; □, T = 298.15 K; ■, T = 298.15 K (Spedding *et al.*, 1975a, 1975c); Δ, T = 313.2 K; ∇, T = 328.2 K. The least-squares fits of equations (V.3.2) to (V.3.10) are shown as solid lines.

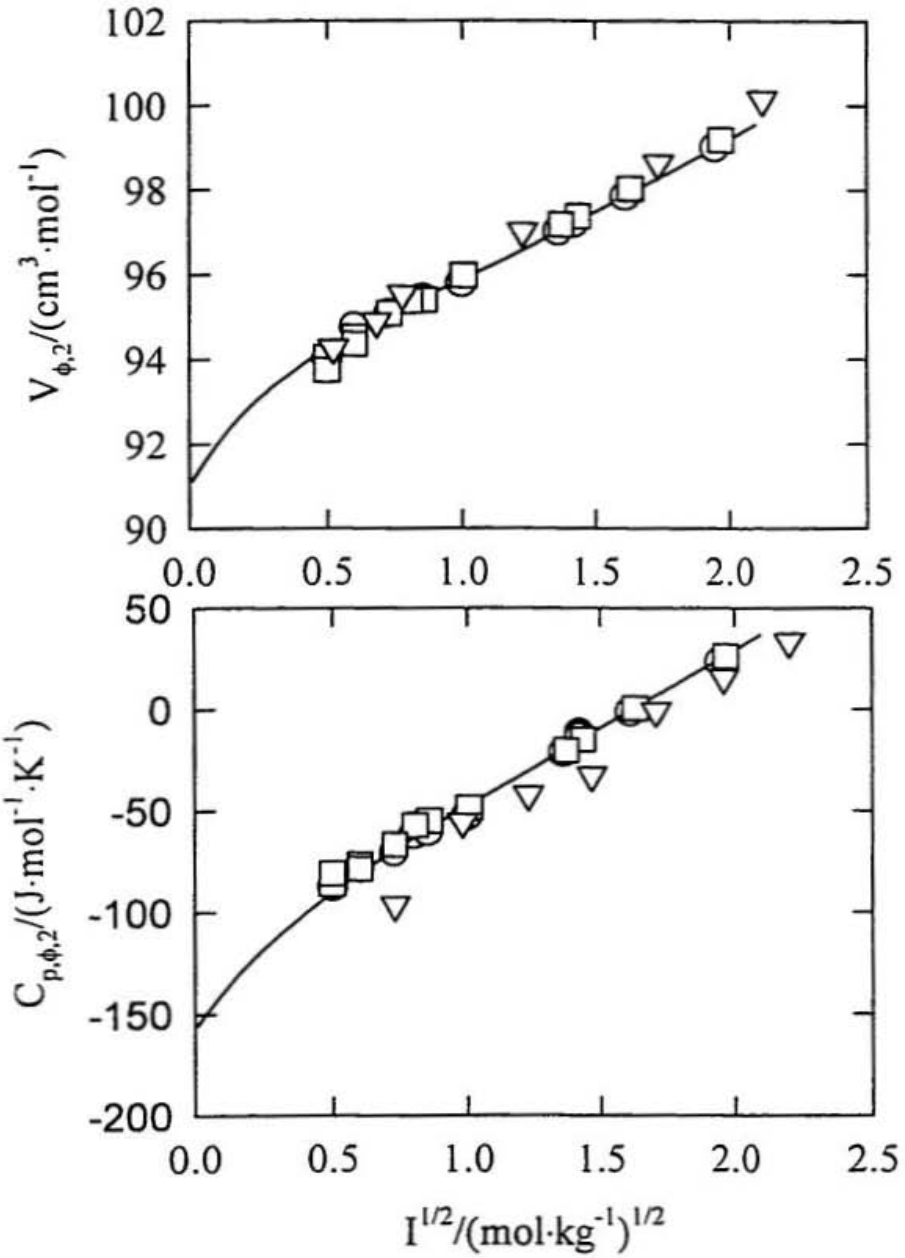


Figure V.5. The apparent molar volumes $V_{\phi,2}$ (upper) and apparent molar heat capacities $C_{p,\phi,2}$ (lower) of $Eu(ClO_4)_3$(aq) plotted as a function of square root ionic strength $I^{1/2}$ at T = 298.2 K: ○, solutions with pH = 2.2; □, solutions with pH = 3 to 5; ▽, Spedding *et al.*, 1975a, 1975c. The least-squares fits to equations (V.3.2) and (V.3.3) are shown as solid lines.

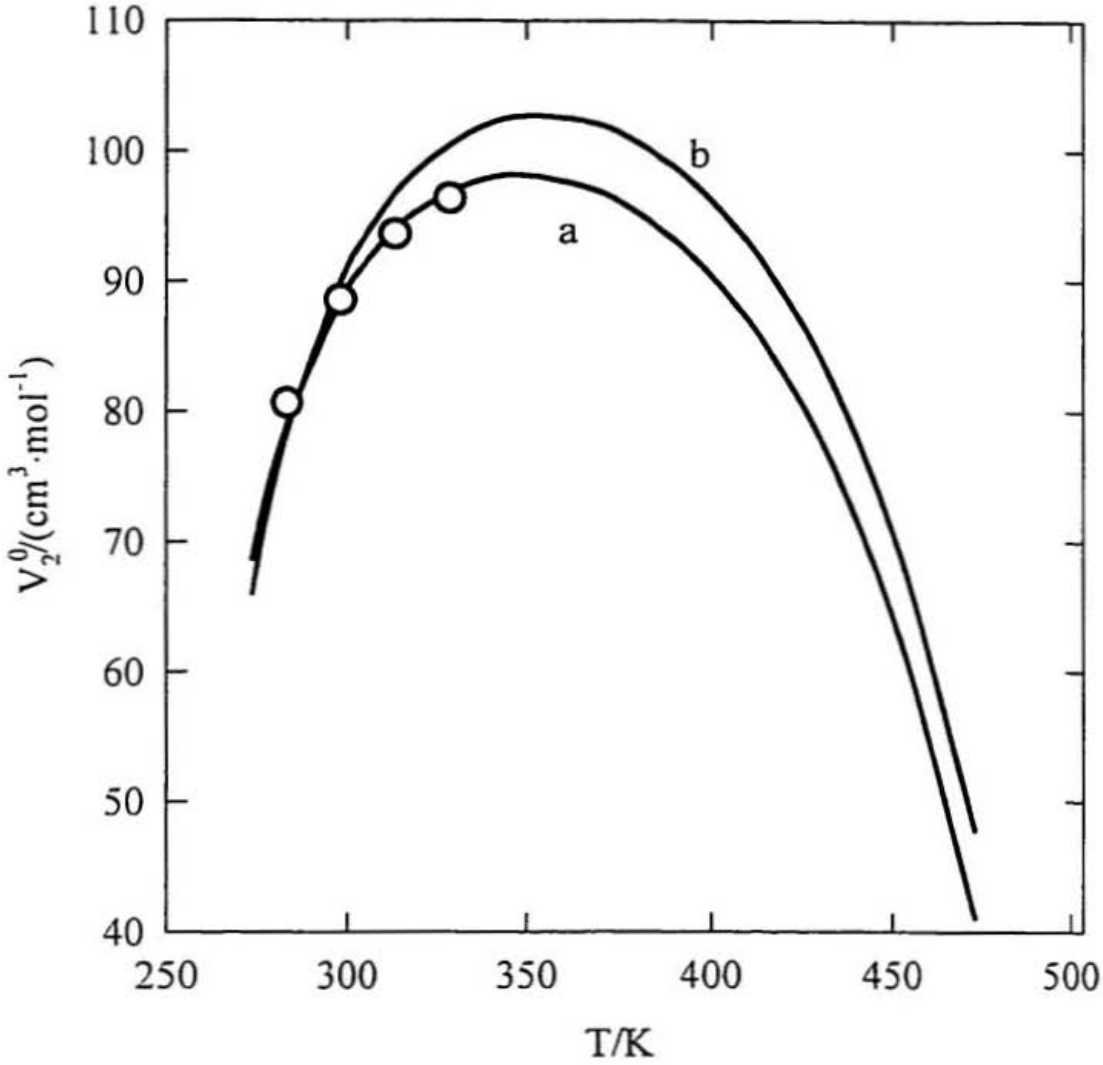


Figure V.6. The standard partial molar volumes of $Nd(ClO_4)_3(aq)$ plotted as a function of temperature: ○, V_2^0 obtained from fitting equation (V.3.3) to the experimental results at each temperature; (a), extrapolated values from equation (V.3.10); (b) extrapolated values from the compilation by Shock and Helgeson (1988).

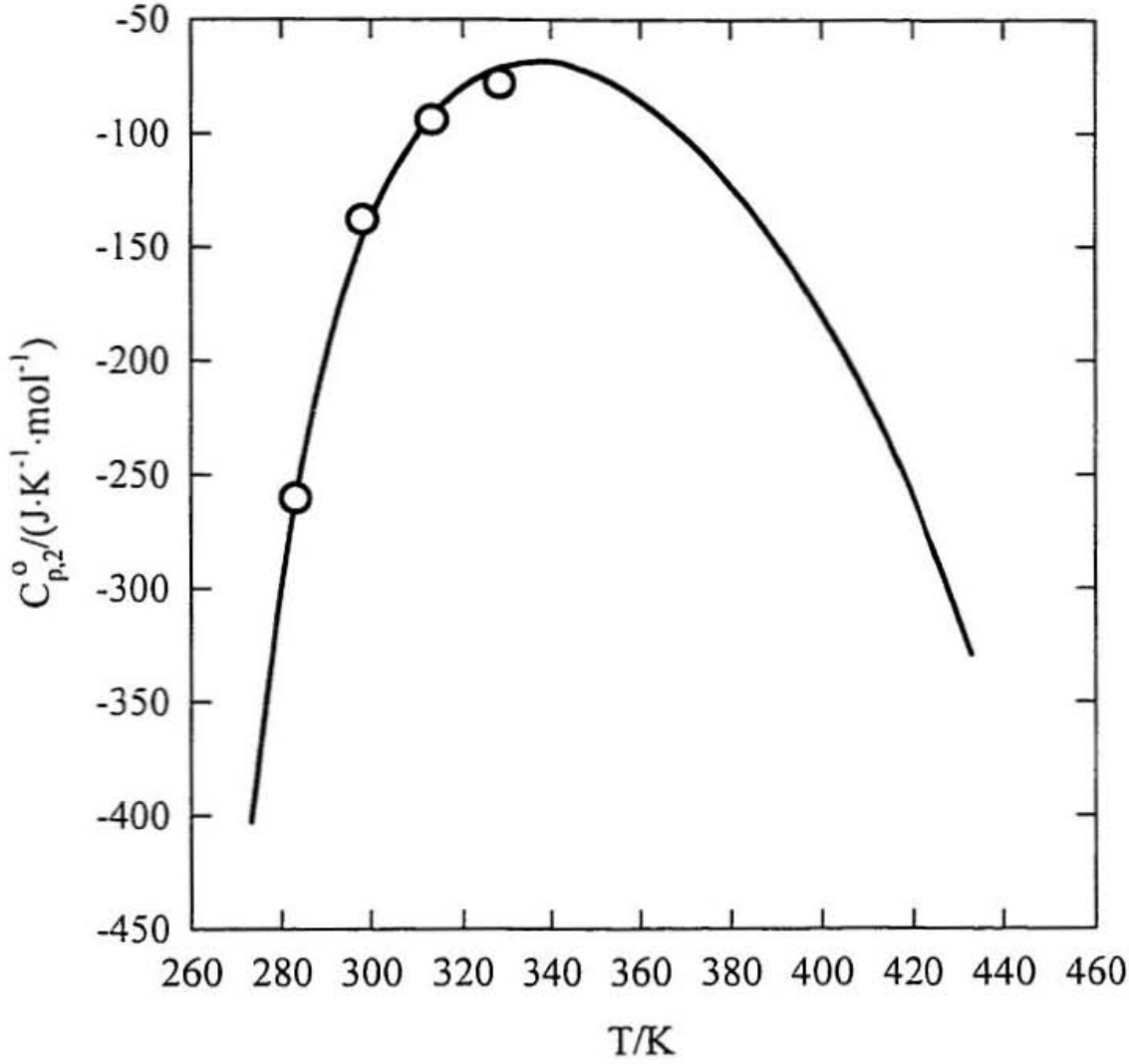


Figure V.7. The standard partial molar heat capacities $C^{\circ}_{p,2}$ of $Yb(ClO_4)_3(aq)$ obtained from fitting equation (V.3.2) to the experimental results at each temperature (shown in circles), and the extrapolation to elevated temperatures by fitting the entire matrix of results to equation (V.3.9a) (shown as a solid line)

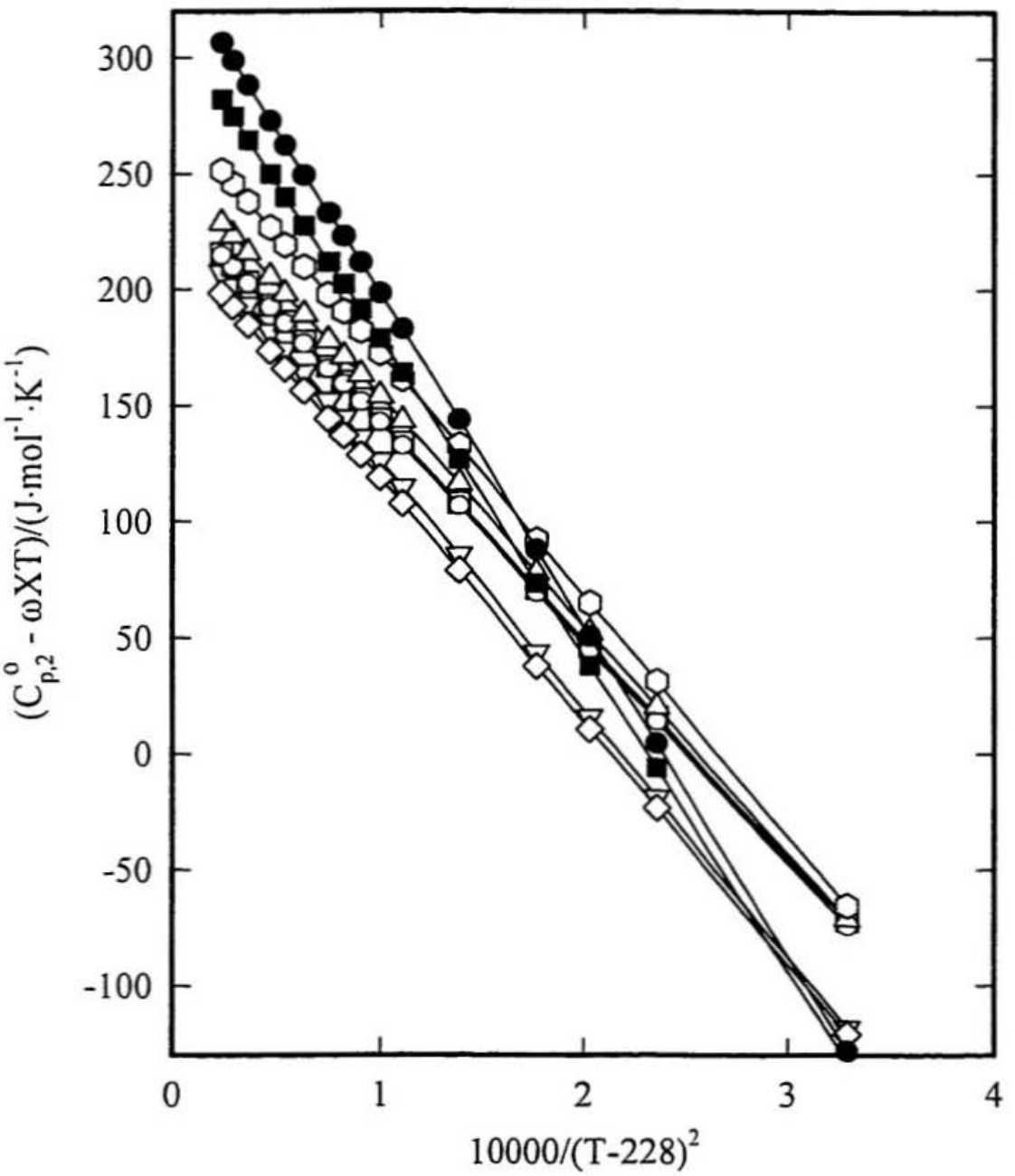


Figure V.8. The temperature dependence of the non-Born terms for aqueous trivalent cations: (a) light lanthanides; ◇, $Nd(ClO_4)_3(aq)$; ▽, $La(ClO_4)_3(aq)$; (b) heavy lanthanides, □, $Eu(ClO_4)_3(aq)$; ○, $Gd(ClO_4)_3(aq)$ Δ, $Er(ClO_4)_3(aq)$; $Yb(ClO_4)_3(aq)$; (c) metals, ●, $Al((ClO_4)_3(aq)$; ■, $Fe(ClO_4)_3(aq)$.

obtained by fitting equation V.3 to our data, agree with Spedding's results to within 0.2 $cm^3 \cdot mol^{-1}$. The average deviations between our results and Spedding's in the molality range of our experiments are 6 $J \cdot K^{-1} \cdot mol^{-1}$, 14 $J \cdot K^{-1} \cdot mol^{-1}$, 14 $J \cdot K^{-1} \cdot mol^{-1}$ and 24 $J \cdot K^{-1} \cdot mol^{-1}$ for $Nd(ClO_4)_3(aq)$, $Eu(ClO_4)_3(aq)$, $Er(ClO_4)_3(aq)$ and $Yb(ClO_4)_3(aq)$, respectively. However, at lower molalities the experimental values for the apparent molar heat capacities do not agree so well. For example, at m = 0.1 $mol \cdot kg^{-1}$, our values for $C_{p,\phi,2}$ of $Nd(ClO_4)_3(aq)$ at T = 298.2 K are more positive than those of Spedding *et al.* by 12 $J \cdot K^{-1} \cdot mol^{-1}$. Those for $Eu(ClO_4)_3(aq)$, $Er(ClO_4)_3(aq)$ and $Yb(ClO_4)_3(aq)$ are more positive by approximately 30 $J \cdot K^{-1} \cdot mol^{-1}$. These systematic differences lead to larger discrepancies in the values obtained for $C^{\circ}_{p,2}$ by means of equation (V.3.2). The standard partial molar heat capacities at T = 298.15 K in table V.1 are more positive than Spedding's results by 38 $J \cdot K^{-1} \cdot mol^{-1}$, 59 $J \cdot K^{-1} \cdot mol^{-1}$, 80 $J \cdot K^{-1} \cdot mol^{-1}$ and 142 $J \cdot K^{-1} \cdot mol^{-1}$ for $Nd(ClO_4)_3(aq)$, $Eu(ClO_4)_3(aq)$, $Er(ClO_4)_3(aq)$ and $Yb(ClO_4)_3(aq)$, respectively. The experimental uncertainties are estimated to be less than 6 $J \cdot K^{-1} \cdot mol^{-1}$ for solutions with m = 0.1 $mol \cdot kg^{-1}$, 4 $J \cdot K^{-1} \cdot mol^{-1}$ for solutions with m = 1.0 $mol \cdot kg^{-1}$, and 10 $J \cdot K^{-1} \cdot mol^{-1}$ at infinite dilution. Apparently the discrepancies are not caused by differences in the solutions themselves because ours were prepared with a procedure identical to that used by Spedding *et al.* (1966d), and the agreement between our values for $V_{\phi,2}$ and those of Spedding *et al.* (1975c) is excellent. Small systematic errors in the heat capacities measured by adiabatic solution calorimetry may account for the large discrepancies at

low molalities. In the series of papers (Spedding *et al.* 1975a, 1975b, 1975c, 1979; 1975; Spedding and Jones, 1966) describing their measurements on aqueous lanthanide salt solutions at T = 298.15 K, the authors noted that the specific heat capacities of several sodium chloride solutions agreed with those reported by Randall and Rossini (1929) to within 0.05%. Randall and Rossini's values for the specific heat capacities and apparent molar heat capacities of NaCl(aq) in the molality range of infinite dilution to m = 1.0 $mol \cdot kg^{-1}$ are systematically lower than modern results (Archer, 1992) by about 0.12% and about 10 $J \cdot K^{-1} \cdot mol^{-1}$, respectively.

The standard partial molar properties of $Nd^{3+}(aq)$, $Eu^{3+}(aq)$, $Er^{3+}(aq)$, and $Yb^{3+}(aq)$ can be calculated by combining the results in table V.1 with values of $C^{\circ}_{p,2}$ and V°_{2} for $HClO_4(aq)$ from Hovey *et al.* (1988) on basis of the usual convention $\{C^{\circ}_{p,2}(H^+, aq) \equiv 0, V^{\circ}_{2}(H^+, aq) \equiv 0\}$, and these are listed in table V.4. Our values for the conventional single-ion standard partial molar volumes V°_{2} at T = 298.2 K are in good agreement with those from the compilation by Shock and Helgeson (1988). The differences for $Nd^{3+}(aq)$, $Eu^{3+}(aq)$, $Er^{3+}(aq)$ and $Yb^{3+}(aq)$ are only 0.5 $cm^3 \cdot mol^{-1}$, 0.2 $cm^3 \cdot mol^{-1}$, 0.4 $cm^3 \cdot mol^{-1}$ and 0.3 $cm^3 \cdot mol^{-1}$, respectively. However, our values for $C^{\circ}_{p,2}$ differ from those compiled by Shock and Helgeson (1988) and Abraham and Marcus (1986) by 69 $J \cdot K^{-1} \cdot mol^{-1}$, 70 $J \cdot K^{-1} \cdot mol^{-1}$, 75 $J \cdot K^{-1} \cdot mol^{-1}$ and 88 $J \cdot K^{-1} \cdot mol^{-1}$, respectively.

Table V.4. Standard partial molar properties of $Ln^{3+}(aq)$ from T = 283.2 K to 328.2 K

$V_2^\phi/(cm^3 \cdot mol^{-1})$					
T/K	$ClO_4^-(aq)$	$Nd^{3+}(aq)$	$Eu^{3+}(aq)$	$Er^{3+}(aq)$	$Yb^{3+}(aq)$
283.2	41.63	-44.3	-41.9	-47.3	-46.4
298.2	44.04	-43.6	-41.1	-42.6	-44.2
313.2	46.24	-45.1	-43.5	-44.3	-45.6
328.2	47.31	-45.6	-44.0	-44.3	-45.9
$C_{p,2}^\circ/(J \cdot K^{-1} \cdot mol^{-1})$					
T/K	$ClO_4^-(aq)$	$Nd^{3+}(aq)$	$Eu^{3+}(aq)$	$Er^{3+}(aq)$	$Yb^{3+}(aq)$
283.2	-62.30	-130.1	-91.0	-87.1	-75.4
298.2	-24.68	-111.9	-83.4	-68.3	-63.9
313.2	-10.22	-96.0	-66.4	-71.0	-63.4
328.2	-4.58	-111.1	-105.8	-91.4	-64.3

V.5 Standard Partial Molar Properties

Spedding and co-workers have systematically studied various properties of the lanthanide salts in aqueous solution at T = 298.15 K. Among the properties studied were apparent molar volumes (Spedding *et al.*, 1966d; Spedding *et al.*, 1975c), apparent molar heat capacities (Spedding *et al.*, 1975a, 1975b, 1979; Spedding and Jones, 1966), heats of dilution (Spedding *et al.*, 1966a), electrical conductivities (Rard and Spedding, 1975), and relative viscosities (Spedding and Pikal, 1966). With the exception of the lanthanide nitrates (Spedding *et al.*, 1979), the variation of each of these properties as a function of ionic radius across the lanthanide series exhibited a discontinuity consistent with the "gadolinium break". Similar behavior has been observed for many other properties of aqueous lanthanide salt solutions, for example, the glass transition temperature (Kanno and Akama, 1987) and the entropy of formation of the LnX^{2+} carboxylate and α-hydroxycarboxylate complexes (Choppin, 1971). The chemical and physical properties of the lanthanide ions are governed mainly by steric and electrostatic effects (Spedding *et al.*, 1966d), and the discontinuities are thought to arise from a change in the hydration number of the aquo-ions in mid-series.

Our values of V_2^ϕ for the six aqueous lanthanide perchlorates at T = 283.2 K, T = 298.2 K and T = 328.2 K are plotted against ionic radius in figure V.9, along with those at T = 298.2 K from Spedding *et al.* (1966d). The plot at T = 298.15 K clearly shows a stepwise decrease in V_2^ϕ of ≈ 5 $cm^3 \cdot mol^{-1}$ between $Gd(ClO_4)_3(aq)$ and $Nd(ClO_4)_3(aq)$ that

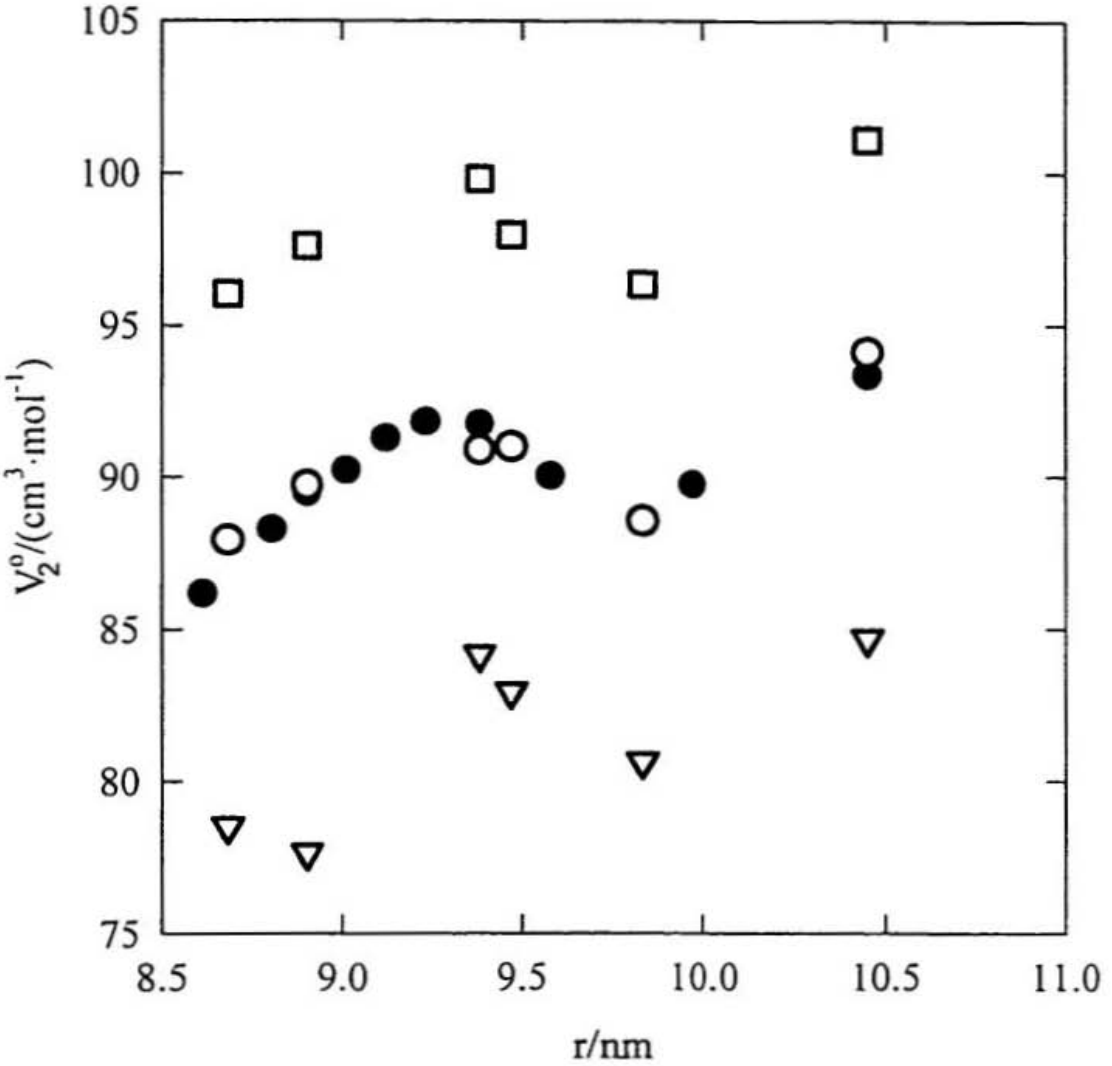


Figure V.9. The standard partial molar volumes V_2^o of aqueous lanthanide perchlorates: ∇, T = 283.2 K, this work; ○, T= 298.2 K, this work; ●, T = 298.15 K, Spedding *et al.* (1975a); □, T = 328.2 K, this work.

interrupts the regular increase with ionic radius, exactly as was reported by Spedding *et al.* (1966d) who attributed the anomaly to a change in hydration number from 8 to 9. X-ray diffraction studies (Habenschuss and Spedding, 1979a, 1979b, 1980), neutron diffraction studies (Cossy *et al.*, 1989; Narten and Hahn, 1983, Yamaguchi *et al.*, 1991), and modelling investigations (Jia, 1987) strongly support this interpretation. The V_2^o results at T = 283.2 K and T = 328.2 K, which are new, show that the effect does not vary significantly with temperature in this range.

Our values of $C_{p,2}^o$ for the six lanthanide perchlorates for each temperature are plotted as a function of ionic radius in figure V.10, along with those for $Al(ClO_4)_3(aq)$ and $Fe(ClO_4)_3(aq)$ (Hovey, 1988). The values for $C_{p,2}^o\{Al(ClO_4)_3,aq\}$ were calculated from those for $AlCl_3(aq)$ (Conti *et al.*, 1992; Hovey and Tremaine, 1986), $HClO_4(aq)$ (Shock and Helgeson, 1988) and HCl(aq) (Tremaine *et al.*, 1986). At T = 298.2 K (figure V.10b), it can be seen that there is a decrease in $C_{p,2}^o$ of ≈ 30 $J \cdot K^{-1} \cdot mol^{-1}$ between the lighter lanthanide ions (La^{3+} and Nd^{3+}) and the heavier lanthanide ions (Gd^{3+}, Eu^{3+}, Er^{3+}, Yb^{3+}). Figure V.10(b) shows the discontinuity in heat capacities much more clearly than similar plots reported by Spedding *et al.* (1975). The effect is even more pronounced at T = 283.2 K (figure V.10a), where the discontinuity is ≈ 45 $J \cdot K^{-1} \cdot mol^{-1}$. The effect is much less apparent at T = 313.2 K (Figure 10c) and, at T = 328.2 K, (Figure V.10d) the discontinuity is less than the experimental scatter.

A similar break in $C_{p,2}^o$ is apparent between the metal- and lanthanide perchlorates.

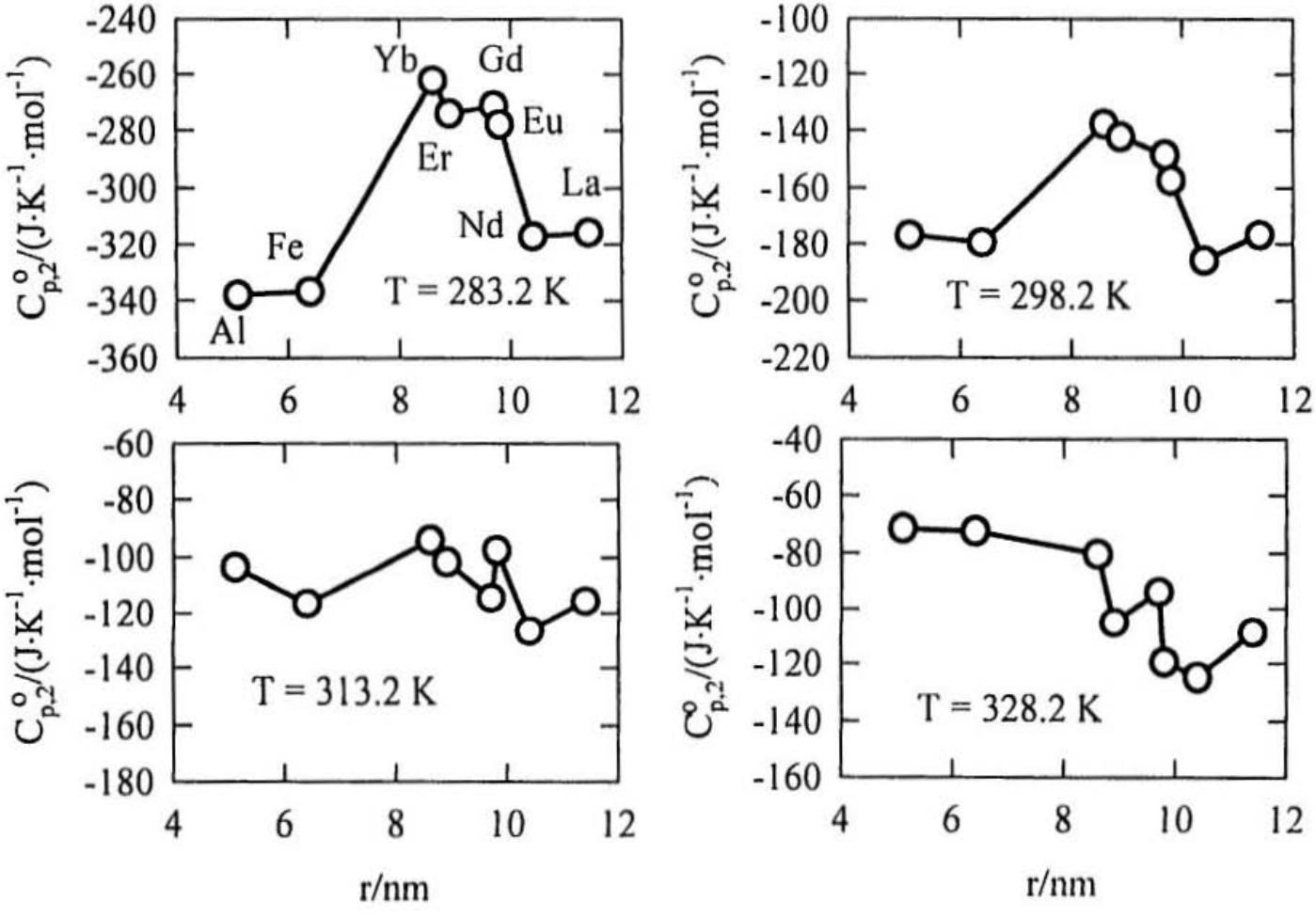


Figure V.10. The standard partial molar heat capacities $C^{o}_{p,2}$ of aqueous lanthanide perchlorates, $Al(ClO_4)_3(aq)$, and $Fe(ClO_4)_3(aq)$ plotted against ionic radius.

At T = 283.2 K, the values of $C^{\circ}_{p,2}$ for $Al(ClO_4)_3(aq)$ and $Fe(ClO_4)_3(aq)$ are ≈ 80 $J \cdot K^{-1} \cdot mol^{-1}$ lower than those for the heavier lanthanide salts. The difference is less at elevated temperatures and, at T = 313.2 K, the break is barely discernable.

This behavior is reflected in the temperature dependance of the non-Born contributions to $C^{\circ}_{p,2}$ in the HKF model, which are plotted in figure V.8. As might be expected, the heavy lanthanides, light lanthanides and metals form three distinct groupings. The non-Born terms arise predominantly from configurational hydration effects (Corti, 1992; Wood *et al.*, 1994). At low temperature, where configurational effects dominate, the non-Born terms for lanthanides lie in two groupings in which the contributions for $La(ClO_4)_3(aq)$ and $Nd(ClO_4)_3(aq)$ differ from those for $Gd(ClO_4)_3(aq)$ and the other rare earths with electronic structures above f^7 by about 40 $J \cdot K^{-1} \cdot mol^{-1}$. The similarity between the values for the metal salts $Fe(ClO_4)_3(aq)$ and $Al(ClO_4)_3(aq)$, and the light lanthanide salts $La(ClO_4)_3(aq)$ and $Nd(ClO_4)_3(aq)$ at T = 283.2 K appears to be coincidental. At elevated temperatures (T > 333 K) the non-Born terms are smooth functions of ionic radius.

V.6 Hydration Effects

The structure of hydrated lanthanide ions has been investigated using X-ray diffraction (Habenschuss and Spedding, 1979a, 1979b, 1980; Smith and Wertz, 1977a, 1977b; Steel and Wertz, 1977; Johansson and Yokoyama, 1990; Matsubara *et al.*, 1988),

neutron diffraction (Cossy *et al.*, 1989; Narten and Hahn, 1983; Yamaguchi *et al.*, 1991), extended X-ray absorption spectroscopy (EXAFS) (Yamaguchi *et al.*, 1988), Raman spectroscopy (Kanno and Hiraishi, 1980; Kanno and Hiraishi, 1982, 1984), n.m.r. (Cossy *et al.*, 1988), molecular dynamics simulations (Meier *et al.*, 1990), and quantum mechanical calculations (Jia, 1987). Generally, the results from these investigations suggest that lighter lanthanide ions, from La^{3+} (aq) to Nd^{3+}(aq) in the series, have a hydration number of nine; those from Tb^{3+}(aq) to Lu^{3+}(aq) have a hydration number of eight; and those in the middle of the series have a fractional hydration number reflecting an equilibrium between the hydration numbers eight and nine. Recent investigations by isomorphous X-ray scattering (Smith and Wertz, 1977a, 1977b; Steel and Wertz, 1977; Johansson and Yokoyama, 1990; Matsubara *et al.*, 1988) and ^{17}O n.m.r. (Cossy *et al.*, 1988) suggest that some features of ionic hydration may be quite constant across the series. However, the X-ray data (Habenschuss and Spedding, 1979a, 1979b, 1980), neutron diffraction results (Cossy *et al.*, 1989; Narten and Hahn, 1983; Yamaguchi *et al.*, 1991), and modelling investigations (Jia, 1987) strongly support Spedding's interpretation that the anomolies in the thermodynamic properties of the aquo ion arise from a change in hydration number.

Several theoretical and semi-empirical models have been developed to link the structure of the hydrated ions to the thermodynamic properties (Goldman and Bates, 1975; Swaddle and Mak, 1983; Miyakawa *et al.*, 1988; Hahn, 1988). The standard partial

molar Gibbs free energies, enthalpies, and volumes of aqueous electrolytes can be predicted quite well from the models, which usually use the Born equation to describe long range solvent polarization and a physico-chemical treatment of the primary solvation layer based on X-ray or neutron diffraction and gas-phase hydration results. None of these semi-continuum treatments gives an accurate prediction for the standard partial molar heat capacities.

Figure V.11 illustrates the hydration geometries in the primary solvation sphere proposed by several authors (Rizkalla and Choppin, 1991; Miyakawa *et al.*, 1988). Miyakawa *et al.* (1988) recently reported an electrostatic model for calculating the bond energies of 8- and 9-coordinated lanthanide ions based on these structures. The model was used to describe the absorption and emission spectra of aqueous cerium ethyl sulphate at temperatures from 278 K to 328 K (Miyakawa *et al.*, 1988; Okada *et al.*, 1981; Kaizu *et al.*, 1985), based on the premise that there is an equilibrium between $[Ce(H_2O)_9]^{3+}$ and $[Ce(H_2O)_8]^{3+}$. At higher temperatures the equilibrium shifts to favour $[Ce(H_2O)_8]^{3+}$ due to the positive value of $S^\circ\{[Ce(H_2O)_8]^{3+}\} - S^\circ\{[Ce(H_2O)_9]^{3+}\} = 34$ $J \cdot K^{-1} \cdot mol^{-1}$ (Miyakawa *et al.*, 1988). The variation in the hydration numbers from the Miyakawa model across the series is plotted in figure V.12. The values for V° (Ln^{3+},aq) corresponding to these hydration numbers may be estimated from the models of Swaddle and Mak (1983) and Hahn (1988). The agreement with the results from Spedding *et al.* (1966d) and our work is within the experimental uncertainties. We have calculated

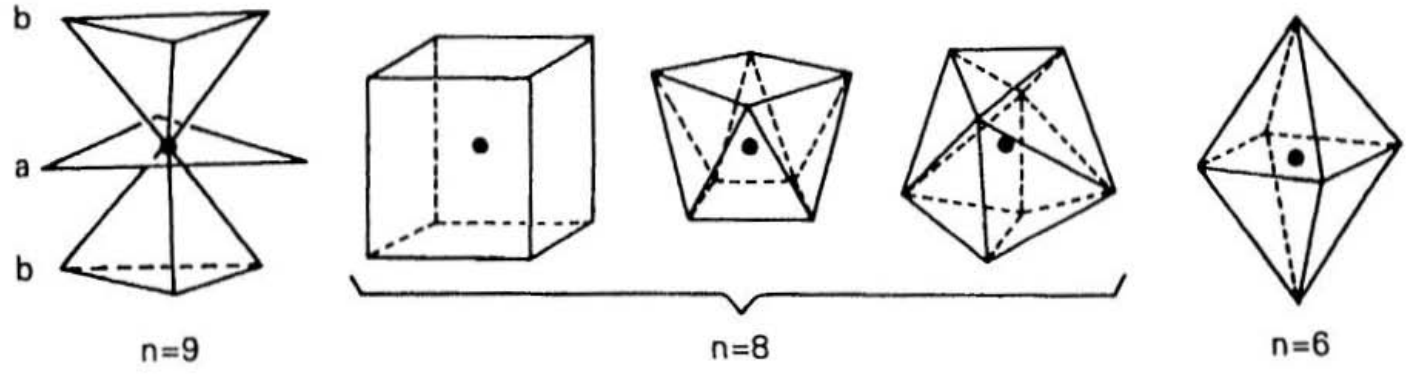


Figure V.11. The geometries of 8- and 9- coordinated $Ln^{3+}(aq)$ cations, and 6-coordinated metal cations as presented by Miyahawa et al. (1988).

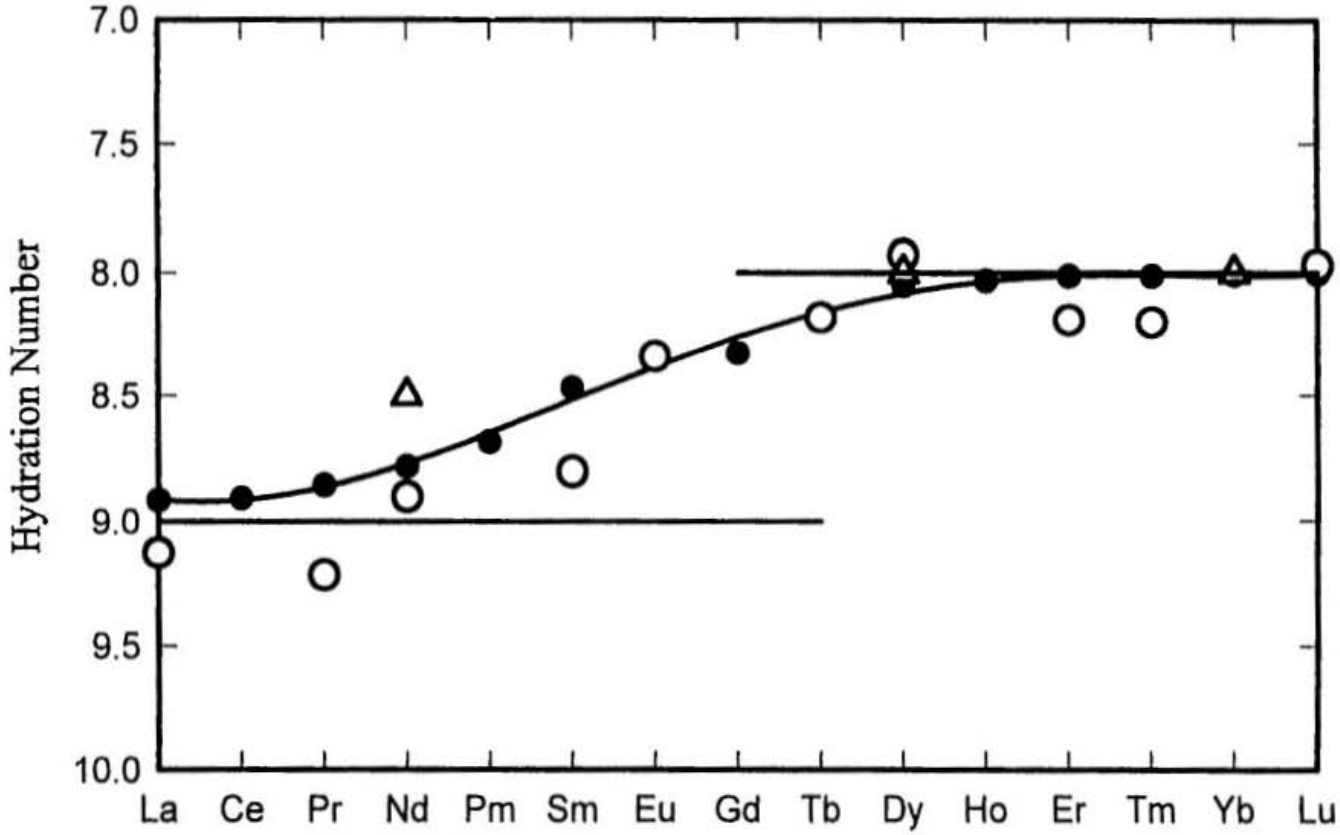


Figure V.12. The hydration number n of $Ln^{3+}(aq)$ plotted in order increasing atomic number: ○, from X-ray diffraction measurements; Δ, from neutron diffraction measurements; ●, the hydration number calculated from Miyakawa *et al.*'s model. See text for references.

hydration numbers at the other temperatures studied here, using a modest extension of the Miyakawa model (see Appendix B), and have found very little change with temperature. This finding, and the rather constant value for the difference in V_2^o between the light and heavy lanthanides in figure V.9, is consistent with observations by Swaddle and Mak (1983) and others, who concluded that the non-Born contributions to V_2^o are dominated by primary solvation effects.

The interpretation of the results for $C_{p,2}^o$ in figure V.10 is more subtle. The standard partial molar heat capacity is traditionally divided into five contributions (Corti, 1992; Wood *et al.*, 1994; Goldman and Bates, 1972; Goldman and Morse, 1975):

$$C_{p,2}^o = C_{p,\,gas}^o + \Delta_s C_{p,\,std\ states}^o + \Delta_s C_{p,I}^o + \Delta_s C_{p,II}^o + \Delta_s C_{p,\,Born}^o , \qquad (V.6.1)$$

where $C_{p,gas}^o$ is the intrinsic heat capacity of the ion, $\Delta_s C_{p,\,std\ states}^o$ is the correction for the difference in standard states between the aqueous and gas phases, $\Delta_s C_{p,I}^o$ and $\Delta_s C_{p,II}^o$ are the contributions to the heat capacity of solvation from the first and second hydration shells, and $\Delta_s C_{p,\,Born}^o$ denotes the contribution of the long-range polarization which can be described well by the Born model (Corti, 1992; Wood *et al.*, 1994). None of the terms except $\Delta_s C_{p,I}^o$ and $\Delta_s C_{p,II}^o$ would be expected to display any significant discontinuity across the lanthanide series. We have attempted two approximate calculations of $\Delta_s C_{p,I}^o$ to determine whether there are sufficient diffences between the 8- and 9-coordinated structures to account for the gadolinium break (see Appendix B). The first assessed the contributions to internal vibrations and rotations within the primary solvation shell,

according to the model of Goldman and Bates (Goldman and Bates, 1972; Goldman and Morss, 1975). The second evaluated the contribution of the chemical relaxation contribution (Woolley and Hepler, 1977) associated with the equilibrium between the two coordination numbers, as calculated from the model by Mikayawa *et al.* (1988), on the basis of the expression:

$$C^{\circ}_{p,2}(Ln^{3+},aq) = (1-\alpha)\, C^{\circ}_{p,2}\,\{[Ln(H_2O)_8]^{3+}\} + \alpha\, C^{\circ}_{p,2}\,\{[Ln(H_2O)_9]^{3+} - \alpha\, C^{\circ}_{p}(H_2O,l) + C^{\circ}_{p}{}^{,rel} \qquad (V.6.2)$$

where α is the fraction in the 9-coordinated hydration structures. The relaxation contribution must always be positive and peaks at a maximum of $C^{\circ}_{p}{}^{,rel} = 40\ J\cdot K^{-1}\cdot mol^{-1}$ for $Sm^{3+}(aq)$ and $Eu^{3+}(aq)$. The contribution of electronic transitions in $Ln^{3+}(aq)$ ions with low lying states is much smaller and was not included in these estimates. The model is consistent with a stepwise difference of about $30\ J\cdot K^{-1}\cdot mol^{-1}$ between the values for $C^{\circ}_{p,2}(Eu^{3+},aq)$ and $C^{\circ}_{p,2}(Nd^{3+},aq)$ at $T = 298.15$ K, similar to that plotted in figure V.10. Estimates of the temperature dependence of α (see Appendix B) indicate that neither the change in hydration number nor the change in the relaxation contribution to $C^{\circ}_{p,2}$ with increasing temperature is sufficiently large to cause the gadolinium break to disappear at $T \geq 328$ K.

These approximate calculations suggest that persistence of the gadolinium break

in V_2^o at temperatures higher than T =298 K is associated with differences in the first hydration shell which are relatively independent of temperature. The disappearance of the gadolinium break in the heat capacities at T > 298.15 K suggests that the heat capacity effect may be caused by changes in the stucture of the second hydration shell with increasing temperature.

V.7 Conclusions

These measurements, as well as those reported in our previous Chapter, provide a new data base for $C_{p,2}^o$, V_2^o, $C_{p,\phi,2}$ and $V_{\phi,2}$ of $La^{3+}(aq)$, $Nd^{3+}(aq)$, $Eu^{3+}(aq)$, $Gd^{3+}(aq)$, $Er^{3+}(aq)$, and $Yb^{3+}(aq)$ over the temperature range 283 K ≤ T ≤ 328 K. At T = 298.2 K, our values of $V_{\phi,2}$ for the lanthanide perchlorates and V_2^o for the lanthanide cations are in excellent agreement with those reported by Spedding *et al.* (Spedding *et al.*, 1966d, 1975c) and those compiled by Shock and Helgeson (1988), which are based on Spedding's data. The standard partial molar volumes for $La^{3+}(aq)$, $Nd^{3+}(aq)$, $Eu^{3+}(aq)$, $Gd^{3+}(aq)$, $Er^{3+}(aq)$, and $Yb^{3+}(aq)$ at T = 298.2 K can be considered well established. We believe our values of $C_{p,2}^o$ are more accurate than the values determined in the classic papers by Spedding *et al.* (1966d, 1975a, 1975b), which were made before the availablity of Picker flow calorimeters. These new experimental results should be used in preference to estimated values (Shock and Helgeson, 1988), which have been the only data for the heat capacity functions of the rare earth cations available at temperatures other than 298

K. Our results for the temperature dependance of V_2^o and $C_{p,2}^o$ suggest that interesting changes in the secondary hydration shell of the hydrated aquo ions occur at temperatures near the freezing temperature.

Chapter VI. Densities and Apparent Molar Volumes of $Gd(CF_3SO_3)_3(aq)$ and $La(CF_3SO_3)_3(aq)$ at Temperatures up to 472 K and Pressures up to 30 MPa

VI.1 Introduction

Accurate thermodynamic properties of aqueous electrolytes at elevated temperatures and pressures are required for calculating speciation, solubility, and mass transport of minerals and oxides in industrial, geochemical and hydrometallurgical systems. This work is a continuation of the work on the thermodynamic properties of $M^{3+}(aq)$ species described in previous chapters, in which the rare earth ions were used as model compounds to explore the effects of ionic radius on partial molar heat capacities and volumes under near ambient conditions. In this chapter we report the apparent molar volumes of aqueous gadolinium trifluoromethanesulfonate (triflate) at temperatures from T = 278 to 472 K and pressures up to 30 MPa. The $Gd^{3+}(aq)$ ion is significant because of its position near the middle of the lanthanide series (f^7), which seems particularly sensitive to subtle hydration effects, and because the early heat capacity measurements of Jekel *et al.* (1964) on $Gd^{3+}(aq)$ played a major role in the development of correlations for predicting heat capacity data at elevated temperatures.

Spedding and co-workers have determined various thermodynamic properties of the lanthanide salts in aqueous solution at T = 298.15 K and 0.1 MPa (Spedding *et al.*, 1966a, 1966b, 1975a, 1975b, 1975c). We have reported the apparent molar heat

capacities and volumes of $LaCl_3(aq)$, $La(ClO_4)_3(aq)$ and $Gd(ClO_4)_3(aq)$ from temperatures T = 283 K to T = 338 K at p = 0. 1 MPa in Chapters IV and V. Because the aqueous triflate anion $CF_3SO_3^-$ has a high resistance to both reductive and oxidative cleavage and is a very weak complexing agent (Leonard and Swaddle, 1975; Lawarance, 1986), we chose the $Gd(CF_3SO_3)_3$ salt for our volumetric measurements at elevated temperatures.

VI.2 Experimental

Densities at T ≤ 318 K were measured using a Paar DMA 60 densimeter. A Paar DMA 512 remote cell with a stainless-steel vibrating tube was used for measurements at elevated pressures; a Paar DMA 602 HP remote cell with a glass vibrating tube was used for measurements at 0.1 MPa. The temperature of the vibrating tube assemblies was controlled to ± 0.01 K by circulating a thermostated mixture of (ethene glycol + water). A 100Ω platinum RTD (Omega) calibrated against a secondary standard 25Ω RTD (Instrulab) was used to monitor the temperature. The pressure of the densimeters was maintained with a pressure generator (HIP Co.) and was measured with a pressure transducer (Precise Sensors, Inc.). Densities at T > 318 K were measured with a platinum-cell vibrating-tube densimeter at Oak Ridge National Laboratory. The details of this densimeter and the procedure for the density measurement were described by Simonson *et al.* (1994).

Distilled, deionized water and a 5.694 $mol \cdot kg^{-1}$ NaCl(aq) solution were used as

reference fluids for the calibration of the densimeters. The densities of water were calculated from the equation of state of Hill (1990), while the densities of NaCl(aq) were calculated from the equation of state of Archer (1992). The stock solutions of $Gd(CF_3SO_3)_3(aq)$ and $La(CF_3SO_3)_3(aq)$ were prepared from the oxide (Aldrich, mass fraction 0.999) and triflic acid (Alfa, mass fraction 0.99) according to the procedure given in Chapter IV. The final pH of the stock solution with m = 0.72 mol·kg^{-1} was about 2.7. A 0.0021 mol·kg^{-1} $HCF_3SO_3(aq)$ solution was used to dilute the stock solution of $Gd(CF_3SO_3)_3(aq)$ to make more dilute solutions with pH = 2.7 for measurements at T ≥ 373 K. The 0.0021 mol·kg^{-1} $HCF_3SO_3(aq)$ solution and the stock solution were initially placed in two Teflon displacement bags and forced to mix and flow into the densimeter tube by a twin-barrelled displacement pump. Different concentrations were achieved by changing volumetric delivery ratios from the two barrels of the pump.

VI.3 Results

Apparent molar volumes $V_{\phi,2}$ for $Gd(CF_3SO_3)_3(aq)$ and $La(CF_3SO_3)_3(aq)$ were calculated from the experimental density differences $(\rho_i^* - \rho)$ and the densities of water ρ_i^* according to the definition:

$$V_{\phi,2} = 1000(\rho_i^* - \rho)/(m\rho\rho_i^*) + M/\rho\,, \qquad \text{(VI.3.1)}$$

where M = 604.436 g·mol^{-1} and M = 586.09 g·mol^{-1} are the molar masses for

$Gd(CF_3SO_3)_3$ and $La(CF_3SO_3)_3$, respectively, and m is the molality of solutions. The densities of water ρ_1^* were taken from the equation of state of Hill (1990) and are listed in table VI.1. The densities ρ and the calculated $V_{\phi,2}$ at each experimental temperature, pressure, and molality are listed in tables A.VI.1 and A.VI.2.

VI.3.1 Concentration Dependence of $V_{\phi,2}$ for $La(CF_3SO_3)_3$(aq)

The Pitzer ion-interaction equation for a 3-1 charge-type strong electrolyte was used to represent the concentration dependence of $V_{\phi,2}$:

$$V_{\phi,2} = V_2^\circ + 6A_V/b \ln(1+bI^{1/2}) + 6RTm[\beta^{(0)V} + 2\beta^{(1)V}f(I)] \qquad \text{(VI.3.2)}$$

where V_2° is the standard partial molar volume; A_V is the Debye-Huckel limiting slope as defined by Bradley and Pitzer (1979) and evaluated using the dielectric constant of water of Archer and Wang (1990); and $b = 1.2\ kg^{1/2}\cdot mol^{-1/2}$; T is the temperature; $R = 8.314\ J\cdot K^{-1}\cdot mol^{-1}$; and $\beta^{(0)V}$ and $\beta^{(1)V}$ are two fitting parameters. The function f(I) is given by

$$f(I) = \left\{1 - (1 + aI^{1/2})\exp(-aI^{1/2})\right\}/(a^2 I) \qquad \text{(VI.3.3)}$$

where $a = 2.0\ kg^{1/2}\cdot mol^{-1/2}$ and I is the ionic strength.

The third viral coefficient usually appearing in equation 5 was neglected since the molalities used for this work are below 1 $mol\cdot kg^{-1}$. It was assumed that $\beta^{(1)V}$ is independent of pressure and that V_2° and $\beta^{(0)V}$ are linear functions of the isothermal

compressibility of water as in the following expressions:

$$V_\phi^\circ = a_1(T) + a_2(T)\beta_1^*(T) \qquad \text{(VI.3.4)}$$

$$\beta^{(0)V} = a_3(T) + a_4(T)\beta_1^*(T) \qquad \text{(VI.3.5)}$$

where $\beta_1^*(T)$ is the isothermal compressibility of water.

Equations (VI.3.2) to (VI.3.5) were fitted to the experimental apparent molar volumes at each temperature by the method of least squares with weights proportional to the solution molality. The standard partial molar volumes V_2^o determined from these fits are listed in table VI.2 and values for the parameters in equations (VI.3.4) and (VI.3.5) and $\beta^{(1)V}$ from the Pitzer equation (VI.3.2) are listed in table VI.3. The fitted and experimental values of $V_{\phi,2}$ are plotted in figures VI.1 to VI.3. With the exception of data below 0.09 mol·kg^{-1}, the fit lies within the estimated experimental uncertainty.

VI.3.2 Temperature- and Pressure-Dependence of $V_{\phi,2}$ for $Gd(CF_3SO_3)_3$(aq)

The Pitzer theory does not consider the temperature dependence of V_2^o, $\beta^{(o)V}$ and $\beta^{(1)V}$. In Chapter III, it was shown that the sharp increase of $V_2^o(NaCF_3SO_3, aq)$ from temperatures of 273 K to ~ 373 K can be described well by the function $\{c_1 + c_2/(T - 228)\}$ with two adjustable parameters c_1 and c_2. It was also demonstrated by Anderson *et*

Table VI.1. Standard partial molar volumes V_2^o of $La(CF_3SO_3)_3(aq)$ from equation (VI.3.2).

	V_2^o /($cm^3 \cdot mol^{-1}$)		
p/MPa	T = 278.33 K	T = 298.03 K	T = 318.06 K
		$La(CF_3SO_3)_3$	
0.1	184.46	185.56	189.01
7.0	191.46	192.04	194.02
30.0	195.17	195.64	197.09

Table VI.2. Parameters for the standard partial molar volumes and excess properties $\beta^{(1)V}$ in equations (VI.3.2), (VI.3.4), and (VI.3.5) for $La(CF_3SO_3)_3(aq)^*$.

	T = 278.33/K	T = 298.03/K	T = 318.06/K
$\beta^{(1)V}$/($kg \cdot mol^{-1} \cdot MPa^{-1}$)	-3.195×10^{-3}	-2.775×10^{-3}	-3.303×10^{-3}
a_1/($cm^3 \cdot mol^{-1}$)	243.22	226.87	221.10
a_2/($cm^3 \cdot MPa \cdot mol^{-1}$)	-1.196×10^{5}	-7.814×10^{4}	-5.869×10^{4}
a_3/($kg \cdot mol^{-1} \cdot MPa^{-1}$)	-1.816×10^{-3}	-1.015×10^{-3}	-6.070×10^{-4}
a_4/($kg \cdot mol^{-1}$)	4.201	2.359	1.388

* $\beta^{(0)V} = a_3(T) + a_4(T)\,\beta_1^*(T)$; $V_1^o = a_1(T) + a_2(T)\,\beta_1^*(T)$

Table VI.3. The values of A_v in equation (VI.3.2) and the densities of $H_2O(l)$ and NaCl(aq) (m = 5.6940 mol·kg^{-1}) used in this work (Hill, 1990; Archer, 1992)

T/K	p/MPa	ρ_i^*/(kg·m^3)	ρ_{NaCl}/(kg·m^3)	Av/(cm^3·kg$^{1/2}$·mol$^{-3/2}$)
373.33	7.07	961.481	1143.381	4.000
372.97	26.11	970.275	1150.357	3.685
423.12	7.08	920.779	1108.081	7.248
423.17	25.61	930.624	1115.454	6.510
472.40	7.17	869.827	1068.843	14.126
472.40	25.50	882.531	1077.279	12.086

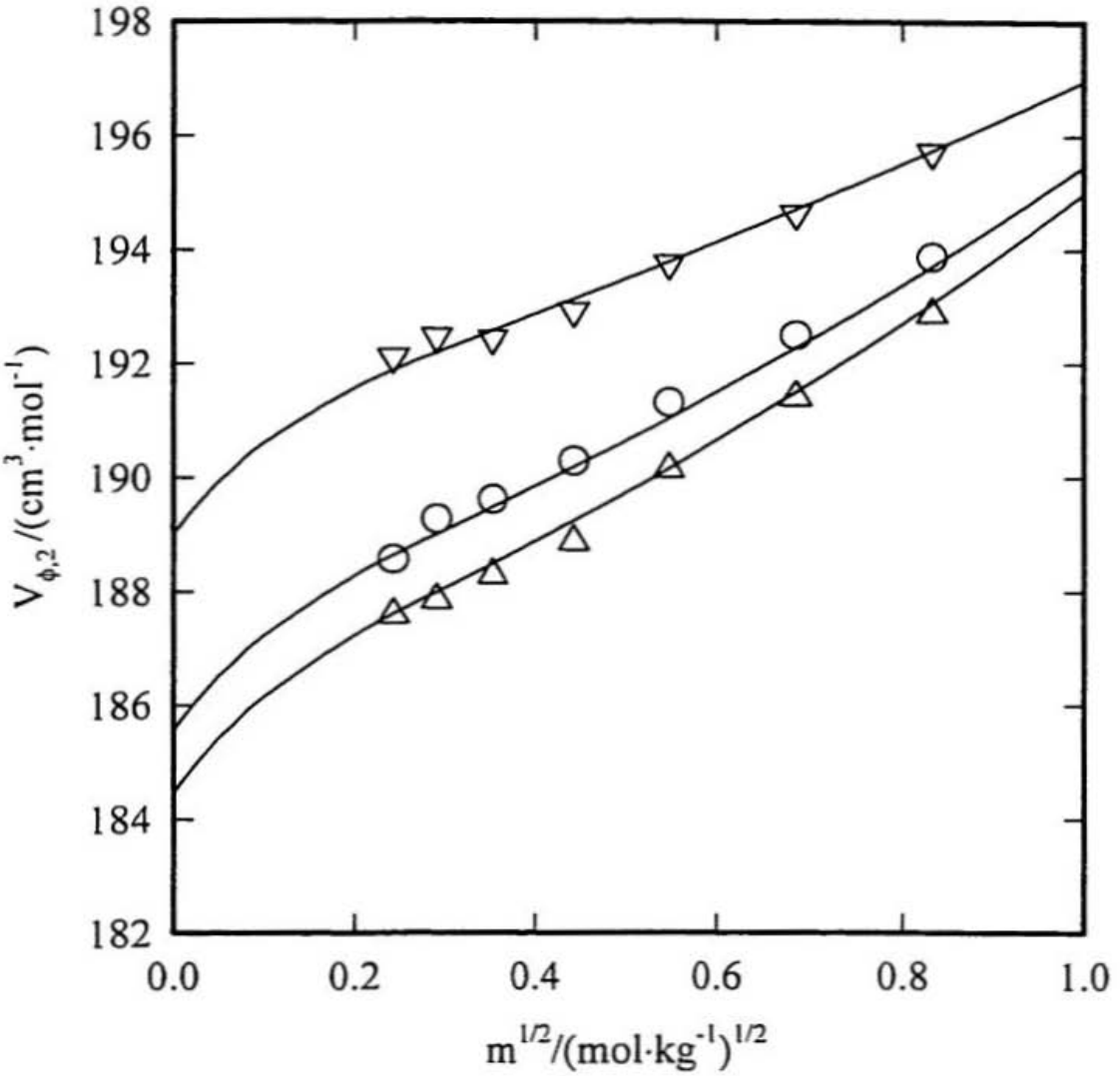


Figure VI.1. Apparent molar volumes of $La(CF_3SO_3)_3(aq)$ at 278 K and at 0.1 MPa (Δ), 7.0 MPa (O) and 30.0 MPa (∇). The solid lines show values calculated according to equation (VI.3.2) and parameters in tables VI.2 and VI.3.

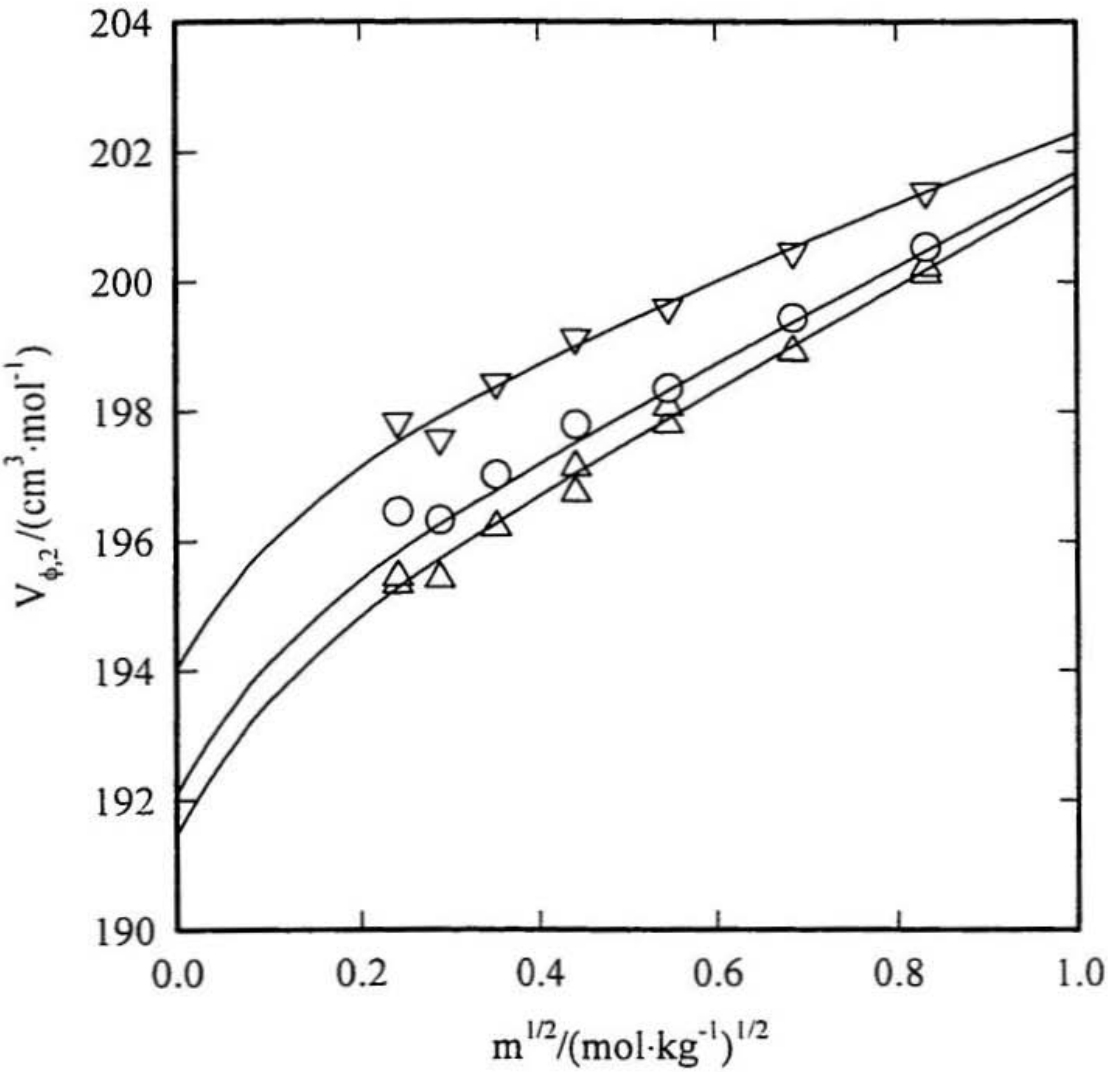


Figure VI.2. Apparent molar volumes of $La(CF_3SO_3)_3(aq)$ at 298 K and at 0.1 MPa (Δ), 7.0 MPa (O) and 30.0 MPa (∇). The solid lines show values calculated according to equation (VI.3.2) and parameters in tables VI.2 and VI.3.

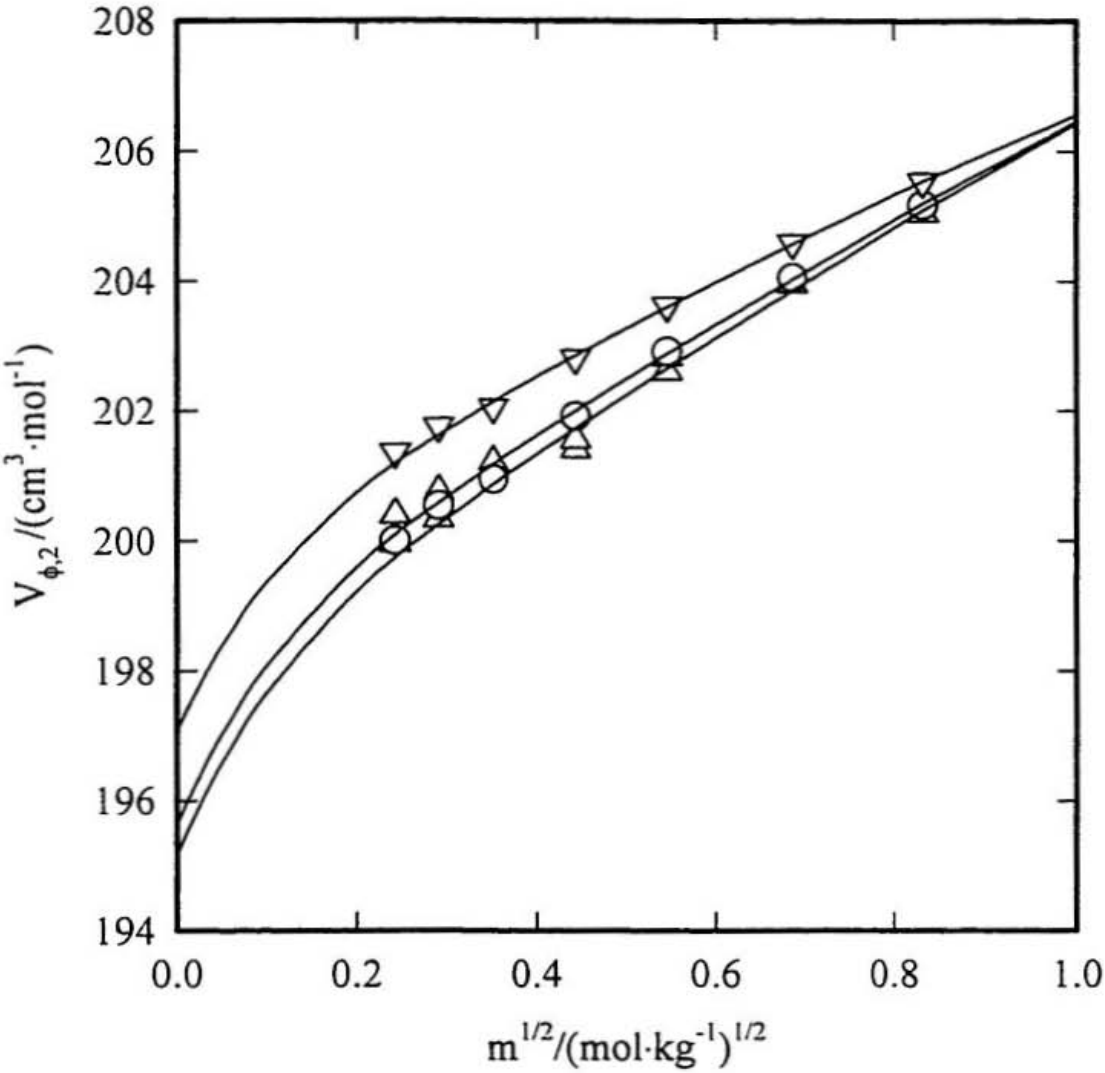


Figure VI.3. Apparent molar volumes of $La(CF_3SO_3)_3(aq)$ at 318 K and at 0.1 MPa (Δ), 7.0 MPa (O) and 30.0 MPa (∇). The solid lines show values calculated according to equation (VI.3.2) and parameters in tables VI.2 and VI.3.

al. (1991), Oakes *et al.* (1995), and Tremaine *et al.* (1996) that the compressibility of the solvent water $\beta_1^* = -(1/V)(\partial V/\partial p)_T$ was a good independent variable to formulate empirical equations which represent the nonlinear behaviour of V_2^o with respect to pressure and temperature. The following empirical expressions were used to represent the temperature and pressure dependence of V_2^o, $\beta^{(o)V}$ and $\beta^{(1)V}$:

$$\beta^{(o)V} = c_1 + c_2 T + c_3/T \qquad \text{(VI.3.6)}$$

$$\beta^{(1)V} = c_4 + (c_5 + c_6 T)p/(T - 228) + c_7\beta_1^* + c_8(\beta_1^*)^2 T \qquad \text{(VI.3.7)}$$

$$V_2^o = c_9 + (c_{10} + c_{11}p)/(T - 228) + c_{12}\beta_1^* + c_{13}\beta_1^* T^2 \qquad \text{(VI.3.8)}$$

where p is pressure and β_1^* is the isothermal compressibility of water.

Equations (VI.3.2), and (VI.3.6) to (VI.3.8) were fitted to the experimental data for $Gd(CF_3SO_3)_3(aq)$ at all temperatures, pressures and molalities by the method of least squares with weights proportional to the solution molality. Values of the adjustable parameters in equations (VI.3.6) to (VI.3.8) obtained in the fitting are listed in table VI.4. Deviations between the calculated $V_{\phi,2}$ and observed $V_{\phi,2}$ are shown in figure VI.4. The calculated values for $V_{\phi,2}$ minus the Debye-Hückel limiting law (DHLL) term according to equation (VI.3.2) are compared with the experimental results in figures VI.5 and VI.6.

Table VI.4. Coefficients for equations (VI.3.2) and (VI.3.6) to (VI.3.8) describing the temperature and pressure dependence of the parameters V_2^o, $\beta^{(o)V}$, and $\beta^{(1)V}$ for $Gd(CF_3SO_3)_3(aq)$*

Coefficient	For $\beta^{(o)V}$	Coefficient	For $\beta^{(1)V}$	Coefficient	For V_2^o
c_1	$2.62142 \cdot 10^{-3}$	c_4	$-1.35802 \cdot 10^{-2}$	c_9	$2.05821 \cdot 10^{2}$
c_2	$-5.71357 \cdot 10^{-6}$	c_5	$-1.47524 \cdot 10^{-2}$	c_{10}	$-1.80408 \cdot 10^{3}$
c_3	$-2.85310 \cdot 10^{-1}$	c_6	$4.15251 \cdot 10^{-5}$	c_{11}	9.56900
		c_7	$4.23018 \cdot 10^{1}$	c_{12}	$6.14879 \cdot 10^{2}$
		c_8	$-1.26656 \cdot 10^{2}$	c_{13}	$-4.56595 \cdot 10^{-1}$

* The units of temperature T, pressure, and compressibility β_1^* in equations (VI.3.2) and (VI.3.6) to (VI.3.8) are K, MPa, and MPa^{-1}, respectively.

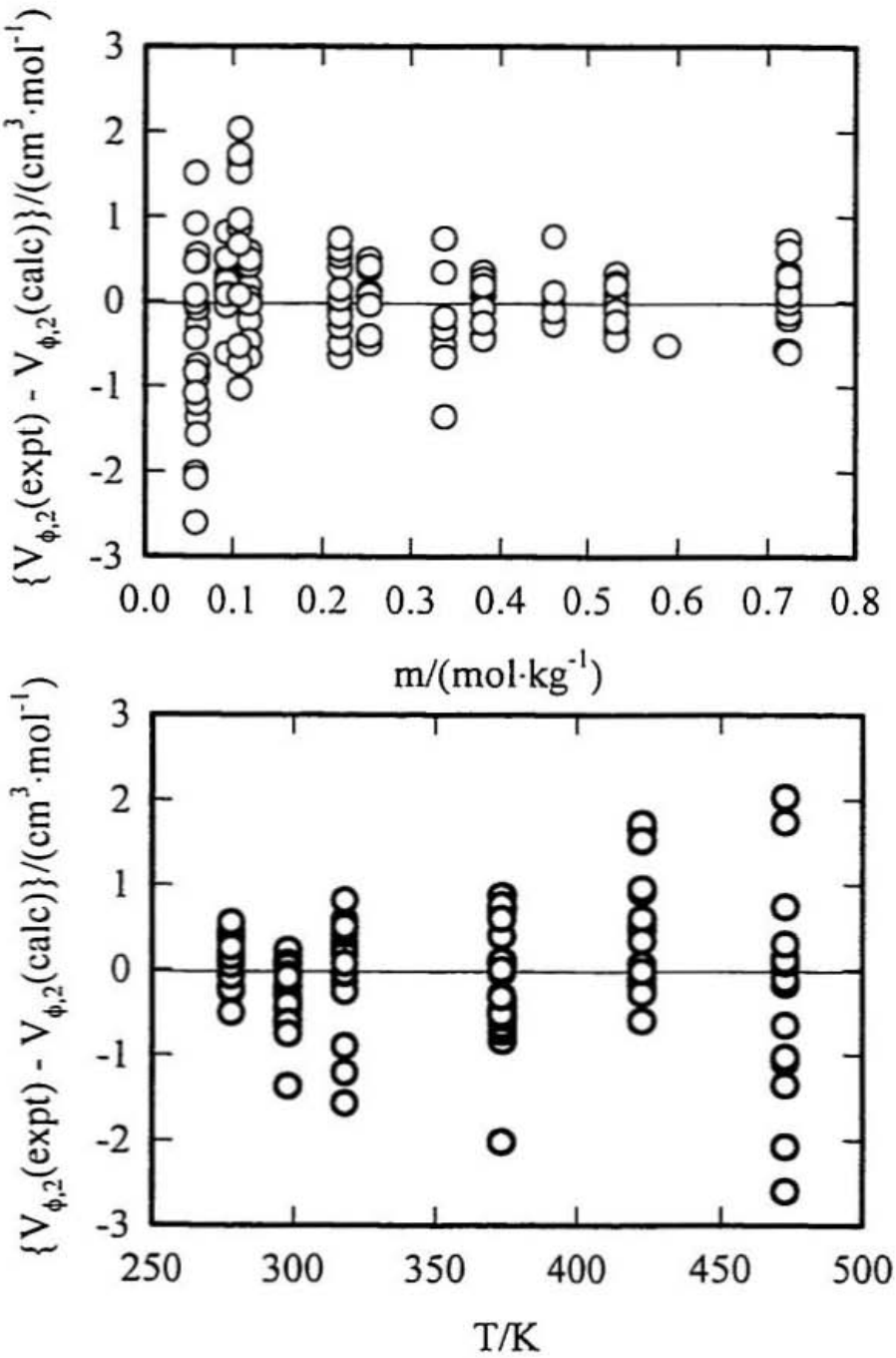


Figure VI.4. $V_{\phi,2}\{Gd(CF_3SO_3)_3, aq\}$ observed minus $V_{\phi,2}\{Gd(CF_3SO_3)_3, aq\}$ calculated from equations (VI.3.2), and (VI.3.6) to (VI.3.8) plotted aganist temperature and molality.

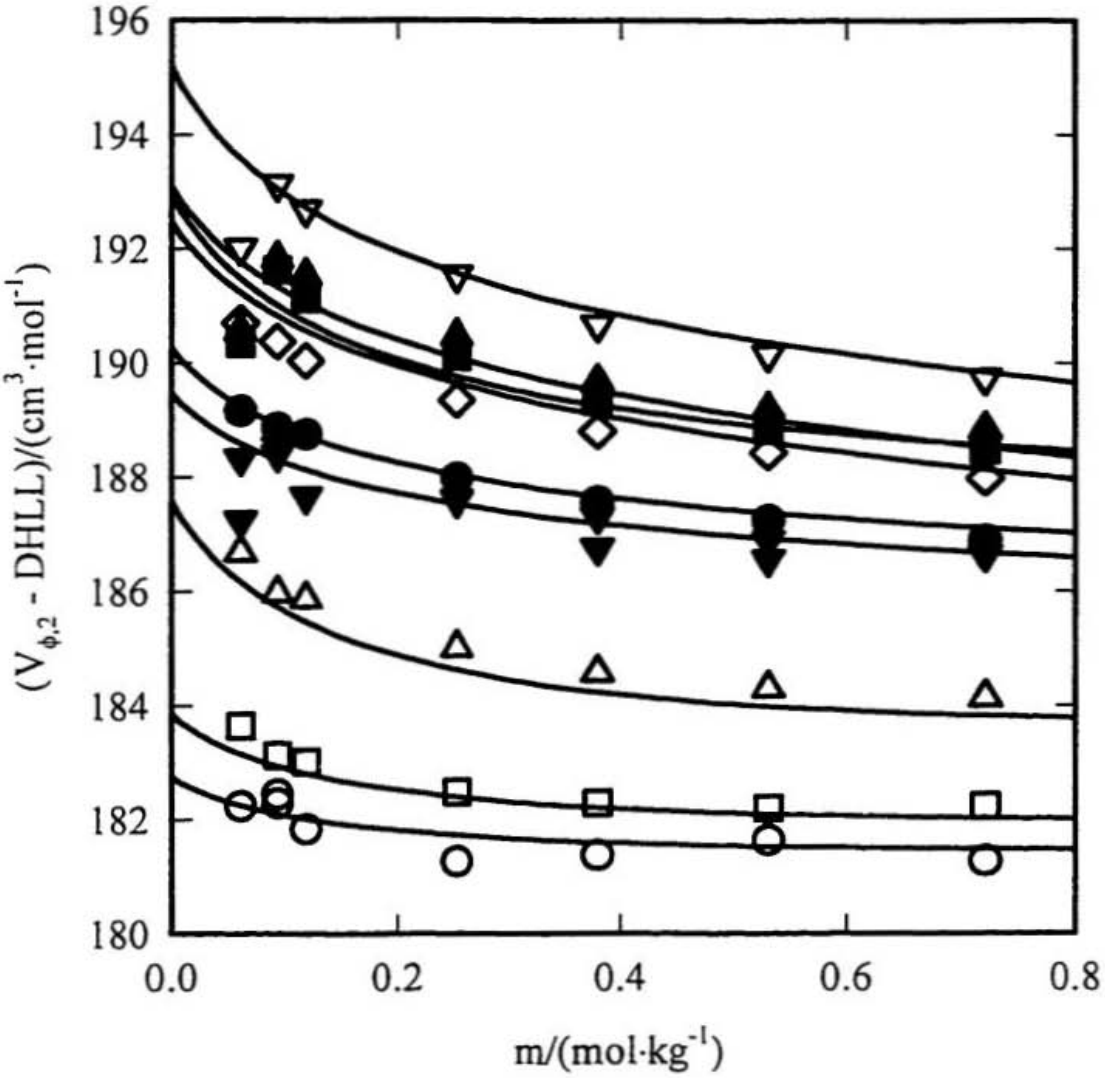


Figure VI.5. $V_{\phi,2}\{Gd(CF_3SO_3)_3, aq\}$ minus the Debye-Hückel limiting slope term according to equation (VI.3.2) plotted against molality: ○, T = 278.33 K, p = 0.1 MPa; □, T = 278.33, p = 7.0 MPa; Δ, T = 278.33 K, P = 30.0 MPa; ▼, T = 298.03 K, p = 0.1 MPa; ●, T = 298.03 K; p = 7.0 MPa; ◇, T = 298.03, p = 30.0 MPa; ■, T = 318.06 K, p = 0.1MPa; ▲, T = 318.06 K, p = 7.0 MPa; ∇, T = 318.06 K, p = 30.0 MPa.

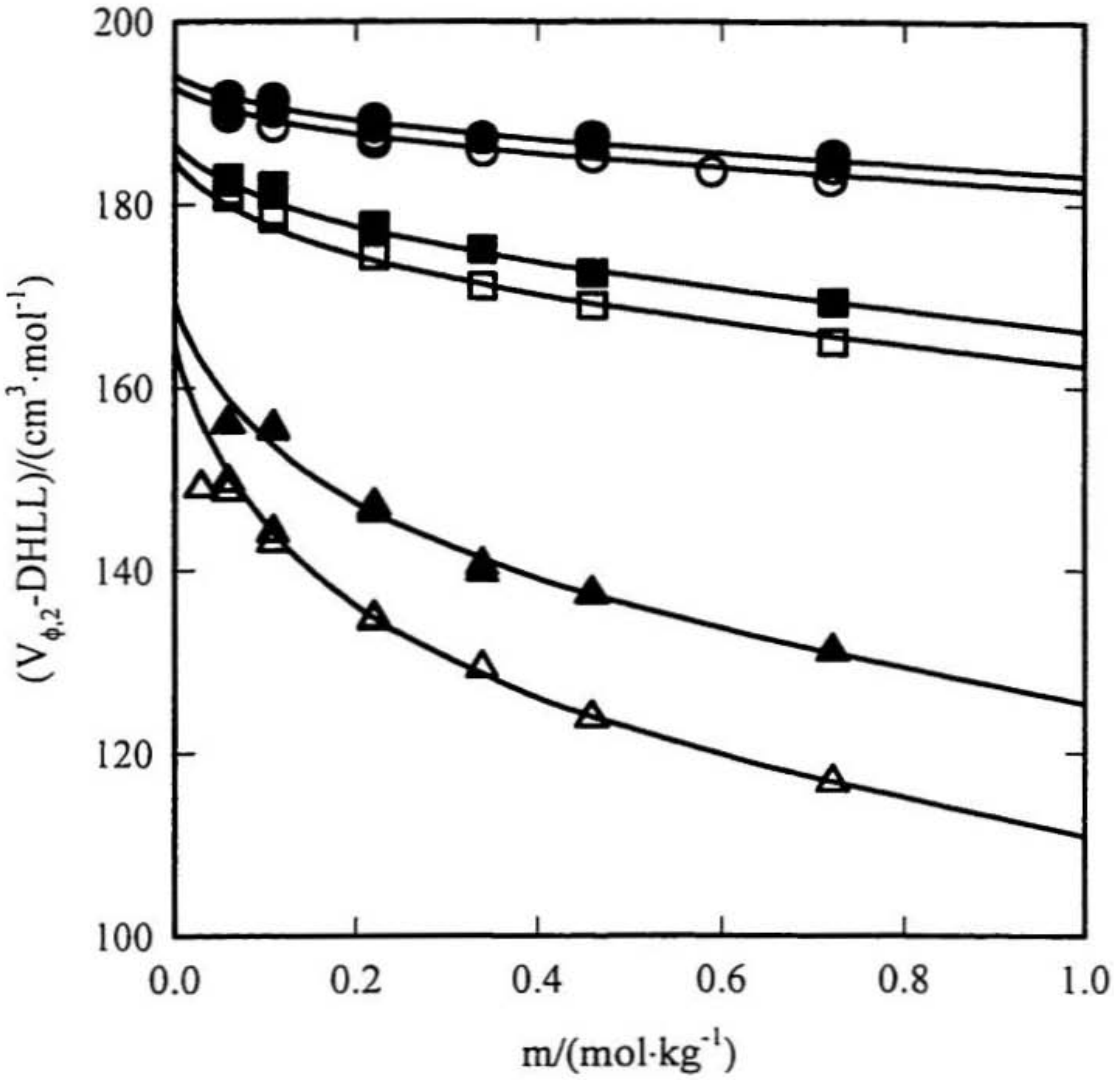


Figure VI.6. $V_{\phi,2}\{Gd(CF_3SO_3)_3, aq\}$ minus the Debye-Hückel limiting slope term according to equation (VI.3.2) plotted against molality: Δ, T = 373.33 K, p = 7.07 MPa; ▲, T = 372.97, p = 26.11 MPa; □, T = 423.12, p = 7.08 MPa; ■, T = 423.17, p = 25.61 MPa; ○, T = 472.40 K, p = 7.17 MPa; ●, T = 472.40, p = 25.50 MPa.

Smoothed values of $V_{\phi,2}$ calculated from equation (VI.3.2) at rounded values of molality, temperature, and pressures $p = p_{sat}$ and $p = 25.0$ MPa are presented in table VI.5 and figure VI.7. The temperature dependence of $\beta^{(0)V}$ and $\beta^{(1)V}$ is illustrated in figure VI.8.

VI.4 Discussion

The hydrolysis of trivalent lanthanides has been critically reviewed by Baes and Mesmer (1976), who concluded that $Gd^{3+}(aq)$ cation does not undergo appreciable hydrolysis in solutions with $pH < 6$ at $m < 1.0$ mol·kg^{-1}. In Chapters IV and V, we confirmed this conclusion by demonstrating that the apparent molar heat capacities $C_{p,\phi,2}$ and $V_{\phi,2}$ for the solutions of $La(ClO_4)_3(aq)$ and $Gd(ClO_4)_3(aq)$ with $3.3 \leq pH \leq 5.3$ agreed with those for solutions with 0.01 mol·kg^{-1} excess $HClO_4$ after the contribution of $HClO_4(aq)$ was subtracted by means of Young's rule. The degree of hydrolysis of aqueous lanthanides at elevated temperature is not known. To suppress any possible hydrolysis of $Gd^{3+}(aq)$, 0.0020 mol·kg^{-1} triflic acid solution was used to dilute the stock solution. At the time when the work was done, no data for $V_{\phi,3}(CF_3SO_3H, aq)$ were available to make the Young's rule correction in $V_{\phi,2}(Gd(ClO_4)_3, aq)$ in the usual way. A calculation using recently reported values for $V_{\phi,3}(CF_3SO_3H, aq)$ in Chapter III shows that the more rigorous calculation changes the values for $V_{\phi,2}\{Gd(ClO_4)_3, aq\}$ by less than 1 cm^3·mol^{-1}.

The sources of error in the measured relative densities for this type of vibrating-

Table VI.5. $V_{\phi,2}$ for $Gd(CF_3SO_3)_3(aq)$ at $p = p_{sat}$ and p= 25.0 MPa

	Molality/(mol·kg^{-1})							
T/K	0	0.05	0.10	0.20	0.30	0.45	0.60	0.72
				$p = p_{sat}$				
278.15	182.73	186.20	187.14	188.28	189.06	189.94	190.63	191.10
298.15	189.57	193.36	194.30	195.41	196.16	197.02	197.69	198.13
318.15	192.57	197.06	198.10	199.32	200.13	201.03	201.71	202.15
338.15	193.61	199.13	200.39	201.82	202.74	203.74	204.47	204.92
373.15	192.38	200.56	202.40	204.43	205.70	207.01	207.91	208.44
423.15	184.04	198.46	201.49	204.79	206.87	209.01	210.48	211.34
473.15	162.63	186.46	189.97	193.78	196.50	199.76	202.34	204.02
				p = 25.0 MPa				
278.15	186.64	189.35	189.92	190.62	191.15	191.80	192.36	192.75
298.15	192.39	195.58	196.24	197.03	197.60	198.28	198.84	199.22
318.15	194.79	198.69	199.50	200.44	201.09	201.82	202.39	202.77
338.15	195.50	200.37	201.40	202.55	203.31	204.13	204.74	205.11
373.15	194.10	201.35	202.93	204.65	205.72	206.79	207.51	207.92
423.15	186.55	199.25	201.97	204.88	206.66	208.40	209.52	210.13
473.15	168.79	190.01	193.77	197.79	200.69	203.20	205.20	206.38

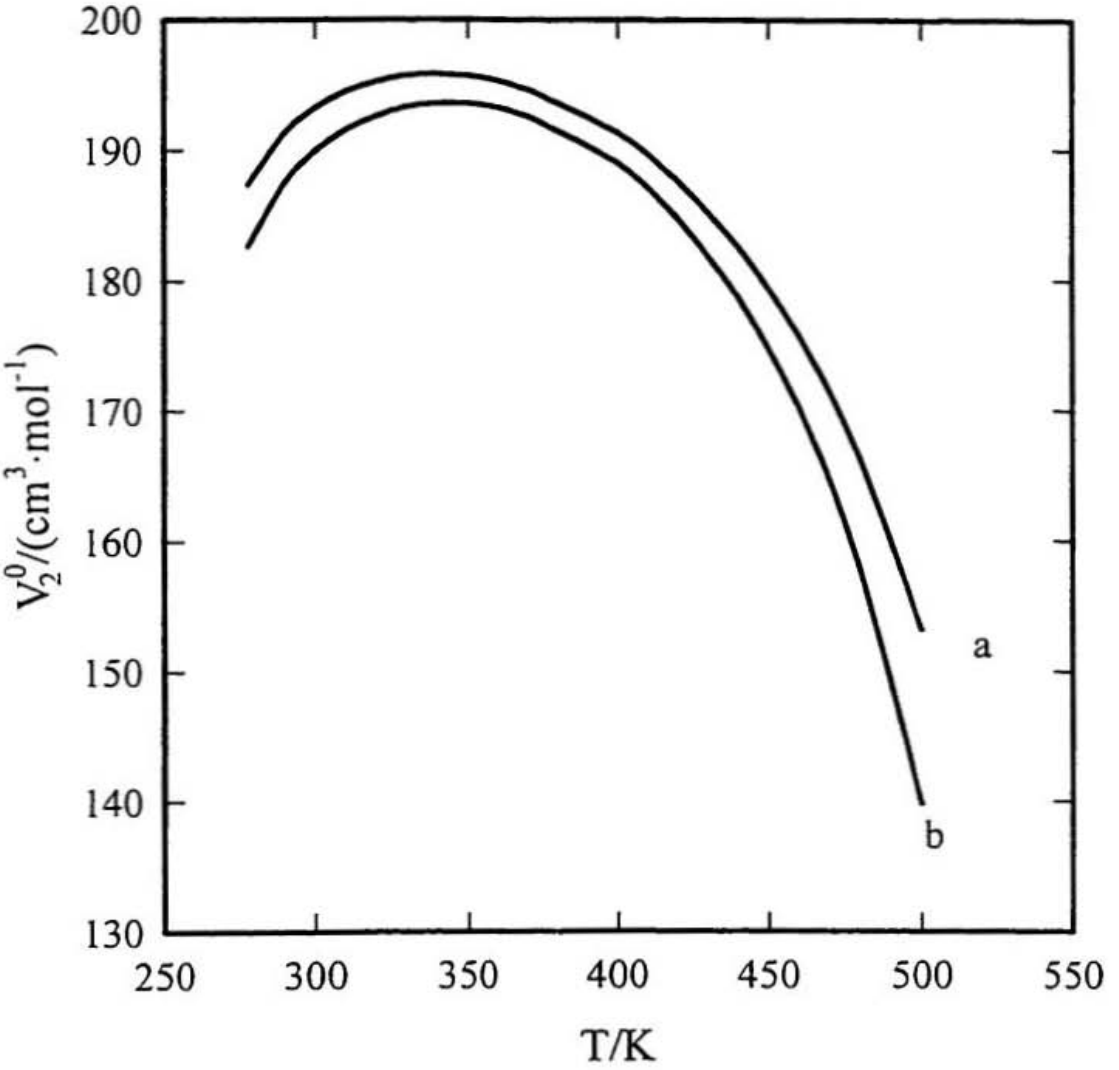


Figure VI.7. V_2° calculated from equation (VI.3.8) plotted against temperature: (a), p = 25.0 MPa; (b), $p = p_{sat}$.

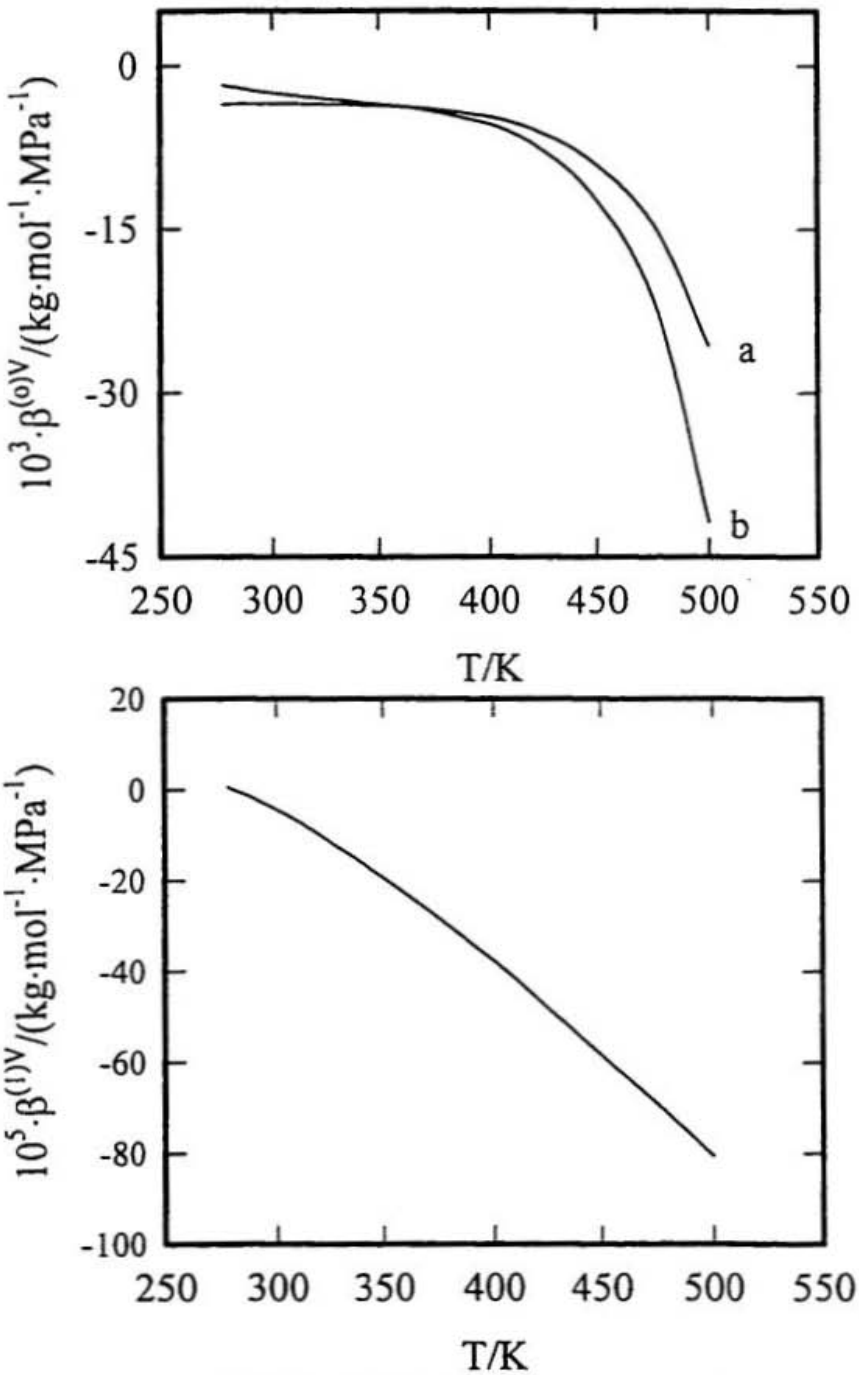


Figure VI.8. $\beta^{(0)V}$ (upper) and $\beta^{(1)V}$ (low) plotted against temperature: (a), p = 25.0 MPa; (b), $p = p_{sat}$.

tube densitometer have been discussed by Oakes *et al.* (1995). We estimated that uncertainty in densities for the most dilute solution (m = 0.058053 mol·kg^{-1}) was 0.1 kg·m^{-3} and that the uncertainty for the most concentrated solution (m = 0.7230 mol·kg^{-1}) was about 0.3 kg·m^{-3}. Those error limits in density lead to uncertainties of 2.2 cm^3·mol^{-1} in $V_{\phi,2}$ for the solution with m = 0.05805 mol·kg^{-1} and 0.5 cm^3·mol^{-1} for the solution with m = 0.72300 mol·kg^{-1}. As shown in figure (VI.3.4), equations (VI.3.2) nad (VI.3.6) to (VI.3.8) represent the experimental results to within the estimated errors.

It has been demonstrated that the solution molalities calculated from the delivery ratios of the high precision Ruska pump are reliable (Oakes *et al.*, 1995; Simonson *et al.*, 1994). To confirm the accuracy of the molalities in this work, two dilutions of a NaCl(aq) solution with m = 5.6940 mol·kg^{-1} were made with the volumetric delivery ratios 1:1 and 1:5 {NaCl(aq) to water} at system pressure p = 6.72 MPa, to yield solutions with m = 2.6854 mol·kg^{-1} and m = 0.86252 mol·kg^{-1}. The measured relative densities ($\rho - \rho_1^*$) for those two solutions at p = 6.72 MPa and T = 373.18 K were 94.57 kg·m^{-3} and 32.62 kg·m^{-3}, respectively, and these agree well with the values 94.64 kg·m^{-3} and 32.56 kg·m^{-3} calculated from the equation of state given by Archer (1992). To minimize the effect of errors in molality, the solution with m = 0.058053 mol·kg^{-1} was directly pushed into the densimeter tube so that its concentration was not affected by the operational condition of the Ruska pump.

VI.4.1 The Effect of Pressure on $V_{\phi,2}$

The pressure effect on $V_{\phi,2}$ is pronounced at temperatures $T \leq 298$ and $T \leq 473$ K. In contrast, $V_{\phi,2}$ at p = 7.0 MPa are almost identical to $V_{\phi,2}$ at p = 26 MPa at T = 423 K over the whole concentration range studied (figure VI.9). This suggests that there is a minimun temperature dependence of apparent molar compressibility $\kappa_{\phi,2} = -(\partial V_{\phi,2}/\partial p)_{T,m}$. A similar phenomena was observed for NaCl(aq) (Tanger and Helgeson, 1988; Simonson, 1994). The increase of $\kappa_{\phi,2}$ at elevated temperatures is predicted by the Born model. Configurational hydration effect may account for the decrease of $\kappa_{\phi,2}$ in the low temperature range.

Compressibility methods have been used to determine the hydration number for cations at T = 298.15 K (Janenas, 1978; Rizkalla and Choppin, 1991). Under the strong electrostatic field of the ion, the water molecules in the immediate vicinity of the ion are incompressible compared to the free molecules of the solvent. If the hydrated cation is assumed to be incompressible and embedded in a continuous solvent, then

$$(\partial V_{\phi,2}/\partial p)_T = nV\beta + 55.51(V_1^*\beta_1^* - V\beta)/m \qquad \text{(VI.4.1)}$$

where m is the solution molality, V is the volume of the solution containing 1 kg solvent and m moles of solute, V_1^* is the molar volume of water, β_1^* is the compressibility of water, and β is the compressibility of the solution.

Apparently, $\kappa_{\phi,2}$ is affected by the number of water molecules in the

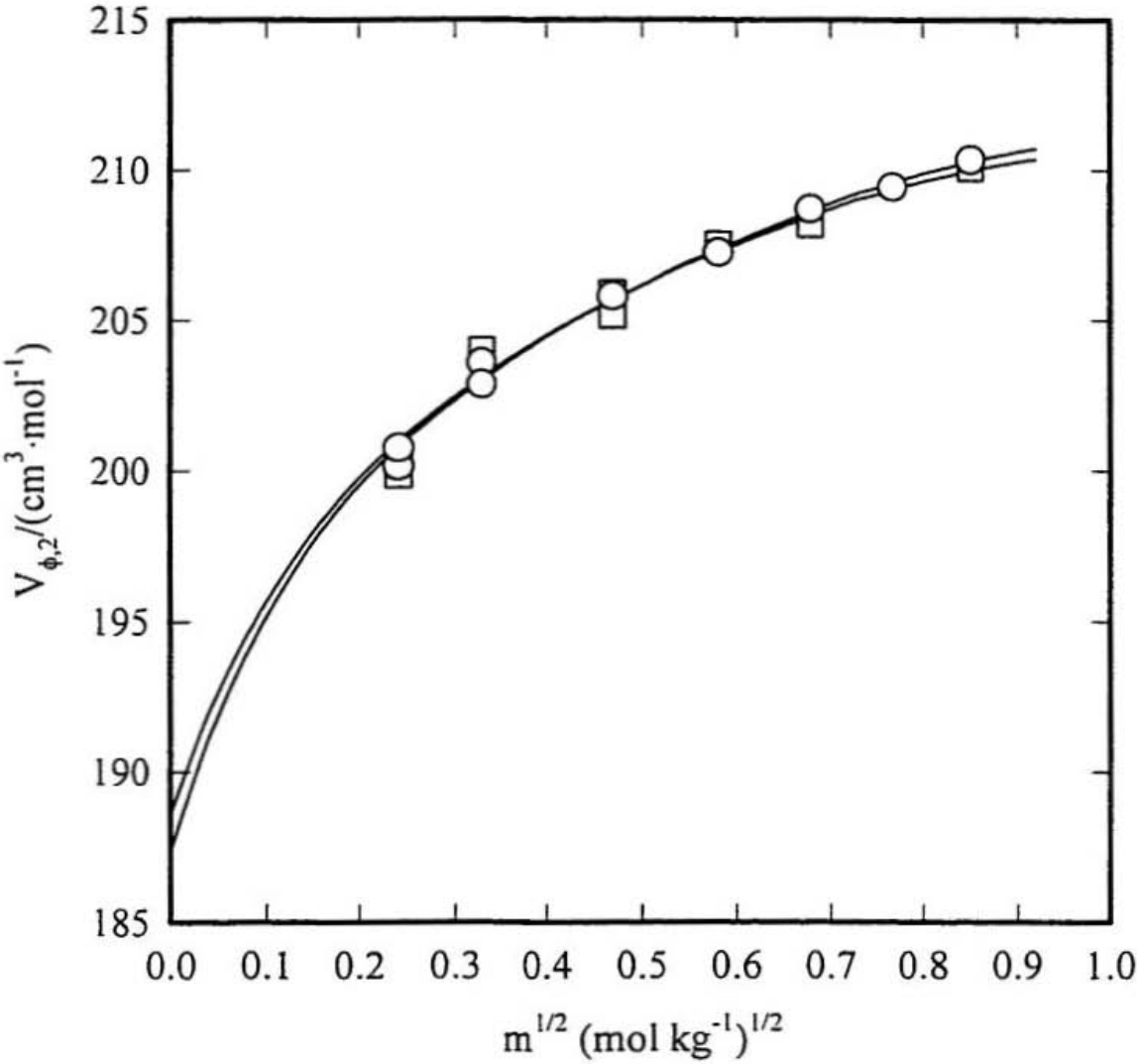


Figure VI.9. $V_{\phi,2}$ plotted against the square root molality at T = 423 K: ○, p = 7.08 MPa; □, p = 25.61 MPa.

incompressible first hydration shell. Aqueous lanthanide cations have hydration numbers between 8 and 9 in the first hydration shell while aqueous cations such as $Na^+(aq)$, $Li^+(aq)$, and $Ca^{2+}(aq)$ have hydration numbers of six or less (Ohtaki and Radnai, 1993). Thus, according to equation (VI.4.1), the pressure dependence of $V_{\phi,2}$ for trivalent lanthanide ions at ambient condition is expected to be more pronounced than that for ordinary 1:1 and 2:1 electrolytes, provided the contribution from the anions is small. The pressure dependence of $V_{\phi,2}\{Gd(CF_3SO_3)_3, aq\}$ is pronounced compared to that for $NaCF_3SO_3(aq)$ as shown in Chapter III. One cannot calculate the absolute value for $Gd^{3+}(aq)$ without the compresibility value for $H^+(aq)$. On the conventional scale, $\{\kappa^o(H^+, aq) \equiv 0\}$, the value of $\kappa^o(Gd^{3+}, aq) = 0.16\ cm^3 \cdot mol^{-1} \cdot MPa^{-1}$ at T = 298.15 K was calculated from our data for $Gd(CF_3SO_3)_3(aq)$, $NaCF_3SO_3(aq)$, and $HCF_3SO_3(aq)$. It is greater than the values $\kappa^o(Na^+, aq) = 0.031\ cm^3 \cdot mol^{-1} \cdot MPa^{-1}$, $\kappa^o(Li^+, aq) = 0.029\ cm^3 \cdot mol^{-1} \cdot MPa^{-1}$, and $\kappa^o(Ca^{2+}, aq) = 0.076\ cm^3 \cdot mol^{-1} \cdot MPa^{-1}$ compiled by Tanger and Helgeson (1988). This may reflect the unusual structure of the hydrated lanthanide cations.

VI.4.2 The Standard Partial Molar Volume V_2^o of $Gd^{3+}(aq)$

Standard partial molar volumes based on the convention ($V_2^o(H^+, aq) \equiv 0$) were calculated for $Gd^{3+}(aq)$ from values of $V_2^o\{Gd(CF_3SO_3)_3, aq\}$ and $V_2^o(CF_3SO_3^-, aq)$. These are presented in table VI.6 and in figure VI.10, along with values of $V_2^o(Gd^{3+}, aq)$ obtained from data for $V_2^o\{Gd(ClO_4)_3, aq\}$ in Chapter IV and values of $V_2^o(ClO_4^-, aq)$ taken from

Table VI.6. Conventional standard partial molar volumes $V_2^o(Gd^{3+}, aq)/(cm^3 \cdot mol^{-1})$ at p = p_{sat}

T/K	283.15	298.15	313.15	328.15	343.15	373.15	423.15	473.15
V_2^o	-33.08	-34.41	-36.41	-39.13	-42.06	-49.15	-63.79	-82.59
	(-36.01)[a]	(-39.73)	(-41.89)	(-44.37)				

[a] The numbers in the parentheses are calculated from $V_2^o\{Gd(CF_3SO_3)_3, aq)$ and $V_2^o(HCF_3SO_3, aq)$

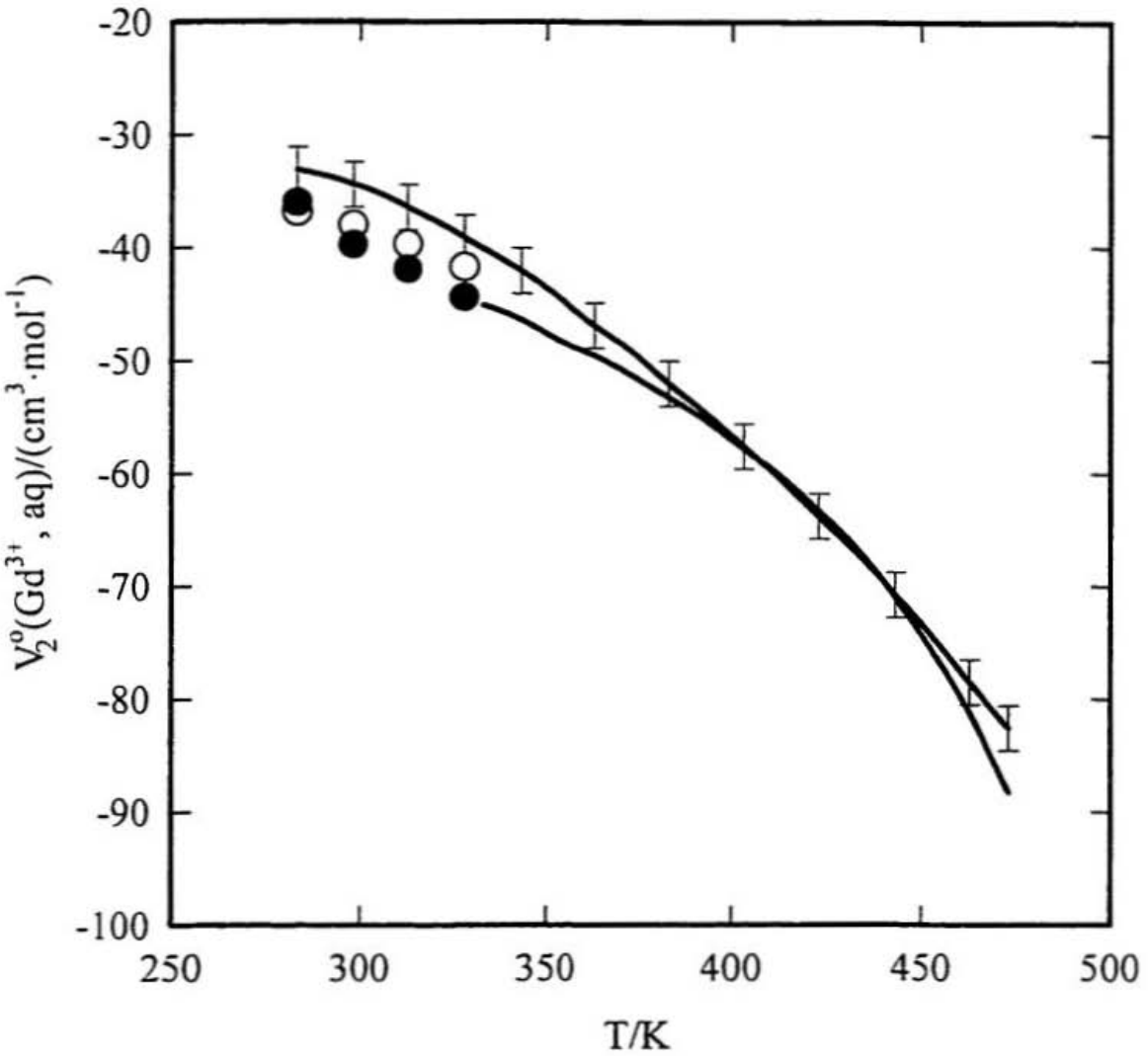


Figure VI.10. $V_2^o(Gd^{3+}, aq)$ plotted against temperature: ○, calculated from values for $V_2^o\{Gd(CF_3SO_3)_3, aq\}$ and $V_2^o(HCF_3SO_3, aq)$; ●, calculated from experimental values for $V_2^o\{Gd(ClO_4)_3, aq\}$ and $V_2^o(ClO_4^-, aq)$ (Tanger and Helgeson, 1988); solid line, calculated from values for $V_2^o\{Gd(ClO_4)_3, aq\}$ predicted in Chapter IV and $V_2^o(ClO_4^-, aq)$ (Tanger and Helgeson, 1988); solid line with error bars, calculated from values for $V_2^o\{Gd(CF_3SO_3)_3, aq\}$ and $V_2^o(NaCF_3SO_3, aq)$ (Chapter III). Error bars show the estimated error limits for $V_2^o\{Gd(CF_3SO_3)_3, aq\}$.

the compilation by Tanger and Helgeson (1988). Although values for $V_2^o(Gd^{3+}, aq)$ obtained from the triflate salt and sodium triflate are systematically more positive than those from the perchlorate salt by about 5 $cm^3 \cdot mol^{-1}$ in the same temperature range, the agreement between the values of $V_2^o(Gd^{3+}, aq)$ obtained from $V_2^o\{Gd(CF_3SO_3)_3, aq\}$ and $V_2^o\{Gd(ClO_4)_3, aq\}$ is satisfactory, since the combined errors in the calculation of $V_2^o(Gd^{3+}, aq)$ could be as large as 7 $cm^3 \cdot mol^{-1}$. The values of $V_2^o(Gd^{3+}, aq)$ at $340\ K \leq T \leq 473\ K$ and the saturation pressure of water calculated from $V_2^o\{Gd(CF_3SO_3)_3, aq\}$ are in excellent agreement with those calculated from values of $V_2^o\{Gd(ClO_4)_3, aq\}$ extrapolated from the results at low temperature (Chapter IV).

VI.5 Conclusion

The values of $V_2^o(Gd^{3+}, aq)$ at $278\ K < T < 473\ K$ and $0.1\ MPa < p < 25\ MPa$ are the first reported volumetric properties for trivalent cations at these conditions. The pronounced effect of pressure on V_2^o at near $T = 298.15\ K$ reflects the unusual hydration structure of aqueous lanthanide ions. The agreement between values of $V_2^o(Gd^{3+}, aq)$ from this measurement on $Gd(CF_3SO_3)_3(aq)$ and those extrapolated from our low-temperature data for $Gd(ClO_4)_3(aq)$ strongly supports the HKF approach for aqueous trivalent salts.

Part Three. Thermodynamics of (Methanol + water) at Elevated Temperature and Pressure

Chapter VII Excess Molar Volumes and Densities of (Methanol + Water) at Temperatures between 323 K and 573 K and Pressures of 7.0 MPa and 13.5 MPa

VII.1 Introduction

A knowledge of the (p, V_m, T) properties of (methanol + water) over a wide range of temperature and pressure is of interest in understanding the role of hydrogen bonding and other non-electrostatic effects on solvation. Densities ρ and excess molar volumes V_m^E for this system are available at ambient conditions (McGlashan and Williamson, 1976; Benson and Kiyohara, 1980; Patel and Sandler, 1985), and some data at temperatures T < 348 K and pressures up to 350 MPa have been reported (Götze and Schneider, 1980; Easteal and Woolf, 1985a, 1985b; Kubota *et al.*, 1987). Other thermodynamic properties, such as excess molar heat capacity and excess molar enthalpy, are known only at temperatures near T = 298.15 K (Benson *et al.*, 1982; Lama and Lu, 1965; Duttachoudhury and Mathur, 1974). Pressure-dependent excess molar enthalpies of (methanol + water) have been reported by Simonson *et al.* (1987) at temperatures up to 573 K, from which V_m^E can be derived. The only other measurements for (methanol + water) at temperatures above 348 K that have been reported are the critical temperatures (Griswold and Wong, 1952; Marshall and Jones, 1974), one point on the critical pressure locus (Griswold and Wong, 1952), and (vapour + liquid) equilibrium data (Griswold and Wong, 1952; Ohe, 1989, 1990). This Chapter presents the results of experimental

measurements to determine ρ and V_m^E of $\{xCH_3OH + (1 - x)H_2O\}$ from ambient to near-critical conditions (temperature range, 323 K ≤ T ≤ 573 K ; pressures, p = 7.0 MPa and p = 13.5 MPa).

VII.2 Experimental

Measurements were made in a stainless steel-cell vibrating-tube densimeter, constructed according to the design of Albert and Wood (1983), as modified by Corti and Fernandez-Prini (1990). The densimeter and the flow system for injecting fluids have been described in Chapter II.

Methanol solutions were prepared by diluting Spectro-grade methanol (mass fraction 0.998, Caledon Laboratories Ltd.) with water by mass. Nanopure water with resistivity >17 MΩ·cm was used as the primary reference fluid at all conditions studied in this work, while D_2O supplied and analysed by Atomic Energy of Canada Ltd. (mass fraction 0.9958 of D_2O, mass fraction 0.0042 of H_2O) was used as the second reference fluid for experiments at temperatures below 523 K. For higher temperatures, CO_2 from Matheson Gas Products Canada (mass fraction 0.998) was used as the second reference fluid. The densities of H_2O and D_2O were obtained from the equations of state reported by Hill (1990) and Hill *et al.* (1982), respectively. The tabulated densities for D_2O were corrected for the content of H_2O by Raoult's law approximation. Densities of CO_2 were interpolated from the values tabulated by Angus *et al* (1976), by means of a cubic spline

function. These agree with more recent data (Friend and Huber, 1994) to within 0.1 $kg \cdot m^{-3}$ at T = 573 K. The difference affects the values of $(\rho - \rho_w)$ in table A.VII.1 by no more than 0.05 $kg \cdot m^{-3}$. The overall accuracy of the densimeter was tested by measuring the bubble point pressure of water at 573.83 K. The results agreed with Hill's equation of state (Hill, 1990) to within $\delta T < 0.1$ K or $\delta p < 0.05$ MPa. These equations of state and instrument calibration are all based on the ITS 68 temperature scale. The conversion to ITS 90 affected the results by less than 0.04 K.

VII.3 Results

If the densimeter tube vibrates harmonically at its resonance frequency, the density of a fluid in the vibrating-tube is given, without any approximation, by

$$\rho = \rho_w + K(\tau - \tau_w) \qquad \text{(VII.3.1)}$$

where ρ and ρ_w are the densities of a fluid and the reference fluid (water), respectively; τ and τ_w are the resonance periods for the fluid and water, respectively; and K is a characteristic constant determined by calibration with two reference fluids of known densities.

Excess molar volumes were obtained from the experimental densities for $\{xCH_3OH + (1 - x)H_2O\}$ according to the usual definition:

$$V_m^E = \{xM_a + (1-x)M_w\}/\rho - xM_a/\rho_a - (1-x)M_w/\rho_w \qquad \text{(VII.3.2)}$$

where V_m^E is the excess molar volume; M_a and M_w are the molar masses of methanol ("alcohol") and water, respectively; and ρ_a and ρ_w are the densities of methanol and water, respectively. The densities of water used in the calculation of V_m^E were obtained from Hill's equation of state for water (Hill, 1990), while ρ of methanol was obtained from Goodwin's equation of state (Goodwin, 1987). The ρ and the V_m^E of $\{xCH_3OH + (1 - x)H_2O\}$ are tabulated in table A.VII.1 at each experimental temperature, pressure, and mole fraction.

The densities of pure methanol were also determined in this work at the same temperatures and pressures as the measurements for $\{xCH_3OH + (1 - x)H_2O\}$. The results are listed in table A.VII.2. A small correction for the water content of the methanol was made at each temperature using the mole-fraction dependence of density from our own data for $\{xCH_3OH + (1 - x)H_2O\}$. These corrections are also listed in table A.VII.2. Figure VII.1 plots the differences between our density values for methanol and those calculated from the equation of state (EOS) reported by Goodwin (1987). The average absolute deviation observed for the total of 28 points is 0.33 $kg \cdot m^{-3}$. This value is consistent with the overall experimental uncertainty which we estimate to be 0.40 $kg \cdot m^{-3}$, according to the method described by Majer *et al.* (1991) and Corti *et al.* (1990). The average relative deviation from Goodwin's equation of state is only 0.066 per cent, much less than 0.67 per cent that the EOS derivates from experimental densities determined by Stray *et al.* (1986), to which Goodwin has given the largest statistical

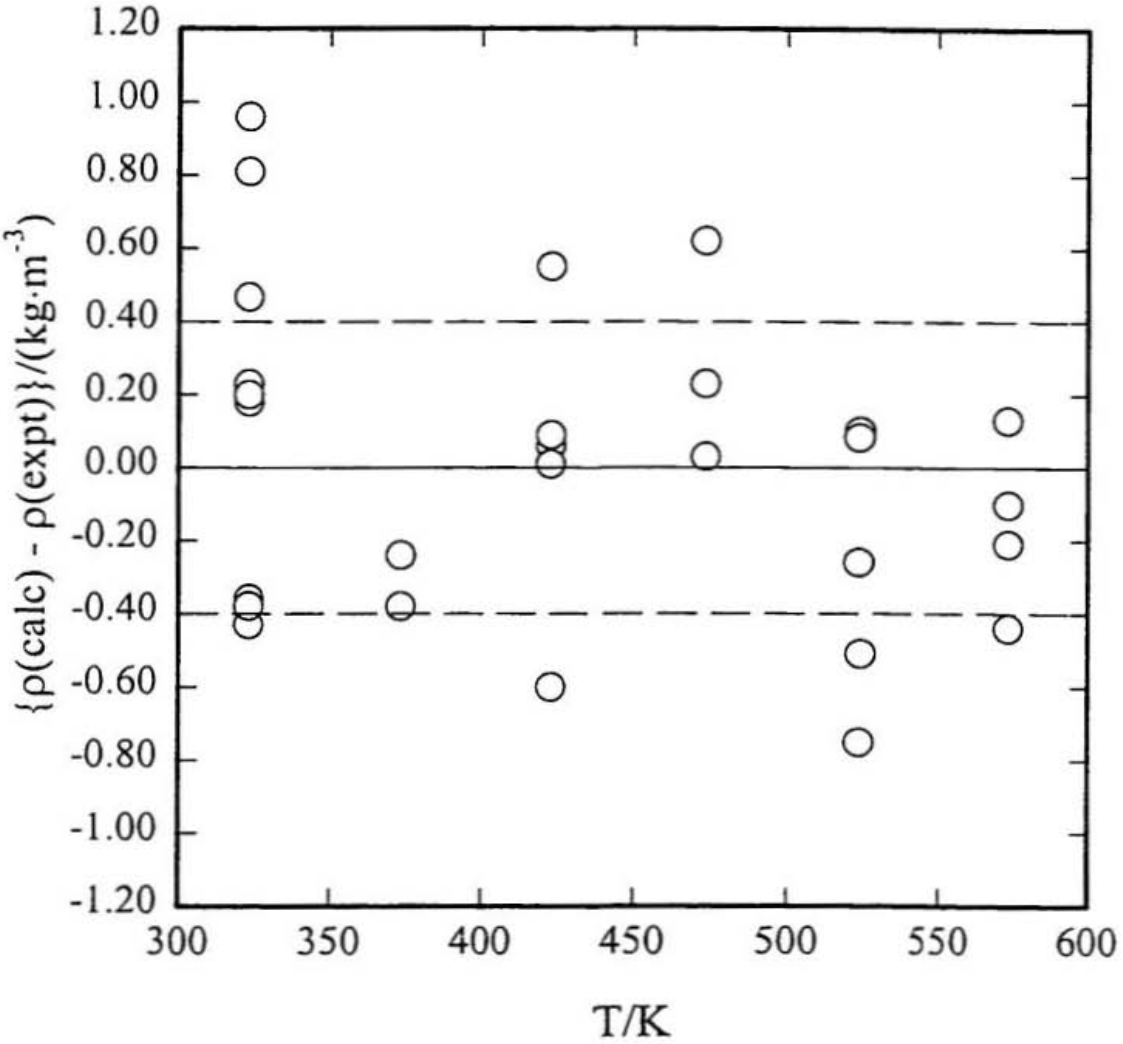


Figure VII.1. Deviations of the experimental densities of pure methanol ρ(expt) from those of Goodwin's equation of state ρ(calc). Dashed lines show the experimental uncertainty.

weight when optimizing the parameters in the EOS.

Plots of V_m^E against x are presented in Figures VII.2 to VII.4, along with values estimated by Simonson *et al.* (1987) from $\{V_m^E - T(\partial V_m^E/\partial T)_p\} = (\partial H_m^E/\partial p)_{T,x}$. None of the densimeter measurements at T < 573 K showed the large density fluctuations associated with the formation of a gas phase in this equipment, and we conclude that the experimental pressures exceeded the saturation pressure for all the data in figures VII.2 to VII.4. Figure VII.5 is a schematic plot of the mole fraction dependance of the molar volumes V_m at constant pressure and temperature, as inferred from our V_m^E data. Clearly, the results at T ≤ 473 K in figures VII.2 and VII.3 lie on isotherm-isobars in the one-phase liquid region (curve d in figure VII.5). The V_m^E data at T = 573 K and p = 13.5 MPa are consistent with a narrow region of (vapour + liquid) phase separation at 0.41 < x < 0.49 (curve c in figure VII.5). However, while the densimeter measurements at x = 0.40888 and x = 0.49641 did show slightly exagerated density fluctuations, none of the very large instabilities typical of two phase (liquid + vapour) mixtures were observed. The possibility that the data were measured just above the critical isotherm-isobar (curve c′ in figure VII.5) is discussed below in Section VII.6. The critical pressure locus for (methanol + water) has not been reported in the literature.

VII.4 Corresponding-States Model

The difficulties in representing ρ and V_m^E of liquid mixtures within the

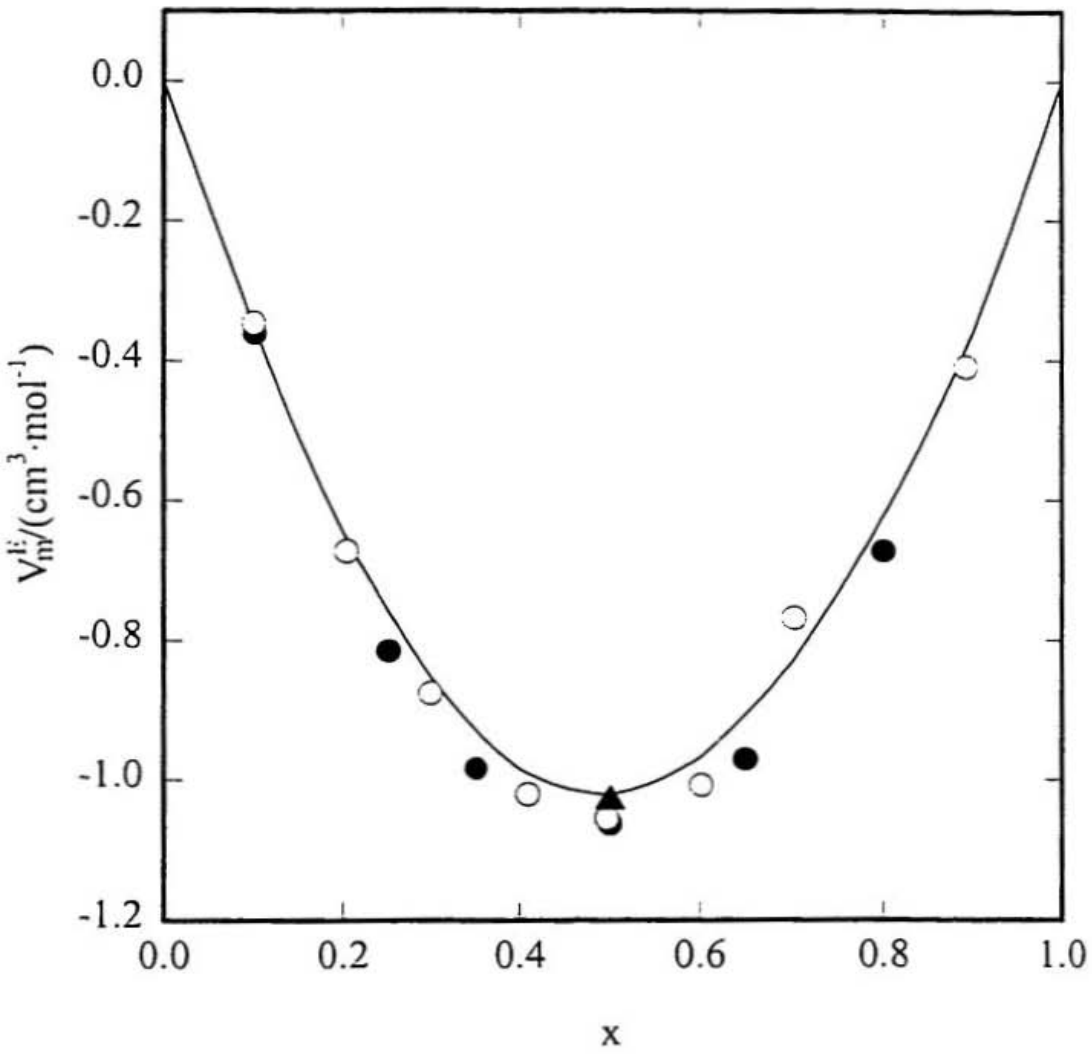


Figure VII.2. Comparison of excess molar volume V_m^E at T = 323 K and p = 0.1 MPa: ○, this work; —, the model; ●, Easteal and Woolf (1985a); ▲, Götze and Schneider (1980).

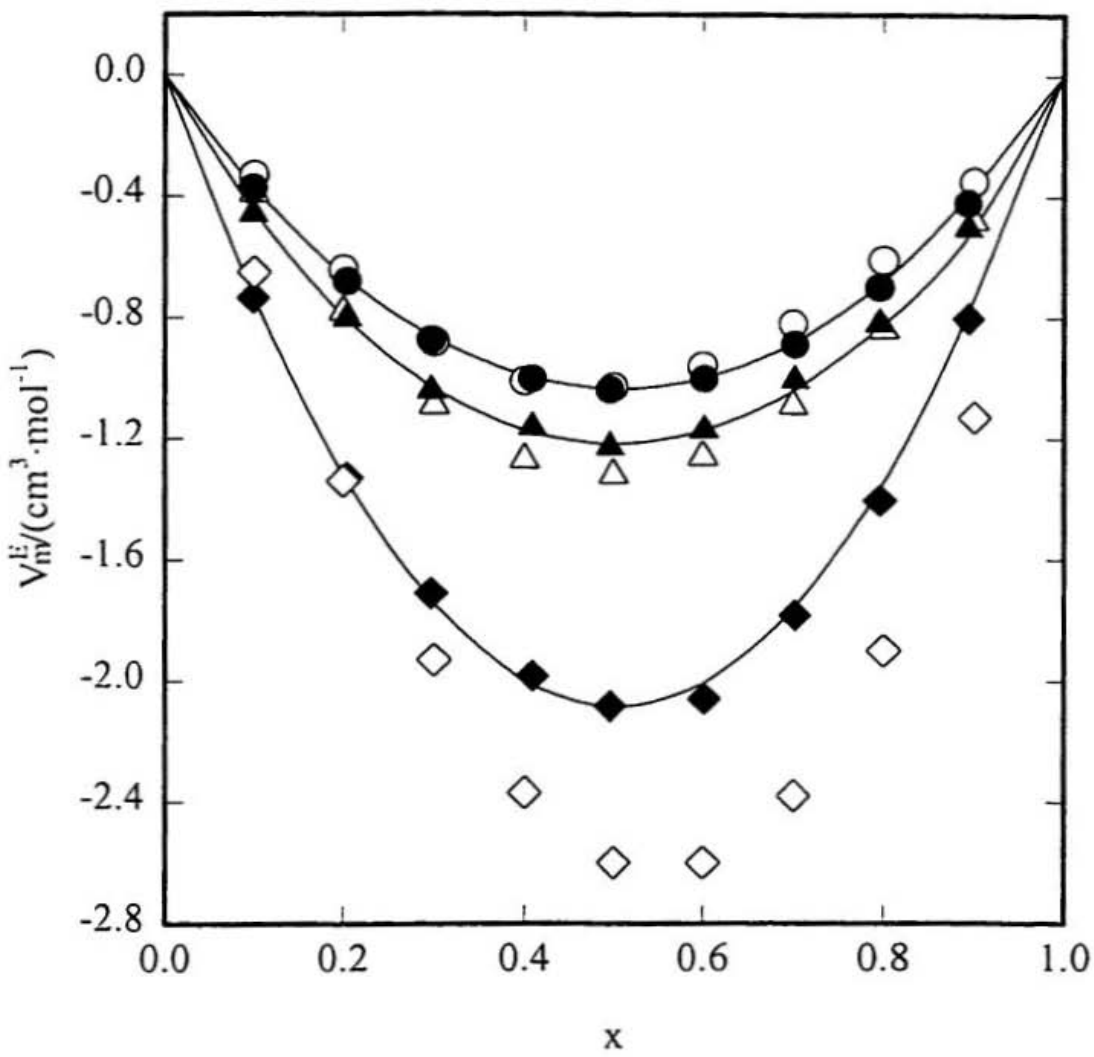


Figure VII.3. Comparison of V_m^E in this work with V_m^E reported by Simonson *et al.* (1987) at p = 7.0 MPa. Solid lines show the values calculated from the model: ●, this work at T = 373 K; ○, Simonson *et al.* at T = 373 K; ▲, this work at T = 423 K; △, Simonson *et al.* at T = 423 K; ◆, this work at T = 473 K; ◇, Simonson *et al.* at T = 473 K.

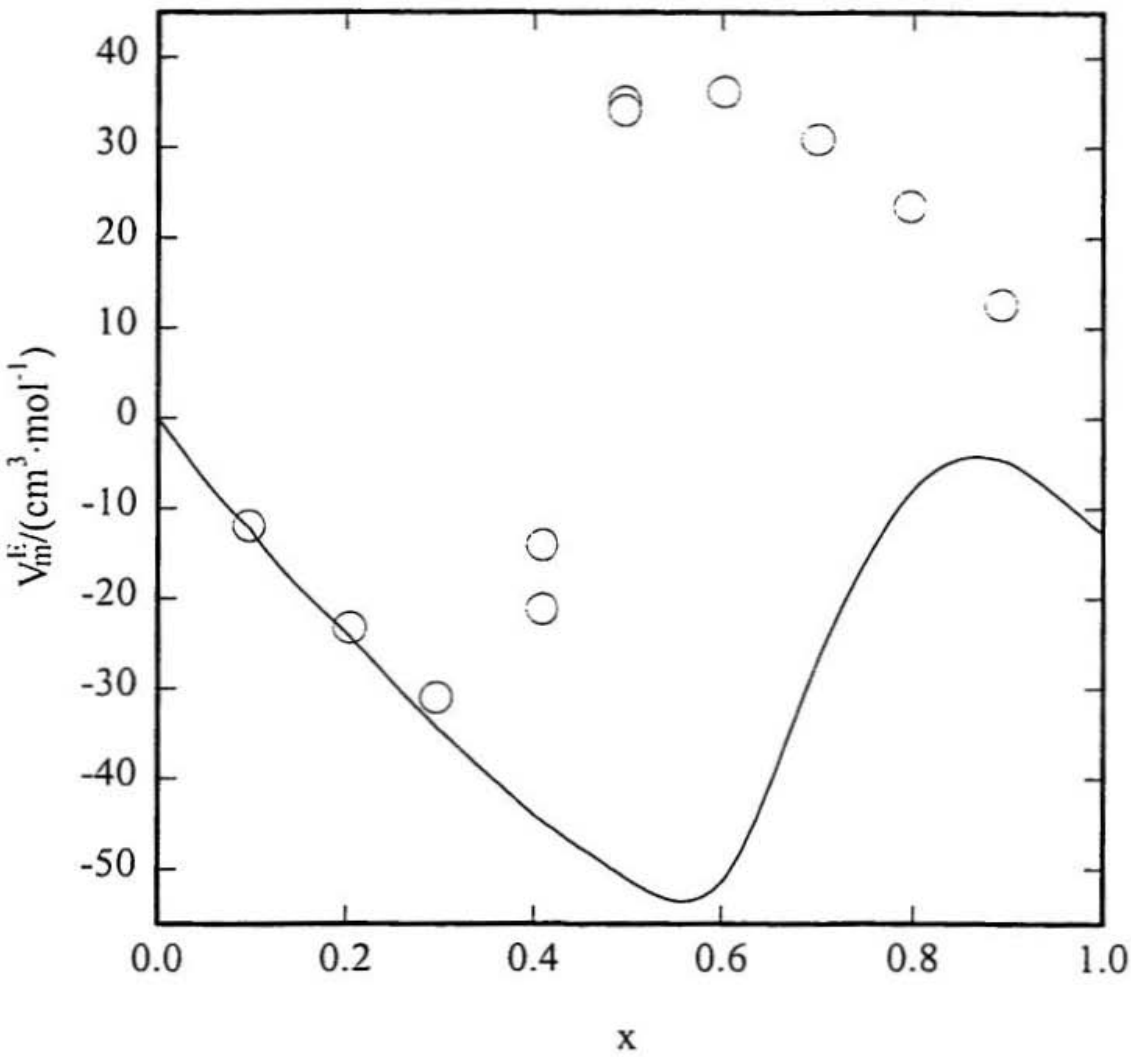


Figure VII.4. Excess molar volumes V_m^E of $\{xCH_3OH + (1 - x)H_2O\}$ at T = 573.6 K and p = 13.7 MPa: ○, experimental; —, the model.

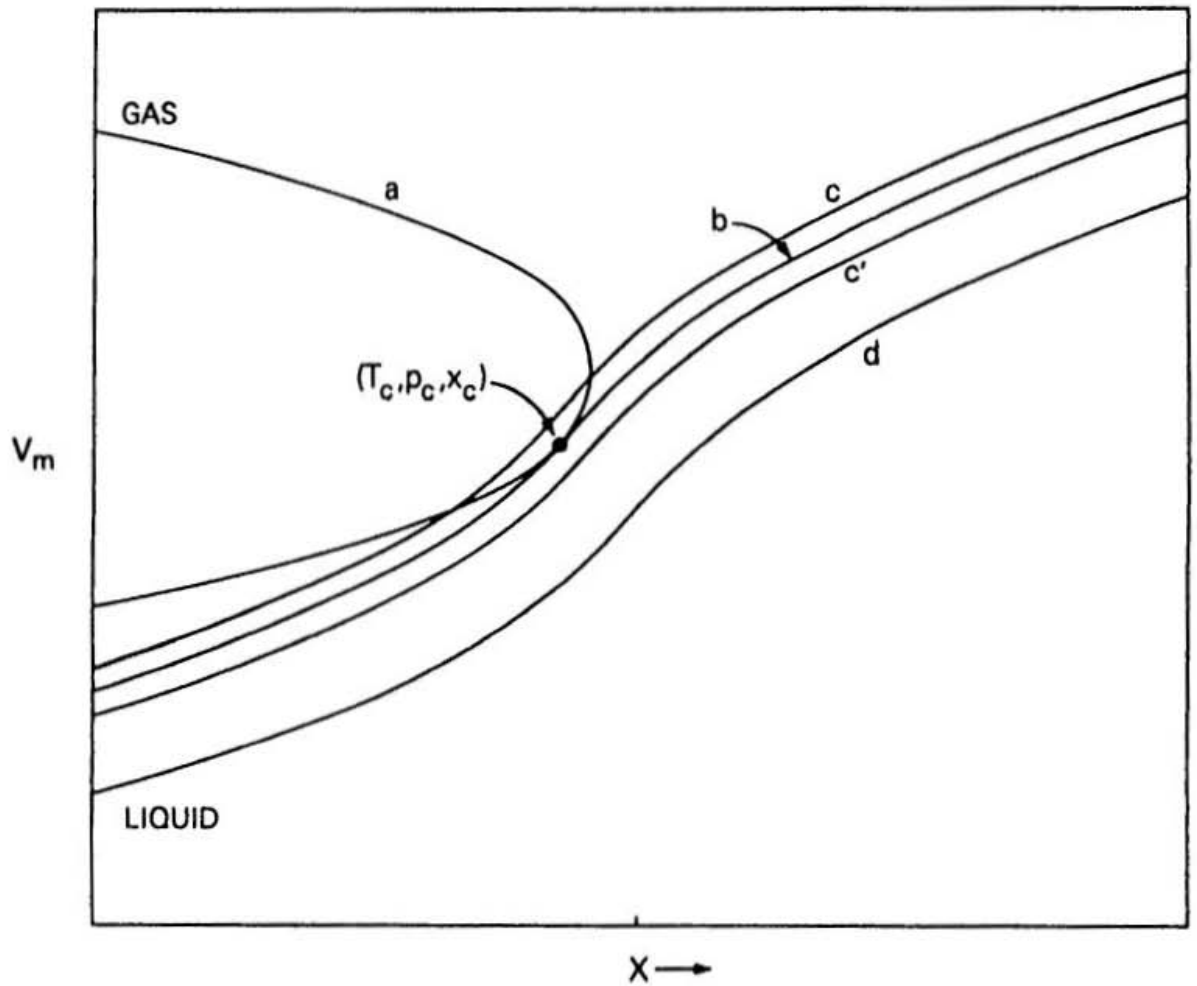


Figure VII.5. A schematic diagram of the dependence of V_m on x at p = 13.5 MPa: a, the (liquid + vapour) phase boundary; b, the critical isotherm isobar if p_c = 13.5 MPa at T_c = 573 K; c and c', the two possible isotherm-isobars at T = 573 K, c, p_c < 13.5 MPa, c', p_c > 13.5 MPa; and d, the isotherm isobar at T = 523 K and p = 13.5 MPa.

experimental uncertainty, over a wide range of temperature and pressure, are well known. Equations of state of the van der Waals type and some corresponding-states models are not adequate for describing the properties of many polar hydrogen-bonded liquid mixtures (Prausnitz *et al.*, 1986). Purely empirical relationships often require complex expressions. For example, Benson and Kiyohara (1980) reported that twelve empirical parameters, plus the molar volumes V^* of the pure components, are needed to reproduce V_m^E of $\{xCH_3OH + (1 - x)H_2O\}$ at $p = 0.1$ MPa in the temperature range $288\ K < T < 308\ K$. A major problem in modelling the behavior of V_m^E for liquid mixtures over a wide range of temperature and pressure is the need to include a representation of the critical behavior for both the mixture and the pure components. Classical critical behavior may have a profound effect on V_m^E, even at temperatures and pressures well-removed from the critical locus (Wormald, 1986; Levelt Sengers, 1991). In this study, we chose to treat the data for V_m^E in the liquid state with a one-fluid corresponding-states model as a pragmatic approach to address the difficult problem. Because we wish to describe *excess* properties, we chose to use pure water as a reference fluid, and to model the differences between the reduced compression factors of the mixtures and those of pure water as calculated from the Hill equation of state, which is accurate to better than 2×10^{-5} under these conditions (Hill, 1990).

By definition, corresponding-states models for mixtures must be based on a well-defined critical locus, or an appropriately formulated "pseudo-critical" locus (Prausnitz *et*

al., 1986; Reid *et al.*, 1987). No accurate measurements for the critical properties of (methanol + water) have been reported, except for the critical temperatures measured by Marshall and Jones (1974), and one point on the critical pressure locus at x = 0.773 reported by Griswold and Wong(1952). Although we attempted to use formulations based on these experimental values, the mixing rule developed by Prausnitz and Gunn (1958) for calculating the pseudocritical temperature T_{cm} and pressure p_{cm} was found to be more successful in reproducing the data for $\{xCH_3OH + (1 - x)H_2O\}$ at $T \leq 523$ K with a simple corresponding states model. Thus, T_{cm} and p_{cm} were calculated from the expressions (Reid *et al.*, 1987):

$$T_{cm} = x T_{ca} + (1-x) T_{cw} \qquad \text{(VII.4.1)}$$

$$p_{cm} = T_{cm}[(x p_{ca} V_{ca}/T_{ca} + \{(1-x) p_{cw} V_{cw}/T_{cw})/(x V_{ca} + (1-x) V_{cw}\}] \qquad \text{(VII.4.2)}$$

Here, $T_{ca} = 512.60$ K and $T_{cw} = 647.126$ K are the critical temperatures for methanol and water, respectively; $p_{ca} = 8.09464$ MPa and $p_{cw} = 22.055$ MPa are the critical pressures of methanol and water, respectively; and $V_{ca} = 119.05$ $cm^3 \cdot mol^{-1}$ and $V_{cw} = 55.948$ $cm^3 \cdot mol^{-1}$ are the critical molar volumes of methanol and water, respectively.

Figure VII.6 presents a relative deviation plot of the compression factors $Z = pV_m/RT$ for H_2O and $\{xCH_3OH + (1-x)H_2O\}$ at the same reduced temperatures and at the same reduced pressures,

$$T_r(T,x) = T/T_{cm} \qquad \text{(VII.4.3)}$$

$$p_r(p,x) = p/p_{cm} \qquad \text{(VII.4.4)}$$

where T_{cm} and p_{cm} for $\{xCH_3OH + (1 - x)H_2O\}$ are the pseudocritical values calculated from equations (VII.4.1) and (VII.4.2). Except for the points in the supercritical region which are not included in figure VII.6, the values for the compression factors agree to within 6 per cent and, for pure methanol, the agreement with the reduced compression factor of water is within 2 percent.

In generalized corresponding-states models (Leach *et al.*, 1968; Gallagher *et al.*, 1993), the Pitzer acentric factor or more complex expressions are used to represent departures from the two-parameter law of corresponding-states. Here, we have used an arbitrary function $\theta(T,p,x)$ to express the relative deviation of the compression factor of the mixture Z_m from that of pure water Z_w at the same reduced temperature and pressure:

$$Z_m(T_r,p_r,x) = Z_w(T_r,p_r)\{1 - \theta(T,p,x)\} \qquad \text{(VII.4.5)}$$

The mole-fraction dependence of θ at the experimental temperatures and pressures is plotted in figure VII.6 over the range $0 \le x \le 1$; it is a smooth function of the mole fraction and the data points for pure methanol are consistent with the results for (methanol + water). The temperature dependence of θ is more pronounced than the

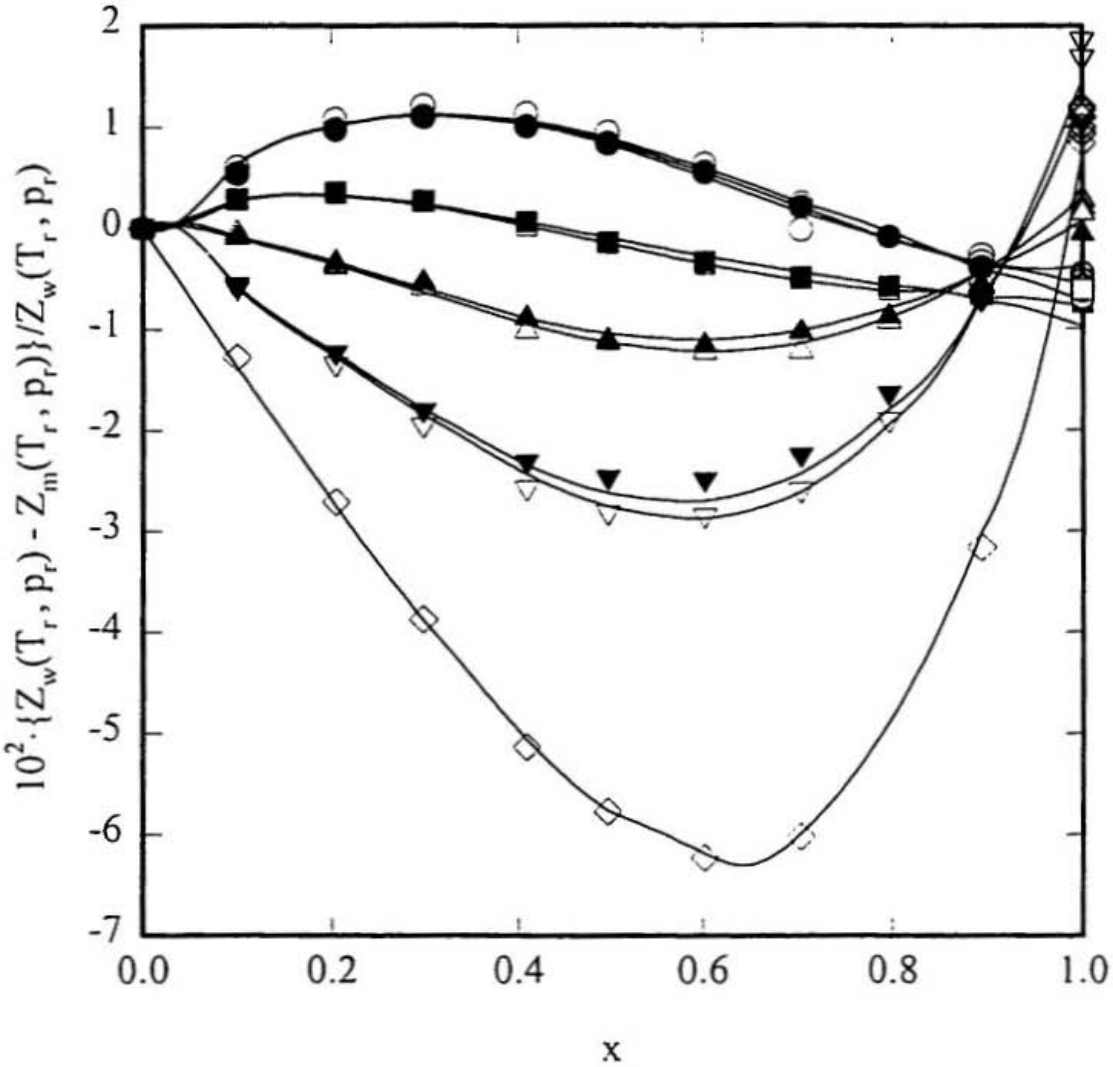


Figure VII.6. The relative differences between the reduced compression factors of $\{xCH_3OH + (1-x)H_2O\}$ and H_2O, $\{Z_w(T_r, p_r) - Z_m(T_r, p_r, x)\}/Z_w(T_r, p_r)$, at the following temperatures and pressures: ○, T = 323 K and p = 0.1 MPa; ●, T = 323 K and p = 7.0 MPa and p = 13.5 MPa; □, T = 373 K and p = 7.0 MPa; ■, T = 373 K and p = 13.5 MPa; △, T = 423 K and p = 7.0 MPa; ▲, T = 423 K and p = 13.5 MPa; ▽, T = 473 K and p = 7.0 MPa; ▼, T = 473 K and p = 13.5 MPa; ◇, T = 523 K and p = 13.5 MPa. The solid lines show the values calculated from the corresponding-states model equation (VII.4.5).

pressure dependence.

Since $\theta \to 0$ as $x \to 0$, the following formula was used to treat the mole fraction dependence:

$$\theta(T,p,x) = a_1(T,p)x + x(1-x)\sum_{i=2}^{4}\{a_i(T,p)\cdot(2x-1)^{i-2}\} \qquad \text{(VII.4.6)}$$

The second term in equation (VII.4.6) is similar to the formula which is frequently used for representing the excess properties of mixtures. The pressure and temperature dependence of each composition-independent parameter in equation (VII.4.6) is given by the expressions

$$a_1 = a_{11} + a_{12}(p/p_{ca})(T/T_{ca}) + a_{13}(T/T_{ca})^2 + a_{14}(T/T_{ca})^3 + a_{15}(T/T_{ca})^4 \qquad \text{(VII.4.7)}$$

$$a_2 = a_{21} + a_{22}T/T_{ca} + a_{23}(p/p_{ca})(T/T_{ca})^2 + a_{24}(T/T_{ca})^3 \qquad \text{(VII.4.8)}$$

$$a_3 = a_{31} + a_{32}T/T_{ca} + a_{33}(p/p_{ca})(T/T_{ca})^2 + a_{34}(T/T_{ca})^3 \qquad \text{(VII.4.9)}$$

$$a_4 = a_{41} + a_{42}T/T_{ca} + a_{43}(p/p_{ca})(T/T_{ca})^2 + a_{44}(T/T_{ca})^3 \qquad \text{(VII.4.10)}$$

The use of temperatures and pressures expressed relative to the critical values for methanol T_{ca} = 512.6 K and p_{ca} = 8.09464 MPa was found to be a convenient way to avoid ill-conditioned convergence properties when fitting these equations to $\theta(T,p,x)$.

The last terms in equations (VII.7) to (VII.10) are used to account for the significant changes in θ for pure methanol as the temperature approaches T_{cs}. All of the experimental densities for (methanol + water) and methanol, except for the data at T = 573 K and p = 13.5 MPa, were used to optimize the parameters in equations (VII.7) to (VII.10) by means of the Marquardt-Levenburg algorithm in the commercial Sigmaplot[c] code. The values obtained for the parameters in equations (VII.7) to (VII.10) are listed in table VII.1. The relative compression factors calculated from equation (VII.4.5) are shown as solid lines in figure VII.6. In figure VII.7, two deviation plots are given which compare the calculated ρ and V_m^E with the experimental results. The average absolute deviation between the calculated and experimental compression factors is 0.0005, which corresponds to an average absolute relative deviation of 0.05 per cent according to the definition of θ in equation (VII.4.5). The ρ and the V_m^E at round temperatures, pressures, and mole fractions are listed in table VII.2.

Plots of the fitted results for V_m^E against x are compared with the experimental data in figures VII.3 to VII.5. Clearly, the model reproduces the data at $T \leq 523$ K to within the estimated experimental uncertainties. The model is less successful in reproducing the behaviour of V_m^E at 573 K at $x > 0.4$, as illustrated in figure VII.4. This is, in part, a consequence of our use of the pseudo-critical parameters given by equations (VII.4.1) and (VII.4.2), and the fact that the true critical pressure locus required to optimize θ near T_{cm} is unknown. A more serious problem is that no one-fluid model of the type used here can

Table VII.1 Parameters in equations (VII.4.7) to (VII.4.10).

j	i=1	i=2	i=3	i=4
1	30.815526	-8.4138196	-55.375755	-37.246685
2	-0.34426008	43.241434	106.99546	75.787649
3	-311.13782	1.4665548	1.9711896	1.3846997
4	517.55990	-59.140300	-67.186932	-44.405032
5	-235.58141			

Table VII.2 Densities ρ, excess molar volumes V_m^E, partial molar volumes V_a and V_w, isothermal compressibilities κ_m and cubic expansion coefficients α_m of $\{xCH_3OH+(1-x)H_2O\}$

x	ρ	V_m^E	V_a	V_w	$10^4 \cdot \alpha_m$	$10^4 \cdot \kappa_m$
	$kg \cdot m^{-3}$	$cm^3 \cdot mol^{-1}$	$cm^3 \cdot mol^{-1}$	$cm^3 \cdot mol^{-1}$	K^{-1}	MPa^{-1}
			T = 323.15 K, p = 0.1 MPa			
0.00	988.03	0.000	38.19	18.23	4.57	4.42
0.10	958.60	-0.355	38.73	18.20	5.96	5.05
0.20	931.82	-0.645	39.34	18.10	7.27	5.74
0.30	906.74	-0.858	39.96	17.89	8.41	6.50
0.40	882.89	-0.985	40.53	17.58	9.34	7.34
0.50	860.06	-1.021	41.03	17.17	10.07	8.28
0.60	838.24	-0.968	41.43	16.69	10.64	9.35
0.70	817.53	-0.831	41.71	16.18	11.17	10.57
0.80	798.11	-0.623	41.86	15.71	11.78	11.97
0.90	780.21	-0.363	41.93	15.37	12.66	13.60
			T = 323.15 K, p = 7.0 MPa			
0.00	991.02	0.000	37.98	18.18	4.57	4.34
0.10	961.96	-0.336	38.51	18.15	5.92	4.94
0.20	935.52	-0.609	39.10	18.05	7.20	5.60
0.30	910.83	-0.808	39.68	17.85	8.30	6.31
0.40	887.45	-0.928	40.21	17.56	9.18	7.10
0.50	865.17	-0.964	40.67	17.18	9.85	7.98
0.60	843.92	-0.916	41.04	16.73	10.35	8.95
0.70	823.74	-0.789	41.31	16.24	10.80	10.05
0.80	804.72	-0.590	41.48	15.74	11.33	11.30
0.90	786.96	-0.331	41.56	15.29	12.14	12.72
			T = 323.15 K, p = 13.5 MPa			
0.00	993.79	0.000	37.79	18.13	4.56	4.26
0.10	965.08	-0.321	38.32	18.10	5.89	4.85
0.20	938.94	-0.581	38.88	18.00	7.13	5.47
0.30	914.60	-0.771	39.42	17.82	8.20	6.15

Table VII.2 Continued

x	ρ	V_m^E	V_a	V_w	$10^4 \cdot \alpha_m$	$10^4 \cdot \kappa_m$
	$kg \cdot m^{-3}$	$cm^3 \cdot mol^{-1}$	$cm^3 \cdot mol^{-1}$	$cm^3 \cdot mol^{-1}$	K^{-1}	MPa^{-1}
0.40	891.65	-0.886	39.92	17.55	9.04	6.89
0.50	869.85	-0.923	40.35	17.19	9.65	7.71
0.60	849.11	-0.882	40.70	16.77	10.10	8.61
0.70	829.39	-0.764	40.97	16.28	10.48	9.62
0.80	810.67	-0.573	41.15	15.74	10.95	10.75
0.90	792.97	-0.312	41.25	15.18	11.71	12.02
			T = 373.15 K, p = 7.0 MPa			
0.00	961.58	0.000	40.35	18.74	7.39	4.79
0.10	927.43	-0.372	41.13	18.69	8.64	5.59
0.20	896.58	-0.662	41.84	18.57	9.80	6.49
0.30	868.42	-0.868	42.46	18.36	10.82	7.49
0.40	842.56	-0.992	42.98	18.08	11.69	8.64
0.50	818.71	-1.037	43.42	17.72	12.39	9.96
0.60	796.59	-1.002	43.78	17.28	12.96	11.48
0.70	775.94	-0.885	44.07	16.74	13.40	13.26
0.80	756.43	-0.680	44.31	16.03	13.77	15.36
0.90	737.70	-0.372	44.48	15.06	14.14	17.87
			T = 373.15 K, p = 13.5 MPa			
0.00	964.54	0.000	40.11	18.68	7.28	4.69
0.10	930.85	-0.345	40.87	18.64	8.50	5.45
0.20	900.43	-0.610	41.54	18.52	9.61	6.30
0.30	872.76	-0.798	42.11	18.33	10.57	7.24
0.40	847.50	-0.912	42.57	18.08	11.37	8.30
0.50	824.35	-0.955	42.96	17.77	11.98	9.50
0.60	802.99	-0.928	43.28	17.37	12.44	10.87
0.70	783.06	-0.827	43.55	16.86	12.76	12.44
0.80	764.14	-0.639	43.79	16.13	13.00	14.26
0.90	745.72	-0.341	43.98	15.06	13.22	16.38

Table VII.2 Continued

x	ρ	V_m^E	V_a	V_w	$10^4 \cdot \alpha_m$	$10^4 \cdot \kappa_m$
	$kg \cdot m^{-3}$	$cm^3 \cdot mol^{-1}$	$cm^3 \cdot mol^{-1}$	$cm^3 \cdot mol^{-1}$	K^{-1}	MPa^{-1}
			T = 423.15 K, p = 7.0 MPa			
0.00	920.71	0.000	43.52	19.57	10.03	6.01
0.10	882.02	-0.451	44.53	19.51	11.55	7.17
0.20	847.40	-0.795	45.43	19.35	12.95	8.53
0.30	816.14	-1.035	46.20	19.10	14.28	10.11
0.40	787.81	-1.174	46.84	18.76	15.54	11.99
0.50	762.05	-1.219	47.34	18.35	16.75	14.25
0.60	738.56	-1.174	47.74	17.86	17.87	17.01
0.70	717.04	-1.043	48.04	17.30	18.88	20.42
0.80	697.16	-0.823	48.27	16.61	19.74	24.73
0.90	678.52	-0.503	48.43	15.68	20.39	30.28
			T = 423.15 K, p = 13.5 MPa			
0.00	924.26	0.000	43.17	19.49	9.82	5.83
0.10	886.21	-0.391	44.15	19.44	11.26	6.92
0.20	852.20	-0.681	44.98	19.29	12.58	8.17
0.30	821.67	-0.877	45.66	19.07	13.79	9.61
0.40	794.23	-0.987	46.19	18.79	14.92	11.28
0.50	769.54	-1.020	46.59	18.46	15.94	13.25
0.60	747.26	-0.984	46.89	18.09	16.82	15.59
0.70	727.01	-0.880	47.13	17.64	17.54	18.39
0.80	708.39	-0.704	47.33	17.05	18.00	21.78
0.90	690.89	-0.439	47.48	16.19	18.15	25.94
			T = 473.15 K, p = 7.0 MPa			
0.00	868.83	0.000	48.15	20.73	13.37	8.47
0.10	824.60	-0.736	49.53	20.66	15.70	10.42
0.20	785.29	-1.321	50.87	20.42	17.95	12.82
0.30	749.79	-1.744	52.10	20.01	20.26	15.80
0.40	717.40	-2.001	53.20	19.42	22.71	19.60
0.50	687.70	-2.089	54.12	18.66	25.37	24.55

Table VII.2 Continued

x	ρ	V_m^E	V_a	V_w	$10^4 \cdot \alpha_m$	$10^4 \cdot \kappa_m$
	$kg \cdot m^{-3}$	$cm^3 \cdot mol^{-1}$	$cm^3 \cdot mol^{-1}$	$cm^3 \cdot mol^{-1}$	K^{-1}	MPa^{-1}
0.60	660.38	-2.009	54.88	17.75	28.28	31.20
0.70	635.19	-1.762	55.46	16.66	31.50	40.43
0.80	611.82	-1.346	55.90	15.33	35.17	53.88
0.90	589.82	-0.735	56.22	13.46	39.65	74.78
			T = 473.15 K, p = 13.5 MPa			
0.00	873.52	0.000	47.59	20.62	12.94	8.09
0.10	830.24	-0.530	48.89	20.55	15.11	9.86
0.20	791.90	-0.922	50.08	20.35	17.16	11.96
0.30	757.59	-1.175	51.11	20.00	19.20	14.51
0.40	726.70	-1.293	51.96	19.55	21.28	17.64
0.50	698.88	-1.287	52.61	19.02	23.41	21.53
0.60	673.85	-1.171	53.06	18.46	25.56	26.44
0.70	651.46	-0.964	53.34	17.96	27.63	32.75
0.80	631.57	-0.693	53.47	17.58	29.50	41.01
0.90	614.10	-0.387	53.50	17.42	31.00	52.06
			T = 523.15 K, p = 13.5 MPa			
0.00	809.60	0.000	54.68	22.25	17.96	12.99
0.10	758.49	-1.399	56.74	22.14	21.75	16.50
0.20	713.44	-2.563	58.87	21.76	25.55	21.02
0.30	672.73	-3.459	61.00	21.05	29.62	26.97
0.40	635.38	-4.056	63.03	19.95	34.18	35.02
0.50	600.81	-4.329	64.87	18.44	39.43	46.24
0.60	568.71	-4.258	66.46	16.50	45.60	62.46
0.70	538.84	-3.826	67.76	14.09	53.08	87.01
0.80	510.94	-3.006	68.77	11.02	62.57	126.23
0.90	484.56	-1.743	69.50	6.85	75.38	193.01

Table VII.2 Continued

x	ρ	V_m^E	V_a	V_w	$10^4 \cdot \alpha_m$	$10^4 \cdot \kappa_m$
	$kg \cdot m^{-3}$	$cm^3 \cdot mol^{-1}$	$cm^3 \cdot mol^{-1}$	$cm^3 \cdot mol^{-1}$	K^{-1}	MPa^{-1}
			T = 573.15 K, p = 13.5 MPa			
0.00	722.72	0.000	68.21	24.93	29.49	27.69
0.10	658.40	-12.22	72.96	24.66	37.98	39.04
0.20	600.80	-23.85	78.95	23.58	48.15	57.04
0.30	546.38	-34.62	86.69	20.95	62.11	88.41

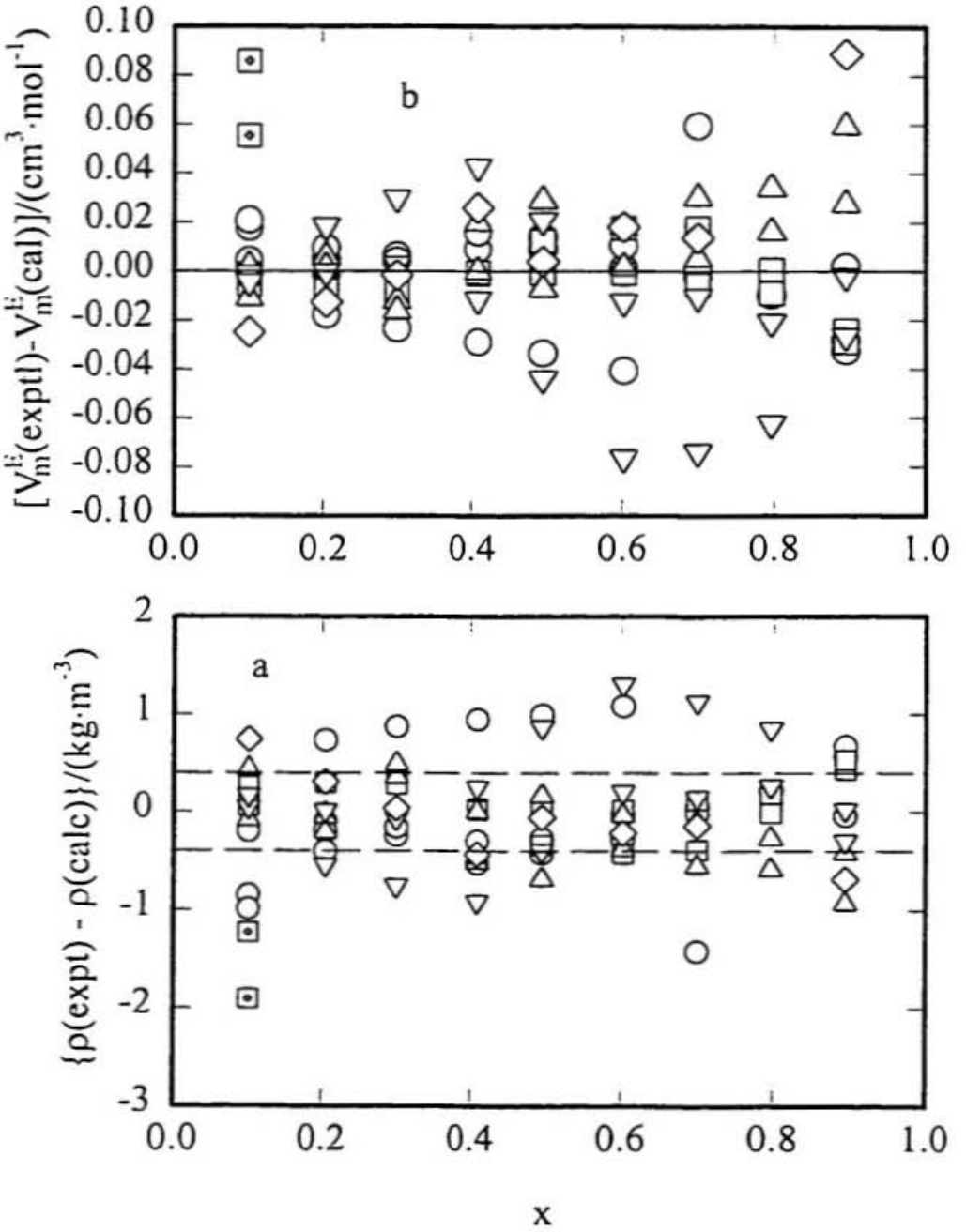


Figure VII.7. Deviations of (a) experimental excess molar volumes V_m^E(expt) from those V_m^E(calc) calculated from the model; (b) deviations of the experimental densities ρ(expt) from those ρ(calc) calculated from the model: ○, T = 323 K; △, T = 373 K; □, T = 423 K; ▽, T = 473 K; ◇, T = 523 K; ⊞, T = 573 K.

adequately describe the divergent properties of two component mixtures in the near-critical region because such models are physically unrealistic (Levelt Sengers, 1991; Griffiths and Wheeler, 1970). Thus, although the fit to the data at T = 573 K can be improved by expanding θ, we have not done so. The model has been used to represent only the V_m^E of the mixtures in the liquid phase at T = 573 K (i.e. $x < 0.4$) and at lower temperatures.

VII.5 Comparison with Literature

Our results for V_m^E are compared in figure VII.2 with those reported by Easteal and Woolf (1985), and Götze and Schneider (1980) at T = 323 K and p = 0.1 MPa. The three sets of data agree to within the combined experimental uncertainties. However, V_m^E calculated from the model, shown as a solid line in figure VII.2, are more positive than our own and Easteal and Woolfs' results by 0.02 $cm^3 \cdot mol^{-1}$. This small systematic error arises from the small statistical weight of the low pressure data, since only the 8 points at p = 0.1 MPa from our work were included when optimizing the parameters in equation (VII.4.6).

We know of no directly measured experimental values for the ρ and V_m^E at temperatures above 373 K to compare with our results. However, as noted above, Simonson *et al.* (1987) have reported values for V_m^E $\{xCH_3OH + (1-x)H_2O\}$ at temperatures up to 523 K and pressures up to 40 MPa derived from the results of

pressure-dependent enthalpy-of-mixing measurements at high temperatures. A comparison of our results with Simonson *et al.*'s at p = 7.0 MPa and temperatures T = (373, 423 and 473 K) is shown in figure VII.3. The agreement at T = 373 K and T = 423 K is reasonable since only volumetric data at T = 298.15 K were used in their modelling. The disagreement at T = 473 K and p = 7.0 MPa is significant. It apparently arises because the curvature in $(\partial H_m^E/\partial p)_{T,x}$, which is quite pronounced under these conditions, is not well represented by the model used by Simonson *et al.* (1987).

Extrapolating the corresponding-states model to p = 20 MPa, yields values for V_m^E that can be compared with those estimated by Simonson *et al.* at T = 373 K and T = 423 K. These are presented in figure VII.8. There is a systematic difference of 0.1 $cm^3 \cdot mol^{-1}$ for x > 0.5 which may arise either from the expression used in this work to describe the simple pressure dependence of θ, or from the model used by Simonson *et al.*(1987) to describe the pressure-dependence of $(\partial H_m^E/\partial p)_{T,x}$. The model appears to give accurate predictions of the V_m^Es of aqueous methanol solutions in the range x < 0.6 at pressures well in excess of the experimental conditions. It may be accurate at elevated pressures over the entire composition range.

VII.6 Partial Molar Volumes, Isothermal Compressibility and Cubic Expansion Coefficient

Molar volumes of $\{xCH_3OH + (1 - x)H_2O\}$ were obtained from the compression

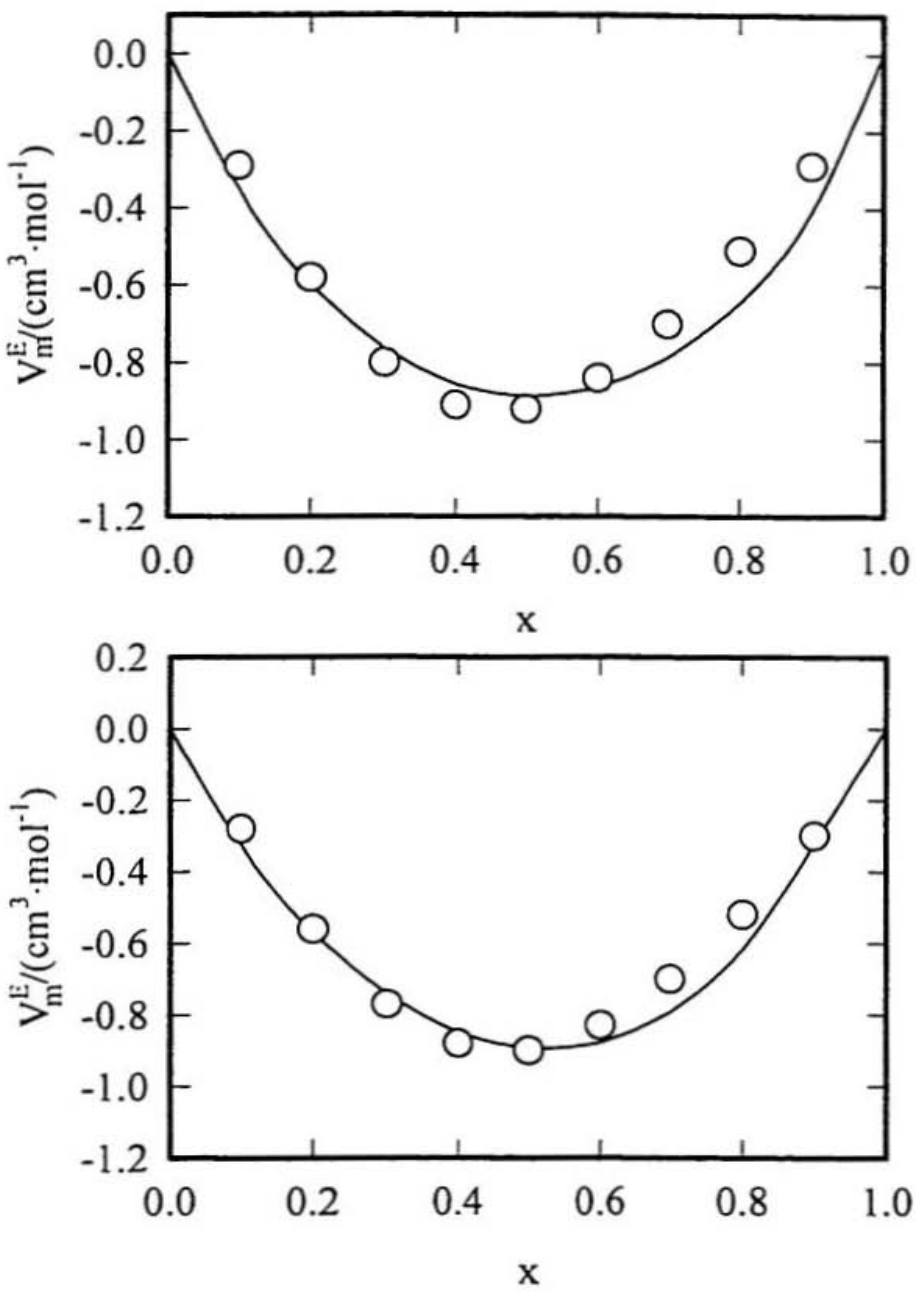


Figure VII.8. Comparison of V_m^E predicted by the model (solid lines) with V_m^E estimated: o, by Simonson et al. (1987); (a) p = 20.0 MPa and T = 373 K, (b) p = 20.0 MPa and T = 423 K.

factor parameters using the expression

$$V_m = R Z_w(T_w, p_w, x)\{1 - \theta(T, p, x)\}\, T/p \qquad \text{(VII.6.1)}$$

where V_m is the molar volume; R is the gas constant; Z_w is the compression factor of water at temperature $T_w = T_{cw}T_r$ and pressure $p_w = p_{cw}p_r$. The partial molar volumes V_a and V_w are defined in terms of the molar volume by

$$\bar{V}_a = V_m - (1 - x)(\partial V_m/\partial x)_{T,p} \qquad \text{(VII.6.2)}$$

$$\bar{V}_w = V_m - x(\partial V_m/\partial x)_{T,p} \qquad \text{(VII.6.3)}$$

The values of V_a and V_w are evaluated through the following derivatives:

$$(\partial V_m/\partial x)_{T,p} = (\partial Z_w/\partial x)_{T,p}(1 - \theta)RT/p - Z_w RT(\partial\theta/\partial x)_{T,p}/p \qquad \text{(VII.6.4)}$$

$$(\partial Z_m/\partial x)_{T,p} = (\partial Z_w/\partial T_w)_{p_w}(\partial T_w/\partial x)_T + (\partial Z_w/\partial p_w)_{T_w}(\partial p_w/\partial x)_p \qquad \text{(VII.6.5)}$$

$$(\partial Z_w/\partial p_w)_{T_w} = Z_w(1/p_w - \kappa_w) \qquad \text{(VII.6.6)}$$

$$(\partial Z_w/\partial T_w)_{p_w} = Z_w(\alpha_w - 1/T_w) \qquad \text{(VII.6.7)}$$

where α_w and κ_w are the cubic expansion coefficient and the isothermal compressibility, respectively, of water at the same reduced temperature and at the same reduced pressure as the (methanol + water). The value of V_a and V_w are listed in table VII.2 . Comparisons with results reported by Easteal and Woolf (1985b) at T = 323 K and p = 0.1 MPa are shown in figure VII.9. The results from our model agree with the results from Easteal and Woolf to within 0.2 $cm^3 \cdot mol^{-1}$, except for the limiting values of V_a in dilute aqueous solutions at $x > 0.8$.

Expressions for the bulk cubic expansion coefficient α_m and isothermal compressibility κ_m of $\{xCH_3OH + (1 - x)H_2O\}$ may be obtained from equation (VII.6.1) through simple algebra. These are given by

$$\kappa_m = \kappa_w p_{cw}/p_{cm} + Z_w(\partial\theta/\partial p)_{T,x}/Z_m \qquad \text{(VII.6.9)}$$

$$\alpha_m = \alpha_w T_{cw}/T_{cm} - Z_w(\partial\theta/\partial T)_{p,x}/Z_m \qquad \text{(VII.6.10)}$$

The values of α_m and κ_m are listed in table VII.2. Comparisons with the results reported by Easteal and Woolf (1985b) at T = 323 K and p = 0.1 MPa are shown in figures VII.10. The results from our model are systematically higher that the results from Easteal and Woolf, although the agreement is within 10 per cent.

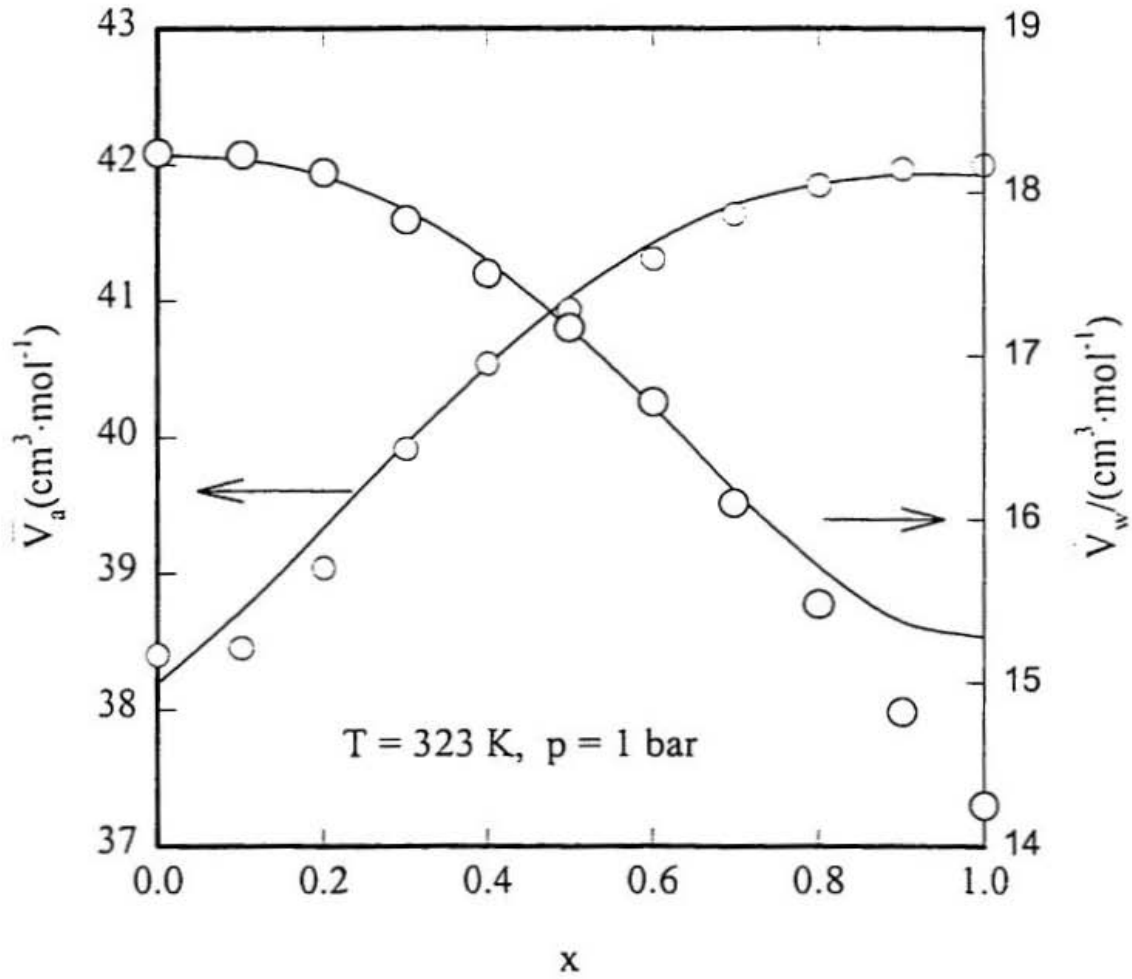


Figure VII.9. Comparison of partial molar volumes V_a and V_w calculated from the corresponding-states model (solid lines) with those from Easteal and Woolf (1985a) (○) at T = 323 K and p = 0.1 MPa.

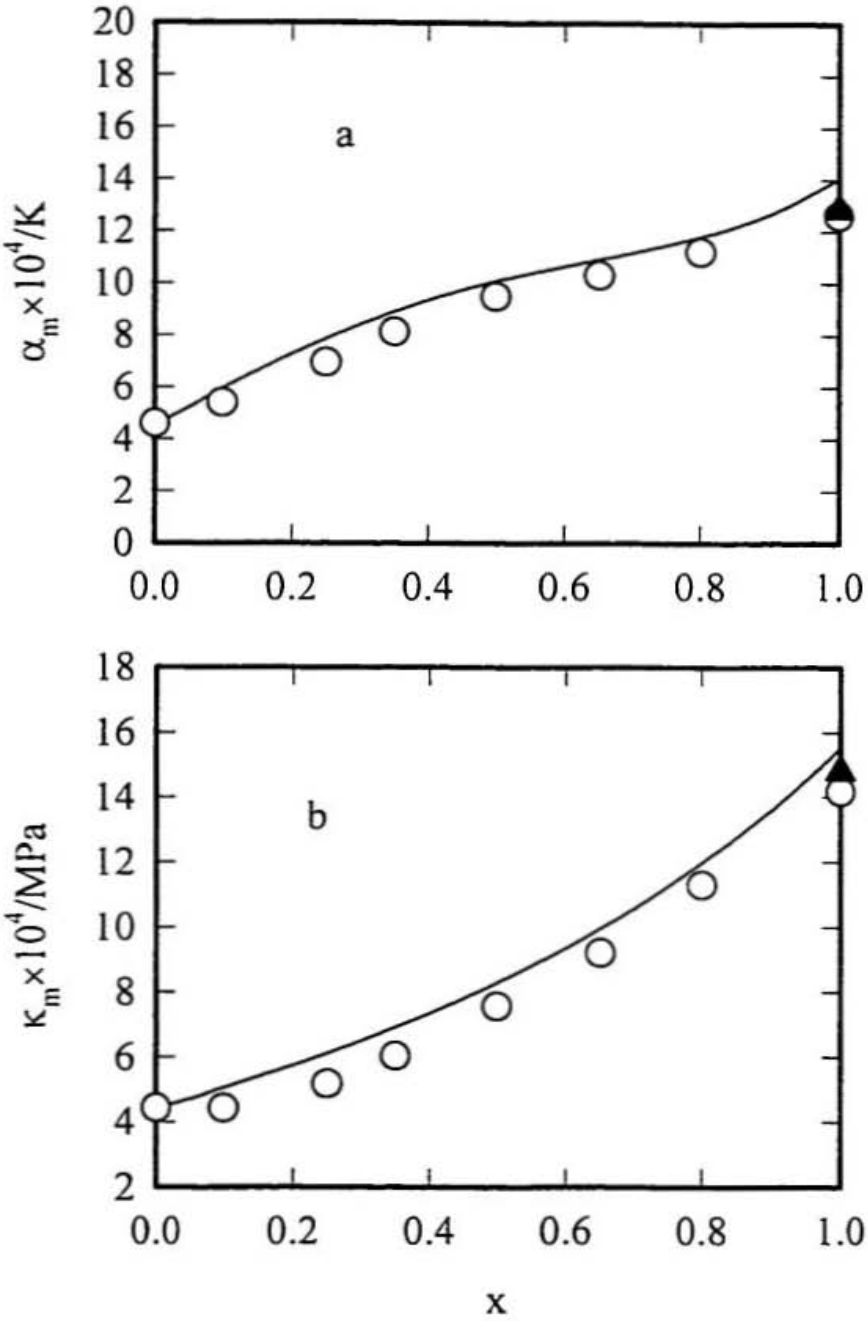


Figure VII.10. Comparison of (b) isothermal compression κ_m and (a) cubic expansion coefficient α_m with those from Easteal and Woolf (1985b) (○) at T = 323 K and p = 0.1 MPa. The values for methanol, ▲, were calculated from Goodwin's equation of state.

VII.7 Near-Critical Behaviour at T = 573.6 K and p = 13.7 MPa

Only a few studies of the behaviour of V_m^E for aqueous non-electrolytes in the near-critical region have been reported (Levelt Sengers, 1991; Biggerstaff and Wood, 1988; Japas, 1992; Franck, 1987), and it is of interest to examine the mole-fraction dependence of $V_m^E\{xCH_3OH + (1 - x)H_2O\}$ at T = 573.6 K and p = 13.7 MPa (figure VII.4) in more detail. The phase diagram of the (methanol + water) system appears to be of type I in the classification of van Konynenburg and Scott (van Konynenburg and Scott, 1980; Marshall and Jones, 1974), i.e., the critical line originates at pure methanol and terminates at pure water . The critical temperature locus reported by Marshall and Jones (1974) is plotted in figure VII.11. No critical pressures for this system have been cited in the literature except for the value p_{cm} = 8.41 MPa at x = 0.773 reported by Griswold and Wong (1952) . From the plot of the critical temperature locus in figure VII.11, it is apparent that the $\{xCH_3OH + (1 - x)H_2O\}$ with $x > 0.45$ at T = 573.6 K lie in the supercritical region ($T > T_{cm}$), and the mixtures with $x < 0.40$ lie in the liquid region i.e. $T < T_{cm}$. The measurement for the solution with x = 0.40888 was made at or just below its critical temperature. While the behavior of V_m^E is consistent with a narrow range of (vapour + liquid) equilibrium, the absence of instabilities in the densimeter measurements at x = 0.40888 and x = 0.49641 is not consistent with this result. It appears that p = 13.5 MPa is at or above the critical pressure, i.e. $p_{cm} < 13.5$ MPa at x = 0.40888, or that only a very narrow two-phase region exists at p = 13.5 MPa in the range $0.41 < x$

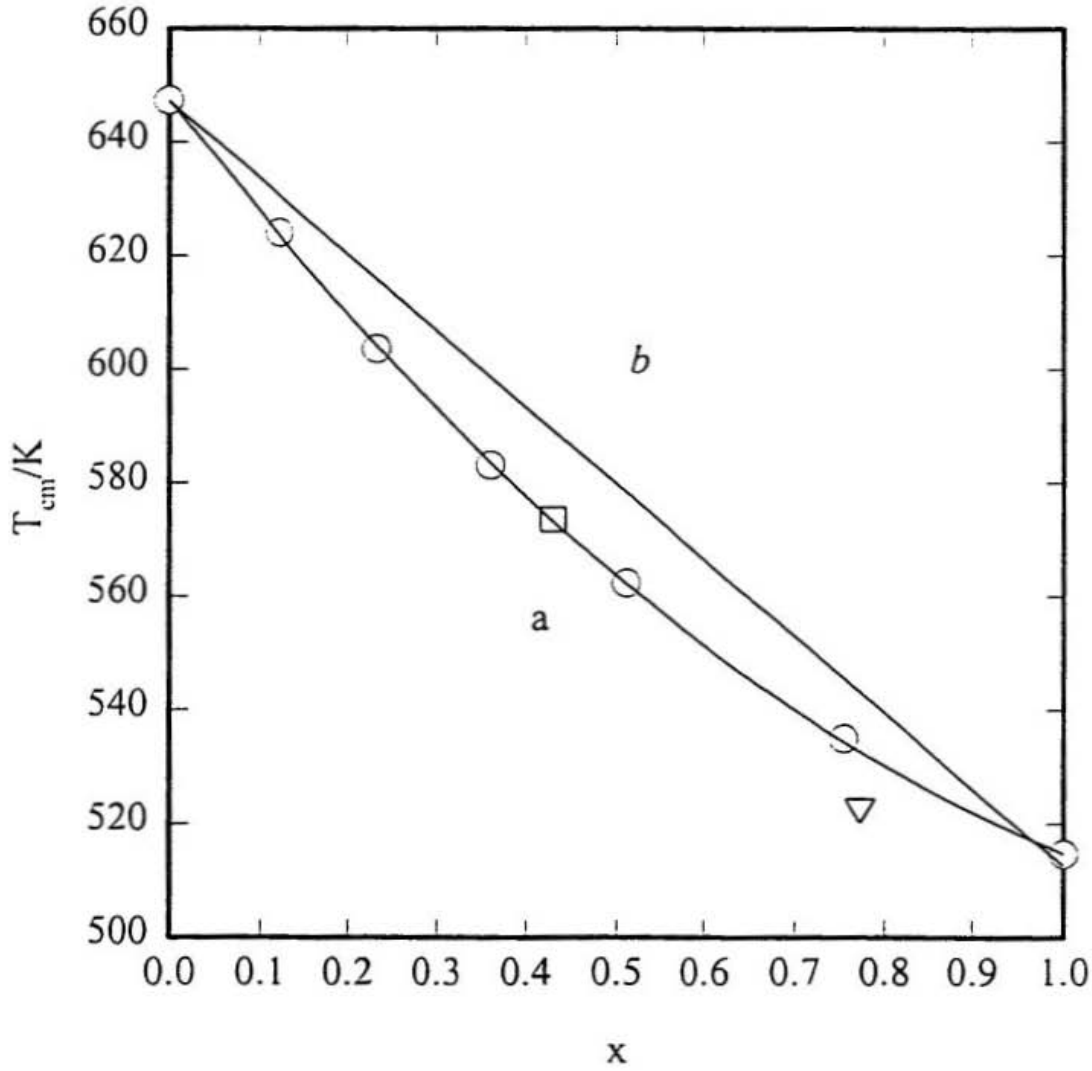


Figure VII.11. Critical temperatures T_c of $\{xCH_3OH + (1 - x)H_2O\}$: — and ○, Marshall and Jones (1974); ▽, Griswold and Wong (1952); □, estimated from the plot of V_m^E against x (figure VII.4) by assuming $V_m^E = 0$ at the critical point. Curve a is the critical temperature locus. Curve b is the pseudocritical temperature locus (equation VII.4.1).

< 0.49. This result, and the value $p_c = 8.41$ MPa at $x = 0.733$ reported in reference VII.11, suggest that the true critical pressure locus lies well below the pseudo-critical locus represented by equation (VII.4.2). Simonson *et al.* (1987) have observed linear behaviour in H_m^E at $T = 573$ K and $p = 20$ MPa which they speculated may reflect two phase behavior. Our volumetric measurements, which are more sensitive to phase separation effects, do not support this suggestion but measurements over a wider range of pressures would clearly be of interest.

Values for the molar volume V_m are plotted in figure VII.12, for comparison with the schematic phase diagram in figure VII.5. The behaviour of V_m for a volatile solute along the critical isotherm-isobar (curve b in figure VII.5) has been discussed by Levelt Sengers (1991) and Chang and Levelt Sengers (1986). The magnitude of V_m increases sharply as the fluid passes from the liquid to supercritical conditions at x_c. The resulting deviations from the ideal volume of mixing, shown by line (b) in figure VII.12, cause V_m^E to shift from negative to positive values, as was observed experimentally (figure VII.4).

The magnitude of V_m^E near x_c is similar to values observed by Franck and coworkers for simple mixtures at $p >> p_c$ (Franck, 1987) although the sigmoid shape is much more pronounced. On the assumption that our measurements did correspond to a supercritical isobar ($p_{cm} < 13.5$ MPa at $x = 0.40888$), the behaviour of $(\partial V_m/\partial x)_{p,T}$ has been estimated by fitting a cubic spline function to the V_m data in figure VII.12 and differentiating the result. The function $(\partial V_m/\partial x)_{p,T}$, plotted in figure VII.13, displays a

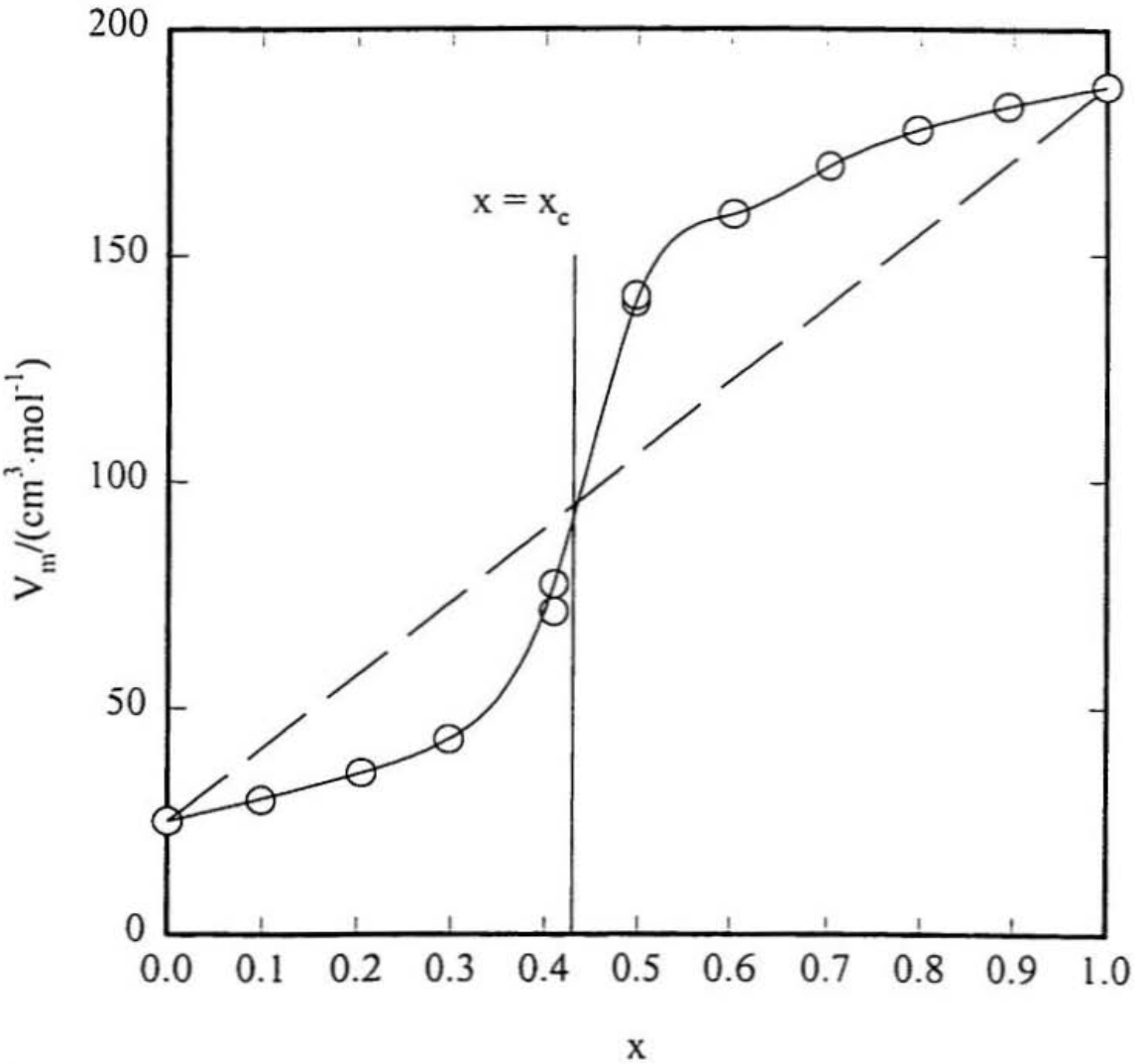


Figure VII.12. Molar volumes V_m of $\{xCH_3OH + (1 - x)H_2O\}$ at T = 573.6 K and p = 13.7 MPa: ○, experimental ; Solid curve a shows the smoothed values obtained by cubic spline functions with linear end conditions; Dashed line is the straight line connecting the critical molar volume of water and the critical molar volume of methanol; The vertical line shows the critical mole fraction at T = 573.6 K.

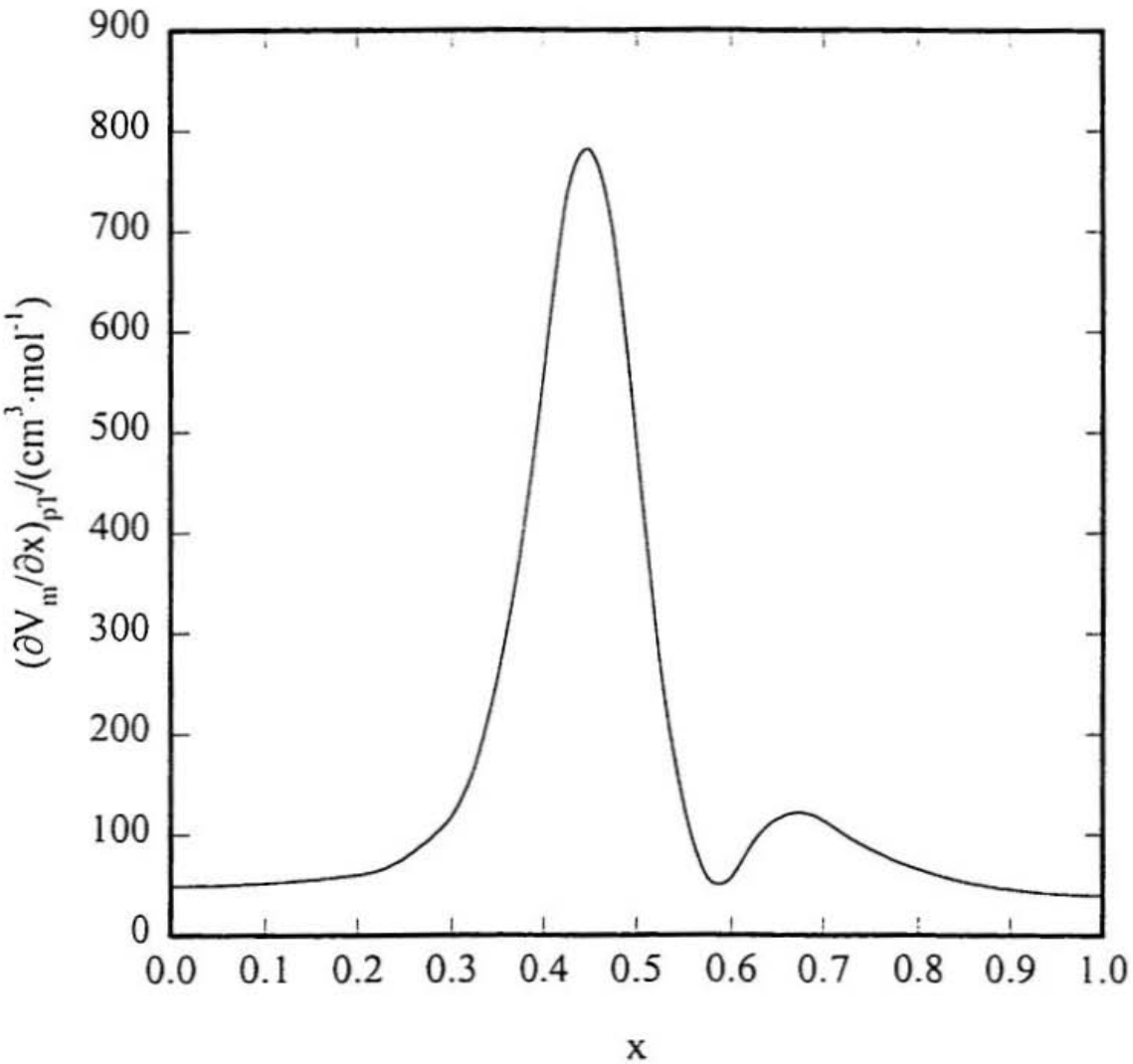


Figure VII.13. Values for $(\partial V_m/\partial x)_{p,T}$ at T = 573.6 K and p = 13.7 MPa corresponding to the cubic spline function in figure VII.12.

sharp maximum corresponding to the point of inflection of V_m at $x \approx x_c$. It is now well understood, both from classical and non-classical theories (Levelt Sengers, 1991; Griffths and Wheeler, 1970; Chang and Levelt Sengers, 1986), that $(\partial V_m/\partial x)_{p,T}$ for two-component mixtures along the critical isotherm-isobar is finite, except at the limits $x \to 0$ and $x \to 1$ where it is strongly divergent. The magnitude of $(\partial V_m/\partial x)_{p,T}$ is rather large (corresponding to $V_2 = 520$ cm^3·mol^{-1} from equation VII.6.2), implying either that small, heavily hydrogen-bonded solutes display large maxima in $(\partial V_m/\partial x)_{p,T}$ at finite concentrations, or that the experimental data do lie in the (vapour + liquid) equilibrium region. Additional measurements should be made to determine whether this behaviour persists at pressures that are clearly higher that p_c, and to determine accurate values for the phase boundaries in this important system. The limiting values of V_2 at $x \to 0$ in table VII.2 are the standard partial molar volumes for methanol in water, V_2°. Although the increase is not as great as that observed by Biggerstaff and Wood (1988) for dilute (argon + water), (xenon + water) and (ethylene + water) mixtures , the increase in V_2° with temperature along the p = 13.5 MPa isobar is consistent with a positive divergence at the critical point of methanol.

Part Four. Concluding Summary, References, and Appendices

Chapter VIII. Concluding Summary

It has been demonstrated in the previous chapters that our measurements provide important new thermodynamic data for many aqueous systems over a wide range of temperature and pressure. These accurate data have been used to test theoretical and empirical models and to explore the effects of the ionic hydration on the thermodynamic properties of aqueous electrolytes. The major contributions of this research are described below.

This research has provided temperature-dependent apparent molar volumes $V_{\phi,2}$ and apparent molar heat capacities $C_{p,\phi,2}$ for $La^{3+}(aq)$, $Nd^{3+}(aq)$, $Eu^{3+}(aq)$, $Er^{3+}(aq)$, $Gd^{3+}(aq)$, and $Yb^{3+}(aq)$ from 283 K to 338 K. The values for $C_{p,\phi,2}$ are the first temperature-dependent measurements to be made on the rare-earth cations with modern flow microcalorimeters. The systematic variations of the standard partial molar properties, V_2^o and $C_{p,2}^o$, across the lanthanide series were examined by using these results to evaluate the parameters in the non-Born terms of the HKF equations. Our values for V_2^o at 298.2 K are in excellent agreement with those reported by Spedding and co-workers. However, the discrepancy between our values for $C_{p,2}^o$ and those of Spedding *et al.* are substantial. We believe that our results are preferred over Spedding *et al.*'s because new calorimetric techniques and the latest theoretical models were used in our

investigation. It is worthwhile to mention that the correlations for estimating temperature-dependent values of $C^{o}_{p,2}$ and V^{o}_{2} that were developed by Shock and Helgeson (1988) are based on Spedding *et al.*'s data at T = 298.15 K. Since these differ substantially from our experimental values, the descriptions of the temperature-dependence of $C^{o}_{p,2}$ and V^{o}_{2} in thermodynamic databases and the associated computer codes that are based on Spedding *et al.*'s data certainly need to be revised.

We have clearly shown that the behaviour of $C^{o}_{p,2}$ is dominated by structural hydration effects at temperatures near 298.15 K. The plot of the non-Born terms against the temperature function $10^{4}/(T - 228)^{2}$ suggests that $C^{o}_{p,2}$ at high temperature are determined primarily by the size and the charge of the ions. The systematic changes in $C^{o}_{p,2}$ and V^{o}_{2} acrose the series at 283.2 and 298.2 K correspond to changes in the hydration number. The gadolinium break for $C^{o}_{p,2}$ becomes ill-defined at $T \geq 313.2$ K while the systematic change in V^{o}_{2} persists over the same temperature range. This suggests that the heat capacity effect may be caused by dramatic changes in the structure of the second hydration shell with decreasing temperature while the volume effect is associated with the primary hydration number. Thus, the gadolinium break for $C^{o}_{p,2}$ is expected to be even more pronounced at supercooled temperatures.

This research has contributed a platinum-cell vibrating tube densimeter, along with the high pressure sampling system and temperature control system, to our research group at Memorial University. We have demonstrated that the platinum-cell densimeter

can be used to study the volumetric properties for aqueous electrolytes at temperatures up to 600 K and 300 bars with a precision similar to other high-temperature densimeters reported by Majer *et al.* (1991), Corti *et al.* (1992), and Simonson *et al.* (1994).

We have used the densimeter, and a similar instrument at Oak Ridge National Laboratory, to make volumetric measurements on gadolinium triflate at elevated temperatures and pressures. These are the first reported standard partial molar volumes at elevated temperatures for an aqueous trivalent salt. In order to calculate values of $V_2^o\{Gd^{3+}, aq\}$ from our data for $V_2^o\{Gd(CF_3SO_3)_3, aq\}$, we also measured the apparent molar volumes for sodium triflate, $NaCF_3SO_3(aq)$. The measurements of $V_{\phi,2}(NaCF_3SO_3,aq)$ provided primary reference data for an important non-complexing anion being used by several groups in the study of hydrothermal solution thermodynamics. The temperature-dependent values of $V_2^o\{Gd(CF_3SO_3)_3, aq\}$, along with values for $C_{p,2}^o$ $(AlCl_3,aq)$ and $C_{p,2}^o$ $(GdCl_3,aq)$ (Hovey and Tremaine,1988; Conti *et al.* 1992; Jekel *et al.*, 1964) reveal that trivalent cations have a sharper increase in both $C_{p,2}^o$ and V_2^o, and a lower temperature for the maximum in $C_{p,2}^o$ and V_2^o, than univalent and bivalent ions. It was also found that the effect of pressure on $V_2^o\{Gd(CF_3SO_3)_3, aq\}$ at temperatures near 298.15 K was more pronounced than that for common 1:1 and 2:1 aqueous electrolytes. This behaviour could be due to the larger primary hydration shell for trivalent lanthanide cations. This interpretation suggests that the pressure effect on V_2^o should also be pronounced for non-lanthanide trivalent salts such $Al(CF_3SO_3)_3$ and

$Fe(CF_3SO_3)_3$, which have a well-defined first hydration shell with six water molecules and a distinguishable second hydration shell, at temperature near 283 K.

The conventional values for $V_2^o(Gd^{3+}, aq)$ calculated from our values for $V_2^o\{Gd(CF_3SO_3)_3, aq\}$ and $V_2^o(HCF_3SO_3, aq)$ confirmed that extrapolations of low temperature data using the HKF model for the effective radius of trivalent cations in the Born equation are surprisingly successful.

Although it would be useful to examine the behaviour of other M^{3+} cations under hydrothermal conditions, the results for $Gd^{3+}(aq)$ and $Al^{3+}(aq)$ suggest that the functions for V_2^o and $C_{p,2}^o$ are described quite well by the HKF Born model. At low temperatures, the systematic differences in V_2^o and $C_{p,2}^o$ due to hydration effects are large, and not well understood. These would merit further study, especially under supercooled conditions were the effects should be VERY large. Although the Picker calorimeter is not suitable for studying supercooled solutions, experimental methods to measure heat capacities of supercooled water have been developed by Rasmussen *et al.* (1973a and 1973b) and these could be employed to obtain $C_{p,\phi}$ for aqueous electrolytes at temperatures below 273.15 K. Such data would provide new information about the structure of hydrated ions.

We note that aqueous triflic acid is an interesting system in which to investigate the competition between ionic solvation effects and hydrogen-bonding effects. Although triflic acid, the strongest monobasic organic acid, is a strong electrolyte in aqueous solutions, its thermodynamic properties do not increase monotonously with increasing

molality like other common aqueous strong acids. We suggest that the abnormal concentration-dependence of $V_{\phi,2}$(HCF_3SO_3, aq) can be accounted for by variations in the multi-layer hydrogen-bonding network structure of aqueous trifilic acid solutions at different concentrations.

The behaviour of $C_{p,\phi,2}$ and $V_{\phi,2}$ at elevated temperatures is intimately related to the critical locus of the aqueous system in question. Our volumetric measurements on (methanol + water) mixtures are the first reported pVT data for this important hydrogen-bonded system under hydrothermal conditions. The V_m^E data obtained from our vibrating tube densimeter at $T < 473$ K are consistent with those estimated from the pressure-. dependence of H_m^E obtained by Simonson *et al.* (1987) and, more recently, by Wormald *et al.* (1996) from flow calorimetry. We have developed a provisional extended corresponding-states model to represent V_m^E and the densities of $\{xCH_3OH + (1-x)H_2O\}$ mixtures to within the experimental uncertainties. The model can be also used to calculate partial molar volumes, isothermal compressibilities, and cubic expansion coefficients for the mixtures to a reasonable precision. The success of the corresponding states approach demonstrates that the system is remarkably well-behaved under these conditions over the entire range of mole fractions, despite the fact that both components are strongly hydrogen bonded. Accurate volumetric data should be measured at higher pressures near the critical locus, and at temperatures near 573.15 K and pressure near 20 MPa where Simonson *et al.* (1987) have suggested a two phase region may exist, before a

comprehensive equation of state treatment can be developed.

References

Abraham, M. H.; Lizzi, J. (1978), Calculations on Ionic Solvation Part 2. — Entropies of Solation of Gaseous Univalent Ions Using an One-Layer Continuum Model, *J. Chem. Soc., Faraday Trans. I*, **74**, 2858-2867.

Abraham, M. H.; Marcus, Y. M. (1986), The Thermodynamics of Solvation of Ions Part I. - The Heat Capacity of Hydration at 298.15 K, *J. Chem. Soc. Faraday Trans. I.*, **82**, 3255-3274.

Abraham, M. H.; Matteoli, E.; Liszi, J. (1983), Calculation of the Thermodynamics of Solvation of Gaseous Univalent Ions in Water from 273 to 573 K, *J. Chem. Soc. Faraday Trans. I.*, **79**, 2781-2800.

Albert, H. J.; Wood, R. H. (1984), High-Precision Flow Densimeter for Fluids at Temperatures to 700 K and Pressures to 40 MPa, *Rev. Sci. Instrum.*, **55**, 589-593.

Anderson, G. M.; Castet, S.; Schott, J.; Mesmer, R. E. (1991), The Density Model for Estimation of Thermodynamic Parameters of Reactions at High Temperatures and Pressures, *Geochim. Cosmochim. Acta*, **55**, 1769-1779.

Angus, S.; Amstrong, B.; de Reuck, K. M. (1976), International Thermodynamic Tables of the Fluid State. Vol. 3: Carbon dioxide. Pergamon: Oxford.

Antal, M. J. Jr. (1995), Water: A Traditional Solvent Pregnant with New Applications, p 24-32 in Physical Chemistry of Aqueous Systems: Meeting the Needs of Industry, White, H. J.; Sengers, J. V.; Neumann, D. B.; Bellows, J. C., ed., Begell House: New York.

Archer, D. G. (1992), Thermodynamic Properties of NaCl + H_2O System II. Thermodynamic Properties of NaCl(aq), NaCl-2H_2O(cr), and Phase Equilibria, *J. Phys. Chem. Ref. Data*, **21**, 793-821.

Archer, D. G.; Wang, P. (1990), The Dielectric Constant of Water and Debye-Hückel Limiting Law Slopes, *J. Phys. Chem. Ref. Data*, **19**, 371-411.

Atkins, P. W. (1990), Physical Chemistry, 4th ed., W. H. Freeman: New York.

Avedikian, L.; Perron, G.; Desnoyers, J. E. (1974), Apparent Molal Volumes and Heat Capacities of Some Alkali Halides and Tetraalkylammonium Bromides in Aqueous Tert-Butanol Solutions, *J. Solution Chem.*, **4**, 331-346.

Baes, C. F.; Mesmer, R. E. Jr. (1976), The Hydrolysis of Cations, Wiley: New York.

Balicheva, T. G.; Ligus, V. I.; Fialkov, Y. Y. (1973), Infrared Absorption Spectra of Trifluoromethanesulphonic Acid and Its Solutions, *Russ. J. Inorg. Chem.*, **18**, 1701-1703.

Ben-Naim, A. (1992), Statistical thermodynamics for Chemists and Biochemists, Plenum Press: New York.

Benson, G. C.; D'Arcy, P. J. (1982), Excess Isobaric Heat Capacities of Water-n-Alcohol Mixtures, *J. Chem. Eng. Data*, **27**, 439-442.

Benson, G. C.; Kiyohara, O. (1980), Thermodynamics of Aqueous Mixtures of Nonelectrolytes. I. Excess Volumes of Water-n-Alcohol Mixtures at Several Temperatures, *J. Solution Chem.*, **9**, 791-804.

Biggestaff, D. R.; Wood, R. H. (1988), Apparent Molar Volumes of Aqueous Argon, Ethylene and Xenon from 300 to 715 K, *J. Phys. Chem.*, **92**, 1988-1994.

Blum, L. (1975), Mean Spherical Model for Asymmetric Electrolytes I. Method of Solution, *Mol. Phys.*, **30**, 1529-1535.

Blum, L.; Hoye, J. S. (1977), Mean Spherical Model for Asymmetric Electrolytes. 2. Thermodynamic Properties and the Pair Correlation Function, *J. Phys. Chem.*, **81**, 1311-1315.

Bontha, J. R.; Pintauro, P. N. (1992), Prediction of Ion Solvation Free Energies in a Polarizable Dielectric Continuum, *J. Phys. Chem.* **96**, 7778-7782.

Bradley, D. J.; Pitzer, K. S. (1979), Thermodynamics of Electrolytes. 12. Dielectric Properties of Water and Debye-Hückel Parameters to 350 °C, *J. Phys. Chem.*, **83**, 1599-1603.

Breen, P. J.; Horrocks, W. D. Jr. (1983), Europium (III) Luminescence Excitation Spectroscopy Inner-Sphere Complexation Europium (III) by Chloride, Thiocyanate, and Nitrate Ions, *Inorg. Chem.*, **22**, 536-540.

Bucher, M.; Poter, T. L. (1986), Analysis of the Born Model for Hydration of Ions, *J. Phys. Chem.*, **90**, 3406-3411.

Bull, F. -X.; Planche, H.; Furst, W.; Renon, H. (1985), Representation of Deviation

from Ideality in Concentrated Aqueous Solutions of Electrolytes using a Mean Spherical Approximation Molecular Model, *AIChE J.*, **31**, 1233-1240.

Burkin, A. R., (1966), The Chemistry of Hydrometallurgical Processes, D. Van Nostrand: Princeton.

Chang, R. F.; Levelt Sengers, J. M. H. (1986), Behavior of Dilute Mixtures near the Solvent's Critical Point, *J. Phys. Chem.*, **90**, 5921-5927.

Chang, R. F.; Morrison, G.; Levelt Sengers, T. M. H. (1984), The Critical Dilemma of Dilute Mixtures, *J. Phys. Chem.*, **88**, 3389-3391.

Chen, Z.; Detellier, C. (1992), Interaction of La(III) with Anions in Aqueous Solutions. A ^{139}La NMR Study, *J. Solution Chem.*, **21**, 941-951.

Choppin, G. R. (1971), Structure and Thermodynamics of Lanthanide and Actinide Complexes in Solution, *Pure & Appl. Chem.* **27**, 23-41.

Cobble, J. W.; Lin, S. W. (1990), Chemistry of Steam Cycle Solutions: Properties, in The ASME Handbook on Water Technology for Thermal Power Systems, Cohen, P. Ed., 545-658.

Cobble, J. W.; Murray, R. C.; Sen, U. (1981), Field and Structure Behaviour of Electrolytes, *Nature*, **291**, 566-568.

Conti, G.; Gianni, P. G.; Matteoli, E. (1992), Apparent Molar Heat Capacity of Aqueous Hydrolyzed and Non-Hydrolyzed $AlCl_3$ between 50-150 °C, *Geochim. Cosmochim. Acta*, **56**, 4125-4133.

Conway, B. E. (1981), Ionic Hydration in Chemistry and Biophysics, Elsevier: New York.

Corti, H. R. (1992), in High Temperature Aqueous Solutions: Electrolyte Solutions, Chapter 5. Fernandez-Prini, R. J.: editor. CRC Press, Boca Raton, FL.

Corti, H. R.; Fernandez-Prini, R.; Svarc, F. (1990), Densities and Partial Molar Volumes of Aqueous Solutions of Lithium, Sodium, Potassium Hydroxides up to 250 °C, *J. Solution Chem.*, **19**, 793-809.

Cossy, C.; Barnes, A. C.; Enderby, J. E. (1989), The Hydration of Dy^{3+} and Yb^{3+} in

Aqueous Solution: A Neutron Scattering First Order Difference Study, *J. Chem. Phys.*, **90**, 3254-3260.

Cossy C.; Helm, L.; Merbach, A. E. (1988), Oxygen-17 Nuclear Magnetic Resonance Kinetic Study of Water Exchange on the Lanthanide (III) Aqua Ions, *Inorg. Chem.*, **27**, 1973-1979.

Cossy, C.; Merbach, A. E. (1988), Recent Developments in Solvation and Dynamics of the Lanthanide (III) Ions, *Pure & Appl. Chem.*, **60**, 1785-1796.

Dandurand, J. -L.; Schott, J. (1992), Prediction of Ion Association in Mixed-Crustal Fluids, *J. Phys. Chem.*, **96**, 7770-7777.

Delaplane, R. G.; Lundgren, J. O.; Olovsson, I. (1975), Hydrogen Bond Studies. XCVII. The Crystal Structure of Trifluoromethanesulphonic Acid Dihydrate, $H_5O_2^+CF_3SO_3^-$, at 225 and 85 K, *Acta Cryst.* **B31**, 2202-2207.

Delaplane, R. G.; Lundgren, J. O.; Olovsson, I. (1975), Hydrogen Bond Studies. CVI. The Crystal Structure of $2CF_3SO_3H.H_2O$, *Acta Cryst.* **B31**, 2208-22013.

Desnoyers, J.; Jolicoeur, C. (1983), Ionic Solution in Comprehensive Treatise of Electrochemistry, Conway, B, B.; Bockris, J. O.; Yeager, E., ed., Plenum Press, New York.

Desnoyers, J. E.; Visser, C. de; Perron, G.; Picker, P. (1976), Reexamination of the Heat Capacities Obtained by Flow Microcalorimetry. Recommendation for the Use of a Chemical Standard, *J. Solution Chem.*, **5**, 605-616.

Dogonadze, R. R.; Kalman, E.; Kornyshev, A. A.; Ulstrup, J. (1985), The Chemical Physics of Solvation, Elsevier: New York.

Dooley, B.; Bursik, A., (1995), State of the Art in Fossil Plant Cycle Chemistry, p 33-47 in Physical Chemistry of Aqueous Systems: Meeting the Needs of Industry, White, H. J.; Sengers, J. V.; Neumann, D. B.; Bellows, J. C., ed., Begell House: New York.

Duttachoudhury, M.; Mathur, H. B. (1974), Heats of Mixing of n-Butyl Amine-Water and n-Butyl Amine-Alcohol Systems, *J. Chem. Eng. Data*, **19**, 145-147.

Easteal, A. J.; Woolf, L. A. (1985), (p, V_m, T, x) Measurements for $\{(1 - x)H_2O + xCH_3OH\}$ in the Range 278 to 323 K and 0.1 to 280 MPa I. Experimental Results,

Isothermal Compressibilities, Thermal Expansivities, and Partial Molar Volumes, *J. Chem. Thermodyn.*, **17**, 49-62.

Easteal, A. J.; Woolf, L. A. (1985), (p, V_m, T, x) Measurements for {(1 - x)H_2O + xCH_3OH} in the Range 278 to 323 K and 0.1 to 280 MPa II.Thermodynamic Excess Properties, *J. Chem. Thermodyn.*, **17**, 69-82.

Eisengerg, D.; Kauzmann, W. (1969), The Structure and Properties of Water, Oxford.

Eley, D. D.; Evans, M. G. (1938), Heats and Entropy Changes Acccompanying the Solution of Ions in Water, *Trans. Faraday Soc.*, **34**, 1093-1112.

Ellis, A. J.; McFadden, I. M. (1972), Partial Molar Volumes of Ions in Hydrothermal Solutions, *Geochim Cosmochim. Acta*, **36**, 413-426.

Fabes, L.; Swaddle, T. W. (1975), Reagents for High Temperature Aqueous Chemistry: Trifluoromethanesulfonic Acid and Its Salts, *Can. J. Chem.*, **53**, 3053-3059.

Frank, E. U. (1987), Fluids at High Pressures and Temperatures, *J. Chem. Thermodyn.*, **19**, 225-242.

Franks, F.; Smith, H. T. (1967), Apparent Molal Volumes and Expansibilities of Electrolytes in Dilute Aqueous Solution, *Trans. Faraday Soc.*, **63**, 2586-2598.

Friend, D. G.; Huber, M. L. (1994), Thermophysical Property Standard Reference Data from NIST, *Int. J. Thermophys.*, **15**, 1279-1288.

Gallagher, J. S.; Crovetto, R.; Levelt Sengers, J. M. H. (1993), The Thermodynamic Behavior of the CO_2-H_2O System from 400 to 1000 K, up to 100 MPa and 30% Mole Fraction of CO_2, *J. Phys. Chem. Ref. Data*, **22**, 431-449.

Gates, J. A. (1985), Thermodynamics of Aqueous Electrolyte Solutions at High Temperatures and Pressures, Ph. D. Thesis, University of Delaware.

Goldman, S.; Bates, R. G. (1972), Calculation of Thermodynamic Functions for Ionic Hydration, *J. Phys. Chem.*, **94**, 1476-1484.

Goldman, S.; Morss, L. R. (1975), Semi-empirical Calculations on the Free Energy and Enthalpy of Hydration for the Trivalent Lanthanides and Actinides, *Can. J. Chem.*, **53**, 2695-2700.

Goodwin, R. D. (1987), Methanol Thermodynamic Properties from 176 to 673 K at Pressures to 700 Bar, *J. Phys. Chem. Ref. Data*, **16**, 799-892.

Götze, G.; Schneider, G. M. (1980), Excess Volumes of Liquid Mixtures at High Pressures IV. Pressure Dependence of Excess Gibbs Energies, Excess Entropies, and Excess Enthalpies of Aqueous Non-Electrolyte Mixtures up to 250 MPa, *J. Chem. Thermodyn.*, **12**, 661-672.

Grant-Taylor, D. F. (1981), Partial Molal Volumes of Sodium Chloride Solutions at 200 Bar, and Temperatures from 175 to 350 °C, *J. Solution Chem.*, **10**, 621-630.

Griffiths, R. B.; Wheeler, J. C. (1970), Critical Points in Multicomponent Systems, *Phys. Rev. A.*, **2**, 1047-1064.

Griswold, J.; Wong, S. Y. (1952), Chem. Eng. Progr., Symp. Ser., 48, 18 (cited by Hicks, C. P.; Young, C. L. (1975), The Gas-Liquid Critical Properties of Binary Mixtures, *Chem. Rev.*, **75**, 119-175).

Guggenheim, E. A.; Turgeon, J. C. (1955), Specific Interaction of Ions, *Trans. Faraday Soc.*, **51**, 747-761.

Haar, L.; Gallagher, J. S.; Kell, G. S. (1984), NBS/NRC Steam Tables (Hemisphere, Washington)

Habenschuss, A.; Spedding, F. H. (1979a), The Coordination (Hydration) of Rare Earth Ions in Aqueous Chloride Solutions from X-Ray Diffraction. I. *J. Phys. Chem.*, **70**, 2797-2806.

Habenschuss, A.; Spedding, F. H. (1979b), The Coordination (Hydration) of Rare Earth Ions in Aqueous Chloride Solutions from X-Ray Diffraction. II. *J. Phys. Chem.*, **70**, 3758-3763.

Habenschuss, A.; Spedding, F. H. (1980c), The Coordination (Hydration) of Rare Earth Ions in Aqueous Chloride Solutions from X-Ray Diffraction. III. $SmCl_3$, $EuCl_3$, and Series Behavior, *J. Phys. Chem.*, **73**, 442-450.

Hahn, R. L. (1988), Volumes of Aqua Ions from Measured Neutron Radial Distribution Functions, *J. Phys. Chem.*, **92**, 1668-1675.

Helgeson, H. C.; Kirkham, D. H. (1976), Theoretical Predictions of the Thermodynamic Behaviour of Aqueous Electrolytes at High Pressures and Temperatures. III. Equation of State for Aqueous Species at Infinite Dilution, *Am. J. Sci.*, **276**, 97-240.

Helgeson, H. C.; Kirkham, D. H.; Flowers, G. C. (1981), Theoretical Predictions of the Thermodynamic Behaviour of Aqueous Electrolytes at High Pressures and Temperatures. IV. Calculation of Activity Coefficient, Osmotic Coefficients, and Apparent Molar and Standard and Relative Partial Molar Properties to 600 °C and 5 kb, *Am. J. Sci.*, **281**, 1249-1516.

Herrington, T. M.; Pethybridge, A. D.; Roffey, M. G. (1985), Densities of Hydrochloric, Hydrobromic, Hydroiodic, and Perchloric Acids 25 to 75 °C, *J. Chem. Eng. Data*, **30**, 264-267.

Hill, P. G. (1990), A Unified Fundamental Equation for the Thermodynamic Properties of H_2O, *J. Phys. Chem. Ref. Data*, **19**, 1233-1274.

Hill, P. G.; MacMillan, D. C.; Lee, V. J. (1982), A Fundamental Equation of State for Heavy Water, *J. Phys. Chem. Ref. Data*, **11**, 1-14.

Ho, P. C.; Palmer, D. A. (1995), Electrical Conductances of Aqueous Sodium Trifluoromethanesulfonate from 0 to 450 °C and Pressures to 250 MPa, *J. Solution Chem.*, **24**, 753-769.

Holm, N. G. (1992), Marine Hydrothermal Systems and the Origin of Life: Report of SCOR Working Group 91, Kluwer Academic: Boston.

Holmes, H. F.; Busey, R. H.; Simonson, J. M.; Mesmer, R. E. (1987), The Enthalpy of Dilution of HCl(aq) to 648 K and 40 MPa, Thermodynamic Properties, *J. Chem. Thermodyn.*, **19**, 863-890.

Holmes, H. F.; Busey, R. H.; Simonson, J. M.; Mesmer, R. E. (1994), $CaCl_2$(aq) at Elevated Temperatures. Ethalpies of Dilution, Isopiestic Molalities, and Thermodynamic Properties, *J. Chem. Thermodyn*amics, **26**, 271-298.

Holmes, H. F.; Mesmer, R. E. (1986a), Thermodynamics of Aqueous Solutions of the Alkali Metal Salfates, *J. Solution Chem.*, **15**, 495-518.

Holmes, H. F.; Mesmer, R. E. (1986b), Isopiestic Studies of Aqueous Solutions at Elevated Temperatures VIII. The Alkali-Metal Sulfates, *J. Chem. Thermodyn.*, **18**, 263-

275.

Hovey, J. K. (1988), Thermodynamics of Aqueous Solutions, Ph. D. Thesis, University of Alberta

Hovey, J. K.; Hepler, L. G.; Tremaine, P. R. (1988), Apparent Molar Heat Capacities and Volumes of Aqueous $HClO_4$, HNO_3, $(CH_3)_4NOH$ and K_2SO_4 at 298.15 K, *Thermochim. Acta*, **126**, 245-253.

Hovey, J. K.; Tremaine, P. R. (1986), Thermodynamics of Aqueous Aluminum: Standard partial molar heat capacities of Al^{3+} from 10 to 55 °C, *Geochim. Cosmochim. Acta*, **50**, 453-459.

Jekel, E. C.; Criss, C. M.; Cobble, J. W. (1964), The Thermodynamic Properties of High Temperature Aqueous Solutions. VIII. Standard Partial Molal Heat Capacities of Gadolinium Chloride from 0 to 100°, *J. Am.Chem. Soc.*, **86**, 5404-5407.

Isono, T. (1984), Density, Viscosity, and Electrolytic Conductivity of Concentrated Aqueous Electrolyte Solutions at Several Temperatures. Alkaline-Earth Chlorides, $LaCl_3$, Na_2SO_4, $NaNO_3$, NaBr, KNO_3, KBr, and $Cd(NO_3)_2$, *J. Chem. Eng. Data*, **29**, 45-52.

Japas, M. L. (1992), Chapter 5, Dilute Solutions near Critical Conditions, in High-Temperature Aqueous Solutions: Thermodynamic Properties, Fernandez-Prini, R. J.: editor. CRC Press: Boca Raton, FL.

Jia, Y. Q. (1987), Quantum Chemical Studies on the Hydrated Ions of the Rare Earths, *Inorg. Chim. Acta*, **133**, 331-336.

Johansson, G.; Eakita, H. (185), X-Ray Investigation of the Coordination and Complex Formation of Lanthanide Ions in Aqueous Perchlorate and Selenate Solutions, *Inorg. Chem.*, **24**, 3047-3052.

Johansson, G.; Yokoyama, H. (1990), Inner- and Outer-Sphere Complex Formation in Aqueous Erbium Halide and Perchlorate Solutions. An X-ray Diffraction Study Using Isostructural Substitution, *Inorg. Chem.*, **29**, 2460-2466.

Kaizu, Y.; Miyakawa, K.; Okada, K.; Kobayashi, H.; Sumitani, M.; Yoshihara, K. (1985), Aqualigand Dissociation of $[Ce(OH_2)_9]^{3+}$ in the 5d – 4f Excited State, *J. Am. Chem. Soc.*,

107, 2622-2626.

Kanno, H.; Akama, Y. (1987), A Glass Formation Study of Aqueous Rare Earth Electrolyte Solutions, *J. Phys. Chem.*, **91**, 1263-1266.

Kanno, H.; Hiraishi, J. (1980), Raman Spectroscopic Evidence for a Discrete Change in Coordination Number of Rare Earth Aquo-Ions in the Middle of the Series, *Chem. Phys. Lett.*, **75**, 553-556.

Kanno, H.; Hiraishi, J. (1982), A anomalous Concentration Dependence of the Inner-Sphere Hydration Number Change in Aqueous $EuCl_3$ and $GdCl_3$ Solutions, *Chem. Phys. Lett.*, **86**, 1488-1990.

Kanno, H.; Hiraishi, J. (1988), Raman Study of Aqueous Rare-Earth Nitrate Solutions in Liquid and Glassy States, *J. Phys. Chem.*, **88**, 2787-2792.

Kell, G. S.; Whalley, E. (1975), Reanalysis of the Density of Liquid Water in the Range 0-150 °C, *J. Chem. Phys.*, **62**, 3496-3503.

Kell, G. G.; McLaurin, G. E.; Whalley, E. (1978), The PVT Properties of Water: IV. Liquid water in the Range 150-350 °C, from Saturation to 1 kbar, *Phil. Trans. Roy. Soc. London. Ser. A*, **360**, 389.

Kell, G. S.; McLaurin, G. E.; Wahlley, E. (1989), PVT Properties of Water. VII. Vapour Densities of Light and Heavy Water from 150 to 500 °C, *Proc. Roy. Soc. A (London)*, **425**,49.

Kestin, J.; Sengers, J. V. (1986), New Interactional Formulations for the Thermodynamic Properties of Light and Heavy Water, *J. Phys. Chem. Ref. Data*, **15**, 305-320.

Kiyohara, O.; Perron, G.; Desnoyers, J. E. (1975), Volumes and Heat Capacities of Cyclic Ethers and Amines in Water and of Some Electrolytes in These Mixed Aqueous Solvents, *Can. J. Chem.*, **53**, 2591-2597.

Kratky, O.; Leopold, H.; Stabinger, H. (1969), Dichtemessungen an Flüssigkeiten und Gasen auf 10^{-6} g/cm^3 bei 0.6 cm^3 Präparatvolumen, *Angew. Phys.*, **27**, 273-277.

Kubota, H.; Tanaka, Y.; Makita, T. (1987), Volumetric Behavior of Pure Alcohols and Their Water Mixtures under High Pressures, *Int. J. Thermophys.*, 8, 47-70.

Lama, R. F.; Lu, B. C. Y. (1965), Excess Thermodynamic Properties of Aqueous Alcohol

Solutions, *J. Chem. Eng. Data*, **10**, 216-219.

Lawrance, G. A. (1986), Coordinated Trifluoromethanesulfonate and Fluorosulfate, *Chem. Rev.*, **86**, 17-33.

Lee, L. L. (1988), Molecular Thermodynamics of Nonideal Fluids, Butterworths: Boston.

Leach, J. W.; Chappelear, P. S.; Leland, T. W. (1968), Use of Molecular Shape Factors in Vapor-Liquid Equilibrium Calculations with the Corresponding States Principle, *AIChE J.*, **14**, 568-576.

Leduc, P.; Desnoyers, J. E. (1973), Apparent Molal Heat Capacities and Volumes of Tetrabutylammonium Carboxylates and Related Solutes in Water at 25 °C, *Can. J. Chem.*, **51**, 2993-2996.

Levelt Sengers, J. M. H. (1991), Supercritical Fluid Technology: Reviews in Modern Theory and Applications, Chapter 1. Bruno, J. J.; Ely, J. F.: editor. CRC Press: Boca Raton, FL.

Levelt Sengers, J. M. H. (1995), Significant Contributions of IAPWS to the Power Industry, Science and Technology, p 1-12 in Physical Chemistry of Aqueous Systems: Meeting the Needs of Industry, White, H. J.; Sengers, J. V.; Neumann, D. B.; Bellows, J. C., ed., Begell House: New York.

Levelt Sengers, J. M. H.; Everhart, C. M.; Morrison, G.; Pitzer, K. S. (1986), Thermodynamic Anomalies in Near-Critical Aqueous NaCl Solutions, *Chem. Eng. Commun.*, **47**, 315-328.

Levelt Sengers, T. M. H.; Given, J. A. (1993), Critical Behaviour of Ionic Fluids, *Mol. Phys.*, **80**, 899-913.

Levelt Sengers, J. M. H.; Kamgar-Parsi, R.; Bulfour, F. W.; Sengers, J. V. (1983), Thermodynamic Properties of Steam in the Critical Region, *J. Phys. Chem. Ref. Data*, **12**, 1-28.

Lindsay, W. T. (1990), Chemistry of Steam Cyle Solutions: Principles, in The ASME Handbook on Water Technology for Thermal Power Systems, Cohen, P. Ed., 341-544.

Lundgren, J. O. (1978), Hydrogen Bond Studies. CXXXI. The Crystal Structure of Trifluoromethanesulphonic Acid Pentahydrate, $H_3O^+CF_3SO_3^-.4H_2O$, *Acta Cryst.* **B34**, 2432-2435.

Lundgren, J. O. (1978), Hydrogen Bond Studies. CXXX. The Crystal Structure of Trifluoromethanesulphonic Acid Tetrahydrate, $H_9O_4^+CF_3SO_3^-$, *Acta Cryst.* **B34**, 2428-2431.

L'vov, S. N.; Zarembo, V. I.; Gilyarov, V. N. (1981), High-Precision Study of Volume Properties of Water Solution of Sodium Chloride under High Pressures, *Geokhimiya*, **4**, 505-516.

Majer, V.; Crovetto, R.; Wood, R. H. (1991), A New Version of Vibrating-Tube Flow Densitometer for Measurements at Temperatures up to 730 K, *J. Chem. Thermodyn.*, **23**, 333-344.

Majer, V.; Hui, L.; Crovetto, R.; Wood, R. H. (1991), Volumetric Properties of Aqueous 1-1 Electrolyte Solution near and above the Critical Temperature of Water. 1. Densities and Apparent Molar Volumes of NaCl(aq) from 0.0025 $mol \cdot kg^{-1}$ to 3.1 $mol \cdot kg^{-1}$, 604.4 K to 725.5 K, and 18.5 MPa to 38.0 MPa, *J. Chem. Thermodyn.*, **23**, 213-229.

Marcus, Y. (1986), The Hydration Entropies of Ions and Their Effects on the Structure of Water, *J. Chem. Soc., Faraday Trans I.*, **82**, 233-242.

Marcus, Y. (1993), Thermodynamics of Solvation of Ions. Part 6. -The Standard Partial Molar Volumes of Aqueous Ions at 298.15 K, *J. Chem. Soc. Faraday Trans.*, **89**, 713-718.

Marsh, K. N.; O'Hare, P. A. G.: eds. (1994), Solution Calorimetry, Blackwell Scientific Publications: Oxford.

Marshall, W. L.; Jones, E. V. (1974), Liquid-Vapor Critical Temperatures of Several Aqueous-Organic and Organic-Organic Solution Systems, *J. Inorg. Nucl. Chem.*, **36**, 2319-2323.

Mastroianni, M.; Criss, C. M. (1972), Standard Partial Molal Heat Capacities of Sodium Perchlorate in Water from 0 - 90 °C and in Anhydrous Methanol from -5 - 55 °C., *J. Chem. Eng. Data*, **17**, 222-226.

McGlashan, M. L.; Williamson, A. G. (1976), Isothermal Liquid-Vapor Equilibria for System Methanol-Water, *J. Chem. Eng. Data*, **21**, 196-199.

Meier, W.; Bopp, P.; Probst, M. M.; Spohr, E.; Lin, J. L. (1990), Molecular Dynamics Studies of Lanthanum Chloride Solutions, *J. Phys. Chem.*, **94**, 4672-4682.

Miyakawa, K.; Kaizu, Y.; Kobayashi, H. (1988), An Electrostatic Approach to the Structure

of Hydrated Lanthanoid Ions, *J. Chem. Soc., Faraday Trans. I.* **84**, 1517-1529.

Muirhead-Gould, J. S.; Laidler, K. J. (1967), Discontinuous Model for Hydration of Monatomic Ions, *Trans. Faraday Soc.*, **63**, 944-952.

Narten, A. H.; Hahn, R. N. (1983), Hydration of the Nd^{3+} Ion in Neodymium Chloride Solutions Determined by Neutron Diffraction, *J. Phys. Chem.*, **87**, 3193-3197.

Oakes, C. S.; Simonson, J. M.; Bondnar, R. J. (1995), Apparent Molar Volumes of Aqueous Calcium Chloride to 250 °C, 400 Bars, and from Molalities of 0.242 to 6.150, *J. Solution Chem.*, **24**, 897-916.

Ohe, S. (1989), Vapor-Liquid Equilibrium Data at High Pressure. Elsevier: Amsterdam.

Ohe, S. (1990), Vapor-Liquid Equilibrium Data at High Pressure. Elsevier: Amsterdam.

Ohtaki, H.; Radnai, T. (1993), Structure and Dynamics of Hydrated Ions, *Chem. Rev.*, **93**, 1157-1204.

Okada, K.; Kaizu, Y.; Kobayashi, H. (1981), Aqualigand Dissociation of 5d – 4f Excited $[Ce(OH_2)_9]^{3+}$ in Aqueous Solution, *J. Chem. Phys.*, **75**, 1577-1578.

Outhwaite, C. W.; Molero, M.; Bhuiyan, L. B. (1991), Symmetrical Poisson-Boltzmann and Modified Poisson-Boltzmann Theories, *J. Chem. Soc., Faraday Trans.*, **87**, 3227-3230.

Outhwaite, C. W.; Molero, M.; Bhuiyan, L. B. (1993), Primitive Model Electrolytes in the Modified Poisson-Boltzmann Theory, *J. Chem. Soc., Faraday Trans.*, **89**, 1315-1320.

Palmer, D. A.; Drummond, S. E. (1988), Potentiometric Determination of the Modal Formation Constants of Ferrous Acetate Complexes in Aqueous Solutions to High Temperatures, *J. Phys. Chem.*, **92**, 6795-6800.

Patel, N. C.; Sandler, S. I. (1985), Excess Volumes of the Water/Methanol, n-Heptane/Ethyl acetate, n-Heptane/n-Butyraldehyde, and n-Heptane/Isobutyraldehyde Systems, *J. Chem. Eng. Data*, **30**, 218-222.

Phutela, R. C.; Pitzer, K. S.; Suluja, P. P. S. (1987), Thermodynamics of Aqueous Magnesium Chloride, Calcium Chloride, and Strontium Chloride at Elevated Temperatures, *J. Chem. Eng. Data*, **32**, 76-80.

Picker, P.; Ludec, P. A.; Desnoyers, J. E. (1971), Heat Capacity of Solutions by Flow Microcalorimetry, *J. Chem. Thermodyn.*, **3**, 631-642.

Picker, P.; Tremblay, E.; Jolicoeur, C. (1974), A High-Precision Digital Readout Flow Densimeter for Liquids, *J. Solution Chem.*, **3**, 377-384.

Pirajno, F. (1992), Hydrothermal Mineral Deposits, Springer-Verlog: New York.

Pitzer, K. S. (1973), Thermodynamics of Electrolytes. I. Theoretical Basis and General Equations, *J. Phys. Chem.*, **77**, 268.

Pitzer, K. S. (1989), Fluids, Both Ionic and Non-ionic, Over Wide Ranges of Temperature and Composition, *J. Chem. Thermodyn.*, **21**, 1-17.

Pitzer, K. S. (1990), Critical Phenomena in Ionic Fluids, *Acc. Chem. Res.*, **23**, 333-338.

Pitzer, K. S. (1991), Ion Interaction Approach: Theory and Data Correlation, in Activity Coefficients in Electrolyte Solutions, 2nd Edition, Pitzer ed., CRC press: Boston, Chapter 3.

Pitzer, K. S.; Brewer, L. (1961), Thermodynamics, 2nd ed., McGruw-Hill: New York.

Pogue, P. F.; Atkinson, G. (1988), Apparent Molal Volumes and Heat Capacities of Aqueous HCl and $HClO_4$ at 15 - 55 °C, *J. Chem. Eng. Data*, **33**, 495-499.

Prausnitz, J. M.; Gunn, R. D. (1958), *AIChE J.*, **4**, 430-435.

Prausnitz, J. M.; Lichtenthaler, R. N.; de Azevedo, E. G. (1986), Molecular Thermodynamics of Fluid-Phase Equilibria, 2nd edition. Prentice-Hall: Englewood Cliffs.

Pruß, A.; Wagner, W. (1995), A New Equation of State for Water as a Candidate for the New Scientific Formulation of IAPWS, p66-77 in Physical Chemistry of Aqueous Systems: Meeting the Needs of Industry, White, H. J.; Sengers, J. V.; Neumann, D. B.; Bellows, J. C., ed., Begell House: New York.

Quint, J. R.; Wood, R. H. (1985), Thermodynamics of a Charge Hard-Sphere Ion in a Compressible Dielectric Fluid. 2. Calculation of the Ion-Solvent Pair Correlation Function, the Excess Solvation, the Dielectric Constant near the Ion, and the Partial Molar Volume of the Ion in a Water-like Fluid above the Critical Point, *J. Phys. Chem.*, **89**, 380-384.

Randall, M.; Rossini, F. D. (1929), Heat Capacities in Aqueous Salt Solutions, *J. Am. Chem. Soc.*, **51**, 323-345.

Rard, J. A. (1985), Chemistry and Thermodynamics of Europium and Some of Its Simpler Inorganic Compounds and Aqueous Species, *Chem. Rev.*, **85**, 555-582.

Rard, J. A.; Spedding, F. H. (1975), Electrical Conductances of Some Aqueous Rare Earth Electrolyte Solutions at 25°. III. The Rare Earth Nitrates, *J. Phys. Chem.*, **79**, 257-262.

Rasmussen, D. H.; and MacKenzie, A. P., (1973), Clustering in Supercooled Water, *J. Chem. Phys.*, **59**, 5003-5013.

Rasmussen, D. H.; and MacKenzie, A. P., (1973), Anomalous Heat Capacities of Supercooled Water and Heavy Water, *Nature*, **181**, 342-344.

Reid, R. C.; Prausnitz, J. M.; Poling, B. E. (1987), The Properties of Gases and Liquids, 4th edition. McGraw-Hill: New York.

Reilly, P. J.; Wood, R. H. (1969), The Prediction of the Properties of Mixed Electrolytes from Measurements on Common Ion Mixtures, *J. Phys. Chem.*, **73**, 4292-4297.

Rizkalla, E. N.; Choppin, G. R. (1991), Hydration and Hydrolysis of Lanthanides, Chapter 103, Handbook on the Physics and Chemistry of Rare Earths. Vol. 15, edited by K. A. Gschmeidner, Jr. and L. Eyring.

Roy, R. N.; Gibbons, J. J.; Peiper, J. C.; Pitzer, K. S. (1983, 1986), Thermodynamics of the Unsymmetrical Mixed Electrolyte HCl-$LaCl_3$, *J. Phys. Chem.*, **87**, 2365-2369.

Rozen, A. M. (1976), The Unusal Properties of Solutions in the Vicinity of the Critical Point of the Solvent, *Russ. J. Phys. Chem.*, **50**, 138-1393.

Saul, A.; Wagner, W. (1989), International Equation for the Saturation Properties of Ordinary Water Substance, *J. Phys. Chem. Ref. Data*, **18**, 1537.

Shabana, A. A. (1990), Theory of Vibration. Volume I: An Introduction, Springer-Verlag: New York.

Shock, H. L.; Helgeson, H. C. (1988), Calculation of the Thermodynamic and Transport Properties of Aqueous Species at High Pressures and Temperatures: Correlation Algorithms for Ionic Species and Equation of State Predictions to 5kb and 1000 °C, *Geochim.*

Cosmochim. Acta, **52**, 2009.

Silber, H. B.; Bakhshandehfar, R.; Contreras, L. A.; Gaizer, F.; Gonsalves, M.; Ismail, S. (1990), Equilibrium Studies of Lanthanide Nitrate Complexation in Aqueous Methanol, *Inorg. Chem.*, **29**, 4473-4475.

Simonson, J. M.; Bradley, D. J.; Busey, R. H. (1987), Excess Molar Enthalpies and the Thermodynamics of (Methanol + water) to 573 K and 40 MPa, *J. Chem. Thermodyn.*, **19**, 479-492.

Simonson, J. M.; Holmes, H. F.; Busey, R. H.; Mesmer, R. E.; Archer, D. G.; Wood, R. H. (1990), Modelling of the Thermodynamics of Electrolyte Solutions to High Temperatures Including Ion Association. Application to Hydrochloric Acid, *J. Phys. Chem.*, **94**, 7675-7681.

Simonson, J. M.; Oakes, C. S.; Bodnar, R. J. (1994), Densities of NaCl(aq) to the Temperature 523 K at Pressures to 40 MPa Measured with a New Vibrating-Tube Densitomter, *J. Chem. Thermodyn.*, **26**, 345-359.

Smith, L. S.; Wertz, D. L. (1977), On the Coordination of La^{3+} in Aqueous $LaBr_3$ Solutioms, *J. Inorg. Nucl. Chem.*, **39**, 95-98.

Smith-Magowan, D.; Wood, R. H. (1981), Heat Capacities of Aqueous Sodium Chloride from 320 to 600 K Measured with a New Flow Calorimeter, *J. Chem. Thermodyn.*, 13, 1047-1073.

Spedding, F. H.; Csejka, D. A.; Dekock, C. W. (1966a), Heats of Dilution of Aqueous Rare Earth Chloride Solutions at 25°, *J. Phys. Chem.*, **70**, 2423-2429.

Spedding, F. H.; Baker, J. L.; Walters, J. P. (1975a), Apparent and Partial Molal Heat Capacities of Aqueous Rare Earth Perchlorate Solutions at 25°C, *J. Chem. Eng. Data*, **20**, 189-195.

Spedding, F. H.; Baker, J. L.; Walters, J. P. (1975b), Apparent and Partial Molal Heat Capacities of Aqueous Rare Earth Chloride Solutions at 25°C, *J. Chem. Eng. Data*, **20**, 438-443.

Spedding, F. H.; Baker, J. L.; Walters, J. P. (1979), Apparent and Partial Molal Heat Capacities of Aqueous Rare Earth Nitrate Solutions at 25°C, *J. Chem. Eng. Data*, **24**, 298-305.

Spedding, F. H.; Jones, K. C. (1966b), Heat Capacities of Aqueous Rare Earth Chloride Solutions at 25 °C, *J. Phys. Chem.*, **70**, 2450-2455.

Spedding, F. H.; Pikal, M. J. (1966c), Relative Viscosities of Some Aqueous Rare Earth Chloride Solutions at 25 °C, *J. Phys. Chem.*, **70**, 2430-2439.

Spedding, F. H.; Pikal, M. J.; Ayer, B. O. (1966d), Apparent Molal Volumes of Some Aqueous Rare Earth Chloride and Nitrate Solutions at 25°, *J. Phys. Chem.*, **70**, 2440-2449.

Spedding, F. H.; Shiers, L. E.; Brown, M. A.; Derer, J. L.; Swabson, D. L.; Habenschuss, A. (1975c), Densities and Apparent Molal Volumes of Some Aqueous Rare Earth Solutions at 25 °C. II. Rare Earth Perchlorates, *J. Chem. Eng. Data*, **20**, 81-88.

Spitzer, J. J.; Olofsson, I. V.; Singh, P. P.; Hepler, L. G. (1979), Apparent Molar Heat Capacities and Volumes of Aqueous Electrolytes at 25 °C: $Cr(NO_3)_3$, $LaCl_3$, $K_3Fe(CN)_6$, and $K_4Fe(CN)_6$, *Can. J. Chem.* **57**, 2798-2803.

Straty, G. C.; Palavra, A. M. F.; Bruno, T. J. (1986), PVT Properties of Methanol at Temperatures to 300 °C, *Int. J. Thermophys.*, **7**, 1077-1089.

Sun, T.; Lenard, J. -L.; Teja, A. S. (1994), A Simplified Mean Spherical Approximation for the Prediction of the Osmotic Coefficient of Aqueous Electrolyte Solutions, *J. Phys. Chem.*, **98**, 6870-6875.

Swaddle, T. W.; Mak, M. K. (1982), The Partial Molar Volumes of Aqueous Metal Cations: their Pridication and Relation to Volumes of Activation for Water Exchange, *Can. J. Chem.*, **61**, 473-480.

Tanger, J. C. IV; Helgeson, H. C. (1988), Calculation of the Thermodynamic and Transport Properties of Aqueous Species at High Pressures and Temperatures: Revised Equation of State for the Standard Partial Molar Properties of Ions and Elecrolytes, *Am. J. Sci.*, **288**, 19-98.

Tanger, J. C. IV; Pitzer, K. S. (1989), Calculation of the Thermodynamic Properties of Aqueous Electrolytes to 1000 °C and 500 bar from a Semicontinuum Model for Ion Hydration, *J. Phys. Chem.*, **93**, 4941-4951.

Tremaine, P. R.; Goldman, S. (1978), Calculation of Gibbs Free Energies of Aqueous Electrolytes to 350 °C from an Electrstatic Model for Ionic Hydration, *J. Phys. Chem.*, 82, 2317-2321.

Tremaine, P. R.; Shvedov, D.; Xiao, C., (1997), Thermodynamic Properties of Aqueous Morpholine and Morpholonium Chloride and Temperature Dependance of Ionization, *J. Phys. Chem.*, **101**, 409-419.

Tremaine, P. R.; Sway, K.; Barbero, J. A. (1986), The Apparent Molar Heat Capacity of Aqueous Hydrochloric Acid from 10 to 140 °C, *J. Solution Chem.*, **15**, 1-22.

Triolo, R; Blum, L.; Floriano, M. A. (1978), Simple Electrolytes in the Mean Spherical Approximation. 2. Study of a Refined Model, *J. Phys. Chem.*, **82**, 1368-1370.

van Konynenburg, P. H.; Scott, R. L. (1980), Critical Lines and Phase Equilibria in Binary Van der Walls Mixtures, *Phill. Trans.*, **298**, 495-540.

Watanasiri, S.; Brule, M. R.; Lee, L. L. (1982), Prediction of Thermodynamic Properties of Electrolytic Solutions using the Mean Spherical Approximation, *J. Phys. Chem.*, **86**, 292-294.

Wei, D.; Blum, L. (1995), Solution Thermodynamic Functions in the Mean Spherical Approximation: Behaviour near the Solvent Critical Region, *J. Chem. Phys.*, **102**, 4217-4226.

Wen, W. Y.; Saito, S. (1964), Apparent and Partial Molal Volumes of Five Symmetrical Tetraalkylammonium Bromides in Aqueous Solutions, *J. Phys. Chem.*, **68**, 2639-2644.

White, D. E.; Wood, R. H. (1982), Absolute Calibration of Flow Calorimeters Used for Measuring Differences in Heat Capacities. A Chemical Standard for Temperatures Between 325 and 600 K, *J. Solution Chem.*, **11**, 223-236.

Wood, R. H.; Buzzard, C. W.; Majer, V. (1989), A Phase-Locked Loop for Driving Vibrating Tube Densimeters, *Rev. Sci. Instrum.* **60**, 493-494.

Wood, R. H.; Carter, R. W.; Quint, J. R.; Majer, V.; Thompson, P. T.; Boccio, J. R. (1994), Aqueous Electrolytes at High Temperatures Comparison of Experiment with Simulation and Continuum Models, *J. Chem. Thermodyn.*, **26**, 225-249.

Wood, R. H.; Quint, J. R.; Groller, J. P. (1981), Thermodynamics of a Charged Hard Sphere in A Compressible Dielectric Fluid. A Modification of the Born Equation to Include the Compressibility of the Solvent, *J. Phys. Chem.*, **85**, 39-44.

Woolley, E. M.; Hepler, L. G. (1977), Heat Capacities of Weak Electrolyte and Ion

Association Reations: Method and Application to Aqueous $MgSO_4$ and HIO_3 at 298 K, *Can. J. Chem.*, **55**, 158-163.

Wormald, C. J. (1986), Heats and Volumes of Mixing in the Critical Region. An Exploration using the Van der Waals Equation, *Flow Phase Equilibria*, **28**, 137-153.

Wormald, C. J.; Badock, L.; Lloyd, M. J., (1996), Excess Enthalpies for (Water + Methanol) at T = 423 K to T = 523 K and Pressures up to 20 MPa. A New Flow Mixing Calorimeter, *J. Chem. Thermodyn.*, **28**, 603-613.

Xiao, C; Bianchi, H.; Tremaine, P. R. (1997), Excess Molar Volumes and Densities of (Methanol + Water) at Temperatures Between 323 K and 573 K and Pressures of 7.0 MPa and 13.5 MPa, *J. Chem. Thermodyn.*, (in press).

Xiao, C.; Tremaine, P. R.; Simonson, J. M. (1996), Apparent Molar Volumes of $La(CF_3SO_3)_3(aq)$ and $Gd(CF_3SO_3)_3(aq)$ at 278K, 298 K, and 318 K at Pressures to 30.0 MPa, *J. Chem. Eng. Data*, **41**, 1075-1078.

Yamaguchi, T.; Nomura, M.; Wakita, H.; Ohtaki, H. (1988), An Extended X-Ray Absorption Fine Structure Study of Aqueous Rare Earth Perchlorate Solutions in Liquid and Glassy States, *J. Chem. Phys.*, **89**, 5153-5159.

Yamaguchi, T.; Tanaka, S.; Watita, H.; Misawa, M.; Okada, I.; Soper, A. K.; Howells, W. S. (1990), Pulsed Neutron Diffraction Studies on Lanthanide (III) Hydration in Aqueous Perchlorate Solutions, *Z. Naturforsch.*, **46a**, 84-88.

Young, T. F.; Smith, M. B. (1954), Thermodynamic Properties of Mixtures of Electrolytes in Aqueous Solutions, *J. Phys. Chem.*, **58**, 716-724.

Appendix A. Tables of Experimental Data

Table A.II.1. The results from the flow-mimicking calibrations at T = 283.2, 288.2, and 298.2 K

F_a/(cm^3·min^{-1})	10^3·ΔW/watt	Fa·ΔW/W_a/(cm^3·min^{-1})	f
	T = 283.2 K		
0.029784	3.0279	0.029594	1.0064
0.029784	3.0312	0.029624	1.0054
0.029785	3.0364	0.029675	1.0037
0.029785	3.0468	0.029741	1.0015
0.034749	3.5506	0.034659	1.0026
0.039713	4.0567	0.039638	1.0019
0.039713	4.0600	0.039688	1.0006
0.039712	4.0361	0.039397	1.0080
0.039715	4.0558	0.039595	1.0030
0.039715	4.0588	0.039632	1.0021
0.049642	5.0838	0.049677	0.9993
0.049640	5.0540	0.049384	1.0052
0.049642	5.0880	0.049654	0.9998
0.049642	5.0643	0.049435	1.0042
0.049642	5.1021	0.049798	0.9969
0.059479	6.0710	0.059479	1.0040
0.059594	6.0705	0.059594	1.0044
0.059637	6.0707	0.059637	1.0055
	T = 288.2 K		
0.039820	3.9263	0.039551	1.0068
0.039820	3.9192	0.039439	1.0097

Table A.II.1. Continued

F_b/(cm^3·min^{-1})	10^3·ΔW/watt	Fa·ΔW/W_d/(cm^3·min^{-1})	f
0.039820	3.9550	0.039814	1.0002
0.039820	3.9272	0.039528	1.0074
		T = 298.2 K	
0.029866	3.6364	0.029635	1.0078
0.029866	3.6603	0.029841	1.0008
0.029864	3.6202	0.029695	1.0057
0.031856	3.8923	0.031884	0.9991
0.031856	3.8843	0.031824	1.0010
0.03982	4.0482	0.039589	1.0058
0.03982	4.0279	0.039391	1.0109
0.03982	4.0512	0.039612	1.0052
0.03982	4.0548	0.039878	0.9985
0.03982	4.0747	0.040066	0.9939
0.049775	5.0698	0.049858	0.9983
0.059728	6.0470	0.059490	1.0040

Table A.III.1. The experimental values of $\{(c_p\rho/c^*_{p,1}\rho^*_1) - 1\}$ and apparent molar heat capacities $C_{p,\phi,2}(HCF_3SO_3, aq)$, where ρ, ρ^*_1, c_p, and $c^*_{p,1}$ are the densities of solution, the densities of water, the specfic heat capacities of solutions, and the specific heat capacities of water, respectively

Molality	$c_p/(J\cdot g^{-1})$	$(c_p\rho/c^*_{p,1}\rho^*_1) - 1$	$C_{p,\phi,2}/(J\cdot K^{-1}\cdot mol^{-1})$
	T = 283.2 K		
0.12391	4.1341	-0.00512	141.2
0.24472	4.0797	-0.00960	147.0
0.27553	4.0664	-0.01066	148.3
0.34284	4.0373	-0.01307	149.6
0.77572	3.8628	-0.02813	152.4
1.06344	3.7563	-0.03777	151.4
1.28900	3.6776	-0.04522	150.6
1.55341	3.5912	-0.05367	150.0
2.02243	3.4491	-0.06832	148.5
2.99526	3.1848	-0.09938	141.0
3.57923	3.0508	-0.11627	138.5
4.33621	2.8951	-0.13752	135.0
4.88265	2.7940	-0.15229	132.6
6.58630	2.5269	-0.19526	126.1
8.11562	2.3384	-0.22906	122.3
	T = 298.2 K		
0.07341	4.1464	-0.00268	164.1
0.11387	4.1285	-0.00407	167.6
0.12391	4.1242	-0.00434	169.3
0.22634	4.0799	-0.00788	170.1

Table A.III.1. Continued

Molality	c_p/(J·g^{-1})	$(c_p\rho/c^*_{p,1}\rho^*_1) - 1$	$C_{p,\phi,2}$/(J·K^{-1}·mol^{-1})
0.24472	4.0722	-0.00846	171.2
0.27553	4.0594	-0.00948	171.9
0.34284	4.0315	-0.001174	171.7
0.43898	3.9922	-0.01499	171.4
0.65870	3.9067	-0.02216	171.3
0.77572	3.8635	-0.02588	171.7
0.88858	3.8219	-0.02956	170.6
1.06340	3.7602	-0.03516	169.4
1.09049	3.7509	-0.03599	169.5
1.28900	3.6837	-0.04232	167.7
1.30461	3.6792	-0.04271	168.3
1.5534	3.5997	-0.05055	166.4
2.02243	3.4606	-0.06495	163.4
2.99526	3.1996	-0.09597	152.9
3.57923	3.0647	-0.11357	148.4
4.33621	2.9087	-0.13543	143.3
4.88265	2.8071	-0.15061	140.1
6.58630	2.5378	-0.19484	131.5
8.11562	2.3477	-0.22932	126.6
	T = 313.2 K		
0.12391	4.1222	-0.00434	174.2
0.24472	4.0711	-0.00840	177.1
0.27553	4.0585	-0.00936	178.0

Table A.III.1. Continued

Molality	$c_p/(J \cdot g^{-1})$	$(c_p\rho/c^*_{p,1}\rho^*_1) - 1$	$C_{p,\phi,2}/(J \cdot K^{-1} \cdot mol^{-1})$
0.34284	4.0309	-0.01160	177.9
0.77572	3.8648	-0.02568	177.2
1.06340	3.7638	-0.03466	176.0
1.28900	3.6877	-0.04193	173.6
1.55341	3.6050	-0.04996	172.6
2.02243	3.4674	-0.06432	169.4
	T = 328.2 K		
0.07341	4.1479	-0.00272	173.1
0.11387	4.1287	-0.00442	161.2
0.22634	4.0825	-0.00813	177.8
0.24472	4.0746	-0.00841	177.2
0.34284	4.0350	-0.01188	180.1
0.43898	3.9966	-0.01498	180.0
0.65870	3.9142	-0.02179	182.5
0.88858	3.8311	-0.02916	181.3
1.06340	3.7712	-0.03472	180.7
1.09049	3.7623	-0.03548	180.8
1.28900	3.6962	-0.04195	178.7
1.30461	3.6912	-0.04229	178.6
1.55341	3.6138	-0.05005	177.3
2.02243	3.4774	-0.06448	174.0
2.99526	3.2222	-0.09423	163.5
3.57923	3.0918	-0.11100	159.7

Table A.III.1. Continued

Molality	$c_p/(J \cdot g^{-1})$	$(c_p\rho/c^*_{p,1}\rho^*_1) - 1$	$C_{p,\phi,2}/(J \cdot K^{-1} \cdot mol^{-1})$
4.33621	2.9370	-0.13294	153.9
4.88265	2.8389	-0.14770	151.2
6.58630	2.5741	-0.19037	142.4
8.11562	2.3891	-0.22306	137.8

Table A.III.2. The experimental values of $\{(c_p\rho/c^*_{p,1}\rho^*_1) - 1\}$ and apparent molar heat capacities $C_{p,\phi,2}(NaCF_3SO_3, aq)$, where ρ, ρ^*_1, c_p, and $c^*_{p,1}$ are the densities of solution, the densities of water, the specfic heat capacities of solutions, and the specific heat capacities of water, respectively

Molality	$c_p/(J\cdot g^{-1})$	$(c_p\rho/c^*_{p,1}\rho^*_1) - 1$	$C_{p,\phi,2}/(J\cdot K^{-1}\cdot mol^{-1})$
	T = 283.15 K		
0.0453	4.1684	-0.00154	151.9
0.0729	4.1542	-0.00231	169.2
0.1104	4.1331	-0.00365	159.0
0.1212	4.1271	-0.00397	157.8
0.1901	4.0927	-0.00568	171.3
0.3562	4.0104	-0.01027	174.6
0.4044	3.9902	-0.01118	182.5
0.5916	3.9072	-0.01528	187.5
0.7340	3.8499	-0.01784	193.6
0.7990	3.8277	-0.01865	200.2
0.8878	3.7922	-0.02024	199.9
1.0355	3.7448	-0.02087	210.6
1.1381	3.7066	-0.02340	209.5
1.2770	3.6625	-0.02486	214.0
1.3478	3.6412	-0.02550	216.3
1.6316	3.5571	-0.02821	221.6
	T = 298.2 K		
0.0729	4.1432	-0.00177	208.8
0.1136	4.1231	-0.00274	208.5
0.3062	4.0037	-0.00683	216.3

Table A.III.2. Continued

Molality	$c_p/(J \cdot g^{-1})$	$(c_p\rho/c^*_{p,1}\rho^*_1) - 1$	$C_{p,\phi,2}/(J \cdot K^{-1} \cdot mol^{-1})$
0.5015	3.9504	-0.01048	221.8
0.7160	3.8664	-0.01400	227.2
0.7990	3.8351	-0.01527	228.1
0.9491	3.7826	-0.01732	232.1
1.2211	3.6932	-0.02068	236.8
1.6825	3.5604	-0.02547	244.3
	T = 313.2 K		
0.0729	4.1414	-0.00167	220.8
0.1104	4.1238	-0.00239	224.8
0.1212	4.1183	-0.00267	221.6
0.1901	4.0866	-0.00403	226.1
0.3562	4.0124	-0.00728	227.3
0.4044	3.9937	-0.00808	233.0
0.5916	3.9170	-0.01129	234.0
0.7340	3.8623	-0.01361	235.3
0.7990	3.8401	-0.01467	238.7
0.8878	3.8064	-0.01589	237.1
1.0355	3.7580	-0.01808	241.6
1.1381	3.7227	-0.01935	241.1
1.2770	3.6792	-0.02113	243.0
1.3478	3.6577	-0.02201	243.8
	T = 328.2 K		
0.0729	4.1445	-0.00191	214.2

Table A.III.2. Continued

Molality	$c_p/(J \cdot g^{-1})$	$(c_p\rho/c^*_{p,1}\rho^*_1) - 1$	$C_{p,\phi,2}/(J \cdot K^{-1} \cdot mol^{-1})$
0.1104	4.1273	-0.00255	224.9
0.1212	4.1228	-0.00262	230.2
0.1901	4.0905	-0.00430	228.1
0.3562	4.0176	-0.00732	232.2
0.4044	3.9972	-0.00855	233.4
0.73399	3.8673	-0.01137	238.2
0.7990	3.8463	-0.01493	243.1
1.0355	3.7618	-0.01916	242.5
1.1381	3.7273	-0.02039	242.8
1.2770	3.6831	-0.02234	243.9
1.3480	3.6608	-0.02334	244.0
1.6316	3.5775	-0.02821	245.7

Table A.III.3. Relative densities and apparent molar volumes $V_{\phi,2}$ of HCF_3SO_3(aq) at p = 0.10 MPa

m	$\rho - \rho_1^*$	$V_{\phi,2}$	m	$\rho - \rho_1^*$	$V_{\phi,2}$
mol·kg^{-1}	kg·m^{-3}	cm^3·mol^{-1}	mol·kg^{-1}	kg·m^{-3}	cm^3·mol^{-1}
	T = 283.15 K			T = 298.15 K	
0.12390	9.29	74.40	0.07241	5.39	76.19
0.24472	18.16	74.50	0.11387	8.32	76.36
0.27553	20.41	74.50	0.22634	16.41	76.33
0.34284	25.23	74.61	0.43898	31.25	76.52
0.77572	55.19	74.80	0.65870	46.12	76.55
1.06344	74.34	74.62	0.88858	61.19	76.56
1.28900	88.80	74.57	1.09049	74.06	76.52
1.55341	105.22	74.65	1.30461	87.34	76.48
2.02243	132.87	74.49	1.55341	102.30	76.43
2.99526	185.97	74.20	2.02243	129.18	76.37
3.57923	214.81	74.14	2.99526	180.48	76.13
4.33621	249.34	74.11	3.57823	208.37	76.07
4.88265	272.39	74.11	4.33621	241.74	76.01
6.58630	335.57	74.23	4.88265	264.03	76.00
8.11562	382.59	74.46	6.58630	325.20	76.05
			8.11562	371.04	76.18
	T = 313.15 K			T = 328.15 K	
0.12391	8.90	77.64	0.07241	5.14	79.74
0.12391	8.88	77.73	0.11387	8.05	78.89
0.24472	17.33	77.97	0.22634	15.56	80.24

Table A.III.3. Continued

m	$\rho - \rho_1^*$	$V_{\phi,2}$	m	$\rho - \rho_1^*$	$V_{\phi,2}$
mol·kg^{-1}	kg·m^{-3}	cm^3·mol^{-1}	mol·kg^{-1}	kg·m^{-3}	cm^3·mol^{-1}
0.24472	17.36	77.82	0.43898	30.01	79.48
0.27553	19.48	77.92	0.65870	44.22	79.59
0.27553	19.48	77.93	0.88858	58.64	79.60
0.34284	24.12	77.91	1.06340	69.16	79.73
0.77572	52.68	78.03	1.09049	70.80	79.71
1.06340	70.83	78.03	1.28900	82.48	79.73
1.28900	84.60	77.95	1.30461	83.55	79.60
1.55341	100.08	77.96	1.55341	97.59	79.61
2.02243	126.24	77.94	2.02243	123.00	79.71
			2.98526	172.75	79.04
			3.57923	199.26	78.99
			4.33620	230.96	78.94
			4.88265	251.53	79.06
			6.58630	310.50	78.89
			8.11562	354.47	78.92

Table A.III.4. Relative densities and apparent molar volumes $V_{\phi,2}$ of $NaCF_3SO_3$(aq)

m	$\rho - \rho_1^*$	$V_{\phi,2}$	m	$\rho - \rho_1^*$	$V_{\phi,2}$
mol·kg^{-1}	kg·m^{-3}	cm^3·mol^{-1}	mol·kg^{-1}	kg·m^{-3}	cm^3·mol^{-1}
T = 283.15 K, p = 0.10 MPa			T = 298.15 K, p = 0.10 MPa		
0.12118	12.18	70.70	0.11362	10.98	74.50
0.35619	35.03	71.20	0.30624	29.08	74.85
0.59162	56.98	71.65	0.50148	46.86	75.05
0.73399	69.94	71.75	0.71603	65.73	75.26
0.88776	83.54	71.94	0.94912	85.59	75.38
1.13814	105.00	72.22	1.22112	107.97	75.45
1.27697	116.60	72.31	1.68251	143.58	75.81
1.34779	122.42	72.37			
T = 313.15 K, p = 0.10 MPa			T = 323.05 K, p =10.60 MPa		
0.07290	6.91	76.55	0.04530	4.22	77.44
0.11035	10.46	76.29	0.07290	6.74	78.33
0.19007	17.93	76.20	0.07290	6.75	78.25
0.40435	37.23	76.98	0.11035	10.38	76.69
0.79898	71.28	77.24	0.40435	36.66	78.32
1.03552	90.77	77.30	0.61459	54.98	78.14
1.63160	136.91	77.49	0.79898	70.29	78.43
			1.03552	89.21	78.77
			1.63160	134.72	78.81
T = 328.15 K, p = 0.10 MPa			T = 373.12 K, p = 0.50 MPa		
0.07290	6.74900	78.74	0.11362	10.13	81.63

Table A.III.3. Continued

m	$\rho - \rho_i^*$	$V_{\phi,2}$	m	$\rho - \rho_i^*$	$V_{\phi,2}$
mol·kg^{-1}	kg·m^{-3}	cm^3·mol^{-1}	mol·kg^{-1}	kg·m^{-3}	cm^3·mol^{-1}
0.11035	10.24	78.23	0.30624	26.66	82.44
0.19007	17.46	78.62	0.50148	42.80	82.92
0.40435	36.50	78.74	0.71603	60.08	82.98
0.79898	69.74	79.11	0.94912	77.93	83.36
1.03552	88.82	79.14	1.22112	98.30	83.34
1.63160	133.76	79.40	1.68251	130.75	83.53
T = 374.77 K, p = 10.01 MPa			T =422.65 K, p = 10.20 MPa		
0.11035	9.81	81.93	0.11362	9.63	86.22
0.19007	16.79	81.94	0.19007	16.10	85.39
0.40435	34.63	83.29	0.30624	25.62	85.91
0.61459	52.04	82.86	0.40435	33.74	85.27
0.79898	66.51	83.14	0.50148	41.54	85.39
1.0355	84.43	83.41	0.71603	57.88	86.17
1.6316	127.02	83.69	0.79898	64.35	85.85
			0.94912	75.31	86.26
			1.03552	81.51	86.36
			1.22112	95.00	86.24
			1.63160	123.16	86.28
			1.68251	126.20	86.55
T = 476.05 K, p = 2.13 MPa			T = 475.93 K, p = 10.18 MPa		
0.11362	9.89	81.52	0.11362	15.94	83.48

Table A.III.3. Continued

m	$\rho - \rho_1^*$	$V_{\phi,2}$	m	$\rho - \rho_1^*$	$V_{\phi,2}$
mol·kg^{-1}	kg·m^{-3}	cm^3·mol^{-1}	mol·kg^{-1}	kg·m^{-3}	cm^3·mol^{-1}
0.30624	25.57	84.72	0.30624	31.60	85.65
0.50148	40.77	86.11	0.50148	46.77	86.80
0.71603	56.82	87.07	0.71603	63.01	87.22
0.94912	73.74	87.55	0.94912	80.35	87.09
1.22112	92.89	87.77	1.22112	99.46	87.46
1.68251	123.45	88.22	1.68251	130.04	87.99
T = 524.85 K, p = 4.56 MPa			T = 523.55 K, p = 10.15 MPa		
0.07290	6.53	74.25	0.04530	3.97	77.99
0.11365	9.93	77.31	0.07290	6.54	74.78
0.30624	26.24	78.41	0.11035	9.74	76.65
0.50148	41.82	80.39	0.19007	16.45	78.63
0.71603	58.39	81.53	0.40435	34.52	78.67
0.94912	75.60	82.65	0.79898	64.33	82.89
1.22112	95.08	83.37	1.03552	81.27	84.15
1.68251	125.98	84.63	1.63160	122.62	84.86
T = 523.57 K, p = 20.40 MPa			T = 573.39 K, p = 10.13 MPa		
0.04530	4.76	52.78	0.11362	11.82	36.60
0.04530	4.12	73.80	0.30624	30.24	45.60
0.07290	6.44	77.60	0.50148	47.57	51.68
0.11035	10.04	73.28	0.71603	65.75	55.91
0.19007	16.90	75.80	0.94912	84.61	59.27

Table A.III.3. Continued

m	$\rho - \rho_1^*$	$V_{\phi,2}$	m	$\rho - \rho_1^*$	$V_{\phi,2}$
mol·kg^{-1}	kg·m^{-3}	cm^3·mol^{-1}	mol·kg^{-1}	kg·m^{-3}	cm^3·mol^{-1}
0.40435	34.25	80.29	1.22112	105.48	62.48
0.61459	50.00	83.61	1.68251	138.90	66.30
0.79898	64.11	83.78			
1.03552	81.38	84.42			
1.63160	121.52	86.17			
T = 573.32 K, p = 19.87 MPa			T = 600.48 K, p = 20.20 MPa		
0.11362	11.16	51.40	0.11362	10.01	3.30
0.30624	28.70	58.25	0.30624	33.59	20.23
0.50148	45.28	62.97	0.50148	51.03	29.21
0.71603	63.03	65.45			
0.94912	81.24	68.05			
1.22112	101.50	70.43			
1.68251	134.03	73.21			

Table A.IV.1. Experimental apparent molar volumes and heat capacities for $LaCl_3$(aq)

m	$\rho - \rho_1^*$	$V_{\phi,2}$	$c_p\rho/(c_{p,1}^*\rho_1^*) - 1$	$C_{p,\phi,2}$
mol·kg^{-1}	g·cm^{-3}	cm^3·mol^{-1}		J·K^{-1}·mol^{-1}
		T = 283.2 K		
0.64862	0.14178	23.32	-0.06817	-349.7
0.54545	0.11999	22.52	-0.05924	-366.7
0.39974	0.088740	21.32	-0.04559	-393.0
0.18744	0.042325	18.62	-0.02314	-441.6
0.11654	0.026441	17.85	-0.01480	-458.7
0.10851	0.024614	17.93	-0.01387	-461.9
0.097344	0.022131	17.48	-0.01255	-468.4
0.050047	0.011431	16.60	-0.006624	-485.9
		T = 298.2 K		
0.64862	0.13996	25.37	-0.06097	-293.6
0.54545	0.11845	24.62	-0.05282	-307.5
0.39974	0.087627	23.42	-0.04043	-329.1
0.18744	0.041698	21.32	-0.02037	-367.2
0.11654	0.026088	20.27	-0.01305	-384.7
0.11654	0.026088	20.27	-0.01304	-384.4
0.10851	0.024308	20.15	-0.01228	-390.2
0.10851	0.024318	20.06	-0.01220	-387.4
0.097344	0.021848	19.78	-0.01100	-390.6
0.097344	0.021858	19.68	-0.01103	-392.6
0.050047	0.011289	18.88	-0.00581	-407.0
		T = 313.2 K		
0.64862	0.13867	26.35	-0.05494	-250.6
0.54545	0.11765	25.11	-0.04757	-265.2
0.39974	0.087056	23.88	-0.03642	-285.2
0.18744	0.041457	21.63	-0.01836	-321.2
0.11654	0.025965	20.35	-0.01171	-336.3
0.10851	0.024171	20.43	-0.01095	-337.8

Table A.IV.1. Continued

m	$\rho - \rho_1^*$	$V_{\phi,2}$	$c_p\rho/(c_{p,1}^*\rho_1^*) - 1$	$C_{p,\phi,2}$
$mol \cdot kg^{-1}$	$g \cdot cm^{-3}$	$cm^3 \cdot mol^{-1}$		$J \cdot K^{-1} \cdot mol^{-1}$
0.097344	0.021720	20.11	-0.009876	-341.3
0.050047	0.011249	18.66	-0.005156	-353.4
		T = 323.2 K		
0.64862	0.13865	25.26	-0.04995	-223.1
0.54545	0.11739	24.42	-0.04340	-236.4
0.39974	0.086801	23.28	-0.03334	-255.9
0.18744	0.041347	20.91	-0.01686	-291.3
0.11654	0.025902	19.55	-0.01078	-306.9
0.10851	0.024135	19.43	-0.01002	-307.0
0.097344	0.021683	19.15	-0.009095	-312.4
0.050047	0.011195	18.38	-0.004857	-330.4
		T = 333.2 K		
0.64862	0.13846	24.64	-0.02012	-30.78
0.54545	0.11713	23.92	-0.01764	-38.89
0.39974	0.086699	22.56	-0.01362	-51.28
0.18744	0.041307	20.08	-0.006943	-73.20
0.11654	0.025886	18.62	-0.004473	-84.58
0.10851	0.024137	18.33	-0.004204	-87.23
0.097344	0.021672	18.18	-0.003811	-89.56
0.050047	0.011224	16.69	-0.002013	-99.98
0.050047	0.011226	16.66	-0.002009	-99.77

Table A.IV.2. Experimental apparent molar volumes and heat capacities for $La(ClO_4)_3$(aq)

m	$\rho - \rho_1^*$	$V_{\phi,2}$	$c_p\rho/(c_{p,1}^*\rho_1^*) - 1$	$C_{p,\phi,2}$
mol·kg^{-1}	g·cm^{-3}	cm^3·mol^{-1}		J·K^{-1}·mol^{-1}
		T = 283.2 K		
0.67688	0.21671	96.18	-0.07009	-59.30
0.49446	0.16224	93.83	-0.05513	-95.89
0.38600	0.12841	92.62	-0.04541	-122.6
0.29593	0.099609	91.47	-0.03637	-145.9
0.16287	0.055771	89.74	-0.02157	-187.3
0.11530	0.039756	88.84	-0.01584	-209.6
0.079062	0.027349	88.83	-0.01104	-217.2
0.072800	0.025183	89.02	-0.01029	-223.2
0.061030	0.021219	87.63	-0.008688	-232.8
0.040850	0.014241	87.31	-0.005912	-243.1
		T = 298.2 K		
0.67688	0.21177	102.1	-0.06423	1.674
0.49446	0.15811	100.9	-0.04967	-20.24
0.38600	0.12505	100.1	-0.04033	-36.28
0.29593	0.097012	99.14	-0.03206	-52.86
0.16287	0.054337	97.63	-0.01869	-80.41
0.11530	0.038673	97.37	-0.01362	-93.47
0.079062	0.026647	96.92	-0.009516	-103.0
0.072800	0.024485	97.82	-0.008813	-101.9
0.061030	0.020572	97.46	-0.007390	-103.0
0.040850	0.013810	97.14	-0.004996	-108.4
		T = 313.2 K		
0.67688	0.20800	106.3	-0.06193	30.99
0.49446	0.15531	105.2	-0.04776	11.62
0.38600	0.12283	104.5	-0.03864	-1.780
0.29593	0.095206	103.9	-0.03054	-13.60

Table A.VI.2. Continued

m	$\rho - \rho_1^*$	$V_{\phi,2}$	$c_p\rho/(c_{p,1}^*\rho_1^*) - 1$	$C_{p,\phi,2}$
mol·kg^{-1}	g·cm^{-3}	cm^3·mol^{-1}		J·K^{-1}·mol^{-1}
0.16287	0.053279	102.9	-0.01779	-37.38
0.11530	0.037922	102.7	-0.01277	-42.55
0.079062	0.026105	102.6	-0.008850	-46.18
0.072800	0.023949	104.0	-0.008184	-41.98
0.061030	0.020238	101.8	-0.006888	-52.54
0.040850	0.013562	102.1	-0.004676	-57.15
		T = 328.2 K		
0.67688	0.20429	110.1	-0.06111	48.64
0.67688	0.20430	110.1	-0.06112	48.52
0.49446	0.15240	109.4	-0.04701	32.34
0.38600	0.12048	109.0	-0.03800	20.57
0.29593	0.093321	108.7	-0.02987	12.74
0.16287	0.052355	107.1	-0.01731	-10.74
0.11530	0.037284	106.7	-0.01240	-15.10
0.079062	0.025691	106.4	-0.008656	-23.18
0.072800	0.023650	106.7	-0.008038	-25.57
0.061030	0.019911	105.7	-0.006715	-27.43
0.040850	0.013360	105.6	-0.004495	-27.06
		T = 338.2 K		
0.67688	0.20261	111.6	-0.06176	47.69
0.49446	0.15125	110.7	-0.04753	30.43
0.38600	0.11957	110.3	-0.03838	19.08
0.29593	0.092727	109.7	-0.03032	7.561
0.16287	0.051923	108.6	-0.01745	-10.43
0.11530	0.037014	108.0	-0.01266	-22.18
0.079062	0.025524	107.4	-0.008881	-33.47
0.072800	0.023440	108.5	-0.008182	-28.91
0.061030	0.019727	107.6	-0.006984	-40.61
0.040850	0.013209	108.2	-0.004541	-23.39

Table A.IV.3. Experimental apparent molar heat capacities $C_{p,\phi}^{expt}$ for $\{La(ClO_4)_3+HClO_4\}(aq)$ mixtures, $C_{p,\phi,3}$ for $HClO_4(aq)$, and $C_{p,\phi,2}$ for $La(ClO_4)_3(aq)$

$m\{La(ClO_4)_3\}$	$m(HClO_4)$	$c_p\rho/(c_{p,1}^*\rho_1^*)-1$	$C_{p,\phi}^{expt}$	$F_3C_{p,\phi,3}$	$C_{p,\phi,2}$
$mol\cdot kg^{-1}$	$mol\cdot kg^{-1}$		$J\cdot K^{-1}\cdot mol^{-1}$	$J\cdot K^{-1}\cdot mol^{-1}$	$J\cdot K^{-1}\cdot mol^{-1}$
		T = 298.2 K			
0.66427	0.005055	-0.06353	-0.7478	0.3051	-1.061
0.48635	0.004451	-0.04948	-25.04	0.2863	-25.56
0.37997	0.004237	-0.04020	-41.20	0.2760	-41.94
0.29120	0.004328	-0.03224	-59.62	0.2728	-60.78
0.16024	0.004384	-0.01883	-84.52	0.1834	-87.02
0.11333	0.004646	-0.01365	-93.32	0.06337	-97.21
0.07746	0.005497	-0.009619	-98.80	-0.2065	-105.6
0.071600	0.004456	-0.008887	-101.1	-0.2346	-107.2
0.060085	0.004183	-0.007535	-104.8	-0.3776	-111.7
0.040221	0.004225	-0.005162	-107.1	-0.8844	-117.4
		T = 313.2 K			
0.66427	0.005055	-0.06144	25.20	0.3634	25.02
0.48635	0.004451	-0.04742	8.016	0.3430	7.743
0.37997	0.004237	-0.03828	-2.399	0.3484	-2.778
0.29120	0.004328	-0.03029	-13.77	0.3840	-14.37
0.16024	0.004384	-0.01781	-40.06	0.4646	-41.63
0.11333	0.004646	-0.01281	-43.70	0.5395	-46.06
0.07746	0.005497	-0.009086	-51.68	0.6840	-56.08
0.07160	0.004456	-0.008304	-48.82	0.5671	-52.46
0.060085	0.004183	-0.007042	-52.92	0.5438	-57.19
0.040221	0.004225	-0.004816	-56.67	0.5411	-63.22

Table A.IV.4. Experimental apparent molar volumes for V_ϕ^{expt} for $\{La(ClO_4)_3 + HClO_4\}(aq)$ mixtures, $V_{\phi,3}$ for $HClO_4(aq)$, and $V_{\phi,2}$ for $La(ClO_4)_3(aq)$

$m\{La(ClO_4)_3\}$	$m(HClO_4)$	$\rho - \rho_1^*$	V_ϕ^{expt}	$F_3V_{\phi,3}$	$V_{\phi,2}$
$mol \cdot kg^{-1}$	$mol \cdot kg^{-1}$	$g \cdot cm^{-3}$	$cm^3 \cdot mol^{-1}$	$cm^3 \cdot mol^{-1}$	$cm^3 \cdot mol^{-1}$
		T = 298.2 K			
0.66427	0.005055	0.2085	101.5	0.3304	101.9
0.48635	0.004451	0.1560	100.1	0.4002	100.6
0.37997	0.004237	0.1236	99.05	0.4891	99.66
0.29120	0.004328	0.0957	98.28	0.6518	99.08
0.16024	0.004384	0.05370	96.24	1.190	97.65
0.11333	0.004646	0.03831	94.95	1.760	97.01
0.07746	0.005497	0.02641	93.49	2.961	96.95
0.07160	0.004456	0.02440	93.76	2.618	96.81
0.06008	0.004183	0.02054	93.14	2.907	96.51
0.04022	0.004225	0.01387	91.26	4.240	96.17
		T = 313.2 K			
0.66427	0.005055	0.2052	105.0	0.3450	105.5
0.48635	0.004451	0.1533	104.2	0.4188	104.8
0.37997	0.004237	0.1212	103.8	0.5124	104.4
0.29120	0.004328	0.09393	103.1	0.6836	104.0
0.16024	0.004384	0.05268	101.2	1.2493	102.7
0.11333	0.004646	0.03756	100.2	1.8489	102.4
0.07746	0.005497	0.02587	98.82	3.111	102.5
0.07160	0.004456	0.02391	99.08	2.751	102.3
0.06008	0.004183	0.02014	98.35	3.055	101.9
0.04022	0.004225	0.01361	95.99	4.456	101.1

Table A.IV.5. Experimental apparent molar volumes and heat capacities for $Gd(ClO_4)_3$(aq)

m	$\rho - \rho_1^*$	$V_{\phi,2}$	$c_p\rho/(c_{p,1}^*\rho_1^*) - 1$	$C_{p,\phi,2}$
mol·kg^{-1}	g·cm^{-3}	cm^3·mol^{-1}		J·K^{-1}·mol^{-1}
		T = 283.2 K		
0.92680	0.31919	96.74	-0.06380	12.04
0.74914	0.26606	95.12	-0.05228	-11.94
0.41074	0.15783	92.15	-0.02673	-73.28
0.17033	0.07543	89.48	-0.003538	-139.28
0.11463	0.05558	89.23	0.002776	-157.19
0.10903	0.05363	88.67	0.003376	-163.60
0.08107	0.04356	88.47	0.006902	-166.70
0.08107	0.04355	88.64	0.006883	-167.02
0.06836	0.03895	88.54	0.008184	-187.91
0.06836	0.03905	87.17	0.008375	-182.04
0.04474	0.03042	87.52	0.011335	-194.13
0.04474	0.03046	86.66	0.011426	-189.25
0.04474	0.03043	87.30	0.011322	-196.19
		T = 298.2 K		
0.92680	0.29952	101.39	-0.074735	53.92
0.74914	0.24694	100.48	-0.063528	37.67
0.41074	0.14067	98.53	-0.038972	-1.98
0.17033	0.06002	96.69	-0.017873	-42.84
0.11463	0.04063	96.46	-0.012322	-52.26
0.10903	0.03874	95.81	-0.011736	-55.34
0.08107	0.02894	95.14	-0.008879	-64.78
0.06836	0.02446	94.66	-0.007505	-67.35
0.04474	0.01606	94.32	-0.004979	-74.04
		T = 313.2 K		
0.9268	0.29447	105.2	-0.07372	71.68
0.74914	0.24265	104.6	-0.06222	59.58

Table A.IV.5. continued

m	$\rho - \rho_1^*$	$V_{\phi,2}$	$c_p\rho/(c_{p,1}^*\rho_1^*) - 1$	$C_{p,\phi,2}$
mol·kg^{-1}	g·cm^{-3}	cm^3·mol^{-1}		J·K^{-1}·mol^{-1}
0.41074	0.13813	103.2	-0.03772	27.97
0.17033	0.058946	101.6	-0.01716	-6.999
0.11463	0.039950	101.1	-0.01177	-14.66
0.10903	0.038004	101.2	-0.01131	-18.54
0.08107	0.028365	100.9	-0.00853	-24.84
0.06836	0.023998	100.2	-0.00736	-37.65
0.04474	0.015748	100.0	-0.00492	-46.66
0.04474	0.015742	100.2	-0.00522	-74.21
		T = 328.2 K		
0.92680	0.29047	107.8	-0.07447	75.41
0.92680	0.29052	107.8	-0.07435	75.84
0.74914	0.23920	107.5	-0.06281	64.64
0.41074	0.13638	105.8	-0.03794	33.41
0.41074	0.13623	106.2	-0.03788	35.38
0.17033	0.05807	105.1	-0.01722	3.13
0.11463	0.03943	104.0	-0.01169	-2.72
0.11463	0.03940	104.2	-0.01162	0.74
0.10903	0.03748	104.4	-0.01113	-1.27
0.10903	0.03746	104.6	-0.01129	-6.71
0.08107	0.02797	104.1	-0.00832	-3.24
0.08107	0.02797	104.1	-0.00860	-18.05
0.08107	0.02796	104.3	-0.00854	-14.02
0.06836	0.02363	104.0	-0.00717	-12.69
0.06836	0.02360	104.3	-0.00726	-16.98
0.04474	0.01552	103.6	-0.00488	-31.73
0.04474	0.01567	100.2	-0.00485	-42.57
		T = 338.2 K		
0.92680	0.28742	109.88	-0.07561	75.43
0.74914	0.23668	109.59	-0.06389	64.09
0.41074	0.13469	108.66	-0.03864	34.94
0.17033	0.05749	107.32	-0.01744	4.34

Table A.IV.5. continued

m	$\rho - \rho_1^*$	$V_{\phi,2}$	$c_p\rho/(c_{p,1}^*\rho_1^*) - 1$	$C_{p,\phi,2}$
$mol \cdot kg^{-1}$	$g \cdot cm^{-3}$	$cm^3 \cdot mol^{-1}$		$J \cdot K^{-1} \cdot mol^{-1}$
0.11463	0.03893	107.19	-0.01204	-4.82
0.10903	0.03711	106.63	-0.01154	-10.28
0.08107	0.02761	107.35	-0.00866	-10.32
0.06836	0.02341	105.92	-0.00728	-14.38
0.06836	0.02338	106.34	-0.00731	-14.25
0.04474	0.01537	105.72	-0.00491	-27.31
0.04474	0.01534	106.45	-0.00490	-24.07

Table A.IV.6. Experimental apparent molar heat capacities $C_{p,\phi}^{expt}$ for $\{Gd(ClO_4)_3+HClO_4\}(aq)$ mixtures, $C_{p,\phi,3}$ for $HClO_4(aq)$, and $C_{p,\phi,2}$ for $Gd(ClO_4)_3(aq)$

$m\{Gd(ClO_4)_3\}$	$m(HClO_4)$	$c_p\rho/(c_{p,1}^{\bullet}\rho_1^{\bullet})-1$	$C_{p,\phi}^{expt}$	$F_3C_{p,\phi,3}$	$C_{p,\phi,2}$
$mol\cdot kg^{-1}$	$mol\cdot kg^{-1}$		$J\cdot K^{-1}\cdot mol^{-1}$	$J\cdot K^{-1}\cdot mol^{-1}$	$J\cdot K^{-1}\cdot mol^{-1}$
		T = 298.2 K			
0.71458	0.09779	-0.06422	33.87	5.19	32.61
0.54768	0.07495	-0.05187	17.63	4.27	15.18
0.38913	0.05325	-0.03832	5.50	3.15	2.67
0.38913	0.05325	-0.03937	-4.91	3.15	-9.16
0.25277	0.03459	-0.02714	-26.33	1.92	-32.11
0.17911	0.02451	-0.01999	-38.47	1.10	-44.98
0.11735	0.01606	-0.01358	-58.00	0.28	-66.26
0.083483	0.01143	-0.00977	-61.64	-0.26	-69.79
0.072617	0.009938	-0.00855	-63.05	-0.45	-71.17
0.043875	0.006004	-0.00527	-73.84	-1.03	-82.78
		T = 313.2 K			
0.71458	0.09779	-0.06306	53.18	6.25	53.34
0.54768	0.07495	-0.05072	39.72	5.06	39.40
0.38913	0.05325	-0.03797	24.15	3.93	22.99
0.25277	0.03459	-0.02595	7.81	2.90	5.57
0.17911	0.02451	-0.01905	-5.06	2.29	-8.36
0.11735	0.01606	-0.01282	-18.81	1.71	-23.32
0.083483	0.01143	-0.009326	-24.77	1.33	-29.67
0.072617	0.009938	-0.008165	-26.82	1.19	-31.84
0.043875	0.006004	-0.004906	-25.98	0.76	-30.40

Table A.IV.7. Experimental apparent molar volumes for V_ϕ^{expt} for {$Gd(ClO_4)_3$ + $HClO_4$}(aq) mixtures, $V_{\phi,3}$ for $HClO_4$(aq), and $V_{\phi,2}$ for $Gd(ClO_4)_3$(aq)

$m\{Gd(ClO_4)_3\}$	$m(HClO_4)$	$\rho - \rho_1^*$	V_ϕ^{expt}	$F_3V_{\phi,3}$	$V_{\phi,2}$
$mol \cdot kg^{-1}$	$mol \cdot kg^{-1}$	$g \cdot cm^{-3}$	$cm^3 \cdot mol^{-1}$	$cm^3 \cdot mol^{-1}$	$cm^3 \cdot mol^{-1}$
		T = 298.2 K			
0.71458	0.09779	0.24074	93.42	5.25	100.2
0.54768	0.07495	0.18818	92.58	5.29	99.23
0.38913	0.05325	0.13625	91.71	5.33	98.20
0.38913	0.05325	0.13626	91.70	5.33	98.18
0.25277	0.03459	0.08999	90.86	5.36	97.20
0.17911	0.02451	0.06420	91.06	5.37	97.42
0.11735	0.01606	0.04255	89.40	5.38	95.52
0.08348	0.01143	0.03037	89.29	5.38	95.40
0.07262	0.009938	0.02644	89.55	5.38	95.69
0.04388	0.006004	0.01606	88.76	5.37	94.80
		T = 313.2 K			
0.71458	0.09779	0.23651	97.19	5.48	104.3
0.54768	0.07495	0.18482	96.58	5.54	103.5
0.38913	0.05325	0.13378	95.98	5.59	102.8
0.25277	0.03459	0.08833	95.37	5.63	102.0
0.17911	0.02451	0.06318	94.89	5.64	101.5
0.11735	0.01606	0.04185	93.52	5.65	99.90
0.08348	0.01143	0.02984	93.93	5.65	100.4
0.07262	0.009938	0.02598	93.98	5.65	100.4
0.04388	0.006004	0.01578	93.32	5.64	99.67

Table A.V.1. Experimental apparent molar heat capacities $C_{p,\phi}^{exptl}$ for $\{Ln(ClO_4)_3+HClO_4\}(aq)$ mixtures, $C_{p,\phi,3}$ for $HClO_4(aq)$, and $C_{p,\phi,2}$ for $Ln(ClO_4)_3(aq)$

$m\{Ln(ClO_4)_3\}$	$m(HClO_4)$	$c_p\rho/(c_{p,1}^{*}\rho_1^{*})-1$	$C_{p,\phi}^{exptl}$	$F_3C_{p,\phi,3}$	$C_{p,\phi,2}$
$mol\cdot kg^{-1}$	$mol\cdot kg^{-1}$		$J\cdot K^{-1}\cdot mol^{-1}$	$J\cdot K^{-1}\cdot mol^{-1}$	$J\cdot K^{-1}\cdot mol^{-1}$
		T=283.2 K			
		$Nd(ClO_4)_3$			
0.69407	0.07900	-0.07006	-42.14	1.11	-48.17
0.53803	0.06124	-0.05793	-69.32	1.27	-78.62
0.38655	0.04400	-0.04484	-102.27	0.74	-114.74
0.22959	0.02613	-0.02874	-138.34	-0.68	-153.33
0.15794	0.01798	-0.02095	-169.18	-1.72	-186.53
0.12169	0.01385	-0.01658	-181.51	-2.37	-199.54
0.12169	0.01385	-0.01657	-183.14	-2.37	-201.34
0.09664	0.01100	-0.01342	-193.16	-2.88	-211.94
0.06612	0.00753	-0.009389	-205.70	-3.60	-225.10
0.03676	0.00418	-0.005382	-218.22	-4.44	-238.11
		$Eu(ClO_4)_3$			
0.62836	0.00721	-0.06030	-30.82	0.14	-31.32
0.43252	0.00702	-0.04546	-68.53	0.15	-69.79
0.33444	0.00672	-0.03698	-91.07	0.06	-92.97
0.30532	0.00633	-0.03430	-97.66	0.02	-99.70
0.16465	0.00593	-0.02025	-135.96	-0.56	-140.28
0.12086	0.00591	-0.01540	-150.39	-1.10	-156.58
0.10656	0.00596	-0.01377	-158.23	-1.40	-165.61
0.08744	0.00597	-0.01148	-163.05	-1.94	-172.10
0.05867	0.00615	-0.008012	-173.36	-3.53	-187.64
0.04025	0.00678	-0.005774	-183.94	-6.09	-207.79
		$Er(ClO_4)_3$			
0.74382	0.06583	-0.06550	4.48	0.75	4.06
0.55722	0.04932	-0.05330	-25.83	1.02	-29.23

Table A.V.1. Continued

$m\{Ln(ClO_4)_3\}$	$m(HClO_4)$	$c_p\rho/(c^*_{p,1}\rho^*_1)-1$	$C_{p,\phi}^{expti}$	$F_3C_{p,\phi,3}$	$C_{p,\phi,2}$
$mol\cdot kg^{-1}$	$mol\cdot kg^{-1}$		$J\cdot K^{-1}\cdot mol^{-1}$	$J\cdot K^{-1}\cdot mol^{-1}$	$J\cdot K^{-1}\cdot mol^{-1}$
0.38967	0.03449	-0.04059	-61.12	0.60	-67.18
0.26451	0.02341	-0.02962	-91.96	-0.22	-99.86
0.17964	0.01590	-0.02129	-121.65	-1.10	-131.22
0.11464	0.01015	-0.01421	-143.94	-2.00	-154.50
0.09292	0.00822	-0.01172	-154.67	-2.37	-165.78
0.07052	0.00624	-0.09062	-162.35	-2.78	-173.67
0.04703	0.00416	-0.06201	-179.41	-3.29	-191.71
		$Yb(ClO_4)_3$			
0.67571	0.06324	-0.06008	1.11	0.98	0.15
049402	0.04623	-0.04793	-32.34	0.99	-36.45
0.35794	0.03350	-0.03741	-62.22	0.46	-68.55
0.22842	0.02138	-0.02585	-98.55	-0.58	-107.13
0.16498	0.01544	-0.01951	-120.09	-1.35	-129.85
0.10357	0.00969	-0.01282	-140.45	-2.30	-151.08
0.07613	0.00712	-0.009639	-156.83	-2.81	-168.43
0.06679	0.00625	-0.008546	-159.09	-3.01	-170.68
0.04124	0.00386	-0.005412	-177.49	-3.60	-190.16
		T=298.2 K			
		$Nd(ClO_4)_3$			
0.69407	0.07900	-0.06436	13.79	4.31	10.56
0.53803	0.06124	-0.05264	-5.59	3.57	-10.19
0.38655	0.04400	-0.04009	-26.69	2.65	-32.67
0.22959	0.02613	-0.02554	-53.69	1.41	-61.38
0.22959	0.02613	-0.02547	-57.04	1.41	-65.10
0.15794	0.01798	-0.01837	-73.30	0.70	-82.42
0.12169	0.01385	-0.01443	-81.61	0.28	-91.21
0.09664	0.01100	-0.01164	-89.31	-0.04	-99.44
0.06612	0.00753	-0.008124	-99.03	-0.49	-109.76
0.03676	0.00418	-0.004613	-109.93	-1.02	-121.31
0.03676	0.00418	-0.004598	-109.19	-1.02	-120.48

Table V.1. Continued

$m\{Ln(ClO_4)_3\}$	$m(HClO_4)$	$c_p\rho/(c^*_{p,1}\rho^*_1)-1$	$C_{p,\phi}^{exptl}$	$F_3C_{p,\phi,3}$	$C_{p,\phi,2}$
$mol\cdot kg^{-1}$	$mol\cdot kg^{-1}$		$J\cdot K^{-1}\cdot mol^{-1}$	$J\cdot K^{-1}\cdot mol^{-1}$	$J\cdot K^{-1}\cdot mol^{-1}$
		$Eu(ClO_4)_3$			
0.04025	0.00678	-0.004911	-76.08	-1.33	-87.34
0.05867	0.00615	-0.006883	-71.29	-0.57	-78.14
0.08744	0.00597	-0.009945	-65.96	-0.11	-70.34
0.10656	0.00596	-0.01185	-58.36	0.04	-61.67
0.12086	0.00591	-0.001334	-57.19	0.12	-60.11
0.16465	0.00593	-0.01777	-50.55	0.26	-52.64
0.30532	0.00633	-0.03043	-20.47	0.40	-21.30
0.33444	0.00672	-0.03253	-10.75	0.43	-11.40
0.33444	0.00672	-0.03267	-12.54	0.43	-13.24
0.43252	0.00702	-0.04084	-0.65	0.45	-1.12
0.62836	0.00721	-0.05527	23.90	0.44	23.73
		$Er(ClO_4)_3$			
0.74382	0.06583	-0.06105	55.73	3.58	56.77
0.74382	0.06583	-0.06107	55.67	3.58	56.70
0.55722	0.04932	-0.04882	35.39	2.91	35.36
0.38967	0.03449	-0.03616	15.84	2.11	14.94
0.38967	0.03449	-0.03633	14.11	2.11	13.06
0.26451	0.02341	-0.02605	-5.92	1.36	-7.92
0.17964	0.01590	-0.01846	-22.31	0.74	-25.08
0.11464	0.01015	-0.01232	-40.08	0.15	-43.79
0.09292	0.00822	-0.01008	-45.66	-0.07	-49.62
0.07052	0.00624	-0.007716	-48.81	-0.34	-52.76
0.07052	0.00624	-0.007814	-54.14	-0.34	-58.57
0.04703	0.00416	-0.005305	-64.33	-0.65	-69.32

Table V.1. Continued

$m\{Ln(ClO_4)_3\}$	$m(HClO_4)$	$c_p\rho/(c^*_{p,1}\rho^*_1)-1$	$C_{p,\phi}^{expt}$	$F_3C_{p,\phi,3}$	$C_{p,\phi,2}$
$mol\cdot kg^{-1}$	$mol\cdot kg^{-1}$		$J\cdot K^{-1}\cdot mol^{-1}$	$J\cdot K^{-1}\cdot mol^{-1}$	$J\cdot K^{-1}\cdot mol^{-1}$
		$Yb(ClO_4)_3$			
0.67571	0.06324	-0.05534	52.09	3.53	53.10
0.49402	0.04623	-0.04309	32.16	2.77	32.13
0.49402	0.04623	-0.04335	30.27	2.77	30.07
0.35794	0.03350	-0.03334	9.74	2.04	8.42
0.35794	0.03350	-0.03328	10.34	2.04	9.08
0.22842	0.02138	-0.02256	-11.54	1.17	-13.90
0.16498	0.01544	-0.01678	-23.32	0.65	-26.21
0.10357	0.00969	-0.01101	-41.31	0.04	-45.22
0.10357	0.00969	-0.1102	-42.34	0.04	-46.35
0.07613	0.00712	-0.008265	-50.66	-0.30	-55.10
0.06679	0.00625	-0.007290	-53.20	-0.40	-57.74
0.04124	0.00386	-0.004570	-60.47	-0.78	-65.29
0.04124	0.00386	-0.004635	-67.82	-0.78	-73.31
		T=313.2 K			
		$Nd(ClO_4)_3$			
0.69407	0.07900	-0.06236	39.42	5.17	38.15
0.53803	0.06124	-0.05071	24.55	4.23	22.64
0.38655	0.04400	-0.03838	7.53	3.31	4.70
0.22959	0.02613	-0.02421	-13.40	2.30	-17.49
0.15794	0.01798	-0.01729	-28.53	1.78	-33.76
0.12169	0.01385	-0.01355	-35.23	1.48	-40.90
0.09664	0.01100	-0.01066	-32.32	1.26	-37.39
0.06612	0.00753	-0.007570	-47.57	0.93	-54.02
0.03676	0.00418	-0.004237	-52.82	0.53	-59.42
		$Eu(ClO_4)_3$			
0.62836	0.00721	-0.05409	47.15	0.52	47.16
0.43252	0.00702	-0.03977	27.06	0.55	26.94
0.30532	0.00633	-0.02931	13.00	0.55	12.71

Table A.V.1. Contiuned

$m\{Ln(ClO_4)_3\}$	$m(HClO_4)$	$c_p\rho/(c^*_{p,1}\rho^*_1)-1$	$C_{p,\phi}^{expti}$	$F_3C_{p,\phi,3}$	$C_{p,\phi,2}$
$mol\cdot kg^{-1}$	$mol\cdot kg^{-1}$		$J\cdot K^{-1}\cdot mol^{-1}$	$J\cdot K^{-1}\cdot mol^{-1}$	$J\cdot K^{-1}\cdot mol^{-1}$
0.33444	0.00672	-0.03179	16.38	0.57	16.12
0.16465	0.00593	-0.01694	-10.68	0.62	-11.71
0.10656	0.00596	-0.01123	-16.58	0.70	-18.24
0.12086	0.00591	-0.01258	-14.09	0.67	-15.48
0.08744	0.00597	-0.009338	-19.87	0.72	-22.00
0.05867	0.00615	-0.006483	-28.40	0.78	-32.24
0.04025	0.00678	-0.004551	-25.86	0.83	-31.18
0.04025	0.00678	-0.004590	-29.84	0.83	-35.83
		$Er(ClO_4)_3$			
0.74382	0.06583	-0.06006	74.40	4.34	76.26
0.55722	0.04932	-0.04763	58.42	3.44	59.84
0.38967	0.03449	-0.03527	40.97	2.64	41.72
0.26451	0.02341	-0.02512	25.30	2.01	25.35
0.17964	0.01590	-0.01773	11.10	1.54	10.40
0.09292	0.00822	-0.009680	-9.00	0.97	-10.85
0.17964	0.01590	-0.01781	9.43	1.54	8.58
0.11464	0.01015	-0.01134	-2.99	1.13	-4.48
0.07052	0.00624	-0.007384	-12.72	0.78	-14.70
0.04703	0.00416	-0.005065	-25.55	0.54	-28.41
		$Yb(ClO_4)_3$			
0.67571	0.06324	-0.05495	68.13	4.22	69.89
0.49402	0.04623	-0.04258	51.30	3.31	52.48
0.35794	0.03350	-0.03256	34.32	2.62	34.67
0.22842	0.02138	-0.02190	17.06	1.92	16.56
0.16498	0.01544	-0.01624	6.96	1.53	5.93
0.10357	0.00969	-0.01053	-5.74	1.11	-7.48
0.07613	0.00712	-0.007950	-15.96	0.87	-18.42
0.06679	0.00625	-000.6951	-13.36	0.78	-15.47
0.04124	0.00386	-0.004385	-25.46	0.50	-28.39
0.04124	0.00386	-0.004368	-22.86	0.50	-25.55

Table V.1. Continued

$m\{Ln(ClO_4)_3\}$	$m(HClO_4)$	$c_p\rho/(c^*_{p,1}\rho^*_1)-1$	$C_{p,\phi}^{expt}$	$F_3C_{p,\phi,3}$	$C_{p,\phi,2}$
$mol\cdot kg^{-1}$	$mol\cdot kg^{-1}$		$J\cdot K^{-1}\cdot mol^{-1}$	$J\cdot K^{-1}\cdot mol^{-1}$	$J\cdot K^{-1}\cdot mol^{-1}$
		T = 328.2 K			
		$Nd(ClO_4)_3$			
0.69407	0.07900	-0.06231	48.79	4.64	49.08
0.53803	0.06124	-0.05066	34.63	4.14	33.96
0.38655	0.04400	-0.03810	20.83	3.58	19.22
0.22959	0.02613	-0.02400	2.39	2.83	-0.49
0.15794	0.01798	-0.01700	-10.70	2.38	-14.57
0.12169	0.01385	-0.01336	-17.67	2.10	-22.02
0.09664	0.01100	-0.01080	-25.62	1.87	-30.62
0.06612	0.00753	-0.007470	-31.49	1.54	-36.74
0.03676	0.00418	-0.004258	-44.46	1.10	-50.75
		$Eu(ClO_4)_3$			
0.62836	0.00721	-0.05376	59.10	0.49	59.28
0.43252	0.00702	-0.03925	42.31	0.58	42.40
0.33444	0.00672	-0.03172	27.67	0.64	27.57
0.30532	0.00633	-0.02954	20.60	0.63	20.38
0.16465	0.00593	-0.01718	-5.317	0.82	-6.36
0.16465	0.00593	-0.01682	3.308	0.82	2.58
0.12086	0.00591	-0.01242	2.626	0.95	1.76
0.05867	0.00615	-0.006605	-26.44	1.34	-30.70
0.10656	0.00596	-0.01132	-9.240	1.02	-10.83
0.08744	0.00597	-0.009634	-22.16	1.11	-24.86
0.04025	0.00678	-0.004872	-45.34	1.65	-54.90
		$Er(ClO_4)_3$			
0.74382	0.06583	-0.06087	77.65	3.80	80.38
0.55722	0.04932	-0.04815	63.30	3.34	65.26
0.38967	0.03449	-0.03556	47.42	2.85	48.51
0.26451	0.02341	-0.02535	35.10	2.40	35.60
0.17964	0.01590	-0.01780	19.80	2.00	19.37
0.11464	0.01015	-0.01174	7.87	1.62	6.81

Table V.1. Continued

$m\{Ln(ClO_4)_3\}$	$m(HClO_4)$	$c_p\rho/(c^*_{p,1}\rho^*_1)-1$	$C_{p,\phi}^{expt}$	$F_3C_{p,\phi,3}$	$C_{p,\phi,2}$
$mol\cdot kg^{-1}$	$mol\cdot kg^{-1}$		$J\cdot K^{-1}\cdot mol^{-1}$	$J\cdot K^{-1}\cdot mol^{-1}$	$J\cdot K^{-1}\cdot mol^{-1}$
0.09292	0.00822	-0.009649	2.07	1.46	0.66
0.07052	0.00624	-0.007537	-8.072	1.26	-10.16
0.04703	0.00416	-0.005208	-23.26	1.01	-26.42
		$Yb(ClO_4)_3$			
0.67571	0.06324	-0.05529	74.02	3.84	76.76
0.49402	0.04623	-0.04257	59.97	3.34	61.93
0.35794	0.03350	-0.03220	47.57	2.89	48.87
0.22842	0.02138	-0.02191	26.62	2.36	26.54
0.16498	0.01544	-0.01621	17.47	2.03	16.89
0.10357	0.00969	-0.01032	12.78	1.62	12.20
0.07613	0.00712	-0.007809	1.23	1.39	-0.17
0.06679	0.00625	-0.006869	1.44	1.29	0.17
0.04124	0.00386	-0.004337	-10.60	0.99	-12.67

[a] $F_3 = m(HClO_4)/[m\{Ln(ClO_4)_3\} + m(HClO_4)]$

Table A.V.2. Experimental apparent molar volumes for V_ϕ^{expt} for $\{Ln(ClO_4)_3 + HClO_4\}(aq)$ mixtures, $V_{\phi,3}$ for $HClO_4(aq)$, and $V_{\phi,2}$ for $Ln(ClO_4)_3(aq)$

$m\{Ln(ClO_4)_3\}$	$m(HClO_4)$	$\rho - \rho_1^*$	V_ϕ^{expt}	$F_3V_{\phi,3}$	$V_{\phi,2}$
$mol \cdot kg^{-1}$	$mol \cdot kg^{-1}$	$g \cdot cm^{-3}$	$cm^3 \cdot mol^{-1}$	$cm^3 \cdot mol^{-1}$	$cm^3 \cdot mol^{-1}$
		T=283.2 K			
		$Nd(ClO_4)_3$			
0.69407	0.07900	23.250	86.66	4.38	91.65
0.53803	0.06124	18.387	85.09	4.37	89.90
0.38655	0.04400	13.466	83.54	4.37	88.18
0.22959	0.02613	8.160	81.78	4.36	86.23
0.15794	0.01798	5.674	80.47	4.35	84.78
0.12169	0.01385	4.387	80.40	4.34	84.71
0.12169	0.01385	4.393	79.94	4.34	84.20
0.09664	0.01100	3.499	79.71	4.33	83.96
0.06612	0.00753	2.404	79.20	4.32	83.40
0.03676	0.00418	1.338	79.86	4.31	84.15
		$Eu(ClO_4)_3$			
0.62836	0.00721	21.188	93.17	0.48	93.75
0.43252	0.00702	14.933	91.27	0.68	92.06
0.33444	0.00672	11.694	90.05	0.84	91.00
0.30532	0.00633	10.710	89.87	0.87	90.85
0.16465	0.00593	5.881	88.12	1.48	89.76
0.12086	0.00591	4.350	87.00	1.98	89.17
0.10656	0.00596	3.854	85.88	2.25	88.31
0.08744	0.00597	3.177	85.08	2.71	87.99
0.05867	0.00615	2.154	82.95	4.02	87.22
0.04025	0.00678	1.501	79.41	6.08	85.68
		$Er(ClO_4)_3$			
0.74382	0.06583	26.316	87.74	3.48	91.71
0.55722	0.04932	20.144	86.34	3.48	90.19
0.38967	0.03449	14.383	84.58	3.48	88.28
0.26451	0.02341	9.908	83.46	3.47	87.07

Table A.V.2. Continued

$m\{Ln(ClO_4)_3\}$	$m(HClO_4)$	$\rho - \rho_1^*$	V_ϕ^{expl}	$F_3V_{\phi,3}$	$V_{\phi,2}$
$mol \cdot kg^{-1}$	$mol \cdot kg^{-1}$	$g \cdot cm^{-3}$	$cm^3 \cdot mol^{-1}$	$cm^3 \cdot mol^{-1}$	$cm^3 \cdot mol^{-1}$
0.17964	0.01590	6.817	81.63	3.46	85.09
0.11464	0.01015	4.387	80.72	3.45	84.10
0.09292	0.00822	3.570	80.00	3.45	83.33
0.07052	0.00624	2.714	80.09	3.44	83.44
0.04703	0.00416	1.820	78.87	3.44	82.11
			$Yb(ClO_4)_3$		
0.67571	0.06324	24.496	86.81	3.67	90.93
0.49402	0.04623	18.308	85.12	3.66	89.08
0.35794	0.03350	13.479	83.91	3.66	87.76
0.22842	0.02138	8.749	82.12	3.65	85.82
0.16498	0.01544	6.375	81.09	3.64	84.69
0.10357	0.00969	4.027	80.79	3.63	84.38
0.07613	0.00712	2.981	79.18	3.62	82.62
0.06679	0.00625	2.613	79.79	3.62	83.29
0.04124	0.00386	1.624	78.14	3.61	81.50
			T=298.2 K		
			$Nd(ClO_4)_3$		
0.69407	0.07900	22.668	92.78	4.46	98.37
0.53803	0.06124	17.920	91.57	4.50	96.99
0.38655	0.04400	13.110	90.62	4.53	95.89
0.22959	0.02613	7.934	89.60	4.56	94.72
0.22959	0.02613	7.964	88.47	4.56	93.46
0.15794	0.01798	5.511	88.78	4.56	93.80
0.12169	0.01385	4.265	88.50	4.57	93.48
0.09664	0.01100	3.400	88.08	4.57	93.02
0.06612	0.00753	2.337	87.59	4.56	92.47
0.03676	0.00418	1.306	87.00	4.56	91.82
0.03676	0.00418	1.306	86.82	4.56	91.63

Table A.V.2. Continued

$m\{Ln(ClO_4)_3\}$	$m(HClO_4)$	$\rho - \rho_1^*$	V_ϕ^{expt}	$F_3V_{\phi,3}$	$V_{\phi,2}$
$mol \cdot kg^{-1}$	$mol \cdot kg^{-1}$	$g \cdot cm^{-3}$	$cm^3 \cdot mol^{-1}$	$cm^3 \cdot mol^{-1}$	$cm^3 \cdot mol^{-1}$
		$Eu(ClO_4)_3$			
0.62836	0.00721	20.773	98.39	0.50	99.01
0.43252	0.00702	14.630	97.00	0.71	97.85
0.33444	0.00672	11.447	96.18	0.88	97.22
0.33444	0.00672	11.447	96.17	0.88	97.21
0.30532	0.00633	10.486	95.95	0.90	97.02
0.16465	0.00593	5.765	94.03	1.55	95.81
0.12086	0.00591	4.262	93.08	2.08	95.45
0.10656	0.00596	3.768	92.71	2.37	95.40
0.08744	0.00597	3.106	91.86	2.85	95.08
0.05867	0.00615	2.104	90.02	4.24	94.77
0.04025	0.00678	1.463	86.91	6.43	94.02
		$Er(ClO_4)_3$			
0.67571	0.06324	23.943	92.74	3.74	97.33
0.49402	0.04623	17.876	91.66	3.77	96.11
0.49402	0.04623	17.873	91.72	3.77	96.18
0.35794	0.03350	13.160	90.79	3.80	95.13
0.35794	0.03350	13.160	90.78	3.80	95.12
0.22842	0.02138	8.528	89.82	3.82	94.05
0.16498	0.01544	6.210	89.17	3.82	93.34
0.10357	0.00969	3.928	88.57	3.82	92.68
0.10357	0.00969	3.930	88.43	3.82	92.52
0.07613	0.00712	2.899	88.15	3.82	92.21
0.06679	0.00625	2.546	87.98	3.82	92.04
0.04124	0.00386	1.578	87.53	3.82	91.54
0.04124	0.00386	1.580	87.21	3.82	91.19
		$Yb(ClO_4)_3$			
0.67571	0.06324	23.943	92.74	3.74	97.33
0.49402	0.04623	17.876	91.66	3.77	96.11
0.49402	0.04623	17.873	91.72	3.77	96.18
0.35794	0.03350	13.160	90.79	3.80	95.13

Table A.V.2. Continued

$m\{Ln(ClO_4)_3\}$	$m(HClO_4)$	$\rho - \rho_1^*$	V_ϕ^{expd}	$F_3V_{\phi,3}$	$V_{\phi,2}$
$mol \cdot kg^{-1}$	$mol \cdot kg^{-1}$	$g \cdot cm^{-3}$	$cm^3 \cdot mol^{-1}$	$cm^3 \cdot mol^{-1}$	$cm^3 \cdot mol^{-1}$
0.35794	0.03350	13.160	90.78	3.80	95.12
0.22842	0.02138	8.528	89.82	3.82	94.05
0.16498	0.01544	6.210	89.17	3.82	93.34
0.10357	0.00969	3.928	88.57	3.82	92.68
0.10357	0.00969	3.930	88.43	3.82	92.52
0.07613	0.00712	2.899	88.15	3.82	92.21
0.06679	0.00625	2.546	87.98	3.82	92.04
0.04124	0.00386	1.578	87.53	3.82	91.54
0.04124	0.00386	1.580	87.21	3.82	91.19
		T=313.2 K			
		$Nd(ClO_4)_3$			
0.69407	0.07900	22.243	96.86	4.66	102.70
0.53803	0.06124	17.566	96.08	4.70	101.77
0.38655	0.04400	12.851	95.30	4.74	100.87
0.22959	0.02613	7.778	94.46	4.78	99.88
0.15794	0.01798	5.402	93.80	4.79	99.14
0.12169	0.01385	4.182	93.50	4.80	98.80
0.09664	0.01100	3.334	93.06	4.80	98.28
0.06612	0.00753	2.290	92.82	4.80	98.05
0.03676	0.00418	1.281	91.94	4.80	97.07
		$Eu(ClO_4)_3$			
0.62836	0.00721	20.401	102.70	0.52	103.35
0.43252	0.00702	14.354	101.79	0.74	102.68
0.33444	0.00672	11.231	101.08	0.92	102.18
0.30532	0.00633	10.289	100.89	0.95	102.01
0.16465	0.00593	5.655	99.20	1.63	101.08
0.12086	0.00591	4.186	97.89	2.19	100.38
0.10656	0.00596	3.698	97.69	2.49	100.53
0.08744	0.00597	3.048	96.87	3.00	100.27
0.05867	0.00615	2.067	94.56	4.45	99.56

Table A.V.2. Continued

$m\{Ln(ClO_4)_3\}$	$m(HClO_4)$	$\rho - \rho_1^*$	V_ϕ^{expd}	$F_3V_{\phi,3}$	$V_{\phi,2}$
$mol \cdot kg^{-1}$	$mol \cdot kg^{-1}$	$g \cdot cm^{-3}$	$cm^3 \cdot mol^{-1}$	$cm^3 \cdot mol^{-1}$	$cm^3 \cdot mol^{-1}$
0.04025	0.00678	1.435	91.70	6.75	99.24
0.04025	0.00678	1.436	91.60	6.75	99.12
		$Er(ClO_4)_3$			
0.74382	0.06583	0.25163	98.64	3.69	103.35
0.55722	0.04932	0.19254	97.90	3.74	102.50
0.38967	0.03449	0.13730	97.11	3.77	101.60
0.26451	0.02341	0.09459	96.44	3.80	100.84
0.17964	0.01590	0.06493	95.76	3.81	100.08
0.17964	0.01590	0.06492	95.80	3.81	100.13
0.11464	0.01015	0.04179	95.17	3.82	99.44
0.09292	0.00822	0.03394	95.21	3.82	99.48
0.07052	0.00624	0.02587	94.58	3.82	98.80
0.04703	0.00416	0.01732	94.04	3.81	98.21
		$Yb(ClO_4)_3$			
0.67571	0.06324	23.531	96.70	3.90	101.48
0.49402	0.04623	17.564	95.90	3.95	100.55
0.35794	0.03350	12.928	95.20	3.98	99.76
0.22842	0.02138	8.376	94.53	4.00	99.00
0.16498	0.01544	6.100	93.93	4.01	98.33
0.10357	0.00969	3.860	93.32	4.02	97.66
0.07613	0.00712	2.846	93.13	4.02	97.46
0.06679	0.00625	2.498	93.34	4.02	97.68
0.04124	0.00386	1.551	92.25	4.01	96.50
0.04124	0.00386	1.550	92.50	4.01	96.77
		T = 328.2 K			
		$Nd(ClO_4)_3$			
0.69407	0.07900	21.899	99.81	4.76	105.87
0.53803	0.06124	17.290	99.18	4.81	105.11
0.38655	0.04400	12.646	98.58	4.86	104.39
0.22959	0.02613	7.650	98.02	4.90	103.72

Table A.V.2. Continued

$m\{Ln(ClO_4)_3\}$	$m(HClO_4)$	$\rho - \rho_1^*$	V_ϕ^{expt}	$F_3V_{\phi,3}$	$V_{\phi,2}$
$mol \cdot kg^{-1}$	$mol \cdot kg^{-1}$	$g \cdot cm^{-3}$	$cm^3 \cdot mol^{-1}$	$cm^3 \cdot mol^{-1}$	$cm^3 \cdot mol^{-1}$
0.15794	0.01798	5.319	97.08	4.92	102.66
0.12169	0.01385	4.115	97.01	4.92	102.57
0.09664	0.01100	3.281	96.60	4.92	102.11
0.06612	0.00753	2.257	95.98	4.92	101.43
0.03676	0.00418	1.262	95.11	4.91	100.47
		$Eu(ClO_4)_3$			
0.62836	0.00721	20.094	105.84	0.53	106.52
0.43252	0.00702	14.142	104.97	0.76	105.91
0.33444	0.00672	11.064	104.35	0.94	105.49
0.30532	0.00633	10.133	104.26	0.97	105.43
0.16465	0.00593	5.570	102.65	1.67	104.62
0.16465	0.00593	5.571	102.58	1.67	104.55
0.12086	0.00591	4.123	101.30	2.24	103.90
0.10656	0.00596	3.644	100.97	2.55	103.93
0.08744	0.00597	3.003	100.22	3.08	103.77
0.05867	0.00615	2.038	97.60	4.57	102.79
0.04025	0.00678	1.415	94.56	6.92	102.39
		$Er(ClO_4)_3$			
0.74382	0.06583	24.816	101.28	3.77	106.14
0.55722	0.04932	18.981	100.75	3.82	105.50
0.38967	0.03449	13.533	100.11	3.87	104.76
0.26451	0.02341	9.298	100.39	3.89	105.04
0.17964	0.01590	6.400	98.93	3.91	103.43
0.11464	0.01015	4.117	98.53	3.91	102.99
0.09292	0.00822	3.348	98.23	3.91	102.66
0.07052	0.00624	2.545	98.40	3.91	102.85
0.04703	0.00416	1.703	98.09	3.91	102.50
		$Yb(ClO_4)_3$			
0.67571	0.06324	23.209	99.36	4.00	104.30
0.49402	0.04623	17.321	9870	4.04	103.52
0.35794	0.03350	1.748	98.15	4.08	102.88

Table A.V.2. Continued

$m\{Ln(ClO_4)_3\}$	$m(HClO_4)$	$\rho - \rho_1^*$	V_ϕ^{expt}	$F_3V_{\phi,3}$	$V_{\phi,2}$
$mol \cdot kg^{-1}$	$mol \cdot kg^{-1}$	$g \cdot cm^{-3}$	$cm^3 \cdot mol^{-1}$	$cm^3 \cdot mol^{-1}$	$cm^3 \cdot mol^{-1}$
0.22842	0.02138	8.258	97.58	4.10	102.22
0.16498	0.01544	6.015	96.96	4.12	101.53
0.10357	0.00969	3.804	96.57	4.12	101.11
0.07613	0.00712	2.807	96.22	4.12	100.72
0.06679	0.00625	2.464	96.43	4.12	100.95
0.04124	0.00386	1.530	95.41	4.11	99.85

[a] $F_3 = m(HClO_4)/[m\{Ln(ClO_4)_3\} + m(HClO_4)]$

Table A.V.3. Experimental apparent molar volumes and apparent molar heat capacities for $Eu(ClO_4)_3(aq)$ at T = 298.2 K

m	$\rho - \rho_1^*$	$V_{\phi,2}$	$c_p\rho/c_{p,1}^*\rho_1^* - 1$	$C_{p,\phi,2}$
$mol \cdot kg^{-1}$	$g \cdot cm^{-3}$	$cm^3 \cdot mol^{-1}$		$J \cdot K^{-1} \cdot mol^{-1}$
0.64552	0.21260	99.19	-0.05621	26.21
0.44400	0.14959	98.03	-0.04153	0.59
0.34294	0.11688	97.38	-0.03340	-14.85
0.31260	0.10692	97.18	-0.03086	-20.10
0.16833	0.058573	95.98	-0.01778	-48.52
0.12356	0.043251	95.40	-0.01322	-54.95
0.10895	0.038191	95.38	-0.01173	-57.12
0.08942	0.031429	95.09	-0.009822	-66.73
0.06003	0.021191	94.53	-0.006719	-76.55
0.06003	0.021201	94.37	-0.006738	-78.54
0.04129	0.014622	94.05	-0.004704	-86.16
0.04129	0.014634	93.75	-0.004640	-80.88

Table A.VI.1. Densities and apparent molar volumes of $La(CF_3SO_3)_3$(aq) and $Gd(CF_3SO_3)_3$(aq)

	p = 0.1 MPa		p = 7.0 MPa		p = 30.0 MPa	
m	ρ	$V_{\phi,2}$	ρ	$V_{\phi,2}$	ρ	$V_{\phi,2}$
$mol \cdot kg^{-1}$	$g \cdot cm^{-3}$	$cm^{-3} \cdot mol^{-1}$	$g \cdot cm^{-3}$	$cm^{-3} \cdot mol^{-1}$	$g \cdot cm^{-3}$	$cm^{-3} \cdot mol^{-1}$
			$La(CF_3SO_3)_3$, T=278.33 K			
0.05843	1.02300	187.59	1.02633	188.57	1.03708	192.11
0.08348	1.03269	187.85	1.03599	189.27	1.04672	192.47
0.12346	1.04796	188.29	1.05123	189.62	1.06195	192.43
0.19639	1.07518	188.88	1.07837	190.29	1.08904	192.92
0.29826	1.11172	190.15	1.11488	191.31	1.12547	193.75
0.46998	1.17014	191.41	1.17320	192.50	1.18369	194.64
0.69312	1.24036	192.88	1.24328	193.88	1.25366	195.72
			$Gd(CF_3SO_3)_3$, T = 278.33 K			
0.06002	1.02477	186.44	1.02809	187.82	1.03890	190.75
0.09289	1.03804	187.41	1.04140	188.05	1.05220	190.77
0.09289	1.03806	187.25				
0.11878	1.04844	187.26	1.05174	188.39	1.06252	191.12
0.25296	1.10044	188.31	1.10366	189.46	1.11440	191.82
0.38042	1.14724	189.40	1.15048	190.25	1.16120	192.34
0.53303	1.20025	190.53	1.20362	191.01	1.21430	192.90

Table A.VI.1. Continued

	p = 0.1 MPa		p = 7.0 MPa		p = 30.0 MPa	
m	ρ	$V_{\phi,2}$	ρ	$V_{\phi,2}$	ρ	$V_{\phi,2}$
$mol \cdot kg^{-1}$	$g \cdot cm^{-3}$	$cm^{-3} \cdot mol^{-1}$	$g \cdot cm^{-3}$	$cm^{-3} \cdot mol^{-1}$	$g \cdot cm^{-3}$	$cm^{-3} \cdot mol^{-1}$
0.72300	1.26261	191.00	1.26562	191.87	1.27627	193.52
			$La(CF_3SO_3)_3$, T=298.04 K			
0.05843	1.01959	195.33	1.02267	196.46	1.03268	197.84
0.08348	1.02909	195.42	1.03218	196.32	1.04221	197.57
0.12346	1.04398	196.21	1.04706	197.02	1.05708	198.43
0.19639	1.07057	196.74	1.07357	197.79	1.08361	199.13
0.29826	1.10627	197.81	1.10936	198.35	1.11942	199.59
0.46998	1.16326	198.91	1.16632	199.44	1.17644	200.46
0.69312	1.23173	200.12	1.23481	200.53	1.24497	201.38
			$Gd(CF_3SO_3)_3$, T = 298.04 K			
0.06002	1.02149	192.20	1.02451	194.06	1.03454	195.42
0.06002	1.02141	193.29				
0.09289	1.03443	194.39	1.03755	194.64	1.04761	195.94
0.09289	1.03442	194.24				
0.11878	1.04462	194.06	1.04769	195.07	1.05778	196.12
0.25296	1.09539	195.91	1.09856	196.18	1.10872	197.24
0.25296	1.09538	195.88				
0.38042	1.14117	196.76	1.14440	196.90	1.15466	197.79

Table A.VI.1 Continued

	p = 0.1 MPa		p = 7.0 MPa		p = 30.0 MPa	
m	ρ	$V_{\phi,2}$	ρ	$V_{\phi,2}$	ρ	$V_{\phi,2}$
$mol \cdot kg^{-1}$	$g \cdot cm^{-3}$	$cm^{-3} \cdot mol^{-1}$	$g \cdot cm^{-3}$	$cm^{-3} \cdot mol^{-1}$	$g \cdot cm^{-3}$	$cm^{-3} \cdot mol^{-1}$
0.38042	1.14137	196.21				
0.53303	1.19316	197.37	1.19637	197.60	1.20670	198.39
0.53303	1.19332	197.04				
0.72300	1.25376	198.09	1.25707	198.20	1.26750	198.86
			$La(CF_3SO_3)_3$, T = 318.06 K			
0.05843	1.01242	199.97	1.01546	200.01	1.02515	201.36
0.08348	1.02170	200.35	1.02479	200.54	1.03450	201.76
0.12346	1.03636	201.22	1.03949	200.95	1.04922	202.05
0.19639	1.06260	201.41	1.06559	201.92	1.07538	202.81
0.19639	1.06255	201.56				
0.29826	1.09759	202.83	1.10070	202.92	1.11058	203.62
0.29826	1.09764	202.61				
0.46998	1.15351	203.96	1.15665	204.05	1.16665	204.59
0.69312	1.22071	205.05	1.22385	205.18	1.23401	205.54
			$Gd(CF_3SO_3)_3$, T = 318.06 K			
0.06002	1.01432	196.42	1.01735	196.53	1.02707	197.66
0.09289	1.02706	198.79	1.03010	198.87	1.03986	199.78
0.11878	1.03707	198.96	1.04010	199.22	1.04990	199.96
0.25296	1.08711	200.27	1.09019	200.46	1.10015	200.98
0.38042	1.13225	200.90	1.13537	201.04	1.14548	201.43

Table A.VI.1 Continued

	p = 0.1 MPa		p = 7.0 MPa		p = 30.0 MPa	
m	ρ	$V_{\phi,2}$	ρ	$V_{\phi,2}$	ρ	$V_{\phi,2}$
mol·kg^{-1}	g·cm^{-3}	cm^{3}·mol^{-1}	g·cm^{-3}	cm^{3}·mol^{-1}	g·cm^{-3}	cm^{3}·mol^{-1}
0.53303	1.18334	201.64	1.18648	201.80	1.19674	202.08
0.72300	1.24282	202.48	1.24601	202.60	1.25644	202.77

Table A.VI.2. Densities ρ and apparent molar volumes $V_{\phi,2}$ of $Gd(CF_3SO_3)_3$(aq)

m	ρ	$V_{\phi,2}$	m	ρ	$V_{\phi,2}$
mol·kg^{-1}	kg·m^{-3}	cm^3·mol^{-1}	mol·kg^{-1}	kg·m^{-3}	cm^3·mol^{-1}
T = 373.33 K, p = 7.07 MPa			T = 372.97 K, P = 26.11 MPa		
0.058053	984.21	200.3	0.058053	993.05	201.7
0.058053	984.19	200.7	0.058053	993.16	199.7
0.107642	1002.9	203.6	0.107547	1012.0	202.6
0.107642	1003.1	202.0	0.107547	1011.8	204.0
0.219979	1044.2	204.1	0.107547	1011.9	203.2
0.219979	1044.1	204.8	0.107547	1011.8	203.8
0.337324	1085.1	205.7	0.219820	1053.3	204.4
0.460021	1125.7	207.1	0.219820	1053.2	204.6
0.588443	1166.7	207.2	0.219820	1053.1	205.3
0.723002	1206.4	209.0	0.337138	1094.4	205.5
0.723002	1207.3	207.7	0.337138	1094.4	205.7
			0.459848	1134.8	207.6
			0.459848	1135.2	206.8
			0.723002	1216.4	208.5
			0.723002	1216.7	208.0
			0.723002	1216.8	207.9
T = 423.12 K, p = 7.08 MPa			T= 423.17 K, p = 25.61 MPa		
0.058053	942.97	200.8	0.058053	952.97	200.3
0.058053	943.00	200.2	0.058053	952.99	199.9
0.107642	961.36	202.9	0.107547	971.28	204.0

Table A.VI.2. Continued.

m	ρ	$V_{\phi,2}$	m	ρ	$V_{\phi,2}$
$mol \cdot kg^{-1}$	$kg \cdot m^{-3}$	$cm^3 \cdot mol^{-1}$	$mol \cdot kg^{-1}$	$kg \cdot m^{-3}$	$cm^3 \cdot mol^{-1}$
0.219979	1001.5	205.8	0.219820	1011.8	205.2
0.337324	1041.5	207.2	0.219820	1011.6	205.9
0.460021	1081.2	208.7	0.337138	1051.8	207.5
0.723002	1160.6	210.4	0.459848	1082.0	208.2
			0.723002	1171.7	210.1
T = 472.40 K, p = 7.17 MPa			T = 472.40 K, p = 25.50 MPa		
0.028893	881.08	177.7	0.058053	904.76	188.5
0.058053	891.95	186.5	0.058053	904.76	188.5
0.058053	891.90	187.5	0.107642	922.75	196.2
0.107642	910.07	191.9	0.107642	922.73	196.5
0.107642	910.16	190.8	0.219979	962.71	198.8
0.219979	949.89	195.8	0.219979	962.60	199.4
0.219979	949.86	196.0	0.337324	1002.5	200.8
0.337324	989.20	199.7	0.337324	1002.7	200.1
0.460021	1028.8	201.3	0.460021	1041.8	203.7
0.723002	1107.0	205.3	0.723002	1120.3	206.9

Table A.VII.1. Densities ρ and excess molar volumes V_m^E of $\{xCH_3OH+(1-x)H_2O\}$

T/K	p/MPa	x	ρ/(kg·m^{-3})	V_m^E/(cm^3·mol^{-1})	
				expt.	calc.
323.21	0.10	0.89350	781.85	-0.410	-0.382
323.17	0.10	0.70229	815.65	-0.769	-0.828
323.16	0.10	0.60172	838.97	-1.008	-0.967
323.15	0.10	0.49641	861.88	-1.056	-1.022
323.14	0.10	0.40888	881.79	-1.021	-0.992
323.17	0.10	0.29674	908.41	-0.876	-0.852
323.13	0.10	0.20398	931.55	-0.673	-0.655
323.15	0.10	0.09879	958.75	-0.346	-0.351
323.20	6.99	0.89350	787.99	-0.348	-0.350
323.17	6.98	0.79623	805.61	-0.609	-0.600
323.17	6.98	0.70229	823.33	-0.788	-0.786
323.13	6.99	0.60172	843.57	-0.914	-0.915
323.19	7.01	0.49641	865.67	-0.955	-0.964
323.20	6.99	0.40888	885.11	-0.926	-0.935
323.17	6.98	0.29674	911.36	-0.797	-0.804
323.14	7.02	0.20398	934.33	-0.613	-0.618
323.08	7.04	0.09879	961.51	-0.314	-0.332
323.16	13.44	0.89350	794.70	-0.364	-0.332
323.17	13.42	0.70229	828.86	-0.761	-0.761
323.18	13.50	0.60172	848.47	-0.870	-0.881
323.16	13.49	0.49641	870.19	-0.909	-0.923

Table A.VII.1. Continued

T/K	p/MPa	x	ρ/(kg·m^{-3})	V_m^E/(cm^3·mol^{-1})	
				expt.	calc.
323.16	13.47	0.40888	889.12	-0.877	-0.892
323.15	13.47	0.20398	937.53	-0.580	-0.590
323.15	13.46	0.09879	964.40	-0.297	-0.318
373.25	7.02	0.89350	739.27	-0.420	-0.396
373.24	7.02	0.79623	757.27	-0.699	-0.690
373.27	7.00	0.70229	775.49	-0.888	-0.882
373.26	7.01	0.60172	796.16	-1.002	-1.001
373.23	7.01	0.49641	819.50	-1.038	-1.037
373.19	7.01	0.40888	840.39	-1.002	-1.000
373.18	7.04	0.29674	869.66	-0.873	-0.863
373.15	7.02	0.20398	895.75	-0.679	-0.672
373.38	7.04	0.09879	927.94	-0.372	-0.366
373.18	13.51	0.89350	747.44	-0.394	-0.365
373.16	13.51	0.79623	764.84	-0.648	-0.649
373.13	13.50	0.70229	782.26	-0.807	-0.824
373.13	13.51	0.60172	802.25	-0.910	-0.927
373.18	13.47	0.49641	824.77	-0.943	-0.956
373.20	13.49	0.40888	845.34	-0.919	-0.919
373.19	13.49	0.29674	873.88	-0.802	-0.793
373.18	13.49	0.20398	899.57	-0.627	-0.620
373.13	13.47	0.09879	931.32	-0.343	-0.342

Table A.VII.1. Continued

T/K	p/MPa	x	ρ/(kg·m^{-3})	V_m^E/(cm^3·mol^{-1})	
				expt.	calc.
423.35	7.00	0.89350	679.06	-0.503	-0.531
423.24	7.00	0.79623	697.53	-0.819	-0.835
423.29	7.00	0.70229	715.85	-1.006	-1.036
423.29	7.00	0.60172	737.98	-1.171	-1.172
423.29	7.00	0.49641	762.94	-1.227	-1.220
423.29	7.00	0.40888	784.75	-1.163	-1.183
423.38	7.00	0.29674	817.22	-1.041	-1.029
423.38	7.00	0.20398	845.65	-0.801	-0.807
423.37	7.00	0.20398	845.84	-0.808	-0.808
423.35	7.00	0.09879	882.71	-0.457	-0.446
423.23	13.50	0.89350	691.04	-0.407	-0.467
423.27	13.47	0.79623	708.33	-0.675	-0.709
423.27	13.50	0.70229	726.36	-0.871	-0.876
423.25	13.53	0.60172	746.46	-0.963	-0.981
423.21	13.52	0.49641	769.67	-0.991	-1.020
423.21	13.53	0.40888	791.92	-0.993	-0.992
423.19	13.53	0.29674	823.11	-0.890	-0.874
423.23	13.53	0.20398	850.82	-0.688	-0.690
423.19	13.52	0.09879	886.55	-0.386	-0.388
473.41	7.01	0.89350	590.87	-0.803	-0.801
473.44	7.01	0.79623	612.50	-1.405	-1.384

Table A.VII.1. Continued

T/K	p/MPa	x	ρ/(kg·m^{-3})	V_m^E/(cm^3·mol^{-1})	
				expt.	calc.
473.44	7.01	0.70229	634.35	-1.783	-1.772
473.46	6.89	0.60172	659.40	-2.059	-2.047
473.44	7.00	0.49641	687.88	-2.083	-2.103
473.41	7.01	0.40888	713.37	-1.984	-2.026
473.41	7.02	0.29674	749.79	-1.710	-1.740
473.40	7.02	0.20398	782.95	-1.329	-1.347
473.40	7.01	0.09879	824.85	-0.733	-0.732
473.30	13.49	0.89350	614.69	-0.445	-0.418
473.25	13.50	0.79623	633.07	-0.775	-0.713
473.27	13.52	0.70229	652.04	-1.037	-0.964
473.27	13.54	0.60172	674.71	-1.246	-1.170
473.26	13.56	0.49641	700.68	-1.332	-1.288
473.26	13.57	0.40888	724.35	-1.307	-1.296
473.33	13.55	0.29674	758.42	-1.169	-1.170
473.32	13.55	0.20398	790.33	-0.936	-0.935
473.31	13.56	0.09879	830.77	-0.531	-0.525
523.24	13.53	0.89350	485.64	-1.760	-1.850
523.28	13.53	0.70229	538.02	-3.813	-3.827
523.25	13.52	0.60172	567.98	-4.248	-4.266
523.27	13.51	0.49641	601.88	-4.348	-4.352
523.23	13.52	0.40888	631.80	-4.076	-4.102

Table A.VII.1. Continued

T/K	p/MPa	x	ρ/(kg·m^{-3})	V_m^E/(cm^3·mol^{-1})	
				expt.	calc.
523.29	13.51	0.29674	673.91	-3.454	-3.452
523.29	13.51	0.20398	711.92	-2.630	-2.617
523.30	13.50	0.09879	759.65	-1.417	-1.392
573.69	13.73	0.89350	166.98	12.594	
573.63	13.74	0.79623	164.28	23.460	
573.65	13.73	0.60172	166.44	36.143	
573.44	13.69	0.49641	177.09	35.073	
573.49	13.73	0.49641	178.94	34.104	
573.69	13.74	0.40888	307.09	-14.036	
573.09	13.59	0.40888	333.04	-21.160	
573.41	13.60	0.29674	514.80	-31.019	-33.622
573.63	13.58	0.20398	585.33	-23.286	-24.024
573.66	13.56	0.09879	657.00	-11.944	-11.999
573.62	13.57	0.09879	656.45	-11.886	-11.972

Table A.VII.2. Densities ρ(expt) of methanol measured in this work and those ρ(calc) from the equation of state (Goodwin, 1987)

T/K	p/MPa	ρ(expt.)/(kg·m^{-3})[a]	δ[b]	ρ(calc)/(kg·m^{-3})
323.19	0.10	762.48	0.50	762.66
323.17	0.10	762.45	0.50	762.68
323.19	0.10	762.99	0.50	762.63
323.16	0.10	761.89	0.50	762.70
323.15	6.99	769.14	0.50	770.10
323.18	7.00	769.88	0.50	770.08
323.15	13.51	776.93	0.50	776.50
323.17	13.44	776.82	0.50	776.44
373.25	6.99	720.49	0.60	720.25
373.21	13.51	729.29	0.60	728.91
423.25	7.01	659.69	0.70	659.75
423.23	7.00	659.74	0.70	659.75
423.29	7.00	659.12	0.70	659.67
423.29	7.00	659.58	0.70	659.67
423.27	13.50	673.63	0.70	673.03
473.48	7.00	568.97	0.80	569.00
473.35	7.01	568.38	0.80	569.00
473.33	13.52	597.58	0.80	597.81
523.31	13.54	460.17	0.90	459.42
523.27	13.57	460.29	0.90	460.03
523.83	13.51	457.45	0.90	456.94
523.72	13.50	456.66	0.90	456.76

Table A.VII.2. Continued

T/K	p/MPa	ρ(expt.)/(kg·m^{-3})[a]	δ[b]	ρ(calc)/(kg·m^{-3})
523.52	13.49	457.63	0.90	457.71
573.29	13.43	164.41	0.00	164.20
573.31	13.43	164.26	0.00	164.16
573.32	13.43	164.58	0.00	164.14

[a] The average absolute deviation, |ρ(expt.) - ρ(calc.)|, is 0.3 kg·m^{-3}.

[b] The densities of methanol have been corrected for the water content (mass fraction 0.001), i.e., ρ(expt.) = ρ(obs.) - δ, where δ was estimated at each temperature from our own experimental data for the mole-fraction dependence of densities.

Appendix B. Hydration Number of Aqueous Lanthanide Ions from Miyakawa's Model

Miyakawa *et al.* (1988) used the following model to calculate the electrostatic bond energy of the hydrated metal ions:

$$U = U_{ML} + U_{LL} + U_p + U_R, \tag{B.1}$$

where U_{ML} is the potential energy due to the electrostatic attraction between the metal ion and the ligand dipoles; U_{LL} is the dipole-dipole repulsion interaction energy between the water molecules, U_p is the work done to form induced dipoles on the water molecules; U_R is the energy associated with the short-range repulsion between the metal ion and the water molecules.

The hydration enthalpy $\Delta_s H°$ was estimated as follows:

$$\Delta_s H^\circ = U + \Delta H_{Born} - (5/2)nRT + n\Delta H_{vap} \tag{B.2}$$

where $\Delta_s H_{Born}$ is the Born hydration enthalpy; ΔH_{vap} is the enthalpy of vaporization of water.

Miyakawa *et al.* (1988) used the model to estimate the hydration enthalpies of the enneahydrated (figure V.11a) and octahydrated (figure V.11c) lanthanide ions. The geometric parameters used for the calculations are taken from the X-ray and neutron

diffraction studies. Miyakawa *et al.* estimated the entropy changes of the following equilibrium

$$[Ln(H_2O)_9]^{3+} = [Ln(H_2O)_8]^{3+} + H_2O$$

from the experimentally determined entropy for La^{3+}(aq)(CN=9) and Lu^{3+}(aq)(CN=8). Knowing the $\Delta_r H°$ for $Ln(H_2O)_9^{3+}$ and $Ln(H_2O)_8^{3+}$ and $\Delta\Delta_r S°$ for the equilibrium above allows $\Delta G°$ for the equilibrium to be obtained. The equilibrium constants are calculated as $K = \exp(-\Delta G°/RT)$.

We assume the average hydration numbers for aqueous lanthanide ions are given by

$$CN = 9 - K/(1+K) \ , \qquad \text{(B.4)}$$

which has been shown in figure V.12.

The heat capacity change $\Delta C_p°$ for the equilibrium is assumed to consist of two terms: the relaxation term $C_{p,rel}°$ associated with the existence of the equilibrium between nine-hydrated ions and eight-hydrated ions, and a term that arises due to the difference in the hydration number:

$$C_p°(CN=8) - C_p°(CN=9) = C_{p,rel}° + \alpha \cdot C_p(H_2O,l) \qquad \text{(B.5)}$$

where $C_{p,rel}°$ is $\Delta H°^2/RT^2 * K/(1+K)^2$. The last term is derived from the assumption that α

{=K/(1+K)} moles of water molecules completely lose any contribution to the heat capacity when they are transfered from bulk water to the first hydration shell. The function $\{C_p^\circ(CN = 8) - C_p^\circ(CN = 9)$ is plotted in figure B.1.

The values for ΔG° at temperatures other than T = 298.15 K can be estimated from ΔG°, ΔH° and ΔS° at T = 298.15 K using:

$$\Delta G^\circ(T) = \Delta H^\circ(T = 298) + (T - 298) * \Delta C_p^\circ + T\Delta S^\circ(T = 298) \qquad \text{(B.6)}$$

It was found that ΔG° did not change significantly, nor did K, the hydration number or $C^\circ_{p,rel}$.

The temperature dependence of C_p° cannot be calculated without knowing the vibrational and rotational contribution of the hydrated water molecules. Kenno and Hiraishi (1980) reported only the totally symmetric stretching vibration frequncy (ν_1) for aqueous lanthanide perchlorate at the glass temperature. No other attempt to measure or estimate all the vibrational modes for the hydrated lanthanide ions has been reported.

Goldman and Bates' model cannot be directly used to estimate the vibrational modes for the hydrated lanthanide ions because of the excessively strong repulsion term used. It is possible to calculate all the vibrational modes for $Ln(H_2O)_8^{3+}$ and $Ln(H_2O)_9^{3+}$ using the classical electrostatic potential functions used in the Miyakawa *et al.*'s model, but it is tedious to do it in a mathematically rigorous way. We chose to use the value for ν_1 reported by Kenno and Hiraishi to estimate the magnitude of the vibrational

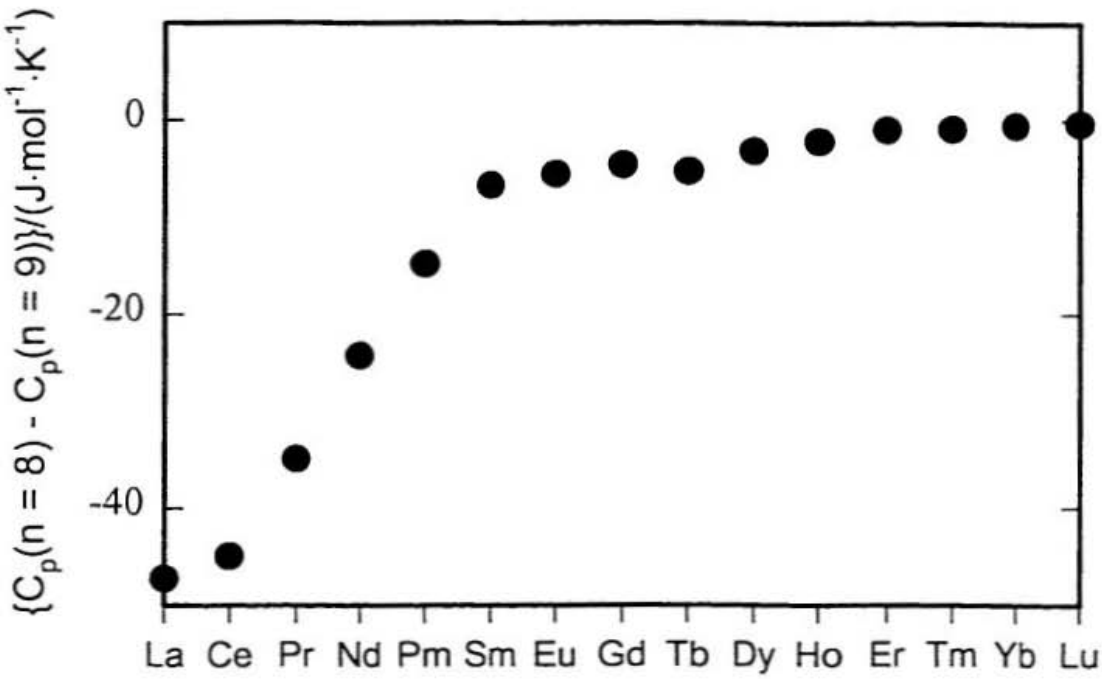


Figure B.1 The gadolinium break estimated from eqution (B.5)

contribution to C_p°.

The vibrational partition function was taken from Goldman and Bates model,

$$\left(\frac{\partial \ln Q_{vib}}{\partial T}\right) = \sum_f \frac{1}{T} \frac{X_f e^{-X_f}}{1 - e^{-X_f}},$$

where $X_j = 1.43868 \nu_j / T$ and ν_j is the vibrational wave number. The contributions to $C_{p,vib}^\circ$ from ν_1 at T = 298.15 K and 328.15 K are obtained by differentiating the equation above and plotted in figure B.2. Although there is a discontinuity in the plot, the gap for $C_{p,vib}^\circ$ calculated from the ν_1 mode is only 0.3 J·K·mol^{-1}, 0.3*(3*CN - 5) J·K·mol^{-1} for 3*CN - 5 modes.

Thus, while the gadolinium break at T = 298.15 K can be explained by Miyakawa *et al.*'s model, the model shows that the difference in heat capacity contribution, $\{C_p^\circ(CN=8) - C_p^\circ(CN=9)\}$, is not sensitive to the temperature change. The contribution to $C_{p,vib}^\circ$ as estimated from the vibrational mode ν_1 is relatively small compared to the gap for $C_{p,vib}^\circ$(40 J·K·mol^{-1}), and the weak temperature dependence of $C_{p,vib}^\circ$ may not be significant to cause the disappearance of the gadolinium break at temperatures higher than T = 298.15 K.

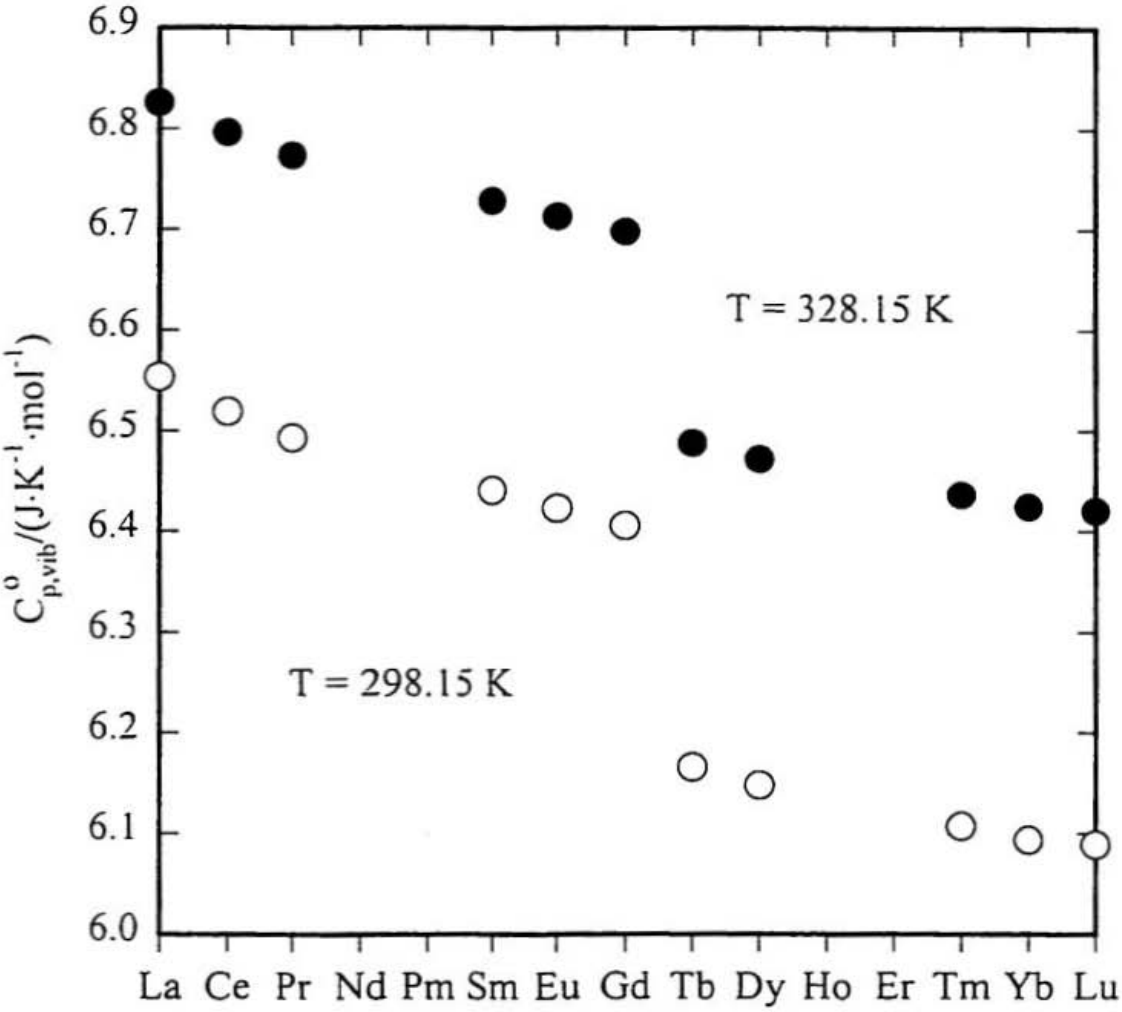


Figure B.2 The heat capacity contributions of the v_1 bands for the $Ln(H_2O)_n^{3+}$

CENTRE FOR NFLD. STUDIES
JUL 18 1978
MEMORIAL UNIVERSITY
OF NEWFOUNDLAND